A Modified Commercial Dynamic Chamber System for Measuring Soil Reactive Nitrogen Fluxes

Moxy Shah

A thesis submitted to the Faculty of Graduate Studies in partial fulfillment of the requirements for the degree of

Master of Science

Graduate Program in Chemistry

York University

Toronto, Ontario

September 2025

© Moxy Shah, 2025

Abstract

Reactive nitrogen compounds (NO, NO_2, HONO, and NH_3; N_r) play an important role in atmospheric processes and pose environmental and health risks. Though studied individually, their interactions at the surface–atmosphere interface remain unexplored. To address this issue, a comprehensive N_r dynamic chamber setup was developed by modifying a commercially available system for GHGs. System modifications to minimize surface loss for N_r were implemented. Proof-of-concept measurements under controlled lab conditions demonstrated that NO, NO_2, HONO, NH_3, and N_2O emissions can be quantified simultaneously. The p-values for the NO, NO_2 and HONO within a specific soil volumetric water content range (20-24%) revealed heterogeneity, suggesting a need to reconsider the soil sampling and handling techniques used in laboratory studies. Emission trends from urea and synthetic magnesium/zinc ammonium carbonate fertilizers provide preliminary insights into N_r release from fertilized soils.

Acknowledgments

Without God's grace, the guidance of my gurus, and the belief that a few special people had in me, I would not have been able to achieve my goals. It is difficult to put this immense gratitude and emotion into words, but I will do my best to convey my appreciation here.

Firstly, thank you to my supervisor, Trevor VandenBoer, for the motivation, feedback, and support throughout my research. I genuinely appreciate the guidance you have provided me in every step of my journey from a naive undergraduate with little knowledge of atmospheric chemistry to becoming a more confident scientist. I am truly grateful for your encouragement and assistance in helping me secure scholarships. I extend my appreciation to my committee members, Cora Young and John Liggio, for their feedback and guidance during my graduate studies.

I am incredibly grateful to the former and current members of both the VDB and CJY research groups for their support. Thanks to Leigh and Fahim for helping me feel comfortable working with chambers. Kifle, you have been an exceptional mentor, always willing to bounce ideas, from which I have learned so much about both research and life in general. Thank you, Danial, for solving my code problems, without which I would not have been able to process the data. Thank you to Leyla for being a mother figure to me; Nasrin, always ready to help; Na-Yung, for rescuing my weirdest lab mishaps; and to Yash, for being the best person to share my grad experience with.

Completing my master's degree would have seemed unattainable without the ongoing support of a few special people in my life. My parents (Hemant and Mayuri), whose unconditional love has been my foundation, and my brother, Darsh, whose belief in me gave me the strength to persevere through every challenge —sorry for bugging you with my codes. These wonderful people have had more patience than I could have asked for. To all my closest friends, your constant motivation and encouragement have been a beacon of light during my darkest days. Kabir, our outings, late-night coffee/chai escapades have kept me going through the time of exhaustion. Pari, our café adventures hold a special place in my heart and thank you for all the check-ins and Zoom meets to keep me focused during the writing process. Dharven, thank you for knowing the right (usually lame) jokes to keep me smiling! Het, Rajvi, Drashti, and Priyal, your pep talks have been my anchor during tough times. Thank you all for believing in me, even when I doubted myself!

Table of Contents

List of Figures

List of Tables

List of Symbols and Abbreviations

±	plus-minus
λ	wavelength
≥	greater than or equal to
≤	less than or equal to
⇌	reversible
℃	degree Celsius
K	kelvin
%	percent
τ	response time
ads	adsorbed
AER	air exchange rate
ADE	acid displacement efficiency
Al	aluminum
AMO	ammonia monooxygenase
AOB	ammonia-oxidizing bacteria
ATP	adenosine triphosphate
AVG	average
cc	cubic centimeter
CIMS	chemical ionization mass spectrometer
CH_4	methane
CO_2	carbon dioxide
cm	centimeter
CRDS	cavity ring-down spectroscopy
EC	eddy covariance
h	hour
HAO	hydroxylamine oxidoreductase
HCl	hydrochloric acid

HCN	hydrogen cyanide
HNO_3	nitric acid
HNCO	isocyanic acid
HVAC	heating, ventilation, and air conditioning
HONO	nitrous acid
IC-CD	ion chromatography-conductivity detection
kt	kiloton
L	liter
LPM	liter per minute
LOD	limit of detection
MC	measurement chamber
MFC	mass flow controller
min	minutes
mg	milligram
g	grams
mL	milliliter
molec cm^{-3}	molecules per cubic centimeters
mt	megaton
m/z	mass-to-charge ratio
n	number of experiments
N/A	not applicable
N cycle	nitrogen cycle
N_2	molecular nitrogen
N_2O_5	dinitrogen pentoxide
NaCl	sodium chloride
NaOH	sodium hydroxide
Na_2CO_3	sodium carbonate
$NaNO_2$	sodium nitrite

NH_3	ammonia
NO	nitrogen oxide
NO_2	nitrogen dioxide
N_2O	nitrous oxide
N_2O_5	dinitrogen pentoxide
NO_3^-	nitrate
NO_2^-	nitrite
NOB	nitrite oxidizing bacteria
NO_x	nitrogen oxides (NO + NO_2)
NO_x^*	nitrogen oxides (NO, NO_2, and NO_y species)
NO_x analyzer	chemiluminescence analyzer that measures NO_x
NVOCs	nitrogen-containing volatile organic compounds
O	singlet oxygen
O_2	molecular oxygen
O_3	ozone
OH	hydroxyl radical
PA	purified air
PAR	photosynthetically active radiation
PFA	perfluoroalkoxy alkane
pH	scale of acidity, -log(H^+)
ppb	parts per billion
ppbv	parts per billion by volume
ppm	parts per million
ppmv	parts per million by volume
ppt	parts per trillion
pptv	parts per trillion by volume
PTFE	polytetrafluoroethylene
s	second

sccm	standard cubic centimeter per minute
SD	standard deviation
SLPM	standard litre per minute
SWC	soil water content
Temp	temperature
tN_r	total reactive nitrogen
RC	reference chamber
REA	relaxed eddy accumulation
RH	relative humidity
RSD	relative standard deviation
RSE	relative standard error
V	volts
VWC	volumetric water content
VOC	volatile organic compounds
WFPS	water-filled pore space
WHC	water holding capacity
ZA	zero air
ZAG	zero air generator

Chapter One: Introduction to reactive nitrogen and its role in atmospheric chemistry

Author's Contributions: MS wrote and TCV edited this work.

1.1 What is reactive nitrogen (N_r) and why do we care?

Nitrogen exists as dinitrogen gas (N_2) in its simplest form and is a critical component of the global biogeochemical cycle (Galloway et al., 2004; Liu, et al., 2020). It makes up 78% of the air in the atmosphere. However, only a small fraction of Earth's atmospheric N_2 is biologically fixed or converted by processes such as lightning to be made available to plants and animals. Atmospheric N_2 is unavailable for most organisms because the two nitrogen atoms in a molecule, held together by a stable triple bond, need to be broken (Zhang et al., 2020). Through natural and anthropogenic processes, nitrogen is converted into reactive forms, which then can be used by living organisms. Reactive nitrogen (N_r) in the atmosphere refers to all nitrogen compounds excluding inert N_2, which constitutes the majority of Earth's atmosphere (Brümmer et al., 2022). The reactive form of nitrogen includes compounds with oxidation number (ON) other than 0, such as inorganic reduced form of nitrogen (NH_x) which include ammonia (NH_3, ON is -3) and ammonium ion (NH_4^+, ON is -3), inorganic chemically oxidized forms like nitrogen oxides (NO_x = nitric oxide (NO, ON is +2) + nitrogen dioxide (NO_2, ON is +4)), nitrous acid (HONO, ON is +3), nitric acid (HNO_3, ON is +5), nitrite ion (NO_2^-, ON is +3), nitrate ion (NO_3^-, ON is +5), nitrous oxide (N_2O, ON is +1), and dinitrogen pentoxide (N_2O_5, ON is +5), gaseous organic nitrates like peroxyacytyl nitrate (PAN), and non-volatile organic nitrogen compounds (i.e., urea, amino acids, amines and proteins) (Galloway et al., 2008). These N_r compounds are mobile and capable of transforming into one another through complex microbial, chemical, and physical processes.

The circulation of N_r occurs within a dynamic biogeochemical cycle that interconnects the atmosphere, soil, water bodies, and living organisms. Reactive nitrogen transforms between forms like NH_4^+, NO_3^-, NO and N_2O. It enters the ecosystem through microbial nitrogen fixation, is taken up by plants or other microbes, and can be released back into the atmosphere through processes like ammonification, nitrification, and denitrification. Transformation also allows N_r to move into water in the form of NH_4^+ and NO_3^-, as well as other water-soluble species, via leaching and runoff, impacting the aquatic ecosystem by fueling algal blooms.

While the nitrogen cycle is essential for supporting life, increasing N_r emissions due to human activities have far-reaching consequences for the environment and human health. Increasing levels of N_r are the root of modern environmental concerns such as acid rain, the formation of the particulate matter ($PM_{2.5}$), and ground-level ozone (O_3). It also causes health issues through the formation of smog and haze, which are linked to respiratory issues like asthma, making air pollution the global second cause of premature mortality (Kinney, 2018; Naureen et al., 2022; Xia et al., 2024). This highlights the need to manage N_r levels in the environment and to have a deep understanding of its sources and sinks throughout global reservoirs. By identifying the key contributors to N_r emissions and the processes that remove or transform it, targeted strategies such as optimizing fertilizer use, implementing regulations to reduce industrial and vehicular NO_x, can be developed to mitigate its adverse effects on the ecosystem, air quality and human health.

1.2 Sources of N_r

1.2.1 Natural sources of N_r

Natural N_r sources include lightning, volcanic activity, wildfires, biomass burning, and biological nitrogen fixation (BNF). These all influence the cycling of nitrogen within terrestrial ecosystems. During thunderstorms, lightning provides a natural pathway for N_r production mainly though NO_x (Schumann & Huntrieser, 2007). High temperatures generated during lightning facilitate the production of NO in the atmosphere from N_2 and O_2. Subsequently, NO is oxidized to NO_2 and further to HNO_3. This process introduces N_r into ecosystems, particularly over tropical continental regions. Lightning contributes a minor amount toward global N_r production, ranging between 1 and 10 Tg N yr^{-1} (Shepon et al., 2007). A recent study showcases how electrically generated hydroxyl radical ($OH^{\cdot}$) might not be consumed immediately by NO but is available to oxidize other pollutants in the atmosphere and contribute to global OH oxidation (Jenkins & Brune, 2025). Volcanic eruptions contribute to N_r production through two primary mechanisms: thermal degradation of atmospheric N_2 and O_2 at high temperatures and the formation of nitrogen compounds during volcanic lightning. During volcanic eruptions, high temperatures (up to 1400–1820 K) in volcanic plumes can fix atmospheric N_2 into reactive forms like NO_x (Aroskay et al., 2023). Explosive eruptions often produce lightning, which creates localized heat and pressure capable of converting N_2 into reactive forms, such as NO_3^- (Aroskay et al., 2023). Recent isotopic studies suggest that high NO_3^- concentrations found in ancient volcanic deposits could be

attributed to volcanic lightning (Aroskay et al., 2023; Contamine et al., 2024). It is estimated that global high-temperature volcanism fixes atmospheric N_2 at rates of approximately 0.028 Tg N yr^{-1}, depending on factors like magma type and eruption temperature (Mather et al., 2004). These processes are thought to play an important role in N_r production, especially during large eruptions. Biomass burning and wildfires are both considered natural sources of N_r, despite the fact that their ignition may be derived from anthropogenic activities, releasing a diverse array of nitrogen-containing compounds into the atmosphere. The nitrogen compounds released during biomass burning originate exclusively from the nitrogen content in the vegetation being combusted. The combustion temperatures when below 1200 °C are insufficient to drive the thermal nitrogen cycle, which would otherwise convert atmospheric N_2 in the presence of O_2 into NO_x (Roberts et al., 2020). As a result, the nitrogen released from biomass burning consists of a wide range of nitrogen species, ranging from NH_3, hydrogen cyanide (HCN), HONO, various nitrogen-containing volatile organic compounds (NVOCs) and NO_x when temperature permits (≥ 1200 °C) (Roberts et al., 2020). During combustion, nitrogen in the fuel undergoes a series of reactions leading to the formation of both gas-phase and particle-bound nitrogen species. Wildfires that occur naturally emit compounds from fully reduced species, such as NH_3, to highly oxidized species, such as isocyanic acid (HNCO), acetonitrile (CH_3CN), including those emitted during biomass burning (Lindaas et al., 2021). These N_r compounds in smoke can undergo oxidation reactions and partition into existing aerosol. The chemistry depends on the presence of oxidants such as OH, O_3, and the NO_3 radical in the atmosphere and is highly complex (Benedict et al., 2017; Lin et al., 2024). Wildfire also releases CO_2 and other GHGs, exacerbating global warming. The release of CO_2 is concerning because it contributes to the positive feedback loop of climate change: as global temperatures rise, the frequency and intensity of wildfires increase, leading to more CO_2 emissions and further warming (Lindaas et al., 2021), but the impacts of the perturbed N_r cycle are still undergoing investigation.

Biogenic sources refer to biologically mediated production of N_r by living organisms, particularly microbes. While microbes are present in other environmental compartments like the aquatic system and the atmosphere, this study will focus solely on terrestrial soil microbes. The primary biogenic source of N_r is biological nitrogen fixation (BNF), a natural process facilitated by nitrogen-fixing microorganisms possessing the nitrogenase enzyme, which can catalyze the conversion of N_2 to NH_3 (Fowler et al., 2013; Galloway et al., 2004; Gruber and Galloway, 2008).

Nitrogen-fixing microorganisms can be free-living archaea or bacteria in soil (e.g., *Azotobacter, Clostridium*, *Bacillus,* and *Klebsiella*) and/or symbiotic with plant roots (e.g., *Rhizobium* and *Bradyrhizobium*) (Maia & Moura, 2014; Zhang et al., 2020). The NH_3 produced through BNF can then be assimilated by plants or transformed into other reactive nitrogen compounds through plant processes like nitrification or denitrification. Biological nitrogen fixation is an essential component of the nitrogen cycle as it adds bioavailable nitrogen to the ecosystem, namely in the form of N_r species like NH_4^+, NO, NO_2, HNO_3, N_2O, and HONO (Fowler et al., 2013). Human activities have amplified N_r production by enhancing BNF through agricultural practices, such as cultivating nitrogen-fixing crops (e.g., soybeans, alfalfa). Globally, BNF contributes to approximately 60 Tg N yr^{-1} on land and 140 Tg N yr^{-1} in the ocean, making it an important natural N_r source (Galloway et al., 2008; Gruber & Galloway, 2008).

1.2.2 Anthropogenic sources of N_r

Anthropogenic N_r has increased more than tenfold compared to pre-industrial levels, now exceeding the annual N_r production estimated from natural sources (Galloway et al., 2004; Liu, Zhang, Xu, Liu, Lu, et al., 2020). Human activities have contributed approximately 210 Tg N yr^{-1} of N_r primarily through industry, agriculture and transportation (Fowler et al., 2013). The combustion of fossil fuels results in NO_x emissions to the atmosphere, and these emissions have risen since the onset of the Industrial Revolution. These human-driven sources of N_r have altered the global N cycle, as N_r is being accumulated in the air, soil and water from the oxidation and/or deposition of these compounds downwind. As N_r moves from the atmosphere to other environmental compartments, it triggers a range of environmental challenges, such as acid rain, eutrophication, and biodiversity loss, as well as human health problems, including respiratory diseases, cardiovascular issues, and the exacerbation of conditions like asthma. Landfills and wastewater treatment plants are also N_r sources in the environment. The decomposition of organic matter in landfills and the treatment of wastewater result in the production of N_r compounds such as N_2O, NH_3, NO_3^- and greenhouse gases (GHGs) like CH_4, CO_2. Landfills are estimated to contribute approximately 3% of global N_2O emissions, with most of these emissions originating from developed countries (Rinne et al., 2005). Similarly, wastewater treatment processes produce effluents containing elevated levels of NH_3, NH_4^+, NO_3^-, NO_2^- and dissolved organic nitrogen (Zhang et al., 2017). Studies have shown that wastewater treatment is a source of HONO through the protonation of NO_2^- (Zhang et al., 2023; Zhou et al., 2011). All of this excess nitrogen could

stimulate algae growth, which can throw the ecosystem out of balance due to a lack of adequate nutrients and sunlight for other organisms present in the water.

The use of nitrogenous fertilizers has led to a marked increase N_r inputs into the environment, with various soil processes actively involved in the nitrogen cycle and facilitating transfer to the atmosphere across the interfacial boundary (**Figure 1.1**).

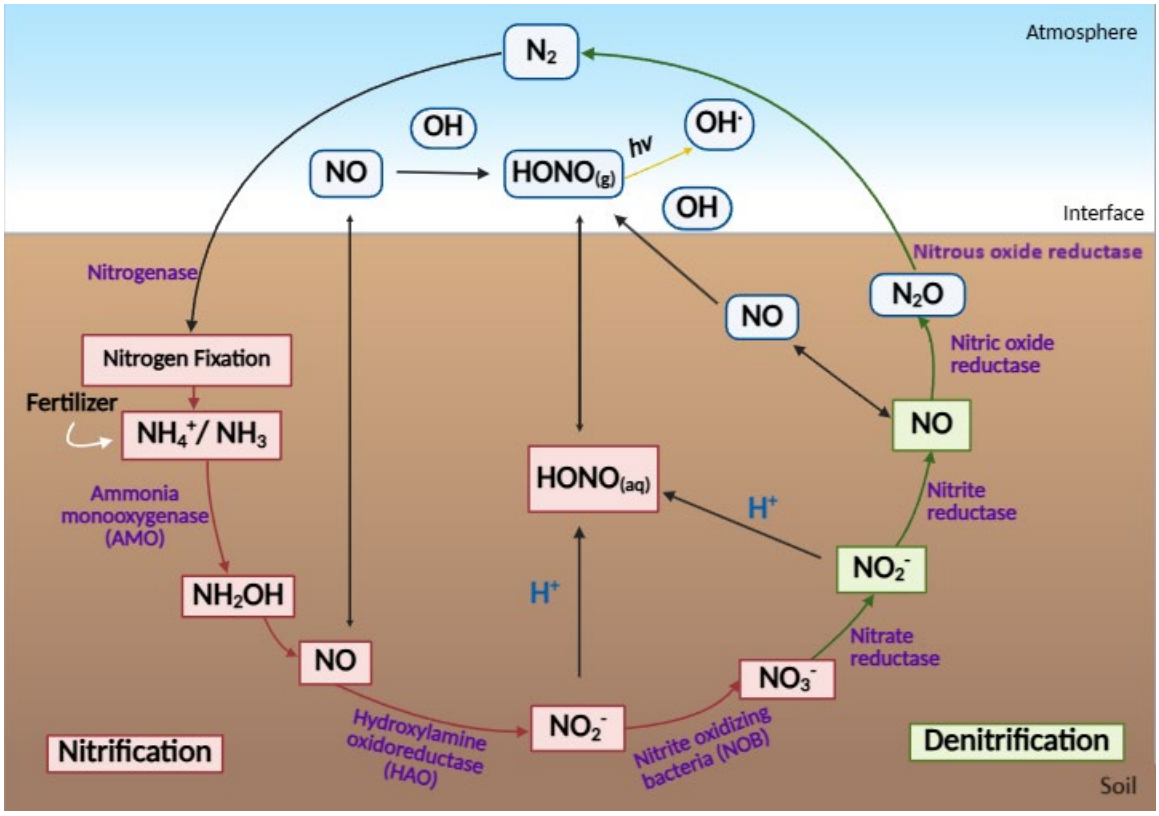

Figure 1.1: Schematic overview of the nitrogen cycle, highlighting the important N_r species at the land-atmosphere interface. Major intermediates involved in the nitrification and denitrification pathways are shown in pink and green boxes, respectively. Specific enzyme for each step of the N cycle is shown in purple. Solid rectangular boxes indicate aqueous species, whereas rectangle with curved edges shows the species partition to the atmosphere. For simplicity, several other known atmospheric sources and sinks of HONO are not depicted.

Soil microbes play a crucial role in N_r emissions through two processes: nitrification and denitrification. Nitrification begins with the conversion of NH_3 to hydroxylamine (NH_2OH) followed by subsequent oxidation by ammonia-oxidizing bacteria (AOB), releasing NO into the atmosphere. Denitrification occurs under anaerobic conditions, causing microbial reduction of NO_3^- to NO_2^- followed by further reduction, again releasing NO (**Figure 1.1**). Atmospheric NO can catalyze the production of tropospheric ozone (O_3) and other photochemical oxidants, causing

local air quality deterioration (Huang et al., 2023; Pan et al., 2022; Tan et al., 2023). The NO reductase (NOR) enzymes in soil microbes reduce NO to N_2O, a key step in denitrification (**Figure 1.1**). Nitrous oxide is a long-lived GHG which causes the depletion of the stratospheric ozone layer (Lehnert et al., 2021; Pan et al., 2022). The major direct emissions are from nitrogen additions in the agricultural sector to about half the total of anthropogenic sources, i.e., 3.6 Tg N yr^{-1} (Tian et al., 2024). The formation of aqueous HONO, due to the protonation of NO_2^- accumulated in soils from microbial nitrification/denitrification, and its subsequent emission to the atmosphere, has been recently recognized as a potential daytime source of gaseous HONO (**Figure 1.1**) (Bhattarai et al., 2021; Nussbaumer et al., 2023; Oswald et al., 2013; Wu et al., 2019). Previous studies have confirmed the release of HONO from soil, both in laboratory and field measurements, which raises interest in its release pathways from the soil (Meusel et al., 2018; Ren et al., 2025; Su et al., 2011; Wu et al., 2019).

Other forms of N_r, such as NH_3, can also volatilize to the overlying atmosphere from soil surfaces through the deprotonation of NH_4^+ in soils. Human activities such as the excessive use of nitrogenous fertilizers and low-efficiency land and waste management practices with respect to N_r have amplified these processes, increasing N_r emissions and their associated environmental impacts. For instance, NH_3 volatilization and N_2O production from agricultural soils are directly linked to fertilizer overapplication (Pan et al., 2022). Thus, effective use of nitrogen is indispensable for both plant growth and the environmental sustainability of humanity.

1.3 Environmental, climatic and health impacts of N_r

Reactive nitrogen gases, including NO_x and NH_3, are significant contributors to air pollution. In the troposphere, NO_x reacts with volatile organic compounds (VOCs) in the presence of sunlight to form O_3 and $PM_{2.5}$, both of which pose a threat to health, including respiratory and cardiovascular issues (Peel et al., 2013). The $PM_{2.5}$ can penetrate the lungs and aggravate conditions like asthma and bronchitis (Peel et al., 2013). Reactions of NO_x also contribute to secondary particulates (e.g., NH_4NO_3) through interactions with NH_3, water vapour and other particles (Finlayson-Pitts & Pitts, 2000; Peel et al., 2013; Seinfeld and Pandis, 2006). Secondary organic aerosols (SOA) are formed in the atmosphere when gas-phase radical species like OH, O_3, and NO_3 react with oxidants (Hallward-Driemeier et al., 2024). Studies show SOA to be highly toxic, possibly due to its strong oxidation potential (Brownwood et al., 2021; Xiang et al., 2023).

The toxicological pathways of SOA are complex, where SOA firstly interacts with membrane receptors, followed by several other pathways, eventually leading to SOA-induced cell death (Xiang et al., 2023).

Ammonia plays a crucial role in neutralizing acidic pollutants like HNO_3 and H_2SO_4, contributing to the formation of fine aerosol nitrates (NH_4NO_3) and sulphates ($(NH_4)_2SO_4$). These aerosols are particulate matter that can lead to haze formation in the atmosphere, and upon their inhalation, can cause respiratory problems (Brownwood et al., 2021; Peel et al., 2013).

Acid rain forms when two pollutants, sulphur dioxide (SO_2) and NO_x, are released into the atmosphere via natural and human activities. The process begins with SO_2 and NO_x undergoing photooxidation in the presence of sunlight, reacting with water and other components present in the atmosphere, to ultimately form sulfuric and nitric acids (Chen et al., 2021). Wind and air currents spread these acidic substances over long distances and eventually precipitate down in the form of wet deposits such as rain, fog, snow, and mist (Mehta, 2010). Overall, N_r contributes to acid rain, which acidifies soil and aquatic systems by lowering the pH, which depletes essential soil nutrients and can lead to biodiversity loss by damaging aquatic organism tissues and organ function (Wang et al., 2020).

Nitrous acid is a major source of the highly reactive photooxidant hydroxyl radical ($OH^{\cdot}$) and NO via its photolysis (Spataro & Ianniello, 2014) (**Figure 1.2**). The RO_2/HO_2 radical produced react with NO to produce NO_2 and an oxy radical (RO). The produced NO_2 photolyze to generate atomic oxygen, which then reacts with O_2 to produce O_3 (Nguyen et al., 2022) (**Figure 1.2**). It has been established that the OH radical is generally the most important trace species in the atmosphere, governing its oxidizing capacity, and therefore, it is essential to control its production, especially in the troposphere (Ramazan et al., 2004).

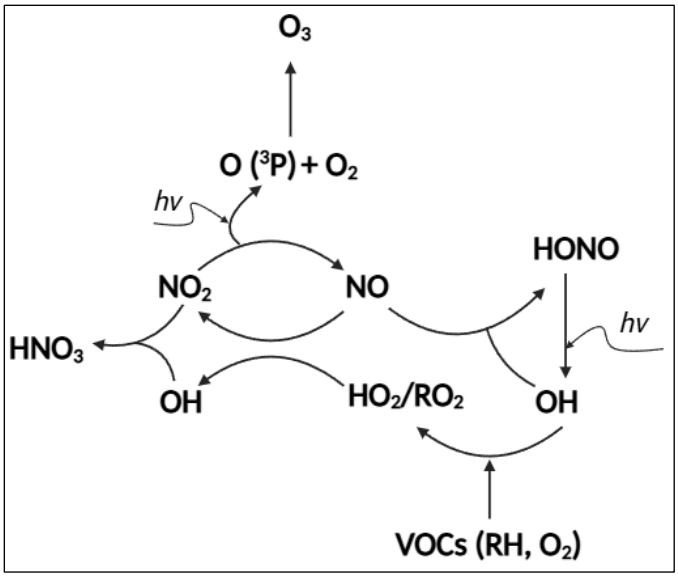

Figure 1.2: Catalytic O_3 production from HONO via OH radical. The hydroxyl radical initiates reactions with VOCs, leading to the production of hydroperoxy radicals (HO_2) and organic peroxy radicals (RO_2). The R represents the organic moiety. In the presence of NO_x, reactions of these radicals establish a cycle that can produce O_3.

Eutrophication is a process in which freshwater and marine ecosystems become over-enriched with nutrients, particularly phosphorus and nitrogen. Nutrients enter the water ecosystems through surface runoff, rainfall, river flow and direct atmospheric N deposition in the form of NH_4^+, NO_3^- and NO_2^- (Baron et al., 2013). When N_r accumulates in water bodies, it overstimulates the growth of algae and aquatic plants, a process known as an algal bloom. As algae and aquatic plants die and decompose, microbial activity increases, consuming dissolved oxygen, creating low to no oxygen conditions for other aquatic organisms (Baron et al., 2013). Thus, an increase in N_r disrupts aquatic ecosystems and can lead to mass die-offs of fish through depletion of the dissolved oxygen the need to live (Paerl et al., 2016).

Nitrous oxide is a long-lived greenhouse gas with a global warming potential 265 times greater than CO_2 over 100 years (IPCC, 2023), making it a significant contributor to global warming. Studies show N_2O is the largest ozone-depleting substance today and is expected to remain the largest throughout the rest of this century (Ravishankara et al., 2009). Nitrous oxide contributes to the depletion of the stratospheric ozone layer by interacting with compounds to form stratospheric NO (**R3**). The produced tropospheric N_2O is transported to the stratosphere and broken down via photolysis, producing $O(^1D)$ and generating approximately 10% of stratospheric NO_x (**R1-R3**) (Portmann et al., 2012).

$$N_2O + h\nu \rightarrow N_2 + O(^1D) \quad \text{(R1)}$$

$$N_2O + O(^1D) \rightarrow N_2 + O_2 \quad \text{(R2)}$$

$$N_2O + O(^1D) \rightarrow 2NO \quad \text{(R3)}$$

All of these gas species mentioned above are linked to either environmental or health issues. Therefore, understanding particularly N_r at the land-atmosphere interphase is important because this is the place where these gases are emitted, deposited or transformed. Studying specifically at the soil-atmospheric interphase would give an idea of which processes/pathways they are released and to what extent in the subsequent sections.

1.4 Reactive nitrogen exchange at the land-atmosphere interface

The exchange of N_r between the Earth's surface and the atmosphere involve numerous production and loss processes driven by both natural and human activities. Reactive nitrogen species are removed from the atmosphere through wet (i.e., dissolution in droplets and subsequent rainout, snow or fog) and dry (i.e., uptake of gases by surfaces like soil, water bodies, etc.) deposition. However, these removal processes are often outpaced by the N_r emission from ground surfaces (Delaria & Cohen, 2023). At the land surface, N_r is released into the atmosphere by microbial nitrogen cycling (i.e., nitrification and denitrification), agricultural activities (e.g., fertilizer application), wildfires, or fossil fuel combustion. Despite advancements, the understanding of N_r exchange remains challenging due to its high spatial and temporal variability and various factors like climate, vegetation cover, and soil/surface properties at the land-atmosphere interface (Ludwig et al., 2001). This complexity is particularly evident in agricultural landscapes, where the balance between nitrogen inputs (i.e., fertilizers, manure) and losses (e.g., emissions, leaching) is dynamic and poorly constrained.

Agricultural activities are among the major contributors to atmospheric N_r emissions, yet their precise magnitude, variability, and transformation pathways remain uncertain (Gong et al., 2025; Tai et al., 2025; Tian et al., 2024; Yang et al., 2024). This knowledge gap has motivated large-scale initiatives such as NASA's FarmFlux campaign, scheduled for the crop-growing season of March–July 2026, to improve the quantification of agricultural emissions. FarmFlux focuses on how gases like NH_3, N_2O, and NO_x are emitted, transported, and transformed in the atmosphere at large spatial scales across US agricultural regions. One of the core challenges in studying N_r exchange

is the interplay between emission and deposition processes across different landscapes. Soils play a pivotal role in mediating N_r emissions due to their dual function as both a source and a sink of nitrogen species. Soil-atmosphere exchange of N_r is primarily thought to be governed by microbial processes such as nitrification and denitrification, with soil factors like pH, moisture, organic matter, and nitrogen availability playing a crucial role in regulating N_r emission (Mosier, 2008; Purchase et al., 2023; Stepniewski et al., 2015). This N_r exchange is intricately linked to agricultural practices, as excessive nitrogen inputs (e.g., fertilizers) amplify emissions of N_r species, namely NO_x, N_2O, HONO, and NH_3 through the soil (Degaspari et al., 2020).

Soils are composed of air-filled pores, water, and organic mineral particles (**Figure 1.3**).

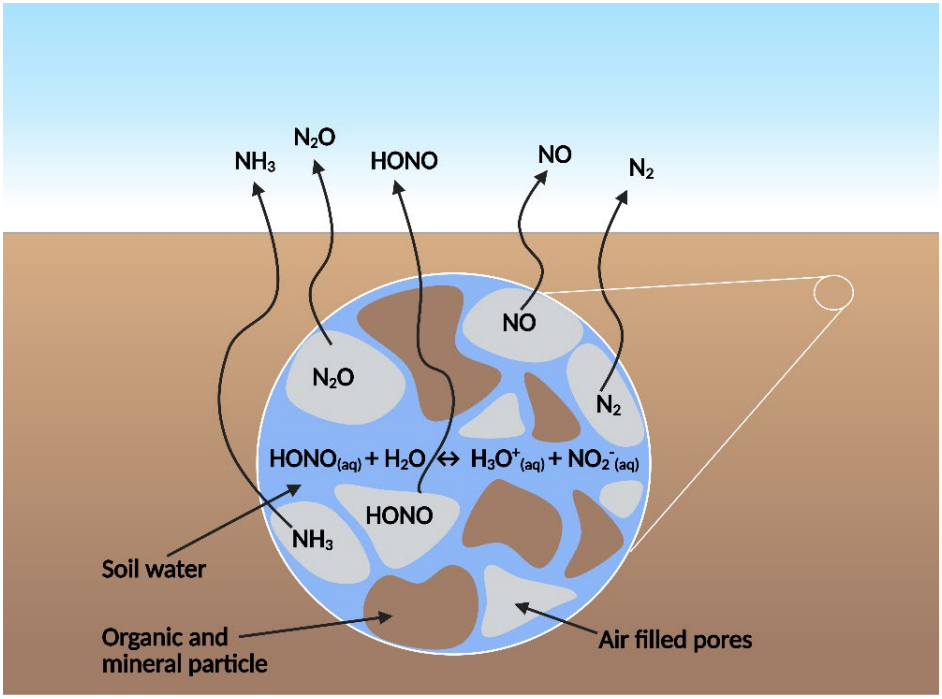

Figure 1.3: A cross-section of the soil matrix showcases the soil phases. Soil is composed of air-filled pores, water, and organic-mineral particles. Air-filled pores facilitate the gas partition between the aqueous phase (i.e., soil water) and the gas phase (air pores) to the atmosphere, releasing gases like NH_3, NO, N_2O, HONO and N_2 from the soil. Acid dissociation of a weak acid like HONO takes place in the aqueous phase via nitrite protonation in acidic soil, followed by volatilization into the atmosphere.

The details of the physical and chemical properties of soils then facilitate constant gas exchange with the atmosphere, whereby gases diffuse into and out of the soil after being produced or consumed therein. Gas diffusivity through soils depends directly on the air-filled porosity and inversely on water content, which controls the movement of the gases to and from the atmosphere

(Mosier, 2008). While soils represent a major component of land-atmosphere N_r exchange, they do not act in isolation. Vegetation, water bodies, and human activities interact with soils to further alter N_r emissions. For instance, N_r emitted from soils can be taken up by vegetation or deposited into aquatic ecosystems (Fowler et al., 2013). To quantify this N_r exchange near the ground surface, various flux measurement techniques are employed, enabling insights into their magnitude and drivers. Large-scale studies like FarmFlux would help address these uncertainties at large spatial scales by integrating their aircraft observations with ground-based flux measurements and atmospheric models to track nitrogen emissions, providing a detailed understanding of how nitrogen moves through the atmosphere (Wolfe et al., 2024). The current state of knowledge on contributing chemical, physical and biological processes governing N_r exchange, and techniques to quantify them are presented in the sections that follow. Highlights of particular knowledge gaps with respect to HONO are provided, as this is a chemical species of emerging interest at the surface-atmosphere interface.

1.5 Pathways leading to atmospheric HONO

1.5.1 Chemical pathways to HONO release

The chemical mechanisms governing HONO sources can be categorized into daytime and nighttime processes. During the day, the only known homogenous gas-phase (i.e., all reactions occur in the gas phase) HONO source is the pressure-dependent third-body reaction where two reactants (i.e., NO and OH) form HONO with the help of a third body molecule, M (usually O_2 or N_2) to stabilize the reaction products and carry away excess energy (**R4**). Given that homogenous gas-phase mechanisms of HONO have been studied extensively and a missing source(s) of HONO still exists, studies speculate that the contribution from heterogeneous sources of HONO to both the daytime and nighttime HONO production pathways is greater than homogeneous sources.

$$NO_{(g)} + OH + M \rightarrow HONO_{(g)} + M \qquad (R4)$$

One recently popularized daytime heterogeneous HONO source is the photolysis of surface adsorbed and/or particulate nitrate (**R5-R7**), where adsorbed HONO at the surface can desorb in **R4** to yield gas-phase HONO under low mixing ratios of NO_x (Sörgel et al., 2011; Wang et al., 2017). The rate and yield of this process are currently debated, as observations no longer are compatible with our established understanding of atmospheric chemistry. Similarly, several

laboratory studies previously showed daytime reaction pathways for HONO production by reaction of NO_2 on photoexcited aerosol surfaces such as soot, humic acid, and TiO_2 (i.e. paint pigment) (Monge et al., 2010; Sörgel et al., 2011; Stemmler et al., 2006). However, the quantification of the importance of these reactions in the real atmospheric environment remains elusive and under debate.

$$HNO_{3\,(ads)} + h\nu \rightarrow NO_{2\,(ads)} + OH \qquad \text{(R5)}$$

$$2NO_{2\,(g)} + H_2O_{(ads)} \rightarrow HONO_{(g)} + HNO_{3\,(ads)} \qquad \text{(R6)}$$

$$HONO_{(aq)} \leftrightarrow HONO_{(g)} \qquad \text{(R7)}$$

During the night, the dominant HONO source in both rural and urban regions is the heterogeneous uptake of NO_2 on surface-adsorbed water (**R6**) (Kleffmann et al., 2005; Ramazan et al., 2004; VandenBoer, Brown, Murphy, Keene, Young, Pszenny, Kim, Warneke, de Gouw, et al., 2013). The uptake of HONO produced by this mechanism can also occur through the adsorption of gas-phase HONO into bulk water on the ground surface and the acid dissociation of HONO back into nitrite and hydronium ion (**R8**).

$$HONO_{(aq)} + H_2O_{(l)} \rightleftharpoons NO_2^-{}_{(aq)} + H_3O^+{}_{(aq)} \qquad \text{(R8)}$$

At sunrise, when evaporation of dew begins, nitrite can be released back into the gas-phase HONO upon protonation through these dynamic equilibria (**R8**) (He et al., 2006; Ren et al., 2020). A nocturnal surface nitrite reservoir can also be displaced by atmospheric photochemical acids (i.e., HNO_3, HCl) the following day and release gas-phase HONO, accounting for up to 30% of the daytime gas-phase HONO (**R7, R8**) (VandenBoer et al., 2015). Recent studies have shown that the role of the ground surface is an important nocturnal sink of gas-phase HONO, which can form a reservoir in the form of NO_2^- that has the potential to be emitted back into gas-phase HONO through these, and perhaps other, processes during the day (Donaldson et al., 2014; VandenBoer et al., 2013).

1.5.2 Biological contribution to HONO production

Evidence from lab studies suggests that biological pathways may play a crucial role in generating intermediate species like HONO through microbial nitrogen transformation pathways (Butterbach-Bahl & Dannenmann, 2011; Caranto & Lancaster, 2017; Kool et al., 2010). Biological nitrogen-

fixing bacteria (BNF) fix atmospheric N_2 into the soil, or nitrogen can be available in the form of NO_x upon lightning, which then feeds into the N-cycle in the form of NH_3 or NO_3^- respectively (**Figure 1.4**).

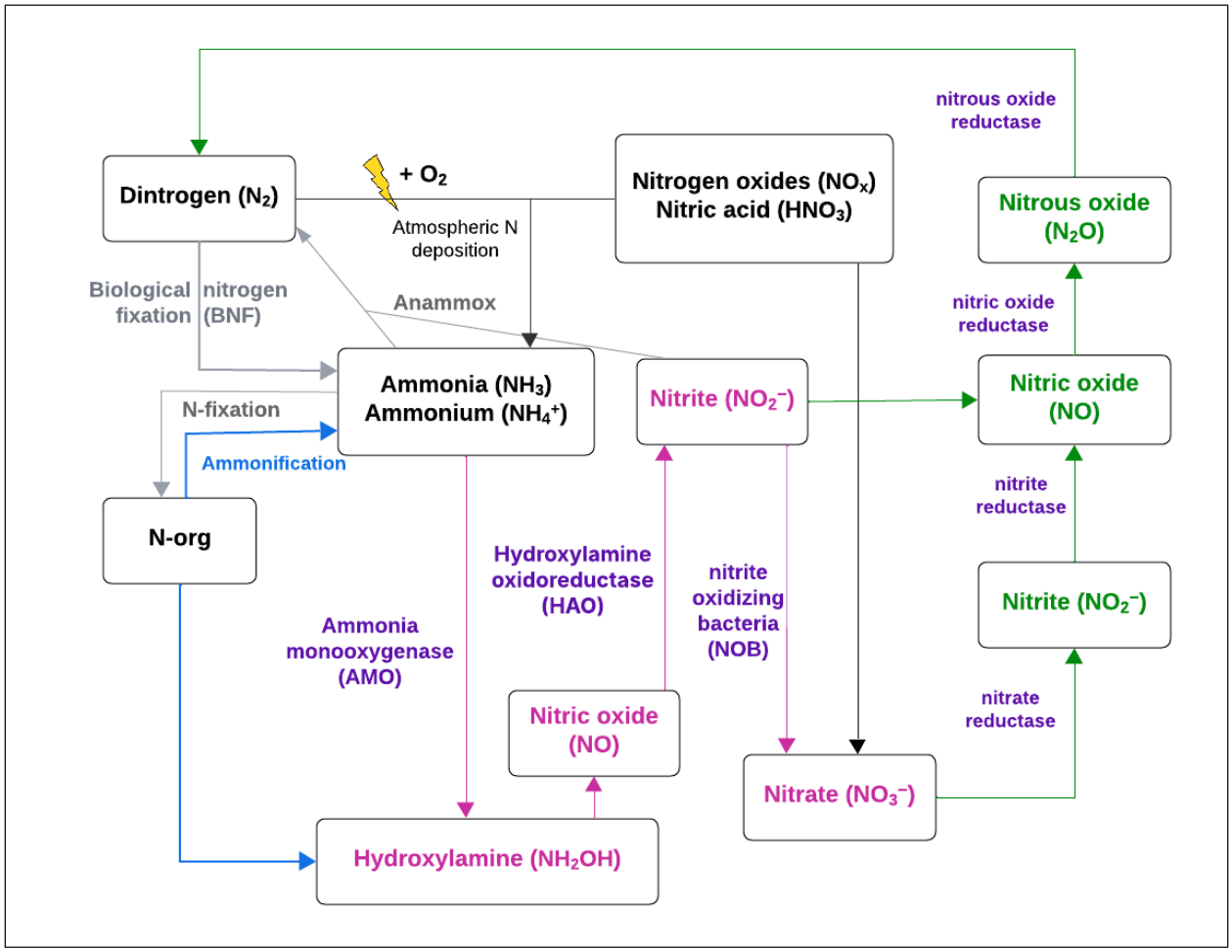

Figure 1.4: A simplified biogeochemical N cycle illustrating the key processes that transform nitrogen into various chemical forms, enabling its movement through the atmosphere, soil, and biosphere. Nitrification encompasses the aerobic oxidation of NH_3, NH_2OH, and NO_2^-, depicted by the pink arrows. Denitrification, represented by the green arrows, is an anaerobic microbial process that reduces NO_3^- and NO_2^- to gaseous nitrogen forms (NO, N_2O, N_2), returning nitrogen to the atmosphere. Mineralization, shown with blue arrows, involves the conversion of organic nitrogen into a bioavailable form for plants and microorganisms. Abiotic processes, indicated by black arrows, encompass chemical transformations of nitrogen that occur independently of microbial activity.

Nitrification is the process where NH_3 and/or NH_4^+ are converted into NO_2^- and NO_3^- by specialized autotrophic bacteria (i.e., ammonia oxidizing bacteria (AOB) and ammonia-oxidizing archaea (AOA) with specific enzymes ammonia monooxygenase and hydroxylamine

oxidoreductase) (**Figure 1.4**). A key by-product of this oxidation through AOB and AOA is NO, as described in Krichels et al. (2024) and Mushinski et al. (2019). This produced NO can transition to the atmosphere or can be converted to NO_2^- by hydroxylamine oxidoreductase (HOA) (**Figure 1.1, 1.4**). The abiotic protonation of NO_2^- in the soil or when soil becomes acidic leads to the production of aqueous HONO (**Figure 1.1**) (Oswald et al., 2013; Su et al., 2011). The relative contribution of AOA and AOB dictates what extent the release of NO and HONO takes place from the soil. This is because the presence of microbial communities like AOA strives for NO as a co-reactant for NH_2OH oxidation, where this could also lead to differences in HONO production (Ermel et al., 2018; Mushinski et al., 2019).

Denitrification occurs under anaerobic conditions, where the stepwise reduction of NO_3^- into N_2 occurs and NO, N_2O are produced as transient intermediates (**Figure 1.1, 1.4**). Nitrate is first reduced to NO_2^- by nitrate reductase. Subsequently, NO_2^- is reduced to NO through the action of nitrite reductase (**Figure 1.4**). Under fluctuating oxygen conditions, where both the anaerobic and aerobic microsites coexist, partial reduction of NO_2^- can lead to HONO formation (**Figure 1.4**). This pathway is particularly active in soils with high water-filled pore space (WFPS), where oxygen diffusion is limited, but occasional oxygen pulses promote nitrifier-denitrifier interactions (Mosier, 2008). In such environments, denitrifiers lacking the nitrous oxide reductase (NOS) enzyme may release higher amounts of N_2O and NO (**Figure 1.4**). This produced NO can partition to the atmosphere and in the presence of OH radical, yields HONO (**Figure 1.1**) (Bhattarai et al., 2021; Butterbach-Bahl et al., 2013).

Despite growing evidence for the importance of biological pathways in HONO emissions, knowledge gaps remain. The microbial community composition, enzyme expression of microbes, N availability, and environmental factors shape the release of NO_x, HONO, and N_2O. Factors like soil pH, moisture, temperature, and nitrogen availability govern the release and abundance of these gases (Pilegaard, 2013; Wang et al., 2021; Wu et al., 2019).

1.6 Influence of abiotic factors on biologically and chemically mediated N_r and GHGs release from the soil

The release of N_r gases and GHGs from soil is governed not only by biological processes but also by a range of abiotic factors that regulate gas production, transformation, and emission. Abiotic

mechanisms shape the environmental conditions under which microbial processes occur and directly drive some of the chemical reactions responsible for gas fluxes at the soil-atmosphere interface. Factors like soil temperature, moisture, pH, redox potential, and mineral composition play critical roles in determining the rates and magnitudes of N_r and GHG emissions (Pilegaard, 2013). Here, the physical and chemical impacts of each abiotic factor will be discussed first, followed by their linkages to biotic systems.

Soil temperature is an important abiotic factor that can influence gas emissions directly by affecting the physical properties of the soil, such as gas diffusivity. Diffusion is the random movement of gas particles in the direction of the concentration gradient (Stępniewski et al., 2011). Larger pores allow more rapid movement of gases than smaller pores; thus, more gas diffusion occurs from soil macropores to the atmosphere. Under steady state, exchange of gases is rapid from the soil, where it is governed by Fick's first law (**Eq. 1**) (Bakker & Hidding, 1970; Stępniewski et al., 2011; Villarreal et al., 2019).

$$F_g = -D\frac{dc}{dx} \qquad \text{(Equation 1)}$$

Where F_g is gas flux density (g m^{-2} s^{-1}), D is the diffusion coefficient (m^2 s^{-1}), $\frac{dc}{dx}$ is the concentration gradient of gas.

Temperature affects the diffusion coefficient, D term, and therefore, as temperature increases, the gas particles collide rapidly, increasing the rate of diffusion. A rise or fall in temperature can also promote the adsorption/desorption. At lower temperatures, adsorption is favoured, whereas at higher temperatures it leads to desorption (**R7**) (Villarreal et al., 2019). The solubility of gases like NH_3, N_2O, and NO decreases with increasing temperature following Henry's law, leading to volatilization of these gases from the soil. For instance, under alkaline conditions, the NH_4^+/NH_3 equilibrium is a prime example of temperature rise, yielding gaseous NH_3. These temperature-induced changes also interact with other abiotic factors like moisture and pH of the soil.

Soil moisture governs the balance between aerobic and anaerobic microbial processes, shaping the pathways for N_r and GHG production. The presence of water can lead to solubilization of gaseous analytes, creating aqueous pathways of transformation favourable, whereas drying enhances the gas phase emissions (Singh et al., 2023). The proportion of WFPS determines oxygen availability in the soil matrix, influencing the prevalence of nitrification versus denitrification (Smith et al.,

2018). Dryness can limit the extent to which gas diffusion takes place. Upon rewetting, the sudden availability of water triggers a burst of microbial activity, stimulating rapid mineralization of organic nitrogen, leading to a release of NH_4^+ and NO_3^- in the soil. Not only that, but soil pH also influences abiotic chemical reactions responsible for gas fluxes. For example, to kick-start the nitrification cycle, the presence of alkaline conditions is needed. Acidic conditions enhance the protonation of NO_2^-, leading to increased HONO emissions (**R6**) (Su et al., 2011). Soil pH is interconnected to redox potential. Under sufficient O_2 (oxic conditions), high soil redox potential (i.e., oxidizing conditions) promotes nitrification and CO_2 production through aerobic respiration (Wu et al., 2019; Zhang et al., 2020).

Mineral composition of soil also plays a crucial role, and a recent study has shown that gases like HONO are released based on the soil composition (Zhu et al., 2021). Zhu et al. (2021) showcases that soil-atmospheric exchange of HONO is not solely dependent on the pH, Henry's law and aqueous N availability but also on amphoteric clay minerals. Evidence suggests that proton transfer reactions that take place on clay mineral surfaces promote the release of HONO from soils that have a neutral pH, despite the pKa of HONO being ~3 (Donaldson et al., 2014a, 2014b; Zhu et al., 2021). Soils consist of iron (hydro)oxides, which can initiate redox reactions of NO_2 (Kebede et al., 2016). To what extent NO_2 is reduced by ferrous iron dictates the outgas of HONO or retention of nitrite in the soil (Kebede et al., 2016). Redox properties of soil organic matter have also been attributed to the presence of quinone moieties (Scharko et al., 2017). Quinones are a class of aromatic compounds that readily transition between three oxidation states (benzoquinone, semiquinone, and hydroquinone) depending on redox conditions. Soil organic matter can reduce NO_2 via the semiquinone or hydroquinone species, enabling it to facilitate NO_2-to-HONO conversion (Scharko et al., 2017).

Many of the above-mentioned abiotic factors, such as soil temperature, moisture, and redox potential, affect biotic processes. Rise in soil temperature reduces the solubility of gases in water while increasing the enzyme efficiency, thereby enhancing microbial activity and increasing soil respiration rates. The temperature-driven effect works in tandem with soil moisture dynamics, which regulate oxygen availability. At low WFPS (≤ 60%), oxygen diffusion is high, promoting nitrification and leading to greater emissions of NO and HONO. At intermediate WFPS (60-80%), denitrification begins to dominate, resulting in increased N_2O production. At high WFPS (> 80%),

complete denitrification occurs, reducing N_2O to N_2 (Butterbach-Bahl et al., 2013). Nitrification, driven by ammonia-oxidizing bacteria (AOB) and archaea (AOA), is most efficient in neutral to slightly alkaline soils (pH 6.5–8.0), where optimal enzyme activity promotes the oxidation of NH_4^+ to NO_3^- (**Figure 1.4**). Alkaline soils favour the volatilization of NH_3, increasing atmospheric nitrogen loss (Schlesinger & Hartley, 1992). This is intertwined with soil redox potential, where the release of gases is based on the availability of electron acceptors and donors (Wu et al., 2019; Zhang et al., 2020). Redox-driven chemical transformations thus contribute to episodic release of N_r from the soil depending on the oxygen conditions (Oswald et al., 2013; Wu et al., 2019). These variables are dynamic in the real-world environment and could be linked with one another, making flux measurements at the soil-atmosphere interphase change over time in response to these abiotic and interlinked biotic drivers. Thus, effective flux measurement techniques are required to capture these in real-time to derive realistic representations in models that attempt to mechanistically couple surface-atmosphere processes.

1.7 Overview of flux measurement techniques

To understand the exchange of gases at environmental interfaces, fluxes are measured using various techniques, including micrometeorological methods, remote sensing, chamber techniques, and more. Flux provides meaningful insight into the deposition and/or emission of gases across a specific area over time to understand their drivers and dynamics.

1.7.1 Micrometeorological methods

Quantifying fluxes of atmospheric gases has been most effectively applied to GHGs at the land-atmosphere interface. Traditional measurement methods, such as eddy covariance (EC), relaxed eddy accumulation (REA), and aerodynamic gradient (AG) methods, have been extensively used for large-scale, continuous flux monitoring (Bao et al., 2022; Pape et al., 2009; Wang et al., 2022). These micrometeorological techniques measure concentration gradients and turbulence to estimate fluxes across interfaces for application to ecosystems, offering long-term insights without disrupting natural processes.

Among these, the EC technique stands out as a widely used and direct approach to measure atmosphere fluxes of non-reactive gases at the ecosystem scale (100 m to 1 km) (Baldocchi, 2003). An eddy is a small circular motion of air caused by temperature fluctuations and wind speed

differences caused by drag induced on airflows moving over surfaces. They range in size from centimetres to tens of meters, lasting from fractions of a second to several minutes. Eddy covariance that quantifies the instantaneous covariance between vertical air motion (upward and downward) and the concentration of trace gases within those air parcels above a ground or canopy surface at a suitable height to obtain a sampling footprint representative of the system under study. By measuring air motion to quantify upward or downward eddies and gas concentration rapidly (at least 1-10 times per second; 1-10 Hz) and over extended periods (typically a minimum of 30–60 minutes per flux value determination), the average flux can be calculated and converted to units of gas emitted from the surface or absorbed into it (Baldocchi, 2014; Baldocchi, 2003). The EC method works best under conditions with steady wind and sufficient turbulence; it is not without limitations. For example, eddy covariance can not be used indoors because there is no natural turbulence (i.e. no source of consistent eddies) and therefore no meaningful covariance to measure. Similarly, at night, EC tends to fail because the Earth's surface cools rapidly, resulting in a temperature inversion in the atmospheric boundary layer. This inversion suppresses vertical mixing because cooler, denser air near the surface will not mix upward into warmer, lighter air above it. For soil–atmosphere fluxes, this means that eddy covariance often cannot measure fluxes at night, as turbulence is frequently absent, resulting in roughly 8-12 hours of a diurnal cycle being data gaps. Other flux measurement approaches are required to capture exchange under such conditions.

The total cost of an EC sonic anemometer system is around $50k USD (IPCC, 2023), while associated gas monitoring systems can be over an order of magnitude more expensive. These include high-quality, fast-response instrumentation, like spectroscopic gas analyzers or mass spectrometers, operating at high frequencies, to resolve chemical fluctuations in the turbulent fluxes measured by the sonic anemometer (Baldocchi, 2003; Kamp et al., 2020). Such instruments exist for N_r gases, like NO_x and NO_y, as described in Geddes & Murphy (2014); Karl et al. (2017); Min et al. (2014), and for NH_3 in Moravek et al. (2019), but are challenged by limitations in the extent of speciation that the analyzers can capture and inlet interaction effects, respectively, but also instrument sensitivity (i.e. capacity to resolve small changes in concentration) and range limits where small fluxes and atmospheric abundances are involved.

To overcome the drawbacks of fast analyzers in the EC method, AG flux measurement methods are an alternative, as they only require making concentration measurements at several heights at a lower time resolution on the order of tens of minutes to hours (Kamp et al., 2020; Laufs et al., 2017). The aerodynamic gradient method utilizes only the vertical concentration gradient (assumes horizontal concentration gradient is negligible) and turbulent diffusivity to determine the vertical gas flux over a surface (Kamp et al., 2020). It is cost-effective and relevant for species like NH_3, for which currently no fast analyzers are available (Kamp et al., 2020). In addition to the EC and AG methods, the REA technique provides another alternative for flux measurement, a technique recently developed for HONO (Ren et al., 2011; Von Der Heyden et al., 2022). The REA method avoids the need for fast-response (≥ 10 Hz) chemical instrumentation by segregating air from updrafts and downdrafts into separate reservoirs, as triggered by a sonic anemometer. Over a predefined period, these reservoirs collect air samples, which are subsequently analyzed by a lower time resolution instrument to determine trace gas concentrations. REA separates the airflow into two sampling lines depending on the sign of the vertical wind velocity (updraft or downdraft), as determined by a sonic anemometer. Fluxes are then calculated using the measured concentration differences (Grelle & Keck, 2021). While REA offers a cost-effective and energy-efficient alternative, it relies on separating upward and downward-moving air under outdoor conditions. Its accuracy depends on turbulence intensity and the capacity to collect the target gases efficiently (Baldocchi, 2003; Kamp et al., 2020).

Unlike EC and REA, which rely on turbulent eddies to transport gases to the measurement height, dynamic chambers create their own controlled air parcel to isolate fluxes directly over the soil surface. This removes the dependence of the measurement technique on the presence of ambient turbulence. The chamber method also addresses the temporal resolution, sensitivity, and detection limit issues of chemical analyzers, as fluxes are accumulated and measured within an enclosed headspace over a defined period. Compared to micrometeorological techniques, chamber methods are relatively inexpensive, easy to deploy and require minimal prior meteorological training and expertise (Tang et al., 2020). Chamber methods can take two forms: static and dynamic. Each has strengths and weaknesses, which depend on analyte properties and atmospheric composition.

1.7.2 The chamber method for N_r flux measurements

The chamber method is a widely used technique for measuring GHG fluxes, especially for N_2O. However, its application for studying the N_r exchange at the soil-atmosphere interface remains less common. Chambers creates a controlled environment for monitoring changes in gas concentration over time, making them useful in settings where micrometeorological techniques may not be feasible when working with reactive N species and small-scale field or heterogeneous plots (Kelsch et al., 2025; Zaman et al., 2011). Chamber methods are particularly well-suited for laboratory-based studies as they are small, lightweight, easily transported and relatively inexpensive (Aneja et al., 2006; Pavelka et al., 2018). Chambers can be of two types: static and dynamic.

Static chambers are chamber that encloses a defined volume of air for a specific continuous period during which an increase or decrease in gas concentration is measured with an analyzer, or a gas sample is collected from the headspace and subject to gas chromatography analysis (Oertel et al., 2016). Static chambers are relatively simple to use; however, they can alter the surface environment over which they are placed, leading to inaccuracies in flux estimates by impacting the temperature, humidity, and gas composition (Pape et al., 2009). This means they can only be installed on a soil collar for a short period before the measured fluxes diverge from their true value under a given set of environmental conditions. This prevents fluxes from being continuously monitored over periods of days to years using such a chamber technique. Prior reports have indicated that static chambers could underestimate CO_2 fluxes by 10-50% in comparison to a dynamic chamber (Norman et al., 1997; Pumpanen et al., 2004; Yu et al., 2013). As this example shows, the dynamic soil-flux chamber overcomes many of the drawbacks of the static chamber and can provide a more accurate and reliable measurement of trace gas exchange fluxes.

The basic principle of using a dynamic chamber system is that it involves flow through the chamber-enclosed surface with ambient air and assumes the measured change in trace gas concentrations inside over time will be greater than those found ambiently, such that fluxes may be inferred. These chambers are typically made of transparent or translucent materials to allow natural light to penetrate, allowing photolytic reaction to occur inside the enclosure. Atmospheric or clean air is continuously added to the headspace of the dynamic chamber, ensuring that environmental conditions remain nearly constant and representative of ambient conditions. During

the measurement period, the chamber is closed, allowing trace gas exchange to occur between the surface and the chamber headspace. Air from the chamber headspace is continuously sampled and analyzed to measure trace gas concentrations. This method has been well established to measure the exchange fluxes of biogenic volatile organic compounds (BVOCs, such as monoterpenes and isoprene) from vegetation and farmland (Kolari et al., 2012; Mochizuki et al., 2018), NH_3 volatilization from cattle manure (Becciolini et al., 2024) and CO_2 fluxes from grasslands (Pape et al., 2009). However, none of these studies have measured the entire suite of N_r that are NO, NO_2, HONO, NH_3 alongside GHGs like N_2O. Only a few studies have used dynamic chambers with minor modifications to measure emissions of gases such as NO, NO_2 and NH_3 (Maggiotto et al., 2000; Pape et al., 2009). Scharko et al. (2015) have shown HONO fluxes from agricultural soils, and Tang et al. (2019) have highlighted both HONO and NO_x fluxes from a farmland. Overall, a dynamic chamber is the best tool to measure N_r flux in a controlled lab setting, providing direct measurements of trace gases from surfaces like soil. It offers a versatile platform for capturing the magnitude, direction, and temporal variability of N_r species. Thus, establishing a validated method for flux measurements is important in assessing surface-atmosphere exchange processes without requiring a complex micrometeorological measurement technique.

1.8 Challenges in measuring N_r fluxes

Non-destructive methods for GHGs like N_2O allow easier flux measurements using spectroscopic techniques because there is no chemical transformation of the analyte (Harris et al., 2020; Rapson & Dacres, 2014). Air is circulated through the analyzer continuously without the need for dilution air and returned into the chamber without altering the sample composition (Stockwell et al., 2018). In contrast, measurements of N_r often require destructive analytical techniques. One of the primary challenges stems from the inherent reactivity and short atmospheric lifetimes of some N_r gases, like NO_x. These gases may be prone to rapid chemical transformations and interactions with other atmospheric constituents, or by interacting with sampling inlet surfaces, making it difficult to capture their true concentrations and fluxes accurately (Seinfeld & Pandis, 1998).

The limitation of using fast-response analyzers to measure NH_3, for example, is the instrument response, which is affected by surface adsorption. It is well-known that adsorption and desorption of NH_3 to and from surfaces, including inlet tubing and fittings, can be notable, leading to delayed signal response and measurement biases (Moravek et al., 2019). There are limited studies that

report simultaneous measurements of NO, NO_2, and HONO. Measurements of NO are well established by chemiluminescence detection (CLD), and it is a widely used technique (Bates, 1992; Kley & McFarland, 1980; Maeda et al., 1980). The gas analyzers required for this measurement are destructive, meaning that dynamic chambers require replacement of the headspace gas with ambient or clean air. For the former approach, this requires ambient NO concentrations not to be rapidly changing during the period of the dynamic chamber closure. In the latter, if the headspace becomes too clean, it may perturb the system from environmental conditions, resulting in inaccurate flux determinations. Past studies have measured NO_2^* (the sum of NO_2 and acidic species like HONO and HNO_3) using passive samplers (Spicer et al., 2001). The same issue extends to the measurement of NO_2 and HONO, as these are also typically measured destructively using CLD. The CLD method provides measurements of NO and NO_y that are used to provide estimates of NO_2 and NO_x (Worton, 2020). Given the difficulty in predicting NO_x, HONO adds another layer of uncertainty due to its surface reactivity and photolabile characteristic, thus requiring accurate and precise detection methods. This characteristic of HONO adsorption/desorption on surfaces leads to uncertainty in detecting not only HONO but also NO_2. Nitrous acid can be formed easily through heterogeneous reactions on wet surfaces like inlet lines, a positive artifact, and within inlet lines, it can undergo wall interactions, leading to a negative artifact (Crilley et al., 2019).

Another challenge is the spatial and temporal variability in N_r exchange processes, as fluxes are influenced by dynamic environmental conditions like soil temperature, moisture, and water content, as well as atmospheric composition, temperature, and relative humidity (Butterbach-Bahl et al., 2013). For instance, soil moisture and temperature fluctuations can influence the rates of nitrification and denitrification, leading to diurnal and seasonal variations in N_2O and NO_x emissions (Davidson et al., 2002). Capturing these variations requires not only precise sampling techniques but also simultaneous monitoring of environmental parameters using specialized sensors and probes. These considerations underscore the importance of selecting appropriate methods and tools, such as dynamic chambers or micrometeorological techniques, to ensure reliable and meaningful measurements of N_r fluxes.

To address these challenges, this thesis focuses on the use of dynamic chamber systems integrated with a suite of destructive gas analyzers, which are particularly well-suited for measuring localized

N_r fluxes. These are applied toward understanding exchange processes at the ground surface-atmosphere interface for agricultural soils, as they are expected to be N_r exchange hotspots. In particular, the dynamic chamber approach will be used in this work to address divergent findings from the literature related to N_r exchange, as such approaches have been widely used in lab studies to suggest that such soils are strong sources of HONO, while the very limited number of field measurements tend to disagree by orders of magnitude.

1.9 The lab-field discrepancy in soil HONO release

A major discrepancy exists between laboratory and field measurements of soil HONO production, where lab fluxes are orders of magnitude higher, raising questions about the underlying mechanisms and influencing factors for emissions being relevantly reproduced in the lab (J. Chen et al., 2023). The lack of HONO measurements from fields under normal use influences the predicted impact it has on atmospheric oxidation capacity, and also is likely to provide a misleading diagnosis for O_3 production when lab-generated rates are used under the assumption that they are reliable proxies (Liu et al., 2023; Xue et al., 2024) (**Figure 1.2**).

In previous studies, significant HONO emissions were estimated from soil samples that reached up to 3000 ng m^{-2} s^{-1} by Su et al. (2011), but were more typically on the order of 340 ng m^{-2} s^{-1} reported by Wang et al. (2021), 250 ng m^{-2} s^{-1} by Oswald et al. (2013) and 200 ng m^{-2} s^{-1} by Meusel et al. (2018). In the case of Su et al. (2011), they adjusted the soil to a pH by adding dilute HCl, in addition to adding $NaNO_2$ solution to the soil sample, which effectively replicates our well-established HONO calibration source (Lao et al., 2020; Roberts et al., 2010). Wang et al. (2021), Oswald et al. (2013) and Meusel et al. (2018) all have aggressively dried small amounts (~7-15.5 g) of their soils using a dry zero air rapidly flushing chamber headspace. These sampling disturbances need to be taken into account, as lab studies use homogenized, sieved, aggressively dried and pre-conditioned soils, which can alter microbial processes and gas fluxes compared to undisturbed field conditions.

In contrast, field measurements retain soils intact and are subject to natural variations in soil properties, microbial activity, and meteorological conditions, which can alter HONO emissions in ways that are supposedly difficult to reproduce in the lab (Song et al., 2023a; Tang et al., 2019). To date, field studies that represent direct comparable field measurement for HONO under ambient conditions have reported fluxes to be ≤2.5 ng m^{-2} s^{-1}, that is, around two orders of magnitude less

than the lab studies (Laufs et al., 2017; Ren et al., 2011; Sörgel et al., 2011; Tang et al., 2020). In real-world environments, the presence of vegetation further complicates the dynamics by altering soil chemistry and gas exchange processes, making it crucial to consider plant–soil–atmosphere interactions when interpreting the release of HONO (Laufs et al., 2017; Schimang et al., 2006). But these complex interactions are even more difficult to simulate realistically in laboratory settings.

The soil NO to HONO ratio gives a value to compare lab-based results to the field data. Laboratory experiments that are typically conducted at controlled soil moisture, temperature, and headspace humidity to isolate specific variables from uncontrolled environmental fluctuations have reported on a similar order of NO emissions as field studies (Bao et al., 2022; Scharko et al., 2015; Wu, Deng, Liu, Xi, Zou, Sha, et al., 2020). However, this study is the first to note the overestimation of HONO relative to NO in a lab setting. When the HONO emission potential curve is misrepresented, that is, when the measured HONO is high in the lab versus low under real soil conditions, then the NO/HONO ratio derived from lab settings will be low compared to field work. This leads to a critical issue when global models use this lab-derived ratio to estimate HONO based on simulated NO emissions. Lab studies have reported the maximum emission potential of the NO to HONO ratio to be below one (Oswald et al., 2013; Wang et al., 2021; Wu et al., 2019). Whereas field measurements ranged from 4.5 up to more than 100 (like the one in this study) (Meng et al., 2024; Tang et al., 2019). These discrepancies highlight the need for improved measurement techniques and standardized protocols to ensure comparability between lab and field studies. By bridging the gap between laboratory and field studies, more reliable estimates of soil-derived HONO and its contribution to atmospheric chemical processes can be derived. This will ultimately enhance our ability to predict and mitigate the environmental impacts of N_r species.

2.0 Thesis objectives

The main objective of this thesis was to develop a dynamic chamber system for the first time to measure a comprehensive suite of N_r fluxes by leveraging modifications on a commercially available chamber for GHG fluxes. This work aims to address a critical gap in the atmospheric chemistry community by providing an in-house and field-deployable in situ measurement system tailored for the investigation of soil-atmospheric exchange processes. The design rationale,

instrumentation integrated with the chambers, and the necessary hardware modifications are comprehensively presented.

To achieve the overarching aim, the study is guided by the following specific objectives:

- Develop and modify commercially available Eosense chambers for in-situ and field soil N_r flux measurements.
- Assess the spatial variability of N_r fluxes, particularly for NO, NO_2, and HONO, from soil collected throughout a managed agricultural field.
- Evaluate the impact of a variety of fertilizer treatments on the magnitude and variability of NO, NO_2, HONO, NH_3 and N_2O fluxes.

These are pursued in the following three thesis chapters and address key aspects of these research goals.

Chapter 2:

This chapter presents the development of a dynamic chamber system for measuring N_r fluxes by modifying commercially available GHG chambers. It describes the necessary hardware modifications to optimize the transfer of N_r species like NO_2, HONO, NH_3 and O_3 while minimizing gas losses. To validate the system, proof-of-concept measurements from agricultural soil are conducted under controlled laboratory conditions. The performance of the modified chamber system is also assessed for its suitability for field deployment, using an in-situ fertilization experiment to demonstrate the contributions of flux terms that exist for reactive gases and the necessity of the reference chamber for their reliability.

Chapter 3:

This chapter assesses N_r flux heterogeneity from randomly gridded soil samples collected across an in-use agricultural field under controlled lab conditions. It particularly characterizes NO, NO_2 and HONO emissions to investigate the spatial variability of fluxes for each species and between them. It investigates whether NO, NO_2 and HONO fluxes remain homogeneous across field samples, where comparable results would indicate that a typical pooled sample would generate consistent N_r fluxes for application at the landscape scale, for example, in an atmospheric chemistry model. Careful attention was given to the design of soil preparation across all samples to ensure comparability of results across the samples while preserving the soil properties. By avoiding practices like aggressive drying, grinding, and the addition of artificial reagents, we aim

to ensure that our samples remain comparable not only to each other but to soils as they exist in the field.

Chapter 4:

In this chapter, we quantify the effects of different nitrogen fertilizers on N_r fluxes by comparing emissions from soils treated with conventional fertilizers like urea versus mechanochemically synthesized magnesium and zinc ammonium carbonate double salts. The study evaluates gaseous emissions of NO, NO_2, HONO, NH_3, and N_2O following the application of these fertilizers, with the amount of total nitrogen volatilized from these double salts.

Chapter 5:

This chapter of the thesis concludes by showcasing the variability of soil N_r emissions with and without fertilizer using the dynamic chamber system. Laboratory experiments confirmed that emissions were heterogeneous even within soils collected from the same field. Experiments using double salt provided further insight into the specifics of the reactive nitrogen species release from the soil. These combined findings contribute to a better understanding of soil nitrogen dynamics. Incorporating this knowledge into modelling frameworks can increase the precision of nitrogen flux estimations at broader regional scales.

2.1 References:

Aneja, V. P., Blunden, J., Claiborn, C. S., & Rogers, H. H. (2006). Dynamic Chamber System to Measure Gaseous Compounds Emissions and Atmospheric-Biospheric Interactions. *Environmental Simulation Chambers: Application to Atmospheric Chemical Processes*, 97–109. https://doi.org/10.1007/1-4020-4232-9_7

Aroskay, A., Martin, E., Bekki, S., Pennec, J.-L. Le, Sarvarino, J., & Temel, A. (2023). Geological evidence of extensive N- fixation by volcanic lightning during very large explosive eruptions. *Proceedings of the National Academy of Sciences*, *120*(2023). https://doi.org/10.1073/pnas

Bakker, J. W., & Hidding, A. P. (1970). *The influence of soil structure and air content on gas diffusion in soils* (Vol. 18).

Baldocchi. (2003). Assessing the eddy covariance technique for evaluating carbon dioxide exchange rates of ecosystems: Past, present and future. *Global Change Biology*, *9*(4), 479–492. https://doi.org/10.1046/j.1365-2486.2003.00629.x

Baldocchi, D. (2014). Measuring fluxes of trace gases and energy between ecosystems and the atmosphere - the state and future of the eddy covariance method. *Global Change Biology*, *20*(12), 3600–3609. https://doi.org/10.1111/gcb.12649

Baldocchi, D. D. (2003). Assessing the Eddy Covariance Technique for Evaluating the Carbon Balance of Ecosystems. *Global Change Biology*, *9*(November 2002), 1–41.

Bao, F., Cheng, Y., Kuhn, U., Li, G., Wang, W., Kratz, A. M., Weber, J., Weber, B., Pöschl, U., & Su, H. (2022). Key Role of Equilibrium HONO Concentration over Soil in Quantifying Soil–Atmosphere HONO Fluxes. *Environmental Science & Technology*. https://doi.org/10.1021/acs.est.1c06716

Baron, J. S., Hall, E. K., Nolan, B. T., Finlay, J. C., Bernhardt, E. S., Harrison, J. A., Chan, F., & Boyer, E. W. (2013). The interactive effects of excess reactive nitrogen and climate change on aquatic ecosystems and water resources of the United States. *Biogeochemistry*, *114*(1–3), 71–92. https://doi.org/10.1007/s10533-012-9788-y

Bates, J. N. (1992). Nitric Oxide Measurement by Chemiluminescence Detection. In *A Companion to Methods in Neurosciences* (Vol. 1, Issue 2).

Becciolini, V., Leso, L., Fuertes Gimeno, E., Rossi, G., Barbari, M., Dalla Marta, A., Orlandini, S., & Verdi, L. (2024). Nitrogen loss abatement from dairy cow excreta through urine and faeces separation: The effect of temperature and exposure period on NH3 fluxes. *Agricultural Systems*, *216*. https://doi.org/10.1016/j.agsy.2024.103898

Benedict, K. B., Prenni, A. J., Carrico, C. M., Sullivan, A. P., Schichtel, B. A., & Collett, J. L. (2017). Enhanced concentrations of reactive nitrogen species in wildfire smoke. *Atmospheric Environment*, *148*, 8–15. https://doi.org/10.1016/j.atmosenv.2016.10.030

Bhattarai, H. R., Wanek, W., Siljanen, H. M. P., Ronkainen, J. G., Liimatainen, M., Hu, Y., Nykänen, H., Biasi, C., & Maljanen, M. (2021). Denitrification is the major nitrous acid production pathway in boreal agricultural soils. *Communications Earth & Environment*, *2*(1), 1–10. https://doi.org/10.1038/s43247-021-00125-7

Brownwood, B., Turdziladze, A., Hohaus, T., Wu, R., Mentel, T. F., Carlsson, P. T. M., Tsiligiannis, E., Hallquist, M., Andres, S., Hantschke, L., Reimer, D., Rohrer, F., Tillmann, R., Winter, B., Liebmann, J., Brown, S. S., Kiendler-Scharr, A., Novelli, A., Fuchs, H., & Fry, J. L. (2021). Gas-Particle Partitioning and SOA Yields of Organonitrate Products from NO3-Initiated Oxidation of Isoprene under Varied Chemical Regimes. *ACS Earth and Space Chemistry*, *5*(4), 785–800. https://doi.org/10.1021/acsearthspacechem.0c00311

Brümmer, C., Rüffer, J. J., Delorme, J. P., Wintjen, P., Schrader, F., Beudert, B., Schaap, M., & Ammann, C. (2022). Reactive nitrogen fluxes over peatland and forest ecosystems using micrometeorological measurement techniques. *Earth System Science Data*, *14*(2), 743–761. https://doi.org/10.5194/essd-14-743-2022

Butterbach-Bahl, K., Baggs, E. M., Dannenmann, M., Kiese, R., & Zechmeister-Boltenstern, S. (2013). Nitrous oxide emissions from soils: How well do we understand the processes and their controls? *Philosophical Transactions of the Royal Society B: Biological Sciences*, *368*(1621). https://doi.org/10.1098/rstb.2013.0122

Butterbach-Bahl, K., & Dannenmann, M. (2011). Denitrification and associated soil N2O emissions due to agricultural activities in a changing climate. *Current Opinion in Environmental Sustainability*, *3*(5), 389–395. https://doi.org/10.1016/j.cosust.2011.08.004

Caranto, J. D., & Lancaster, K. M. (2017). Nitric oxide is an obligate bacterial nitrification intermediate produced by hydroxylamine oxidoreductase. *Proceedings of the National Academy of Sciences of the United States of America*, *114*(31), 8217–8222. https://doi.org/10.1073/pnas.1704504114

Chen, J., Zhang, Y., Kuzyakov, Y., Wang, D., & Olesen, J. E. (2023). Challenges in upscaling laboratory studies to ecosystems in soil microbiology research. *Global Change Biology*, *29*(3), 569–574. https://doi.org/10.1111/gcb.16537

Chen, X., Shan, X., Shi, Z., Zhang, J., Qin, Z., Xiang, H., & Wei, H. (2021). Analysis of the Spatio-temporal Changes in Acid Rain and Their Causes in China (1998-2018). *Journal of Resources and Ecology*, *12*(5), 593–599. https://doi.org/10.5814/j.issn.1674-764x.2021.05.002

Contamine, D., Martin, E., Aroskay, A., Bekki, S., & Szopa, S. (2024). Nitrates production by volcanic lightning during explosive eruptions. EGU24-13523. https://doi.org/10.7185/gold2023.19942

Crilley, L. R., Kramer, L. J., Ouyang, B., Duan, J., Zhang, W., Tong, S., Ge, M., Tang, K., Qin, M., Xe, P., Shaw, M. D., Lewis, A. C., Mehra, A., Bannan, T. J., Worrall, S. D., Priestley, M., Bacak, A., Coe, H., Allan, J., … Bloss, W. J. (2019). *Intercomparison of nitrous acid*

(HONO) measurement techniques in a megacity (Beijing). https://doi.org/10.5194/amt-2019-139

Davidson, E. A., Savage, K., Verchot, L. V., & Navarro, R. (2002). Minimizing artifacts and biases in chamber-based measurements of soil respiration. *Agricultural and Forest Meteorology*, *113*(1–4), 21–37. https://doi.org/10.1016/S0168-1923(02)00100-4

Degaspari, I. A. M., Soares, J. R., Montezano, Z. F., Del Grosso, S. J., Vitti, A. C., Rossetto, R., & Cantarella, H. (2020). Nitrogen sources and application rates affect emissions of N2O and NH3 in sugarcane. *Nutrient Cycling in Agroecosystems*, *116*(3), 329–344. https://doi.org/10.1007/s10705-019-10045-w

Delaria, E. R., & Cohen, R. C. (2023). Measurements of Atmosphere-Biosphere Exchange of Oxidized Nitrogen and Implications for the Chemistry of Atmospheric NOx. *Accounts of Chemical Research*, *56*(13), 1720–1730. https://doi.org/10.1021/acs.accounts.3c00090

Donaldson, M. A., Berke, A. E., & Raff, J. D. (2014). Uptake of gas phase nitrous acid onto boundary layer soil surfaces. *Environmental Science and Technology*, *48*(1), 375–383. https://doi.org/10.1021/es404156a

Donaldson, M. A., Bish, D. L., & Raff, J. D. (2014). Soil surface acidity plays a determining role in the atmospheric-terrestrial exchange of nitrous acid. *Proceedings of the National Academy of Sciences of the United States of America*, *111*(52), 18472–18477. https://doi.org/10.1073/pnas.1418545112

Ermel, M., Behrendt, T., Oswald, R., Derstroff, B., Wu, D., Hohlmann, S., Stönner, C., Pommerening-Röser, A., Könneke, M., Williams, J., Meixner, F. X., Andreae, M. O., Trebs, I., & Sörgel, M. (2018). Hydroxylamine released by nitrifying microorganisms is a precursor for HONO emission from drying soils. *Scientific Reports*, *8*(1), 1–8. https://doi.org/10.1038/s41598-018-20170-1

Finlayson-Pitts, B. J., & Pitts, J. N. (2000). Rates and Mechanisms of Gas-Phase Reactions in Irradiated Organic – NOx – Air Mixtures. In *Chemistry of the Upper and Lower Atmosphere* (pp. 179–263). Academic Press. https://doi.org/10.1016/B978-012257060-5/50008-3

Fowler, D., Coyle, M., Skiba, U., Sutton, M. A., Cape, J. N., Reis, S., Sheppard, L. J., Jenkins, A., Grizzetti, B., Galloway, J. N., Vitousek, P., Leach, A., Bouwman, A. F., Butterbach-Bahl, K., Dentener, F., Stevenson, D., Amann, M., & Voss, M. (2013). The global nitrogen cycle in the twenty-first century. *Philosophical Transactions of the Royal Society B: Biological Sciences*, *368*(1621). https://doi.org/10.1098/rstb.2013.0164

Galloway, J. N., Dentener, F. J., Capone, D. G., Boyer, E. W., Howarth, R. W., Seitzinger, S. P., Asner, G. P., Cleveland, C. C., Green, P. A., Holland, E. A., Karl, D. M., Michaels, A. F., Porter, J. H., Townsend, A. R., Vo¨ro¨smarty, C. J., Vo¨ro, V., & Vo¨ro¨smarty, V. (2004). Nitrogen cycles: past, present, and future. In *Biogeochemistry* (Vol. 70, Issue 2). papers://aa15ed4a-8b41-4036-84a6-41087bba0cd6/Paper/p3387

Galloway, J. N., Townsend, A. R., Erisman, J. W., Bekunda, M., Cai, Z., Freney, J. R., Martinelli, L. A., Seitzinger, S. P., & Sutton, M. A. (2008). Transformation of the nitrogen cycle: Recent trends, questions, and potential solutions. *Science*, *320*(5878), 889–892. https://doi.org/10.1126/science.1136674

Geddes, J. A., & Murphy, J. G. (2014). Observations of reactive nitrogen oxide fluxes by eddy covariance above two midlatitude North American mixed hardwood forests. *Atmospheric Chemistry and Physics*, *14*(6), 2939–2957. https://doi.org/10.5194/acp-14-2939-2014

Gong, C., Wang, Y., Tian, H., Kou-Giesbrecht, S., Vuichard, N., & Zaehle, S. (2025). Uncertainties in fertilizer-induced emissions of soil nitrogen oxide and the associated impacts on ground-level ozone and methane. *EGUsphere*. https://doi.org/10.5194/egusphere-2025-1416

Grelle, A., & Keck, H. (2021). Affordable relaxed eddy accumulation system to measure fluxes of H2O, CO2, CH4 and N2O from ecosystems. *Agricultural and Forest Meteorology*, *307*(June), 108514. https://doi.org/10.1016/j.agrformet.2021.108514

Gruber, N., & Galloway, J. N. (2008). An Earth-system perspective of the global nitrogen cycle. *Nature*, *451*(7176), 293–296. https://doi.org/10.1038/nature06592

Hallward-Driemeier, A. H., Hall, J. R., Spence, K. A., Telicki, B. P., Schaeffer, A. F., Avila, J. C., Albores, I. S., & Carrasquillo, A. J. (2024). Secondary Organic Aerosol Formation and Chemistry from the OH-Initiated Oxidation of Monofunctional C10 Species. *ACS Earth and Space Chemistry*, *8*(5), 907–919. https://doi.org/10.1021/acsearthspacechem.3c00180

Harris, S. J., Liisberg, J., Xia, L., Wei, J., Zeyer, K., Yu, L., Barthel, M., Wolf, B., Kelly, B. F. J., Cendón, D. I., Blunier, T., Six, J., & Mohn, J. (2020). N2O isotopocule measurements using laser spectroscopy: Analyzer characterization and intercomparison. *Atmospheric Measurement Techniques*, *13*(5), 2797–2831. https://doi.org/10.5194/amt-13-2797-2020

He, Y., Zhou, X., Hou, J., Gao, H., & Bertman, S. B. (2006). Importance of dew in controlling the air-surface exchange of HONO in rural forested environments. *Geophysical Research Letters*, *33*(2). https://doi.org/10.1029/2005GL024348

Huang, L., Fang, J., Liao, J., Yarwood, G., Chen, H., Wang, Y., & Li, L. (2023). Insights into soil NO emissions and the contribution to surface ozone formation in China. *Atmospheric Chemistry and Physics*, *23*(23), 14919–14932. https://doi.org/10.5194/acp-23-14919-2023

IPCC. (2023). Climate Change 2021- The Physical Science Basis. *Cambridge University Press*. https://doi.org/https://doi.org/10.1017/9781009157896

Jenkins, J. M., & Brune, W. H. (2025). Spatially separate production of hydrogen oxides and nitric oxide in lightning. *Atmospheric Chemistry and Physics*, *25*(9), 5041–5052. https://doi.org/10.5194/acp-25-5041-2025

Kamp, J. N., Häni, C., Nyord, T., Feilberg, A., & Sørensen, L. L. (2020). The aerodynamic gradient method: Implications of non-simultaneous measurements at alternating heights. *Atmosphere*, *11*(10). https://doi.org/10.3390/atmos11101067

Karl, T., Graus, M., Striednig, M., Lamprecht, C., Hammerle, A., Wohlfahrt, G., Held, A., Von Der Heyden, L., Deventer, M. J., Krismer, A., Haun, C., Feichter, R., & Lee, J. (2017). Urban eddy covariance measurements reveal significant missing NO x emissions in Central Europe. *Scientific Reports*, *7*(1). https://doi.org/10.1038/s41598-017-02699-9

Kebede, M. A., Bish, D. L., Losovyj, Y., Engelhard, M. H., & Raff, J. D. (2016). The Role of Iron-Bearing Minerals in NO2 to HONO Conversion on Soil Surfaces. *Environmental Science and Technology*, *50*(16), 8649–8660. https://doi.org/10.1021/acs.est.6b01915

Kelsch, A., Claß, M., & Brüggemann, N. (2025). Accuracy and sensitivity of NH3 measurements using the Dräger Tube method. *Atmospheric Measurement Techniques*, *18*(6), 1519–1535. https://doi.org/10.5194/amt-18-1519-2025

Kinney, P. L. (2018). Interactions of Climate Change, Air Pollution, and Human Health. In *Current environmental health reports* (Vol. 5, Issue 1, pp. 179–186). Springer. https://doi.org/10.1007/s40572-018-0188-x

Kleffmann, J., Gavriloaiei, T., Hofzumahaus, A., Holland, F., Koppmann, R., Rupp, L., Schlosser, E., Siese, M., & Wahner, A. (2005). Daytime formation of nitrous acid: A major source of OH radicals in a forest. *Geophysical Research Letters*, *32*(5), 1–4. https://doi.org/10.1029/2005GL022524

Kley, D. A., & McFarland, M. (1980). *Chemiluminescence detector for NO and NO2* (Vol. 12).

Kolari, P., Bäck, J., Taipale, R., Ruuskanen, T. M., Kajos, M. K., Rinne, J., Kulmala, M., & Hari, P. (2012). Evaluation of accuracy in measurements of VOC emissions with dynamic chamber system. *Atmospheric Environment*, *62*, 344–351. https://doi.org/10.1016/j.atmosenv.2012.08.054

Kool, D. M., Wrage, N., Zechmeister-Boltenstern, S., Pfeffer, M., Brus, D., Oenema, O., & Van Groenigen, J. W. (2010). Nitrifier denitrification can be a source of N2O from soil: A revised approach to the dual-isotope labelling method. *European Journal of Soil Science*, *61*(5), 759–772. https://doi.org/10.1111/j.1365-2389.2010.01270.x

Krichels, A. H., Greene, A. C., Stephens, E. Z., Zhao, S., Schimel, J. P., Aronson, E. L., Hanan, E. J., & Homyak, P. M. (2024). Nitrifier controls on soil NO and N2O emissions in three chaparral ecosystems under contrasting atmospheric N inputs. *Soil Biology and Biochemistry*, *196*(May), 109482. https://doi.org/10.1016/j.soilbio.2024.109482

Lao, M., Crilley, L. R., Salehpoor, L., Furlani, T. C., Bourgeois, I., Andrew Neuman, J., Rollins, A. W., Veres, P. R., Washenfelder, R. A., Womack, C. C., Young, C. J., & VandenBoer, T. C. (2020). A portable, robust, stable, and tunable calibration source for gas-phase nitrous acid (HONO). *Atmospheric Measurement Techniques*, *13*(11), 5873–5890. https://doi.org/10.5194/amt-13-5873-2020

Laufs, S., Cazaunau, M., Stella, P., Kurtenbach, R., Cellier, P., Mellouki, A., Loubet, B., & Kleffmann, J. (2017). Diurnal fluxes of HONO above a crop rotation. *Atmospheric Chemistry and Physics*, *17*(11), 6907–6923. https://doi.org/10.5194/acp-17-6907-2017

Lehnert, N., Musselman, B. W., Seefeldt, L. C., & Gutenberg-university, J. (2021). Grand Challenges in the nitrogen cycle. *Chemical Society Reviews*, *50*, 3640–3646. https://doi.org/10.1039/d0cs00923g

Lin, M., Horowitz, L. W., Hu, L., & Permar, W. (2024). Reactive Nitrogen Partitioning Enhances the Contribution of Canadian Wildfire Plumes to US Ozone Air Quality. *Geophysical Research Letters*, *51*(15). https://doi.org/10.1029/2024GL109369

Lindaas, J., Pollack, I. B., Garofalo, L. A., Pothier, M. A., Farmer, D. K., Kreidenweis, S. M., Campos, T. L., Flocke, F., Weinheimer, A. J., Montzka, D. D., Tyndall, G. S., Palm, B. B., Peng, Q., Thornton, J. A., Permar, W., Wielgasz, C., Hu, L., Ottmar, R. D., Restaino, J. C., … Fischer, E. V. (2021). Emissions of Reactive Nitrogen From Western U.S. Wildfires During Summer 2018. *Journal of Geophysical Research: Atmospheres*, *126*(2), 1–21. https://doi.org/10.1029/2020JD032657

Liu, L., Zhang, X., Xu, W., Liu, X., Lu, X., Wei, J., Li, Y., Yang, Y., Wang, Z., & Wong, A. Y. H. (2020). Reviewing global estimates of surface reactive nitrogen concentration and deposition using satellite retrievals. *Atmospheric Chemistry and Physics*, *20*(14), 8641–8658. https://doi.org/10.5194/acp-20-8641-2020

Liu, Xue, C., Ye, C., Liu, C., Zhang, C., Wang, J., Zhang, Y., & Liu, J. (2023). The Lack of HONO Measurement May Affect the Accurate Diagnosis of Ozone Production Sensitivity. *ACS Environmental Au*, *3*(1), 18–23. https://doi.org/10.1021/acsenvironau.2c00048

Ludwig, J., Meixner, F. X., Vogel, B., & Forstner, J. (2001). Soil-air exchange of nitric oxide: An overview of processes, environmental factors, and modeling studies. *Biogeochemistry*, *52*(3), 225–257. https://doi.org/10.1023/A:1006424330555

Maeda, Y., Aoki, K., & Munemori, M. (1980). Chemiluminescence Method for the Determination of Nitrogen Dioxide. In *Anal. Chem* (Vol. 52). https://pubs.acs.org/sharingguidelines

Maggiotto, S. R., Webb, J. A., & Thurtell, G. W. (2000). Nitrous and Nitrogen Oxide Emissions from Turfgrass Receiving Different Forms of Nitrogen Fertilizer. *American Society of Agronomy, Crop Science Society of America, and Soil Science Society of America*, *29*, 621–630.

Maia, L. B., & Moura, J. J. G. (2014). *How Biology Handles Nitrite*.

Mather, T. A., Pyle, D. M., & Allen, A. G. (2004). Volcanic source for fixed nitrogen in the early Earth's atmosphere. *Geology*, *32*(10), 905–908. https://doi.org/10.1130/G20679.1

Mehta, P. (2010). *Science behind Acid Rain: Analysis of Its Impacts and Advantages on Life and Heritage Structures*. https://www.researchgate.net/publication/265824342

Meng, F., Han, B., Qin, M., Fang, W., Tang, K., Shao, D., Liao, Z., Duan, J., Feng, Y., Huang, Y., Ni, T., & Xie, P. (2024). Measurement report: Surface exchange fluxes of HONO during the growth process of paddy fields in the Huaihe River Basin, China. In *EGUsphere*. https://doi.org/10.5194/egusphere-2024-2127

Meusel, H., Tamm, A., Kuhn, U., Wu, D., Lena Leifke, A., Fiedler, S., Ruckteschler, N., Yordanova, P., Lang-Yona, N., Pöhlker, M., Lelieveld, J., Hoffmann, T., Pöschl, U., Su, H., Weber, B., & Cheng, Y. (2018). Emission of nitrous acid from soil and biological soil crusts represents an important source of HONO in the remote atmosphere in Cyprus. *Atmospheric Chemistry and Physics*, *18*(2), 799–813. https://doi.org/10.5194/acp-18-799-2018

Min, K. E., Pusede, S. E., Browne, E. C., LaFranchi, B. W., & Cohen, R. C. (2014). Eddy covariance fluxes and vertical concentration gradient measurements of NO and NO2 over a ponderosa pine ecosystem: Observational evidence for within-canopy chemical removal of NOx. *Atmospheric Chemistry and Physics*, *14*(11), 5495–5512. https://doi.org/10.5194/acp-14-5495-2014

Mochizuki, T., Amagai, T., & Tani, A. (2018). Effects of soil water content and elevated CO2 concentration on the monoterpene emission rate of Cryptomeria japonica. *Science of the Total Environment*, *634*, 900–908. https://doi.org/10.1016/j.scitotenv.2018.04.025

Monge, M. E., D'Anna, B., Mazri, L., Giroir-Fendler, A., Ammann, M., Donaldson, D. J., & George, C. (2010). Light changes the atmospheric reactivity of soot. *Proceedings of the National Academy of Sciences of the United States of America*, *107*(15), 6605–6609. https://doi.org/10.1073/pnas.0908341107

Moravek, A., Singh, S., Pattey, E., Pelletier, L., & Murphy, J. G. (2019). Measurements and quality control of ammonia eddy covariance fluxes: A new strategy for high-frequency attenuation correction. *Atmospheric Measurement Techniques*, *12*(11), 6059–6078. https://doi.org/10.5194/amt-12-6059-2019

Mosier, A. R. (2008). Exchange of Gaseous Nitrogen Compounds Between Terrestrial Systems and the Atmosphere. *Nitrogen in the Environment*, 443–462. https://doi.org/10.1016/B978-0-12-374347-3.00013-5

Mushinski, R. M., Phillips, R. P., Payne, Z. C., Abney, R. B., Jo, I., Fei, S., Pusede, S. E., White, J. R., Rusch, D. B., & Raff, J. D. (2019). Microbial mechanisms and ecosystem flux estimation for aerobic NOy emissions from deciduous forest soils. *Proceedings of the National Academy of Sciences of the United States of America*, *116*(6), 2138–2145. https://doi.org/10.1073/pnas.1814632116

Naureen, I., Saleem, A., Aslam, S., Zakir, L., Mukhtar, A., Nazir, R., & Zulqarnain, S. (2022). Potential Impact of Smog on Human Health. *Haya: The Saudi Journal of Life Sciences*, *7*(3), 78–84. https://doi.org/10.36348/sjls.2022.v07i03.002

Nguyen, D. H., Lin, C., Vu, C. T., Cheruiyot, N. K., Nguyen, M. K., Le, T. H., Lukkhasorn, W., Vo, T. D. H., & Bui, X. T. (2022). Tropospheric ozone and NOx: A review of worldwide

variation and meteorological influences. *Environmental Technology and Innovation*, *28*. https://doi.org/10.1016/j.eti.2022.102809

Norman, J. M., Kucharik, C. J., Gower, S. T., Baldocchi, D. D., Crill, P. M., Rayment, M., Savage, K., & Striegl, R. G. (1997). A comparison of six methods for measuring soil-surface carbon dioxide fluxes. *Journal of Geophysical Research Atmospheres*, *102*(24), 28771–28777. https://doi.org/10.1029/97jd01440

Nussbaumer, C. M., Place, B. K., Zhu, Q., Pfannerstill, E. Y., Wooldridge, P., Schulze, B. C., Arata, C., Ward, R., Bucholtz, A., Seinfeld, J. H., Goldstein, A. H., & Cohen, R. C. (2023). Measurement report: Airborne measurements of NOx fluxes over Los Angeles during the RECAP-CA 2021 campaign. *Atmospheric Chemistry and Physics*, *23*(20), 13015–13028. https://doi.org/10.5194/acp-23-13015-2023

Oertel, C., Matschullat, J., Zurba, K., Zimmermann, F., & Erasmi, S. (2016). Greenhouse gas emissions from soils—A review. *Chemie Der Erde*, *76*(3), 327–352. https://doi.org/10.1016/j.chemer.2016.04.002

Oswald, R., Behrendt, T., Ermel, M., Wu, D., Su, H., Cheng, Y., Breuninger, C., Moravek, A., Mougin, E., Delon, C., Loubet, B., Pommerening-Röser, A., Sörgel, M., Pöschl, U., Hoffmann, T., Andreae, M. O., Meixner, F. X., & Trebs, I. (2013). HONO emissions from soil bacteria as a major source of atmospheric reactive nitrogen. *Science*, *341*(6151), 1233–1235. https://doi.org/10.1126/science.1242266

Paerl, H. W., Gardner, W. S., Havens, K. E., Joyner, A. R., McCarthy, M. J., Newell, S. E., Qin, B., & Scott, J. T. (2016). Mitigating cyanobacterial harmful algal blooms in aquatic ecosystems impacted by climate change and anthropogenic nutrients. *Harmful Algae*, *54*, 213–222. https://doi.org/10.1016/j.hal.2015.09.009

Pan, S.-Y., He, K.-H., Lin, K.-T., Fan, C., & Chang, C.-T. (2022). Addressing nitrogenous gases from croplands toward low-emission agriculture. *Npj Climate and Atmospheric Science*, *5*(1). https://doi.org/10.1038/s41612-022-00265-3

Pape, L., Ammann, C., Nyfeler-Brunner, A., Spirig, C., Hens, K., & Meixner, F. X. (2009). An automated dynamic chamber system for surface exchange measurement of non-reactive and reactive trace gases of grassland ecosystems. *Biogeosciences*, *6*(3), 405–429. https://doi.org/10.5194/bg-6-405-2009

Pavelka, M., Acosta, M., Kiese, R., Altimir, N., Brümmer, C., Crill, P., Darenova, E., Fuß, R., Gielen, B., Graf, A., Klemedtsson, L., Lohila, A., Longdoz, B., Lindroth, A., Nilsson, M., Jiménez, S. M., Merbold, L., Montagnani, L., Peichl, M., … Kutsch, W. (2018). Standardisation of chamber technique for CO2, N2O and CH4 fluxes measurements from terrestrial ecosystems. *International Agrophysics*, *32*(4), 569–587. https://doi.org/10.1515/intag-2017-0045

Peel, J. L., Haeuber, R., Garcia, V., Russell, A. G., & Neas, L. (2013). Impact of nitrogen and climate change interactions on ambient air pollution and human health. *Biogeochemistry*, *114*(1–3), 121–134. https://doi.org/10.1007/s10533-012-9782-4

Pilegaard, K. (2013). Processes regulating nitric oxide emissions from soils. *Philosophical Transactions of the Royal Society B: Biological Sciences*, *368*(1621). https://doi.org/10.1098/rstb.2013.0126

Portmann, R. W., Daniel, J. S., & Ravishankara, A. R. (2012). Stratospheric ozone depletion due to nitrous oxide: Influences of other gases. *Philosophical Transactions of the Royal Society B: Biological Sciences*, *367*(1593), 1256–1264. https://doi.org/10.1098/rstb.2011.0377

Pumpanen, J., Kolari, P., Ilvesniemi, H., Minkkinen, K., Vesala, T., Niinistö, S., Lohila, A., Larmola, T., Morero, M., Pihlatie, M., Janssens, I., Yuste, J. C., Grünzweig, J. M., Reth, S., Subke, J. A., Savage, K., Kutsch, W., Østreng, G., Ziegler, W., … Hari, P. (2004). Comparison of different chamber techniques for measuring soil CO 2 efflux. *Agricultural and Forest Meteorology*, *123*(3–4), 159–176. https://doi.org/10.1016/j.agrformet.2003.12.001

Purchase, M. L., Bending, G. D., & Mushinski, R. M. (2023). Spatiotemporal Variations of Soil Reactive Nitrogen Oxide Fluxes across the Anthropogenic Landscape. *Environmental Science and Technology*, *57*(43), 16348–16360. https://doi.org/10.1021/acs.est.3c05849

Ramazan, K. A., Syomin, D., & Finlayson-Pitts, B. J. (2004). The photochemical production of HONO during the heterogeneous hydrolysis of NO2. *Physical Chemistry Chemical Physics*, *6*(14), 3836–3843. https://doi.org/10.1039/b402195a

Rapson, T. D., & Dacres, H. (2014). Analytical techniques for measuring nitrous oxide. In *TrAC - Trends in Analytical Chemistry* (Vol. 54, pp. 65–74). Elsevier B.V. https://doi.org/10.1016/j.trac.2013.11.004

Ravishankara, A. R., Daniel, J. S., & Portmann, R. W. (2009). Nitrous oxide (N2O): The dominant ozone-depleting substance emitted in the 21st century. *Science*, *326*(5949), 123–125. https://doi.org/10.1126/science.1176985

Ren, C., Huang, X., Wang, Y., Zhang, L., Zhou, X., Sun, W., Zhang, H., Liu, T., Ding, A., & Wang, T. (2025). Enhanced Soil Emissions of Reactive Nitrogen Gases by Fertilization and Their Impacts on Secondary Air Pollution in Eastern China. *Environmental Science and Technology*. https://doi.org/10.1021/acs.est.4c12324

Ren, X., Sanders, J. E., Rajendran, A., Weber, R. J., Goldstein, A. H., Pusede, S. E., Browne, E. C., Min, K. E., & Cohen, R. C. (2011). A relaxed eddy accumulation system for measuring vertical fluxes of nitrous acid. *Atmospheric Measurement Techniques*, *4*(10), 2093–2103. https://doi.org/10.5194/amt-4-2093-2011

Ren, Y., Stieger, B., Spindler, G., Grosselin, B., Mellouki, A., Tuch, T., Wiedensohler, A., & Herrmann, H. (2020). Role of the dew water on the ground surface in HONO distribution: A

case measurement in Melpitz. *Atmospheric Chemistry and Physics*, *20*(21), 13069–13089. https://doi.org/10.5194/acp-20-13069-2020

Roberts, J. M., Stockwell, C. E., Yokelson, R. J., De Gouw, J., Liu, Y., Selimovic, V., Koss, A. R., Sekimoto, K., Coggon, M. M., Yuan, B., Zarzana, K. J., Brown, S. S., Santin, C., Doerr, S. H., & Warneke, C. (2020). The nitrogen budget of laboratory-simulated western US wildfires during the FIREX 2016 Fire Lab study. *Atmospheric Chemistry and Physics*, *20*(14), 8807–8826. https://doi.org/10.5194/acp-20-8807-2020

Roberts, J. M., Veres, P., Warneke, C., Neuman, J. A., Washenfelder, R. A., Brown, S. S., Baasandorj, M., Burkholder, J. B., Burling, I. R., Johnson, T. J., Yokelson, R. J., & De Gouw, J. (2010). Measurement of HONO, HNCO, and other inorganic acids by negative-ion proton-transfer chemical-ionization mass spectrometry (NI-PT-CIMS): Application to biomass burning emissions. *Atmospheric Measurement Techniques*, *3*(4), 981–990. https://doi.org/10.5194/amt-3-981-2010

Scharko, N. K., Martin, E. T., Losovyj, Y., Peters, D. G., & Raff, J. D. (2017). Evidence for Quinone Redox Chemistry Mediating Daytime and Nighttime NO2-to-HONO Conversion on Soil Surfaces. *Environmental Science and Technology*, *51*(17), 9633–9643. https://doi.org/10.1021/acs.est.7b01363

Scharko, N. K., Schu, U. M. E., Berke, A. E., Banina, L., Peel, H. R., Donaldson, M. A., Hemmerich, C., White, R., & Ra, J. D. (2015). *Combined Flux Chamber and Genomics Approach Links Nitrous Acid Emissions to Ammonia Oxidizing Bacteria and Archaea in Urban and Agricultural Soil*. https://doi.org/10.1021/acs.est.5b00838

Schimang, R., Folkers, A., Kleffmann, J., Kleist, E., Miebach, M., & Wildt, J. (2006). Uptake of gaseous nitrous acid (HONO) by several plant species. *Atmospheric Environment*, *40*(7), 1324–1335. https://doi.org/10.1016/j.atmosenv.2005.10.028

Schumann, U., & Huntrieser, H. (2007). The global lightning-induced nitrogen oxides source. *Atmospheric Chemistry and Physics*, *7*(14), 3823–3907. https://doi.org/10.5194/acp-7-3823-2007

Seinfeld, J. H., & Pandis, S. N. (1998). *From Air Pollution to Climate Change* (2nd ed.). Wiley.

Seinfeld, J. H., & Pandis, S. N. (2006). *Atmospheric chemistry and physics: from air pollution to climate change.* (2nd edition). John Wiley & Sons.

Shepon, A., Gildor, H., Labrador, L. J., Butler, T., Ganzeveld, L. N., & Lawrence, M. G. (2007). Global reactive nitrogen deposition from lightning NOx. *Journal of Geophysical Research Atmospheres*, *112*(6), 1–14. https://doi.org/10.1029/2006JD007458

Singh, S., Mayes, M. A., Kivlin, S. N., & Jagadamma, S. (2023). How the Birch effect differs in mechanisms and magnitudes due to soil texture. *Soil Biology and Biochemistry*, *179*(January), 108973. https://doi.org/10.1016/j.soilbio.2023.108973

Smith, K. A., Ball, T., Conen, F., Dobbie, K. E., Massheder, J., & Rey, A. (2018). Exchange of greenhouse gases between soil and atmosphere: interactions of soil physical factors and biological processes. *European Journal of Soil Science*, *69*(1), 10–20. https://doi.org/10.1111/ejss.12539

Song, Y., Xue, C., Zhang, Y., Liu, P., Bao, F., Li, X., & Mu, Y. (2023). Measurement report: Exchange fluxes of HONO over agricultural fields in the North China Plain. *Atmospheric Chemistry and Physics*, *23*(24), 15733–15747. https://doi.org/10.5194/acp-23-15733-2023

Sörgel, M., Regelin, E., Bozem, H., Diesch, J. M., Drewnick, F., Fischer, H., Harder, H., Held, A., Hosaynali-Beygi, Z., Martinez, M., & Zetzsch, C. (2011). Quantification of the unknown HONO daytime source and its relation to NO2. In *Atmospheric Chemistry and Physics* (Vol. 11, Issue 20, pp. 10433–10447). https://doi.org/10.5194/acp-11-10433-2011

Spataro, F., & Ianniello, A. (2014). Sources of atmospheric nitrous acid: State of the science, current research needs, and future prospects. *Journal of the Air and Waste Management Association*, *64*(11), 1232–1250. https://doi.org/10.1080/10962247.2014.952846

Spicer, C., Billick, I., & Yanagisawa, Y. (2001). *Nitrous Acid Interference with Passive NO2 Measurement Methods and the Impact on Indoor NO2 Data, Indoor Air*. *11(3)*, 156–161. https://doi.org/10.1034/j.1600-0668.2001.011003156.x

Stemmler, K., Ammann, M., Donders, C., Kleffmann, J., & George, C. (2006). Photosensitized reduction of nitrogen dioxide on humic acid as a source of nitrous acid. *Nature*, *440*(7081), 195–198. https://doi.org/10.1038/nature04603

Stępniewski, W., Sobczuk, H., & Widomski, M. (2011). *Diffusion in Soils* (pp. 214–220). https://doi.org/10.1007/978-90-481-3585-1_273

Stepniewski, W., Stepniewska, Z., & Rozej, A. (2015). Gas Exchange in Soils. *Soil Management: Building a Stable Base for Agriculture*, 117–144. https://doi.org/10.2136/2011.soilmanagement.c8

Stockwell, C. E., Kupc, A., Witkowski, B., Talukdar, R. K., Liu, Y., Selimovic, V., Zarzana, K. J., Sekimoto, K., Warneke, C., Washenfelder, R. A., Yokelson, R. J., Middlebrook, A. M., & Roberts, J. M. (2018). Characterization of a catalyst-based conversion technique to measure total particulate nitrogen and organic carbon and comparison to a particle mass measurement instrument. *Atmospheric Measurement Techniques*, *11*(5), 2746–2764. https://doi.org/10.5194/amt-11-2749-2018

Su, H., Cheng, Y., Oswald, R., Behrendt, T., Trebs, I., Meixner, F. X., Andreae, M. O., Cheng, P., Zhang, Y., & Pöschl, U. (2011). Soil nitrite as a source of atmospheric HONO and OH radicals. *Science*, *333*(6049), 1616–1618. https://doi.org/10.1126/science.1207687

Tai, A. P. K., Luo, L., & Luo, B. (2025). Opinion: Understanding the impacts of agriculture and food systems on atmospheric chemistry is instrumental to achieving multiple Sustainable Development Goals. *Atmospheric Chemistry and Physics*, *25*(2), 923–941. https://doi.org/10.5194/acp-25-923-2025

Tan, W., Wang, H., Su, J., Sun, R., He, C., Lu, X., Lin, J., Xue, C., Wang, H., Liu, Y., Liu, L., Zhang, L., Wu, D., Mu, Y., & Fan, S. (2023). Soil Emissions of Reactive Nitrogen Accelerate Summertime Surface Ozone Increases in the North China Plain. *Environmental Science and Technology*. https://doi.org/10.1021/acs.est.3c01823

Tang, K., Qin, M., Duan, J., Fang, W., Meng, F., Liang, S., Xie, P., Liu, J., Liu, W., Xue, C., & Mu, Y. (2019). A dual dynamic chamber system based on IBBCEAS for measuring fluxes of nitrous acid in agricultural fields in the North China Plain. *Atmospheric Environment*, *196*(May 2018), 10–19. https://doi.org/10.1016/j.atmosenv.2018.09.059

Tang, K., Qin, M., Fang, W., Duan, J., Meng, F., Ye, K., Zhang, H., Xie, P., Liu, J., Liu, W., Feng, Y., Huang, Y., & Ni, T. (2020). An automated dynamic chamber system for exchange flux measurement of reactive nitrogen oxides (HONO and NOX) in farmland ecosystems of the Huaihe River Basin, China. *Science of the Total Environment*, *745*(X), 140867. https://doi.org/10.1016/j.scitotenv.2020.140867

Tian, H., Pan, N., Thompson, R. L., Canadell, J. G., Suntharalingam, P., Regnier, P., Davidson, E. A., Prather, M., Ciais, P., Muntean, M., Pan, S., Winiwarter, W., Zaehle, S., Zhou, F., Jackson, R. B., Bange, H. W., Berthet, S., Bian, Z., Bianchi, D., … Zhu, Q. (2024). Global nitrous oxide budget (1980-2020). *Earth System Science Data*, *16*(6), 2543–2604. https://doi.org/10.5194/essd-16-2543-2024

VandenBoer, T. C., Brown, S. S., Murphy, J. G., Keene, W. C., Young, C. J., Pszenny, A. A. P., Kim, S., Warneke, C., de Gouw, J. A., Maben, J. R., Wagner, N. L., Riedel, T. P., Thornton, J. A., Wolfe, D. E., Dubé, W. P., Öztürk, F., Brock, C. A., Grossberg, N., Lefer, B., … Roberts, J. M. (2013). Understanding the role of the ground surface in HONO vertical structure: High resolution vertical profiles during NACHTT-11. *J. Geophys. Res. Atmos*, *118*, 155–165. https://doi.org/10.1002/jgrd.50721

VandenBoer, T. C., Young, C. J., Talukdar, R. K., Markovic, M. Z., Brown, S. S., Roberts, J. M., & Murphy, J. G. (2015). Nocturnal loss and daytime source of nitrous acid through reactive uptake and displacement. *Nature Geoscience*, *8*(1), 55–60. https://doi.org/10.1038/ngeo2298

Villarreal, R., Lozano, L. A., Melani, E. M., Salazar, M. P., Otero, M. F., & Soracco, C. G. (2019). Diffusivity and sorptivity determination at different soil water contents from horizontal infiltration. *Geoderma*, *338*, 88–96. https://doi.org/10.1016/J.GEODERMA.2018.11.045

Von Der Heyden, L., Wißdorf, W., Kurtenbach, R., & Kleffmann, J. (2022). A relaxed eddy accumulation (REA) LOPAP system for flux measurements of nitrous acid (HONO). *Atmospheric Measurement Techniques*, *15*(6), 1983–2000. https://doi.org/10.5194/amt-15-1983-2022

Wang, C., Fang, Y., An, W., Zeng, C., Wang, W., Sardans, J., Fernández-Martínez, M., & Peñuelas, J. (2020). Acid rain mediated nitrogen and sulfur deposition alters soil nitrogen,

phosphorus and carbon fractions in a subtropical paddy. *Catena*, *195*. https://doi.org/10.1016/j.catena.2020.104876

Wang, Fu, X., Wu, D., Wang, M., Lu, K., Mu, Y., Liu, Z., Zhang, Y., & Wang, T. (2021). Agricultural Fertilization Aggravates Air Pollution by Stimulating Soil Nitrous Acid Emissions at High Soil Moisture. *Environmental Science and Technology*, *55*(21), 14556–14566. https://doi.org/10.1021/acs.est.1c04134

Wang, J., Zhang, X., Guo, J., Wang, Z., & Zhang, M. (2017). Observation of nitrous acid (HONO) in Beijing, China: Seasonal variation, nocturnal formation and daytime budget. *Science of The Total Environment*, *587–588*, 350–359. https://doi.org/10.1016/J.SCITOTENV.2017.02.159

Wang, Y., Fu, X., Wang, T., Ma, J., Gao, H., Wang, X., & Pu, W. (2022). Large Contribution of Nitrous Acid to Soil-Emitted Reactive Oxidized Nitrogen and Its Effect on Air Quality. *Environmental Science and Technology*. https://doi.org/10.1021/acs.est.2c07793

Wolfe, G. M., Fischer, E. V., & Geddes, J. (2024). *NASA Earth Venture Suborbital 4 Program*.

Worton, D. R. (2020). Future Adoption of Direct Measurement Techniques for Regulatory Measurements of Nitrogen Dioxide: Drivers and Challenges. In *Environmental Science and Technology* (Vol. 54, Issue 23, pp. 14785–14786). American Chemical Society. https://doi.org/10.1021/acs.est.0c04709

Wu, D., Deng, L., Liu, Y., Xi, D., Zou, H., Sha, Z., Pan, Y., Hou, L., & Liu, M. (2020). *Comparisons of the effects of different drying methods on soil nitrogen fractions: Insights into emissions of reactive nitrogen gases (HONO and NO)*. https://doi.org/10.1080/16742834.2020.1733388

Wu, D., Horn, M. A., Behrendt, T., Müller, S., Li, J., Cole, J. A., Xie, B., Ju, X., Li, G., Ermel, M., Oswald, R., Fröhlich-Nowoisky, J., Hoor, P., Hu, C., Liu, M., Andreae, M. O., Pöschl, U., Cheng, Y., Su, H., … Sörgel, M. (2019). Soil HONO emissions at high moisture content are driven by microbial nitrate reduction to nitrite: tackling the HONO puzzle. *ISME Journal*, *13*(7), 1688–1699. https://doi.org/10.1038/s41396-019-0379-y

Xia, X., Meng, X., Liu, C., Guo, Y., Li, X., Niu, Y., Lam, K. B. H., Wright, N., Kartsonaki, C., Chen, Y., Yang, L., Du, H., Yu, C., Sun, D., Lv, J., Chen, J., Yang, X., Gao, R., Wu, S., … Qu, C. (2024). Associations of long-term nitrogen dioxide exposure with a wide spectrum of diseases: a prospective cohort study of 0·5 million Chinese adults. *The Lancet Public Health*, *9*(12), e1047–e1058. https://doi.org/10.1016/S2468-2667(24)00264-0

Xiang, W., Wang, W., Du, L., Zhao, B., Liu, X., Zhang, X., Yao, L., & Ge, M. (2023). Toxicological Effects of Secondary Air Pollutants. In *Chemical Research in Chinese Universities* (Vol. 39, Issue 3, pp. 326–341). Springer Science and Business Media Deutschland GmbH. https://doi.org/10.1007/s40242-023-3050-0

Xue, C., Ye, C., Lu, K., Liu, P., Zhang, C., Su, H., Bao, F., Cheng, Y., Wang, W., Liu, Y., Catoire, V., Ma, Z., Zhao, X., Song, Y., Ma, X., McGillen, M. R., Mellouki, A., Mu, Y., & Zhang, Y.

(2024). Reducing Soil-Emitted Nitrous Acid as a Feasible Strategy for Tackling Ozone Pollution. *Environmental Science and Technology*, *58*(21), 9227–9235. https://doi.org/10.1021/acs.est.4c01070

Yang, J. Y., Drury, C. F., Jiang, R., Worth, D. E., Bittman, S., Grant, B. B., & Smith, W. N. (2024). Reactive nitrogen losses from Canadian agricultural soils over 36 years. *Ecological Modelling*, *495*. https://doi.org/10.1016/j.ecolmodel.2024.110809

Yu, L., Wang, H., Wang, G., Song, W., Huang, Y., Li, S. G., Liang, N., Tang, Y., & He, J. S. (2013). A comparison of methane emission measurements using eddy covariance and manual and automated chamber-based techniques in Tibetan Plateau alpine wetland. *Environmental Pollution*, *181*, 81–90. https://doi.org/10.1016/j.envpol.2013.06.018

Zaman, M., Heng, L., & Müller, C. (2011). *Measuring Emission of Agricultural Greenhouse Gases and Developing Mitigation Options using Nuclear and Related Techniques*. https://doi.org/10.1007/978-3-030-55396-8

Zhang, Liu, P., Wang, Y., George, C., Chen, T., Ma, S., Ren, Y., Mu, Y., Song, M., Herrmann, H., Mellouki, A., Chen, J., Yue, Y., Zhao, X., Wang, S., & Zeng, Y. (2023). Unveiling the underestimated direct emissions of nitrous acid (HONO). *Proceedings of the National Academy of Sciences of the United States of America*, *120*(35). https://doi.org/10.1073/pnas.2302048120

Zhang, X., Ward, B. B., & Sigman, D. M. (2020). *Global Nitrogen Cycle: Critical Enzymes, Organisms, and Processes for Nitrogen Budgets and Dynamics*. https://doi.org/10.1021/acs.chemrev.9b00613

Zhou, Oehmen, A., Lim, M., Vadivelu, V., & Ng, W. J. (2011). The role of nitrite and free nitrous acid (FNA) in wastewater treatment plants. *Water Research*, *45*(15), 4672–4682. https://doi.org/10.1016/j.watres.2011.06.025

Zhu, C., Jagdale, G., Gandolfo, A., Alanis, K., Abney, R., Zhou, L., Bish, D., Raff, J. D., & Baker, L. A. (2021). Surface Charge Measurements with Scanning Ion Conductance Microscopy Provide Insights into Nitrous Acid Speciation at the Kaolin Mineral-Air Interface. *Environmental Science and Technology*, *55*(18), 12233–12242. https://doi.org/10.1021/acs.est.1c03455

Chapter Two: Modification and validation of a commercial dynamic chamber for reactive nitrogen and greenhouse gas flux measurements

Moxy Shah[1], Kifle Z. Aregahegn[1], Danial Nodeh-Farahani[1], Leigh R. Crilley[1,‡], Tasnia Hasan[1], Yashar Ebrahimi-Iranpour[1], Fahim Sarker[1], Nick Nickerson[2], Chance Creelman[2], Sarah Morrison[2], Alexander Moravek[1,§], Trevor C. VandenBoer[1,*]

[1] Department of Chemistry, York University, Toronto, Ontario, Canada

[2] Eosense Inc., Dartmouth, Nova Scotia, Canada

[‡] Now at: Atmospheric Services, WSP Australia, Brisbane, QLD, Australia

[§] Now at: German Environment Agency, Department of Air Quality, Dessau-Rosslau, Germany

[*]Communicating author: tvandenb@yorku.ca

The material presented in this chapter has been submitted to *Atmospheric Measurement Techniques* (egusphere-2025-4662), for peer review on 22 September 2025.

Author contributions: TCV designed and oversaw the experiments, acquired funding, wrote parts of the manuscript, and guided writing and revision of all sections of the manuscript. MS wrote the manuscript and performed all the experiments. KZA carried out the multiplexer experiments, conducted data analysis for the fill-empty experiment, provided guidance and feedback on the derivation of the mass balance flux model, and assisted in the revision of the manuscript. LRC helped design the experiments, modify the chambers, write the LabVIEW code, and conduct the pilot field measurements. LRC also contributed to manuscript preparation and revision. FS performed some fill/ empty experiments and the NO_2 loss experiments, designed the custom valve switching system, modified LabVIEW code for the pilot field measurements, and contributed to initial drafts of the manuscript. DF worked up the pilot field study results and derived the dual chamber mass balance flux calculations, along with contributions to the writing and revision of the manuscript. YEI assisted with the GHG fill and empty experiments and the pilot field study site setup. NN, CC, and SM provided technical support with setting up and modifying the chambers and multiplexer, and AM contributed to the initial chamber lab setup and reviewing of the manuscript.

Abstract

Reactive nitrogen compounds (NO, NO_2, HONO, NH_3 and others; N_r) play important roles in atmospheric processes, and their cascading impacts throughout the Earth system have adverse effects on both the environment and human health. The fluxes of these gases at the surface-atmosphere interface have been studied in isolation or in smaller subsets by micrometeorological techniques or chambers, but simultaneous observations of all N_r species alongside standard greenhouse gases (GHGs) as a function of time have not been reported. Here, a dual-dynamic chamber system was developed for N_r by modifying a commercially available system for GHG fluxes for use with destructive analyzers and to account for chemical changes. The resulting platform measures N_r and, by extension, other reactive gases, more widely accessible to the scientific community, as custom chambers do not need to be fabricated.

System modifications to passivate surfaces were implemented, so that N_r gases like NO_2 could be effectively transferred to standard gas analyzers, with an initial 36% loss due to transformations ultimately minimized below analyzer detection limits (~10%) under relevant atmospheric conditions. The modified 72 L chamber did not see a change in the baseline response times for GHGs or NO at a flow rate of 2 L min^{-1}. They retained the same values as an ideal non-reactive trace gas (τ = 37-39 min versus 36 min. The modifications improved the transfer time constants of NO_2, HONO, and NH_3 by up to 2 min, but substantial surface interactions for NH_3 remain. In all cases, a surface interaction term needs to be characterized for these gases to obtain accurate fluxes. Losses of NO_2 and O_3 by known gas phase reactions, or from deposition and reaction on pristine and aged chamber surfaces, were characterized across a range of environmentally relevant relative humidities (RH) and mixing ratios. The final dual-chamber system configuration includes a measurement and reference chamber, which are necessary to implement the corrections for surface effects and chemical transformations when accurately quantifying dynamic fluxes via a mass balance framework.

Proof-of-concept measurements of N_r fluxes from agricultural soil samples under controlled lab conditions as a function of soil water content were able to quantify emissions of NO, NO_2, HONO, NH_3, and N_2O simultaneously, when subject to fertilization experiments using urea, ammonium carbonate and bicarbonate, and ammonium nitrate. Unfertilized replicate agricultural soil samples

showed variability in NO_2 and HONO emissions when prepared with minimal disturbance to the soil structure, with values consistent with those reported by in-situ field measurements. These oppose maximum potential fluxes characterized in prior lab soil manipulations, particularly for HONO relative to NO. Last, fluxes were quantified with destructive gas analyzers in the field with the dual-chamber system on an in-use agricultural soil and included a urea-based fertilizer perturbation to stimulate microbial and chemical transformation and transfer N_r to the atmosphere. The resulting fluxes observed show good agreement with prior reports based on other flux techniques. The mass balance terms within the dual-chamber approach are fully inspected from the pilot deployment in the field, along with an error analysis, to aid in the uptake of this approach by the community.

2.1 Introduction

The nitrogen (N) cycle is a crucial biogeochemical cycle on Earth, essential for sustaining life through the production of nucleic acids, proteins, and other vital biomolecules (Lehnert et al., 2021). Although the carbon cycle receives the most attention due to looming climatic crises caused by greenhouse gases (GHGs) like carbon dioxide (CO_2) and methane (CH_4), the N cycle is closely intertwined with the carbon cycle (Schlesinger, 2020). At the interface of these cycles and the Earth's surface, reactive nitrogen (N_r) species exchanged between ecosystems and the atmosphere have become an area of emerging interest (Lehnert et al., 2021; Wu et al., 2020). Within the atmosphere, N_r species such as nitric oxide (NO) and nitrogen dioxide (NO_2) – collectively referred to as NO_x – ammonia (NH_3), and nitrous acid (HONO) can each be mediated in part through surface-atmosphere exchange, influencing local air or water quality, ecosystem processes, and biodiversity (Lehnert et al., 2021; Richardson et al., 2023; Wu et al., 2020). Meanwhile, the non-reactive nitrous oxide (N_2O) has climate impacts due to its long atmospheric lifetime (~120 years) and potent greenhouse effect (IPCC, 2023).

Reactive nitrogen compounds (NO, NO_2, HONO, and NH_3; N_r) play an important role in atmospheric processes, contributing to the formation of pollutants like ozone (O_3) and secondary organic aerosols (SOA). The exchange of N_r between the Earth's surface and the atmosphere involves numerous production and loss processes driven by both natural and human activities. Reactive nitrogen species are removed from the atmosphere through wet and dry deposition, and

their abundance depends on the net outcome relative to N_r emissions (Delaria and Cohen, 2023). At the land surface, N_r is released into the atmosphere by microbial nitrogen cycling, agricultural activities, wildfires, or fossil fuel combustion (Benedict et al., 2017; Mosier, 2008; Yang et al., 2024). Despite the wealth of knowledge on the environmental importance of N_r, studying N_r at the surface-atmosphere interface with high time resolution and chemical speciation remains a challenge due to its high spatial and temporal variability driven by factors like climate, vegetation cover, and soil/surface properties (Ludwig et al., 2001). For example, recent studies have demonstrated that HONO production at the ground surface plays a major role in the unexplained daytime HONO source and its impact on daytime OH, with vertically resolved measurements confirming that the surface remains a dominant source at all times of day (VandenBoer et al., 2013, 2015; Young et al., 2012). Such observations pose a challenge in studying N_r because suitable equipment for high time resolution atmospheric observations is expensive, limiting the concurrent study of the interplay between emission and deposition for many N_r species to one or a few species at a time. As a result, no systems are currently accessible enough to the scientific community to be deployed across widely different global landscapes, particularly in soils.

Soils play a pivotal role in mediating N_r emissions due to their dual function as both a source and a sink of nitrogenous species. Soil-atmosphere exchange of N_r is thought to be governed by microbial processes such as nitrification and denitrification, with soil factors like pH, moisture, organic matter, and nitrogen availability playing a crucial role in regulating N_r emission (Mosier, 2008; Purchase et al., 2023; Stepniewski et al., 2015). These microbial processes have been demonstrated to drive the formation and release of some N_r species (e.g., NO, NH_3 and N_2O) in addition to assertions that they can support the production and release of HONO via partitioning (Butterbach-Bahl & Dannenmann, 2011; Kool et al., 2010; Mushinski et al., 2019; Oswald et al., 2013; Su et al., 2011). Understanding the exchange of these gases is essential for unravelling the complex interactions between the nitrogen and carbon cycles and their broader environmental impacts from an unprecedented imbalance in the global nitrogen cycle (Richardson et al., 2023). Given the importance of N_r in atmospheric chemistry and its influence on ecosystem processes, it is essential to understand the mechanisms driving its exchange (Fowler et al., 2013). To date, comprehensive exchange systems for studying the full suite of N_r have not been reported.

To quantify N_r exchange for a few explicit species near the ground surface, various flux measurement techniques have been employed, yielding insights into their magnitude and identifying some driving factors. Quantifying fluxes of atmospheric gases has been most effectively applied to GHGs at the surface-atmosphere interface. Traditional measurement methods, such as eddy covariance (EC), relaxed eddy accumulation (REA), and aerodynamic gradient (AG) methods, have been extensively used for ecosystem-scale, continuous flux monitoring, including targeted assessment of most N_r species (e.g., (Bao et al., 2022; Geddes and Murphy, 2014; Kamp et al., 2020; Laufs et al., 2017; Min et al., 2014; Moravek et al., 2014, 2019; Ren et al., 2011; Von Der Heyden et al., 2022; Wang et al., 2022; Wolff et al., 2010). These micrometeorological techniques measure concentrations, concentration gradients, and/or turbulence to estimate fluxes across interfaces applicable to ecosystem-scale processes. When operated continuously, they offer long-term insight without disrupting the natural system. Chamber methods have some advantages compared to micrometeorological techniques, as they are relatively inexpensive, easy to deploy, and require minimal prior meteorological training and expertise (Tang et al., 2020). Chambers are limited to small plots, e.g. making them suitable to study the effect of different fertilizer treatments (Tang et al., 2020). The chamber method is a widely used technique for measuring GHG fluxes, especially for N_2O. However, challenges remain in addressing potential biases introduced by chemical transformations occurring within the chamber and interactions with the chamber surfaces, particularly for N_r species (i.e., NO_2, HONO, NH_3).

Chemical transformations can occur on chamber surfaces or between the point of emission and measurement. Surface interactions such as adsorption, desorption, and heterogeneous reactions can alter the apparent concentration of several N_r species. For example, NO in a chamber could react in the gas phase with O_3 to form NO_2 during the day and NO_3 at night if sufficient O_3 is present to fully titrate NO (R1, R2). Heterogeneous reaction of gas-phase NO_2 on surfaces under humid conditions also produces nitric acid (HNO_3) and HONO (R3) (Kleffmann et al., 2005; Ramazan et al., 2004; VandenBoer et al., 2015). The formed HONO can undergo multiphase processes in the chamber or on enclosed surfaces by partitioning into water according to its Henry's Law constant and then dissociating into nitrite (NO_2^-) and the hydronium ion (H_3O^+) according to its acid dissociation equilibrium constant and the pH (R4, R5) (He et al., 2006; Ren et al., 2020).

Nitrous acid could also photolyze, yielding NO and an OH radical (R6) (Spataro & Ianniello, 2014).

$$NO + O_3 \rightarrow NO_2 + O_2 \quad \text{(R1)}$$

$$NO_2 + O_3 \rightarrow NO_3 + O_2 \quad \text{(R2)}$$

$$2NO_{2\,(g)} + H_2O_{\,(ads)} \rightarrow HONO_{\,(g)} + HNO_{3\,(ads)} \quad \text{(R3)}$$

$$HONO_{\,(g)} \leftrightarrow HONO_{\,(aq)} \quad \text{(R4)}$$

$$HONO_{\,(aq)} + H_2O_{\,(l)} \rightleftharpoons NO_2^-{}_{(aq)} + H_3O^+{}_{(aq)} \quad \text{(R5)}$$

$$HONO + h\nu \rightarrow NO + OH \quad \text{(R6)}$$

These processes in/on the chamber can introduce uncertainty in flux measurements. Characterizing and accounting for chemistry and surface effects in chamber-based methods are necessary to obtain accurate flux measurements of N_r species with a chamber-based system. While static chamber systems typically determine the flux from the change in concentration after closing the chamber cover, traditional dynamic chamber systems use a controlled flow of ambient air through the headspace and retrieve the flux from the concentration difference at the chamber inlet and outlet. With minor modifications, these chambers have previously been applied to agricultural soils and natural ecosystems, demonstrating their utility for measuring emissions of gases such as N_2O and NO_x (Maggiotto et al., 2000; Pape et al., 2009). Their ability to create standardized and reproducible conditions makes them particularly advantageous for studying the driving mechanisms behind gas exchange, yet their application to the full suite of relevant N_r species for surface-atmosphere exchange remains unestablished.

The dynamic chamber method has been reported for measurements of the exchange fluxes of challenging gases like biogenic volatile organic compounds (BVOCs, such as monoterpenes and isoprene) from vegetation and farmland (Kolari et al., 2012; Mochizuki et al., 2018), NH_3 volatilization from cattle manure (Becciolini et al., 2024), N_2O and NO_x from turfgrass (Maggiotto et al., 2000), and NO_x fluxes from grasslands (Pape et al., 2009; Plake, Sörgel, et al., 2015). Scharko et al. (2015) used sealed chambers and Tang et al. (2019), using dynamic chambers, were amongst the first to highlight the potential for both HONO and NO_x fluxes from agricultural

soils as hotspots impacting atmospheric chemistry, which has been implemented in atmospheric models (Ha et al., 2023; Tian et al., 2024).

The complexity of nitrite (NO_2^-) chemical and biological production and loss in soils, coupled with soil properties facilitating gas exchange of HONO, has led to intense interest and debate around discerning the fundamental controls on its surface-atmosphere exchange (R4, R5) (Barney & Finlayson-Pitts, 2000; Huang et al., 2002; Kamboures et al., 2008; Meusel et al., 2018; Mushinski et al., 2019; Purchase et al., 2023; Song et al., 2023; Sörgel et al., 2015; Wang et al., 2021). The same is true for direct emissions of NO_2 from soils, where evidence remains limited (Huber et al., 2024; Zörner et al., 2016). Only a handful of field studies have directly measured soil NO_2 measurements, making it challenging to infer how much NO_2 might be emitted from soils. Gong et al. (2025) estimate that the fertilizer-induced soil NO_x emissions contribute 0.84–2.2 Tg N yr^{-1} globally, with uncertainties partly due to the lack of NO_2 measurements. Their modelling indicates that this underrepresentation likely leads to underestimation of summertime ozone enhancements (0.3–3.3 ppbv) in agricultural hotspot regions. This N_r exchange is intricately linked to agricultural practices, as excessive nitrogen inputs (e.g., fertilizers) amplify emissions of N_r species, namely NO_x, N_2O, HONO, and NH_3 from the impacted soils (Degaspari et al., 2020). This highlights the need for more direct soil NO_2 measurements, as well as better constraints on the broader N_r species emitted from fertilized soils.

Automated dynamic chambers deployed in situ for field observations would provide a platform for capturing (and manipulating) the magnitude, direction, and temporal variability of N_r species or physical variables via the headspace gas or soil amendments while retaining soils in an intact state (Aneja et al., 2006). Thus, establishing an accessible dynamic chamber method for N_r flux measurements is desirable. However, such a platform needs to undergo extensive validation to reduce flux bias from challenging N_r species such as NH_3. This important and necessary first step will allow a wider global study of surface-atmosphere N_r exchange processes.

Here, we modify commercial dynamic chambers originally designed for GHG flux measurements to make them suitable for quantifying the most prevalent N_r gas exchange fluxes at surface-atmosphere interfaces. First, we implement surface and hardware modifications to adapt the commercial chambers to minimize gas adsorption and transformations. We systematically characterized the transfer of both GHGs and N_r species by calculating fill and empty rates,

transformed to time constants, to identify any surface interactions and/or transformations on the chamber surfaces. We then applied our modified commercial dynamic chambers to make flux measurements by equipping them with destructive gas analyzers for HONO and NO_x and a cavity ring-down spectrometer (Picarro G2509) for NH_3, N_2O, CO_2, and CH_4 in lab experiments, or with a fully automated dual-chamber approach under field conditions through a pilot study. Flux bias minimization through a mass balance approach during the pilot study in a real agricultural field is demonstrated for several N_r gases. This community-accessible approach addresses key needs in allowing more researchers to measure N_r exchange at the surface-atmosphere interface, with the capacity to monitor fluxes of all species simultaneously with at least hourly time resolution.

2.2 Materials and methods

2.2.1 Dynamic chambers for field fluxes

2.2.1.1 Description of the custom-modified dual-dynamic chamber system for flux measurement

The dynamic chamber system is composed of two identical commercially available chambers (eosAC-LT®, Eosense, Dartmouth, NS). These are modified and coupled to programmable valves that control the delivery of sample gases to a suite of instrumentation (**Figure 2.1)** to perform reactive gas flux measurements.

The dynamic chambers, constructed out of transparent polyacrylate walls and lids, have an internal volume of 0.072 m^3 and can enclose a surface area of 0.21 m^2. When used on soil surfaces, the chambers are secured with embedded soil collars using custom-made polytetrafluorethylene (PTFE) rings (**Figure 2.S1)** and can be similarly affixed to impervious surfaces. A built-in fan ensures uniform distribution of gases inside the chamber. Ambient air temperature is measured inside the chamber from the fan arm, whereas pressure sensors are embedded in the control box outside the chamber. Each chamber has two auxiliary ports, one internally and the other externally, capable of collecting measurements of environmental properties such as relative humidity (RH), photosynthetically active radiation (PAR), soil temperature, and soil volumetric water content (VWC).

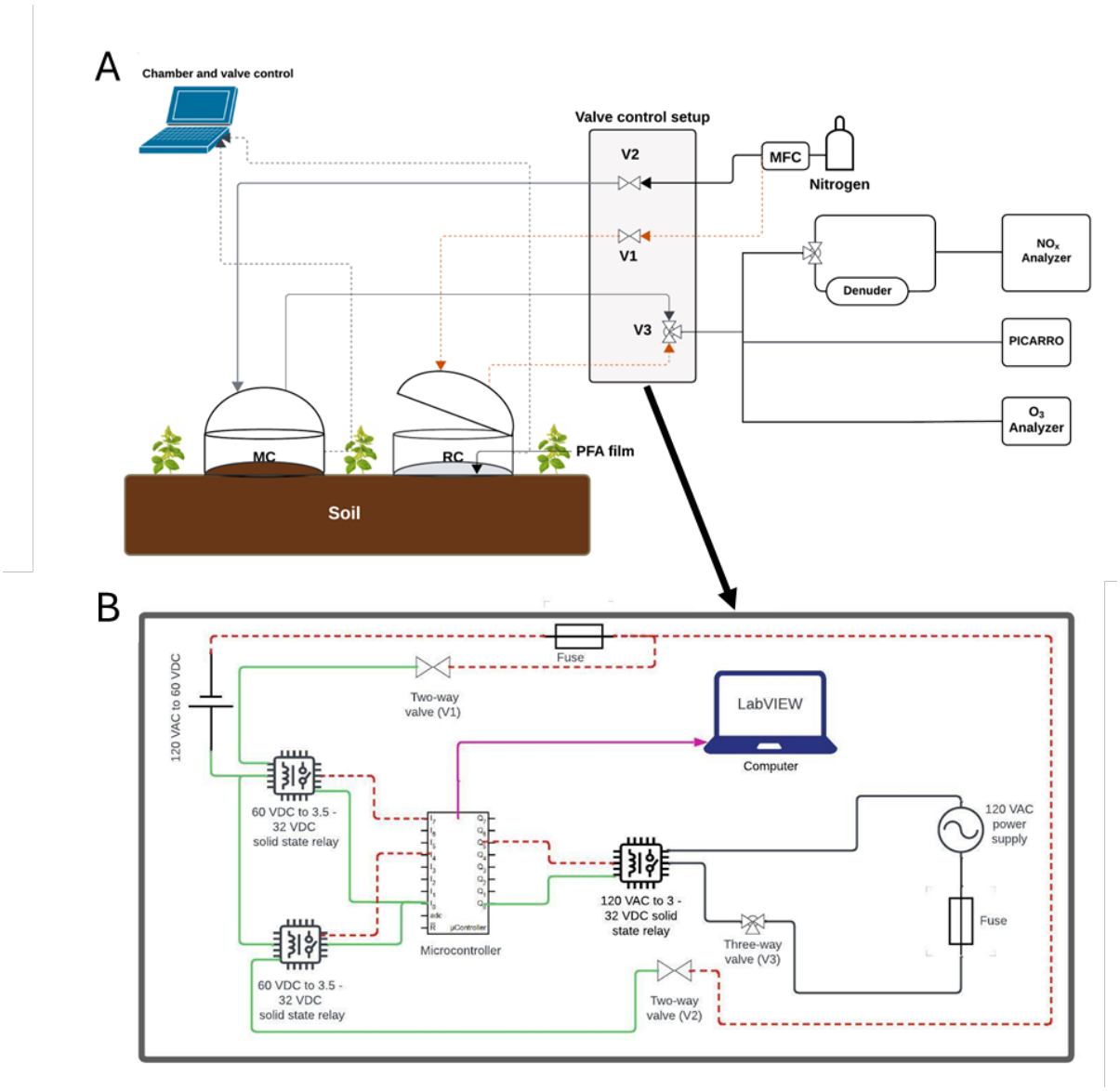

Figure 2.1: (**A)** Schematic of the dynamic chamber system to measure N_r and GHG fluxes. The components of the system include: the chambers, a dilution gas source (nitrogen (N_2) or zero air (ZA)), solenoid valve control, gas transfer lines, and gas analyzers. Grey lines indicate dilution gas flow from a source (e.g. cylinder) to the measurement chamber (MC) and air sampled from the MC to the analyzers. The dashed orange line represents these same flows relative to the reference chamber (RC). Communication lines from the chambers to a computer for automated control and ancillary sensor data collection using the chamber software (eoslink-AC; blue dotted lines). (**B**) The valve control setup for flow control in the complete dynamic chamber system, illustrating electrical components and lines needed for full automation using LabVIEW. It includes two 24 V DC two-way valves (V1 and V2; red dashed lines for negative electric potential, green for positive), with power supplied by solid-state relays, and a three-way 120 V AC valve (V3; black lines) with a power supply and another solid-state relay. The purple arrow represents the USB data acquisition connection from the microcontroller to a computer running the LabVIEW VI for valve control.

For an N_r sampling approach, one of the two chambers is used as the measurement (MC) to enclose an experimental surface while the second chamber acts as a reference (RC) by being sealed at the bottom with a film of 0.002" perfluoroalkoxy alkane (PFA; McMasterr-Carr®, PN: 84955K24). The inert PFA film is held in place between the chamber collar and our custom-made PTFE rings (**Figure 2.S1**). This modification provides a negative control observation for physical interactions on apparatus surfaces and associated chemistry when sampling reactive gases. The use of the RC, therefore, is to facilitate the correction of surface-mediated effects, reactions, and the reduction of bias when determining quantitative flux values.

Reactive gases require continuous correction for surface interactions and/or transformations as ambient levels are dynamic, so the RC component of this system design continuously baselines the physical interactions and chemistry happening on its surfaces both before and after quantifying reactive gas fluxes with the MC. Thus, the measurements are taken every 30 minutes, where one chamber is closed for gas analysis while the other is open to the ambient atmosphere. The sampling time interval was determined based on the lower limit of the range of field HONO flux values reported in the literature to ensure detection in its application during our pilot field study (**see Section 2.6**). The resulting accumulated mixing ratios of HONO in the chamber are well above the 1.4 parts per billion (ppbv) mixing ratio detection limit (LOD) of even a modified NO_x analyzer, such that it can be used for measuring HONO (Crilley et al., 2023; Lao et al., 2020; Zhou et al., 2018; Nodeh-Farahani et al., 2021).

Headspace recirculation to facilitate analyte mixing ratio enhancements for non-destructive spectroscopic GHG analysis is a common measurement approach to decrease flux observation times. Reactive nitrogen measurements, in contrast, are typically destructive techniques that change the identity of the target analyte in the act of quantifying its abundance. To interface with such instruments, the sampled air needs to be replaced (Linde Canada Plc, PN: NI LC250-230) to balance the flow demand in a closed chamber. This balance is delicate even when using mass flow controllers (MFCs) on both incoming and outgoing flows, and the best solution we identified is to provide a slight overflow that takes advantage of the chamber design to vent excess pressure through a short length (~15 cm) of 1/8" ID, ¼" OD tubing that keeps the internal pressure equivalent to ambient. The flow differential between make-up gas and sampling is roughly 400 $cm^3\ min^{-1}$. Such a supply of make-up gas was explored across a range of potential flow rates when

using destructive gas analyzers (e.g., three instruments each sampling at 1 - 4 standard litres per minute, L min^{-1}) to find that 6 L min^{-1} is the upper limit of flow-through where the chamber pressure is not substantially perturbed from ambient and the chamber lid retains its seal.

In the field, a flux measurement cycle begins with closing the RC while the MC is open. At defined intervals, they alternate their open-closed states. Flows of make-up gas to each chamber are modulated with a pair of two-way solenoid valves. When sampling from the RC, one valve (V1; **Figure 2.1**) is open to permit make-up gas flow while the other valve (V2) is closed to prevent the flow from being directed to the MC. On the sampling lines, a three-way solenoid valve (V3) alternates to guide flow from whichever is closed to the suite of gas analyzers. In this work, the gas instrumentation included a modified NO_x chemiluminescent analyzer (NO, NO_2, and HONO), a greenhouse gas and ammonia cavity ringdown spectrometer (H_2O, CO_2, CH_4, N_2O, NH_3), and a UV-absorption ozone (O_3) analyzer. All instrument and operational details are provided in **Section 2.3**.

2.2.1.2 Automated controls: system, data collection and processing

The chamber eosLink-AC software (Eosense Inc., Dartmouth, NS) is used to define the duration of chamber opening and closing cycles, and logs chamber temperature, pressure, and auxiliary sensor data associated with a given eosAC-LT chamber. Each chamber requires a 12 V DC power supply connected by USB to a laptop through a weatherproof communication cable, controlling the chamber lid and data transfer.

When a chamber cycle begins, a text file is generated and includes measurement time elapsed, chamber lid status, chamber temperature and pressure, and auxiliary sensor data. This data file is updated at least once every 10 seconds, varying between 2-8 second intervals, which we average onto a 1-minute time base to match measurements from the slowest gas analyzers. The solenoid valves are modulated by the electrical circuit shown in **Figure 2.1B**. Automation is facilitated by a microcontroller (NI-6509i, National Instruments) programmed with a custom-scripted LabVIEW VI (LabVIEW version 2020). The VI controls valve states (i.e., for V1, V2, and V3) and synchronization of the valve switching with respect to each chamber opening and closing cycle as described in the previous section. The VI also generates its own text file containing valve open/close state and a timestamp to be used for data processing. A custom R script (R Studio

v3.0.1) was developed to process the data file generated by eoslink-AC, data from all reactive gas analyzers, and the VI. Further design information and full details of this sampling strategy and script can be found in **Section S1** of the supporting information, and is available on the GitHub repository alongside our VI (https://github.com/fjs-vdblab/fluxchamber.git).

2.2.1.3 Reactive and greenhouse gas instrumentation for flux measurements

The mixing ratios of NO and NO_2 were measured using a commercially available chemiluminescent NO_x analyzer (EC 9841, American Ecotech, Warren, RI). The calculated LOD determined from sampling dry zero air was 0.84 ppbv, 0.67 ppbv and 1.07 ppbv for NO, NO_x, and NO_2, respectively. The instrument has an operating range of 0 – 20 parts-per-million by volume (ppmv), a sample flow rate of 0.5 L min^{-1}, and reports measurements at a time resolution of 1 minute. To quantify NO_2, it is reduced to NO on a heated molybdenum catalyst (325 °C). To prevent interferences from atmospherically-relevant acidic species in this system (e.g. HONO, HNO_3, and N_2O_5) the sampled air from the chambers during field experiments was passed through a sodium carbonate (Na_2CO_3) coated annular denuder to reduce bias in the NO_2 measurement, as these species and other components of NO_y (e.g. peroxyacetyl nitrate; PAN) may also be reduced to NO (Villena et al., 2012). The Na_2CO_3 denuder was prepared according to the EPA Compendium Method IO-4.2 (Winberry Jr et al, EPA, 1999) to remove atmospheric acids by reactive uptake to the basic coating. As part of our controlled laboratory and pilot field study experiments, this denuder was also used to selectively measure HONO by scrubbing this target gas for a specified period.

A commercial O_3 analyzer (Serinus 10, American Ecotech, Warren, RI) was used to measure mixing ratios, quantify O_3 loss to surfaces, and constrain the reaction of O_3 with NO to form NO_2 in the pilot study sampling. This analyzer employs a non-dispersive UV absorption cell to quantify O_3 in the sampled air. The calculated LOD from sampling zero air is 0.95 ppbv at 1 minute time resolution, with an operating range of 0 to 20 ppmv and a sampling flow rate of 0.5 L min^{-1}. Quality control procedures for the NO_x and O_3 instruments can be found in **Section S2**.

The mixing ratios of greenhouse gases (GHGs) and ammonia (NH_3) sampled from the automated chamber system were measured using a Picarro G2509 which uses cavity ring down spectroscopy

(CRDS) to simultaneously measure nitrous oxide (N_2O), methane (CH_4), carbon dioxide (CO_2), and NH_3 at ppbv levels, as well as water (H_2O) vapor at ppmv. The analyzer has a time response of ~ 8 seconds for N_2O, CH_4, CO_2, H_2O and < 2 min for NH_3. The Picarro G2509 instrument was used for measurements during both the lab experiments and the pilot study campaign. The customized version of the instrument had a sampling flow rate of ~0.23 L min^{-1}, and was equipped with an inlet filter. To minimize adsorption and chemical interactions of NH_3 on instrument surfaces, stainless steel gas handling components, including the inlet bulkhead, were replaced with PFA counterparts. The instrument cavity material was treated with a SilcoNert® coating by the manufacturer. The Picarro G2509 analyzer utilizes cavity ringdown spectroscopy to quantify the mixing ratio of the target analytes, and a full span calibration is not necessary to be performed regularly. Despite this, we validated its calibration and performed quality control checks in our laboratory to ensure the accuracy and stability of the analyzer for all aspects of this work presented below (**Section 2.S2**).

2.2.2 Chamber modifications to minimize NO_2 reactions on chamber surfaces

In order to transfer reactive gases through these chambers, interactions with surfaces need to be limited at all points of potential adsorptive or reactive losses. The custom-made base plate, consisting of two rings made from PTFE sheets with a PFA film pinned between them (**Figure 2.S1**) was used to assess gas interactions on chamber surfaces and acts as the RC for field measurements. From this starting point, commercial components were identified for replacement. First, the gas inlet and outlet push-to-connect fittings in the original chamber configuration have plastic grips, with an internal component made of brass, which is informally known in the atmospheric chemistry community to have strong interactions with nitrogen oxides. These brass fittings were replaced with PTFE Swagelok® bulkhead fittings (PN: T-400-1-4**)** as shown in **Figure 2.S2**. Similarly, the polyacrylate wall and lid surfaces of the chambers were considered, which are, by design, actinically transparent to ensure PAR is transferred to any contained plants or surfaces. To retain this visible radiation transparency, while also making the surface more inert, we applied 0.002” thin PFA film to the inner surfaces using double-sided tape (**Figure 2.S2**).

2.2.3 Chamber modification validation using greenhouse and reactive gases

The design of the chambers by the manufacturer is to transfer GHGs to non-destructive gas analyzers by recirculating the headspace. Before and after our modifications, we had to ensure that

the non-reactive GHGs were still transferred through the system. In addition, we challenged the transfer of N_r gases by controlled gas delivery. It was expected that N_r gases could undergo interactions and/or chemical transformations on the chamber surfaces and sampling tubing that would differ between the unmodified and modified variants. Determining the time constants of fill and decay of these reactive gases in the chamber allowed us to contrast their behaviour against that expected from a modelled theoretical inert trace gas in our system (**Figure 2.2**). Equations used to model mass transfer in our chambers were derived from Pape et al. (2009). The resulting accumulation curve was modelled by the theoretical function:

$$\mu_{fill} = 1 - e^{-\left(\frac{t}{\tau_{fill}}\right)} \quad \textbf{(E1)}$$

$$\tau_{fill} = V/Q_{fill} \quad \textbf{(E2)}$$

Where μ_{fill} represents the normalized mixing ratio of the gas in the chamber at the time t (min) after closing of the chamber compared to the maximum mixing ratio within the measurement cycle, τ_{fill} is theoretical accumulation timescale for transfer of an ideal inert gas (min), V is the volume of the chamber (0.072 m^3), and Q_{fill} represents the total experimental flow rate (2 L min^{-1}). Similarly, the theoretical decay curve when emptying the chamber **(E3)** can be obtained, where τ_{empt} is the theoretical decay timescale for gas transfer (min) and Q_{empt} is again the total experimental flow rate (2 L min^{-1}).

$$\mu_{emp} = e^{\left(-\frac{t}{\tau_{emp}}\right)} \quad \textbf{(E3)}$$

$$\tau_{emp} = \frac{V}{Q_{emp}} \quad \textbf{(E4)}$$

2.2.3.1 Instrumentation and materials for control experiments

Control experiments for the transmission of inert and reactive gases were conducted by filling and emptying the chambers with known quantities of the target gases at mixing ratios relevant to the atmosphere, as well as in quantities that would accumulate during real observations of modest fluxes (e.g. from a fertilized farm field). Measurement of NO, NO_2 and HONO was performed using the modified NO_x analyzer, the GHGs (CO_2, CH_4 and N_2O) and NH_3 with the Picarro G2509, and O_3 with the UV-absorption instrument. Details of the generation of gas concentrations can be found in **Section S3** of the SI.

2.2.3.2 Filling and emptying experiments with N_r, O_3, and GHGs

The positive control experiments filled the chambers in both modified and unmodified configurations, where the time constants were calculated from the measurements to compare against a theoretical inert and perfectly transferred gas (i.e. lost by dilution and removal to analyzers only). In each filling experiment, the chamber was flushed with pure N_2 from a liquid N_2 dewar (Linde Canada, PN: NI LC250-20) until a stable baseline level of each gas mixing ratio was reached; typically, these were values at the analyzer detection limits. Then, a blend of GHGs or one of the N_r analytes was delivered into the chamber along with N_2 as the dilution flow at a total flow rate of 2 L min^{-1}, and this was then sampled at a total of 1.8 L min^{-1} by the analyzers (**Figure 2.S4**). The gases were added to the chamber from their respective calibration sources until the observed concentration (C) reached the known value being delivered (C_0), within error. Since different mixing ratios of the gases were added for these control experiments, the use of normalized concentrations was necessary to facilitate data analysis and visualization. Where surface interactions could be identified (e.g. for NH_3), the role of surfaces versus air exchange has been explored using double exponential fits (see **ES-1 and ES-2 in Section S3**) (Crilley et al., 2023; Ellis et al., 2010; Moravek et al., 2019). The gases were emptied back to the initial baseline level observed with clean dilution gas before starting the next replicate or a new filling experiment with a different target gas. Time constants for filling and emptying were then determined by fitting the experimental observations in Igor Pro8 (Wavemetrics, Portland, OR, US).

Similarly, the Eosense eosMX multiplexer is designed to coordinate chamber flux measurements using eosAC chambers with non-destructive analyzers, such that headspace can be recirculated while the chambers are closed. One of these devices was characterized for the transmission of GHGs and N_r gases, alongside similar modifications. This system is appealing as it has the eosLink-MX software (Eosense, V1.9.07), which is used for communication, scheduling actions, and logging peripheral data from all connected eosAC chambers. It features dedicated chamber tubing inlets and outlets, along with a COMM port supporting up to 12 eosAC chambers. Each chamber channel includes two Swagelok gas fittings for transporting gases to analyzers and for either recirculating, or in the case of N_r measurements, supplying a purging gas to the chamber headspace.

To optimize the performance for N_r species, the original stainless-steel (SS) Swagelok fittings and solenoid valves were compared against replacement PFA tube fittings, bulkhead unions (Swagelok, PFA-420-61), and a PTFE 3-way valve (Clippard, NR1-2-12-G2). A 2 L min^{-1} flow of dry zero air containing the target compounds was passed through either the SS valve with SS fittings or the PTFE valve with PFA fittings for 30 minutes each. The flow was measured before and after the valves to ensure the setup was leak-free. The ratio of the transferred gas amount to the nominal was used to identify impacts of surface interactions on quantitative transmission to downstream gas analyzers. Further details are presented in **Section S4**.

2.2.4 Characterization of NO_2 loss on chamber surfaces

All losses of NO_2 in the chamber were characterized by the addition of known NO_2 mixing ratios to the chamber under a variety of relevant conditions (**Figure 2.S5**). The experiments were performed progressively, starting from the unmodified configuration of the chamber, replacement of fittings, and covering the inner surface with PFA film to quantify their efficacy in minimizing NO_2 loss and/or transformation on chamber surfaces.

Different RH values were produced inside the flux chamber by combining flows of dry zero air (ZA) and one saturated with water vapour by transiting a 500 mL Pyrex impinger filled with deionized water (e.g. equal 1 L min^{-1} flows combine to an RH of 50%). A high-precision, research-grade humidity probe (HMP60, Vaisala Oyj, Finland; ± 3% at 0 - 90% RH, ± 5% at 90 – 100% RH) was connected to the chamber to confirm the set point by measurement in the chamber. The flow from an NO_2 calibration cylinder (Linde Canada; PN: NI NX5MC-AQ; 5.9 (±5%) ppm) was adjusted using an MFC and combined with a dilution flow of ZA to achieve mixing ratios of 5, 7 and 10 ppbv. The total flow rate for these experiments was 2.0 L min^{-1} and a vacuum pump (62.3 L min^{-1}, PN: UZ-07061-22, Gast Manufacturing Inc., Benton Harbor, MI, USA) with an MFC (10 L min^{-1}, PN: 1179C01314CR1BV, MKS instruments Inc, Andover, MA, US) was used to make up the sampling flow beyond the 0.5 L min^{-1} of the NO_x analyzer. The same flow difference stated above was maintained in the chamber, using the built-in vent.

Quantification of NO_2 and HONO in the air sampled from the chamber can be achieved using the alternating solenoid setup depicted in **Figure 2.S5**. The sampled air is switched between two channels – one directly to the NO_x analyzer and the other through a Na_2CO_3-coated denuder – modulated every 5 minutes by a three-way solenoid valve (Fluoroware Galtek 1/4" F-NPT 3-way

solenoid valve, 115V, PN: 203-3414-415. Entegris Inc., MN, US). When the sampled air flows directly to the analyzer, the total mixing ratio of NO_2 and acidic NO_y species, like HONO and HNO_3, is measured and has been termed NO_2^* (Crilley et al., 2023; Lao et al., 2020; Zhou et al., 2019). When the flow is directed through a Na_2CO_3 denuder, it selectively scrubs HONO and HNO_3, leaving behind NO_2 (Possanzini et al., 1983). Under the controlled NO_2 composition used in our experiments, it is expected that HONO will be the only acid present in the sampled air, as such experimental systems have been thoroughly characterized by Finlayson-Pitts et al. (2003),, and HNO_3 is retained on the surfaces (**R3)** (Barney & Finlayson-Pitts, 2000; Huang et al., 2002; Kamboures et al., 2008). As a result, by the differential measurement of mixing ratios recorded in the two channels (**E5**) every 5 minutes, HONO can be quantified.

$$HONO = NO_2^* - NO_2 \qquad \textbf{(E5)}$$

To quantify the amount of NO_2 lost to the chamber surface relative to the mixing ratio of NO_2 added to the chamber during an experiment, the NO_2 loss fraction (f_{NO2}) is informative for mass balance between the two processes. Comparison of each chamber modification on f_{NO2} helps identify which changes are essential in minimizing losses. Experiments using 5 ppbv of NO_2 at 85% RH added to the chamber were used to quantify f_{NO2} in the unmodified configuration (n=3), to derive an upper limit of irreversible loss to surfaces or chemical loss via surface hydrolysis (**R3**). Following the materials characterization experiments, additions of atmospherically relevant 5, 7 and 10 ppbv mixing ratios of NO_2 at three different RH values (45%, 65% and 85%) to the fully modified chamber were used to characterize and develop a correction methodology for the surface loss. The mixing ratios of NO_2 and RH values selected for these experiments are representative of the ambient atmosphere in urban areas (Toronto North Station, ECCC), where the chamber system was envisioned to be deployed.

2.5 Drivers of O_3 loss to chamber surfaces

We tested how modifications and aging of the interior chamber surfaces affected O_3 transfer. It is among the most sensitive/reactive species to transfer through this new system and is expected to drive reactive loss of NO when measuring N_r fluxes. The fraction of O_3 lost to chamber surfaces was first quantified using a clean and unmodified chamber with PTFE bulkhead fittings replacing the push-to-connect brass fittings. Prior to O_3 addition, the chamber was flushed with ZA until the background level of O_3 was at the instrument detection limits. Three mixing ratios of O_3 of 150,

200 and 250 ppb were generated by a GasCal 1100 dilution calibrator with integrated O_3 generator and photometer (American Ecotech, Warren, RI) and added to the chamber for 60 mins or until a constant concentration was reached. Two replicate runs of each addition level were performed.

The fraction of O_3 lost to chamber surfaces was quantified in duplicate on a modified chamber with the interior chamber surfaces covered by brand new 0.002" thick PFA film in a separate set of experiments. The same mixing ratios of O_3 were delivered in duplicate to the modified chamber operated for lab and field experiments, so that the PFA film had been attached to the inner surface of the chamber and exposed to ambient air for more than two years, with 15 days of continuous use in an agricultural field during our pilot study. In all three experiments, the lost fraction of O_3 was determined for each mixing ratio delivered.

2.2.6 Proof of concept N_r fluxes from agricultural soils

2.2.6.1 Soil sample N_r emissions for lab experiments

Randomized soil samples weighing 4-5 kg were collected into Ziplock bags from an eight-plot grid established for an agricultural field site in Lambton County, ON, Canada (43°09'36.0" N 81°55'48.0" W). The samples were used to investigate emissions in the lab with and without the addition of fertilizers. Individual and pooled samples from the field plots were used. Bulk soil samples were prepared for lab-based chamber measurements by removing debris, roots and seeds, followed by oven drying at 35 °C for 24-72 hours on a stainless-steel mesh tray covered with aluminum foil, to prevent alteration of the microbial community from exposure to unrealistic temperature regimes. After drying, samples were stored in Ziploc® bags at room temperature until use.

Ultrapure water (18 MΩ·cm; Milli-Q®, Sigma-Aldrich, St, Louis, US) was added to approximately 350 g of a dry soil sample to achieve ~28% volumetric water content (VWC). The soil sample was loaded into the chamber on a foil-lined tray, and the water content was measured using a soil moisture probe inserted fully into the sample (TEROS 11, VWC range for mineral soils: 0.00 – 0.70 m^3/m^3; accuracy: ± 0.03 m^3/m^3; resolution: 0.001 m^3/m^3, METER Group Inc., WA, USA). The chamber was then sealed against intrusion from room air, and dry ZA was added to the chamber during the drying period. A modified NO_x analyzer measured NO, NO_2 and HONO following our usual configuration, while the Picarro G2509 measured N_2O and NH_3 fluxes. Both instruments monitored unamended soil samples and others fertilized with urea ($CO(NH_2)_2$),

ammonium carbonate (AC, $(NH_4)_2CO_3$), ammonium bicarbonate (ABC, NH_4HCO_3) at rates of 100 kg N ha^{-1}. A similar experiment was conducted with ammonium nitrate (NH_4NO_3) at the same fertilizer rate using only the modified NO_x analyzer. Soil VWC and headspace RH were recorded using auxiliary sensors within the chamber.

2.2.6.2 Field deployment of automated dynamic N_r chambers

The RC and MC setup was deployed to make automated N_r flux measurements from the same agricultural field as the lab-based soil samples described in the prior section. The observations took place in early September 2022 at the end of a soybean cropping season. A detailed description of the campaign and its results is the subject of a separate work, so we provide a brief overview here relevant to demonstrating the utility and procedure of an RC/MC chamber pair to determine fluxes from field observations. The total measurement period was approximately two weeks in duration to test the performance of the designed system. Generally, conditions were hot and dry, without precipitation, and the soybeans surrounding the observed soils were undergoing senescence during the measurement period. The chambers were deployed only on the soil, between crop rows, and operated to quantify fluxes as outlined in **Section S7**. After an initial 7-day period of observing baseline fluxes from the field, an experimental perturbation was conducted to stimulate N_r emissions through the addition of an aqueous urea solution equivalent to 22 kg N ha^{-1} of fertilizer added by broadcast application, followed by washing into the soil by an equivalent of 2.5 cm (1") of rain. The modified NO_x analyzer and the Picarro G2509 were used to measure the N_r and GHG fluxes continuously across both periods.

2.2.7 Soil flux determination

The flux of a gas is the rate at which it is released and/or transferred across a surface or an interface (e.g., soil to atmosphere) per unit area per unit time. Gas fluxes are of high interest in agriculture as they give insight into the uptake or emission of N-bearing gases that may lead to fertilizing, or loss of fertilizing effects, respectively. Fluxes are also important for assessing the state of plants or soils at interfaces through metrics like primary productivity, in which case measurement of a GHG like CO_2 provides the insight (Anthony & Silver, 2024; Li et al., 2016; Okiti et al., 2025). The RC captures environmental fluctuations such as temperature or pressure change and directly observes the interactions of ambient gases with surfaces within the sampling setup, as well as

tracking reactions, allowing for corrections to every net flux (F_{net}) measurement cycle (**E6** for reactive gases and **E7** for non-reactive gases; as derived in **Section S7**).

$$F_{\text{net}} = (\lambda).\left(\frac{V}{A}\left(\frac{\Delta C_m}{\Delta t_m} - \frac{\Delta C_r}{\Delta t_r}\right) + \frac{Q_{\text{out}}}{A}\left(\frac{\int_{t_{1m}}^{t_{2m}} c_m(t)\ dt}{\Delta t_m} - \frac{\int_{t_{1r}}^{t_{2r}} c_r(t)\ dt}{\Delta t_r}\right)\right.$$
$$\left. - \frac{V}{A}\left(\frac{\int_{t_{1m}}^{t_{2m}} R_m(t)\ dt}{\Delta t_m} - \frac{\int_{t_{1r}}^{t_{2r}} R_r(t)\ dt}{\Delta t_r}\right)\right)$$

E6

Where V is the volume of the chamber (m^3), A is the surface area (m^2) enclosed by the chamber and governing the gas flux; Q_{out} is the volumetric flow rate of air exiting the chamber ($m^3\ s^{-1}$; $c_m(t)$ and $c_r(t)$ are target gas concentrations within the measurement and reference chamber (mol m^{-3}), respectively; $\frac{\Delta C_m}{\Delta t_m}$ and $\frac{\Delta C_r}{\Delta t_r}$ represent their corresponding rates of change (mol $m^{-3}\ s^{-1}$); and F_{net} is the resulting net gas flux per unit area (mol $m^{-2}\ s^{-1}$).The terms R_m and R_r denote the instantaneous chemical production or loss rate expressed in units of mol $m^{-3}\ s^{-1}$ for consistency. The dimensionless attenuation factor λ is required to correct for interactions of reactive gases with chamber surfaces. Such surface interactions, which are particularly strong for gases like NH_3, significantly reduce the measured rate of concentration change within the closed chamber (**Figure 4**). Thus, λ is derived as the ratio between a theoretical unattenuated gas and the target gas concentration from controlled deliveries integrated over the chamber closure interval as derived in **Section S7**. The attenuation correction removes bias from chamber-induced artifacts in flux estimates, so that more accurate soil–atmosphere exchange is reported.

$$F_{\text{net}} = \lambda \cdot \frac{P_{\text{air}}}{R \cdot T} \cdot \left(\frac{V}{A}\left(\frac{\Delta X_m}{\Delta t_m} - \frac{\Delta X_r}{\Delta t_r}\right) + \frac{Q_{\text{out}}}{A}\left(\frac{\int_{t_{1m}}^{t_{2m}} X_m(t)\ dt}{\Delta t_m} - \frac{\int_{t_{1r}}^{t_{2r}} X_r(t)\ dt}{\Delta t_r}\right)\right)$$

E7

For inert gases in **E7,** the fluxes can be based on mixing ratios, where $X_m\ and\ X_r$ are the gas volumetric mixing ratios (mol X per mol air), P_{air} is the air pressure (Pa), T is the absolute

temperature (K), and R is the universal gas constant (J mol^{-1} K^{-1}). By comparing the RC and MC observations, we isolate the effects of specific environmental conditions on N_r (**E6**) or GHG (**E7**) exchange fluxes, while accounting for surface effects and chemical transformations in the former.

2.3 Results

2.3.1 Determining time constants of reactive nitrogen and GHGs

The time constants of both filling and emptying the chambers were calculated using concentrations normalized to their initial values, for each N_r gas and GHG. These were used to quantify gas transfer times through the chambers and to confirm performance relative to theory. Where departures were identified, we quantified the extent of surface interactions for the various target analytes, allowing for corrections to be implemented for determining in situ fluxes **(Table 2.1, Figure 2.2)**.

2.3.1.1 Time constants of greenhouse gases (GHGs)

Determination of the GHG time constants allows benchmarking of the chamber performance prior to and after modifications, which then allows us to contrast the behaviour of transferred reactive gases through the chambers. In both the modified and unmodified chambers, the greenhouse gases CO_2, CH_4 and N_2O were anticipated to behave as non-reactive trace gases with little to no physical interactions on chamber surfaces, nor to undergo chemical transformations.

The theoretical fill and empty rates for the chambers with a flow rate of 2 L min^{-1} are 36 min. The average measured time constants of filling with the greenhouse gases CH_4, CO_2, and N_2O in the unmodified chamber were found to be 37 ± 1 min, 37 ± 2 min, and 37 ± 1 min, respectively (**Table 2.1**). During the emptying phase, the average time constants for CH_4, CO_2, and N_2O were 37 ± 1 min, 37 ± 1 min, and 38 ± 2 min, respectively. These measurements are not different from theory within the limits of experimental accuracy, demonstrating that GHGs do not deviate from the values modelled for an ideal trace gas (**Figure 2**). In either experiment, the time constants did not change in the presence of the chamber modifications. Since the GHGs are effectively transferred through both the modified and unmodified configurations of the chamber, the baseline performance of the chambers was not affected by the hardware modifications. Therefore, comparison of these results with the time constants of N_r gases provides a description of their interaction or transformation processes on the modified chamber surfaces.

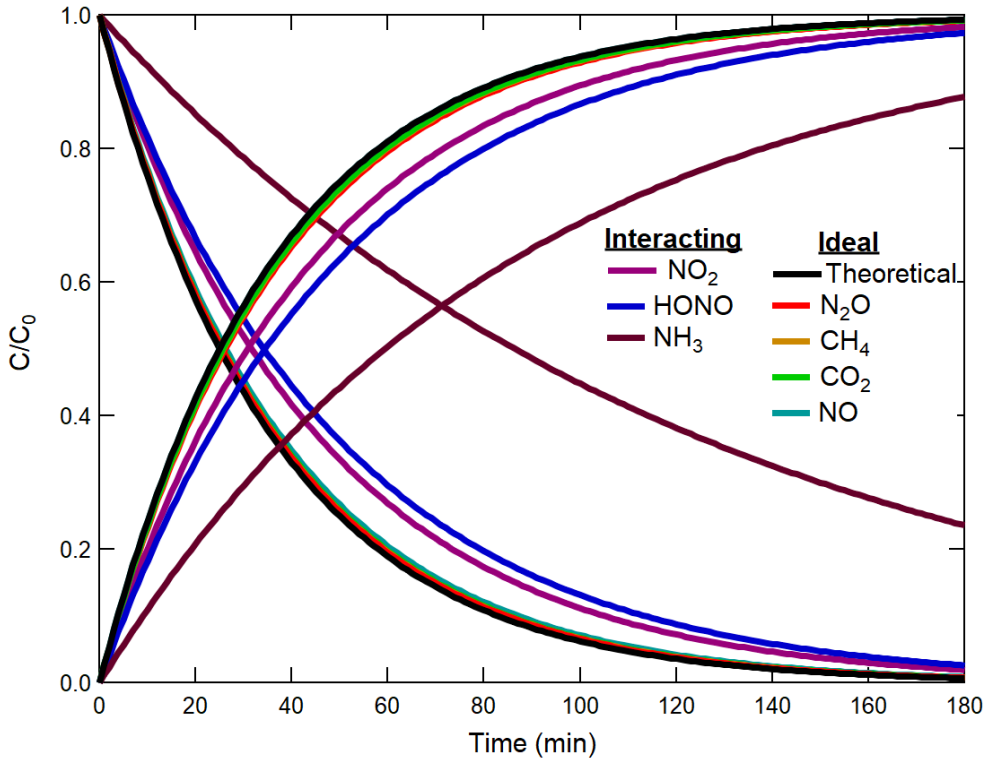

Figure 2.2: Addition of reactive nitrogen gases and greenhouse gases to a modified dynamic chamber. For clarity, the coloured traces show the fitting curves corresponding to the response time in concentration normalized to the delivered value of each gas while filling and emptying the chamber. The black trace corresponds to a perfect non-reactive transfer of an ideal trace gas based on volume transfer in the chamber only. Note that the N_2O, CH_4, CO_2 and NO fill and empty traces all overlap with the theoretical fill and empty curves.

2.3.1.2 Time constants of reactive nitrogen gases

In the modified chamber, the time constant of filling or emptying with NO was 38 ± 1 min. The obtained NO time constants are similar to GHGs, as NO is not expected to have strong surface interactions. The slower time response of the NO_2, HONO, and NH_3 measurements is determined by two processes: (1) the exchange of the sample air volume in the inlet line and the chamber, and (2) the adsorption and desorption of the gas onto and from the chamber surface (Whitehead et al., 2008). Increases in surface interactions were observed for increasingly polar gases in the order of NO_2, then HONO, and most for NH_3 (**Figure 2.2**). The highest change in the time constants between the modified and unmodified configurations was 2.6 ± 2.5 min, observed for HONO, with smaller improvements observed for NO_2 and NH_3 during the filling process. Improved time constants when emptying reactive nitrogen from the chambers had similar trends (**Table 2.1**).

Overall, the deviations for these gases to longer time constants than those expected from an inert molecule can be attributed to their polar, ionizable, and/or reactive nature. For example, NO_2 is lost more readily than NO, possibly through its known reaction on surfaces to make HONO and HNO_3, being lost itself in the process (Finlayson-Pitts et al., 2003). It also has higher water solubility than NO, but lower than for HONO or NH_3. Similarly, a decrease in transmission efficiency for HONO could be explained by its weakly acidic nature (pKa = 3.16) (Silva et al., 2006) and solubility in water (Henry's law constant = 0.48 mol/m^3 Pa; (Schwartz & White, 1981) that facilitate partitioning and dissociation in surface water films, which could generate non-volatile nitrite (NO_2^-) on chamber surfaces. This chemistry will slow the transfer of gas-phase HONO through the chambers, as the NO_2^- would need to protonate before being lost as neutral HONO when repartitioning to the gas phase (**R4, R5)**. Finally, the most delayed transmission rate is for NH_3, likely because it undergoes strong inter-molecule interactions and ionization on the chamber surfaces and/or any interfacial water (Henry's law constant = $5.9*10^{-1}$ mol/m^3 Pa (Orkin et al., 2011); pKa = 9.25 (Lide, 2009), as well as on tubing surfaces and potentially partitioning into the tubing before reaching the analyzer (Pagonis et al., 2017).

The determined surface impact values (D; Table 1) demonstrate an expected greater impact of surfaces when no reactive gas is present in the headspace prior to filling, and a lesser effect during emptying when the surface has been exposed and equilibrated with the analyte, which is commonly referred to as passivation. As a result, increasing delays from NO through NH_3 exist in our N_r gas suite due to increasingly stronger interactions with chamber surfaces and gas handling lines. For NH_3 specifically, the fill has a D value of 89%, while during emptying it is only 23%. This is due to all sample handling surfaces not being passivated prior to filling, similar to our findings with NH_3 transfer for other N_r instruments (Crilley et al., 2023). In contrast, during the emptying process, desorption occurs over previously exposed surfaces ending at the instrument, reducing the extent of surface effects. The surface interactions for these gases are minimized in the modified chambers to facilitate more time-efficient measurements of surface exchange. However, they necessitate the use of the λ term when deployed in the measurement-reference configuration for those N_r species which experience partial transmission, such as NH_3. The λ term is required to obtain accurate values, as the enclosed flux measurement surface should be perturbed for the least amount of time possible when making field measurements, and the chambers cannot be closed for several hours to allow surface-active gases to passivate the lines. In addition, minimizing the

potential for transformations reduces the frequency required for in-field characterization of these processes through positive and negative gas delivery controls. For NO_2, specifically, we sought to quantify this as a function of modifying components of our chambers, as NO_2 is the most reactive gas in our suite.

Table 2.1. Summary of time responses of addition and removal of GHGs and N_r gases to and from a chamber at 2 L min^{-1} in unmodified and modified configurations. Time responses here correspond to a theoretical fill or empty e-folding time response of 36 minutes. Where analytes were observed to undergo surface interactions, a double exponential fit was used to characterize them, with the first time constant representing the known gas exchange rate being fixed at 36 minutes, as this was observed for the non-reactive gases, and the second time constant is reported (*) alongside an assessment of the relative magnitude of surface interactions, through the D-value (%) (Crilley et al., 2023; Ellis et al., 2010; Moravek et al., 2019). Variability shown is one standard deviation of the mean from replicate experiments (n=3).

Gas species	Direction	Unmodified (min)	Modified (min)	Improvement (min)	D (%)
NO	Fill	38.8 ± 0.7	37.8 ± 0.6	1.0 ± 0.7	-
	Empty	37.9 ± 1.5	36.0 ± 0.6	1.9 ± 2.1	-
NO_2	Fill*	18.9 ± 0.6	18.0 ± 3.1	0.9 ± 3.2	94 ± 18
	Empty*	21.2 ± 1.2	20.4 ± 1.4	0.8 ± 1.9	78 ± 21
HONO	Fill*	21.9 ± 1.1	19.3 ± 1.2	2.6 ± 1.6	74 ± 10
	Empty*	23.2 ± 1.4	21.2 ± 0.9	2.0 ± 1.7	71 ± 9
NH_3	Fill*	69.6 ± 0.4	68.2 ± 0.5	1.4 ± 0.6	89 ± 3
	Empty*	76.9 ± 0.8	75.0 ± 4.6	1.9 ± 4.7	23 ± 4
CO_2	Fill	37.9 ± 1.5	37.0 ± 1.8	0.9 ± 2.3	-
	Empty	38.0 ± 1.8	37.0 ± 1.2	1.0 ± 2.2	-
CH_4	Fill	37.9 ± 1.1	36.8± 1.2	1.1 ± 1.6	-
	Empty	39.1± 1.7	37.2 ± 1.2	1.9 ± 2.1	-
N_2O	Fill	38.6 ± 2.1	36.7 ± 1.2	1.9 ± 2.4	-
	Empty	39.7 ± 1.3	37.7 ± 1.6	2.0 ± 2.1	-

2.3.2 Multiplexer modification impacts on gas transfer

The multiplexer (eosMX; Eosense Inc.) allows us to operate up to twelve dynamic chambers simultaneously with a suite of gas analyzers, such as the Picarro G2509, NO_x, and O_3 analyzers. However, the commercial multiplexer is constructed with stainless steel (SS) valves and fittings that would be expected to facilitate strong interactions or losses of target gases in the N_r analyte suite. Valves and fittings made of SS have a higher tendency to chemically interact and/or adsorb reactive gases compared to fluoropolymer replacements. To address this uncertainty, the gas transfer efficiency as a percentage loss in the multiplexer versus a bypass line was evaluated specifically for NH_3 and NO_2, alongside standard GHGs as they passed through fittings and gas handling solenoid valves made of SS or PFA and PTFE replacement parts.

The loss fractions were modest and measurable when connected to the analyzers using minimal lengths of PFA tubing (~50 cm). The most substantial loss of gases was observed on SS, in which the highest reactivity and/or adsorption were expected due to its known tendency to interact with reactive gases (Vaittinen et al., 2014). When the GHGs were delivered after dry zero air into the SS setup for 30 minutes, typical of a chamber closure period, their losses ranged from 10% for N_2O to 19% for H_2O. Meanwhile, NO_2 exhibited 17% loss on the SS surfaces, and the greatest effect was seen for NH_3 with a loss of 38% (**Figure 2.S6**). In contrast, losses on the chemically inert and hydrophobic surface of the PFA fittings and PTFE valve were negligible (<1%) for most gases, except for NH_3, which still exhibited a measurable loss of 11%. Other reports have also shown up to 15% loss of NH_3 at atmospheric pressure on PTFE and PFA surfaces (Ellis et al., 2010; Shah et al., 2006; Vaittinen et al., 2014). While it is expected that the SS would eventually passivate and improve the transmission of the GHGs in a standard recirculation approach, this is not likely to be the case for destructively analyzed N_r and even more so if it facilitates a chemical transformation. Overall, we found that replacing the multiplexer SS valves and fittings with PFA fittings and PTFE valves provided a 9–27% reduction in surface losses of N_r compounds and GHGs. We strongly recommend the use of PTFE and/or PFA materials over SS for more accurate measurement of N_r species when interfacing the dual chamber setup with the destructive N_r analyzers needed for field flux measurements, whether using a custom setup of the commercially available multiplexer.

2.3.3 Minimizing NO_2 losses and determining controlling variables

In addition to the rate of transfer of N_r gases, chamber modifications are necessary to prevent reactive losses. The lost fraction of NO_2 (f_{NO2}) to chamber surfaces was quantified by the addition of known mixing ratios of calibration gas to the chamber in both the unmodified and modified configurations under atmospherically relevant humidities. These experiments enabled us to determine the magnitude of NO_2 lost to the chamber and gas transfer tubing surfaces due to chemical and/or physical transformations, as well as demonstrate the effectiveness of the different chamber modifications in minimizing these losses. For NO_2, a probable chemical transformation pathway is its heterogeneous conversion to HONO (**R3**), which is favourable under atmospherically relevant humidities and the resulting water-adsorbed surfaces expected to exist throughout the chamber and sampling lines.

2.3.3.1 Chamber modification impacts on NO_2 losses

The average fractional loss (f_{NO2}) for an unmodified chamber and one modified with the PFA film and PTFE bulkhead fittings was measured under conditions of 83% RH and 5 ppb of NO_2. Substantial reduction in NO_2 loss and transformation was observed from the implemented modifications. In the original unmodified configuration of the chamber, f_{NO2} was 0.36 ± 0.02 (**Figure 2.S7**). When the interior chamber surfaces were covered with a film of PFA, it was reduced to 0.22 ± 0.03, a relative decrease of 18%. This is consistent with the acrylic chamber surfaces and fasteners to the chamber frame, facilitating physical and/or chemical loss of NO_2.

The film of PFA, along with other fluoropolymers, is known to have excellent chemical resistance and low reactivity towards a range of chemicals, including NO_2 (Ebnesajjad, 2005; Graham et al., 1997). In addition, the superhydrophobic nature of these materials prevents the accumulation of water on the surfaces, which is known to facilitate atmospheric surface reactions of NO_2 (Finlayson-Pitts et al., 2002; Jenkin et al., 1988; Stutz et al., 2002) and create analytical bias in the measurement of trace gases like HONO, especially when instrument gas sampling inlets do not take this into account (Crilley et al., 2019; Von Der Heyden et al., 2022).

The replacement of the brass-lined push-to-connect bulkhead fittings with PTFE led to a similar decrease in f_{NO2}, which was reduced by 17% to a final value of less than 0.05 ± 0.02 (**Figure 2.S7**). These fitting surfaces act as the largest surface-driven NO_2 loss despite their surface area being

very small compared to that of the entire chamber configuration and with a very small contact time against the gas sample (0.012 s per fitting at a flow rate of 2 L min^{-1}).

The loss of NO_2 in the commercially available system is challenging to attribute solely to the heterogeneous hydrolysis reaction. During the characterization experiments, the conditions inside the chamber were matched to those reported by previous lab studies, which have shown that high RH, presence of NO_2, and surface adsorbed water on surfaces favour this loss mechanism (Jenkin et al., 1988; Stutz et al., 2004). The reaction is known to occur on surfaces such as Pyrex (Jenkin et al., 1988) and borosilicate glass (Finlayson-Pitts et al., 2002), but no prior studies to date, nor this study, have demonstrated metallic surfaces as facilitating this mechanism.

Overall, chamber modifications were effective in minimizing NO_2 losses. The inert PTFE fittings dramatically minimized transformations, while PFA film lining the inner chamber surfaces was also effective, but less so. Our results indicate that water-adsorbed and metallic surfaces, such as brass, facilitate substantial loss and/or transformations of NO_2. Further investigation is required to confirm the mechanism(s) at play and is beyond the scope of this work.

2.3.3.2 RH-facilitated NO_2 loss as a function of concentration

A complete characterization of f_{NO2} and the amount of HONO in the fully modified chamber was determined under a range of environmentally relevant RHs and NO_2 concentrations. We found that the absolute and fractional NO_2 losses were highest under the highest RH conditions (85%; **Table 2.2**). However, the f_{NO2} does not appear to follow a concentration-dependent trend across the additions made at lower RHs, with at most 0.4 ppbv NO_2 lost across the remainder of the tests, a value which is equivalent to the LOD of the NO_x analyzer used. This would generate 0.2 ppbv of HONO according to the disproportionation of the hydrolysis mechanism, which is well below the analyzer detection limits. Overall, the modifications successfully reduce NO_2 losses below 10% across all environmentally relevant conditions the chambers are expected to encounter, with our findings here suggesting that the mass lost is nearly constant and independent of NO_2 mixing ratio at RHs below 85%, while being marginally higher at and above this value.

Quantifying f_{NO2} and the amount of HONO made in the chamber is required for the correction of field datasets. Quantifying NO_2 loss to the chamber surfaces allows us to prevent bias when

reporting NO_2 exchange processes on environmental surfaces, as the magnitude of the losses attributed to chamber surfaces versus the surface studied can be corrected. The system, via the reference chamber, can also quantify any changes in these processes over time if standard concentration additions to the headspace are conducted. Consequently, important parameters such as NO_2 deposition fluxes on surfaces can be better estimated (Pape et al., 2009).

Since the inferred HONO mixing ratios from the chamber surfaces across various environmental RHs are nearly invariant at 0.2 ± 0.1 ppbv, it is simple to background correct any observational datasets by subtracting this amount from the total HONO measured in the chamber if a more sensitive analyzer is used during field or lab experiments. In addition, as the NO_2 values expected in most atmospheric gas samples during field measurements are well into the ppbv range (>3.3 ppbv per 30-minute flux measurement for a 1.4 ng m^{-2} min^{-1} emission), the corrections would be easy to implement in post-processing of datasets and have minimal impact on the technical aspects of the analytical determinations.

Table 2.2: Characterization of NO_2 lost in the modified chamber under environmentally relevant ranges of NO_2 and RH. The loss fraction (f_{NO2}) and HONO produced in the chamber were quantified at each of three NO_2 mixing ratios (5, 7, 10 ppbv) delivered at varying relative humidities (RH) to the fully modified chamber. Variability (±) provided is one standard deviation of the mean from replicate experiments (n=3).

RH (%)	NO_2 added (ppbv)	NO_2 lost (ppbv)	f_{NO2}	HONO produced (ppbv)
85	5	0.50 ± 0.01	0.1 ± 0.02	
85	7	0.70 ± 0.04	0.1 ± 0.02	
85	10	0.50 ± 0.07	0.05 ± 0.01	
65	5	0.30 ± 0.10	0.06 ± 0.02	
65	7	0.40 ± 0.09	0.06 ± 0.02	<1.1[a]
65	10	0.30 ± 0.08	0.03 ± 0.01	
45	5	0.30 ± 0.05	0.05 ± 0.01	
45	7	0.40 ± 0.04	0.06 ± 0.00	
45	10	0.30 ± 0.08	0.03 ± 0.01	

[a] _ below instrument detection limit of 1.1 ppbv determined as S/N=3 while sampling zero air

It should be noted that the amount of HONO in the chamber was below the LOD of the NO_x analyzer for HONO (1.07 ppbv), meaning that the upper limit of HONO inferred may perhaps, in fact, be negligible. Therefore, future experiments that wish to detect small N_r fluxes accurately will need to focus on reproducing these experiments with a higher performance instrument, such as a time-of-flight chemical ionization mass spectrometer (ToF-MS) or long-path absorption photometer (LOPAP), which have lower detection limits (Crilley et al., 2019; Lee et al., 2014; Neuman et al., 2016; Reed et al., 2016).

2.3.4 Characterization of O_3 loss in the chamber modified with and without PFA

Ozone loss was observed in both modified and unmodified chamber configurations, with 18% lost to clean lines alone when transferring 30 ppbv. The unmodified chambers lost 45% across all delivered mixing ratios (150-250 ppbv), which are higher than those typically expected in ambient air. This was reduced to 35% when the fluoropolymer modifications were implemented with new clean PTFE fittings and PFA film. When the PFA film was aged by 15 days of ambient sampling and 2 years of exposure to lab air, the losses were substantially exacerbated, reaching 80%. Such outcomes are expected and can be attributed to several factors, primarily involving surface reactions with built-up films of deposited organics, adsorption, and material interactions (Burkholder et al., 2015).

Ozone is known to undergo heterogeneous surface reactions, particularly on materials like glass, metals, or polymers (Plake et al., 2015). These surfaces often contain reactive sites such as hydroxyl groups or adsorbed water molecules that can catalyze the decomposition of O_3 into molecular oxygen (O_2) and other byproducts (George et al., 2015). Adsorption of O_3 on chamber surfaces is another potential pathway for loss. When O_3 molecules interact with surfaces, they may undergo a reaction if the materials are not inert. The use of PFA here was intended to benefit the transfer of O_3, yet despite its high chemical inertness, low reactivity, and resistance to the uptake of many chemicals from gas samples, the subsequent O_3-driven surface reactions are still substantial (Ebnesajjad, 2017). This is likely because, over time, reactive substances from sampled air accumulated through adsorption on the PFA film and/or its defect sites, thereby reducing its effectiveness. The same issue is well-known for PFA tubing used in standard air quality monitoring and is a common maintenance need for O_3 analyzer inlets. Further, physical wear or surface aging might alter the material surface through product formation or exposure of new reaction sites, which

makes it less resistant to further reaction with O_3, and therefore increases the rate of loss over time. This is the case in our aged PFA film results, which emphasizes the importance of regular replacement of the film as part of the N_r system maintenance and that quality control procedures characterizing the chamber material performance with respect to O_3 will provide the highest accuracy of experimental results.

2.3.5 Proof-of-concept reactive nitrogen fluxes using soil samples in the lab

Proof-of-concept flux measurements were performed using the modified dynamic chamber system to demonstrate that emissions of N_r gases from agricultural soil samples can be measured under controlled conditions, similar to many prior reports using custom-built soil chambers (Almand-Hunter et al., 2015; Pape et al., 2009; Tang et al., 2019, 2020).

2.3.5.1 Fluxes of NO, NO_2, and HONO from agricultural soil samples

Emission fluxes were measured from two pooled and two individual soil samples collected from a single agricultural field (**Table 2.3; Section S6**). The average and integrated fluxes of N_2O, NH_3, NO, NO_2, and HONO were assessed under controlled, environmentally realistic, drying conditions of zero air modified to be 65% RH delivered at 3.6 L min^{-1} to the chamber headspace where the soil was contained. The soil started the drying process from a VWC of approximately 25% with the flows held constant for around 4 days or until the VWC reached 15% (**Table 2.3**).

As the soils dried, NO and NO_2 emissions increased, with NO fluxes highest across all replicates and reaching up to 2.50 µg N m^{-2} hr^{-1}. This trend is consistent with the prior work of other researchers, showing peak NO emission potentials when VWC drops below 25% during soil drying, which is when microbial nitrification and denitrification processes are suggested to become more active (Bao et al., 2022; Oswald et al., 2013). The soil VWC at which these maxima occur can vary depending on soil type, texture, and the microbial diversity therein (Ludwig et al., 2001; Schindlbacher et al., 2009). The plot-level replicates from our field had a higher integrated NO flux (i.e., > 2600 µg N m^{-2}), compared to the pooled replicates (<1000 µg N m^{-2}), likely indicating real differences in preserved microbial hotspots, intact plot-level soil aggregates, true spatial variability, and plot-specific N availability (**Table 2.3**). Soil texture and aggregate size, for example, play an important role in building the porous structure of soil, which has implications for the release of gases (Mangalassery et al., 2013). Soil aggregates, therefore, govern the release of gaseous N_r analytes like NO based on the aerobic or anaerobic state of the soil. Here, our low level

of soil manipulation (i.e. not ground, no sieving) will drive some of the variability by preserving these features, which exist across and within real soil systems (Lipiec et al., 2007). Individual plot samples also retain plot-specific microbial communities when working with intact soil, whereas soil grinding can temporarily inhibit microbial activity. While we tried to minimize soil handling and processing extremes in these experiments, a measure of homogeneity was also pursued, and fully intact soil cores were not assessed.

Integrated NO_2 fluxes showed the same trend, with more sample-to-sample variability as one pooled replicate (R2) produced over three times the emissions of R1, despite both experiments being conducted across identical moisture content ranges (**Table 2.3**). Given the limited studies directly measuring NO_2, such as Purchase et al. (2023), this variability is difficult to interpret and highlights the need for more assessments of its production pathways and controls, which our developed chambers show promise for.

The observed average HONO fluxes remained low across all of the samples, ranging from 0.05 to 0.25 μg N m^{-2} hr^{-1} (**Table 2.3**). These values are lower by up to an order of magnitude compared to those reported in other controlled laboratory studies, where HONO fluxes ranging from 250 ng N m^{-2} s^{-1} to 900 μg N m^{-2} hr^{-1} have been reported (Oswald et al., 2013; Su et al., 2011; Wang et al., 2021). These discrepancies are concerning, given recent emphasis from the scientific community on the atmospheric impacts of soil-derived HONO on air quality. Here, the results from our agricultural soil samples may reflect the differences in our methodology, such as the soil handling and preparation steps prior to and during experiments. Many prior reports prepare their samples in ways that strongly deviate from real-world conditions (e.g. initial soil drying temperatures above those occurring under ambient conditions, extreme storage conditions, grinding, sieving, use of dry zero air to flush chambers, etc.). Further drivers of variability within the category of heavily altered samples from the literature include pH, NO_2^- availability, and NH_4^+ or NO_3^- content, all of which are known to influence biotic and abiotic HONO formation pathways (Wu et al., 2019).

Our HONO fluxes from the agricultural soil samples studied here are consistent with field observations under ambient conditions, where average emissions have been reported to largely remain below 2 ng N m^{-2} s^{-1} or 7.2 μg N m^{-2} hr^{-1} (Tang et al., 2019; Xue et al., 2024). This does suggest that greater care in sample preparation, and likely also a widely agreed-upon standard procedure, is needed to study soil HONO emissions relevant to atmospheric models.

The integrated HONO fluxes for the pooled replicates yielded 185 μg N m^{-2} and 146 μg N m^{-2}, respectively. From the individual sample replicates, which were slightly wetter than the pooled, the integrated HONO fluxes were 690 and 739 μg N m^{-2}, which was unexpected because the overall moisture regime accessed by the pooled soil experiments was not lower than those from the plot samples. The drier soils would have been expected to yield greater integrated HONO emissions (Oswald et al., 2013), yet this was not the case. Additional replicates and experimental controls, while beyond the scope of this study, would allow further attribution of the controls over the observed HONO variability.

Table 2.3: Average and integrated fluxes of NO, NO_2, and HONO (in μg N m^{-2} hr^{-1} and μg N m^{-2}, respectively) from agricultural soil samples across two soil VWC ranges. Both the average and integrated fluxes were calculated over a constant period within the noted range of soil VWC. Values are reported as mean ± standard error.

Soil sample	Soil VWC Range (%)	Duration (hr)	Avg Flux (μg N m^{-2} hr^{-1})			Integrated flux (μg N m^{-2})		
			NO	NO_2	HONO	NO	NO_2	HONO
Pooled R1	16-22	125	1.0 ± 0.04	0.05 ± 0.02	0.06 ± 0.02	2400 ± 120	160 ± 50	190 ± 50
Pooled R2	16-22	125	1.0 ± 0.04	0.20 ± 0.02	0.05 ± 0.01	2500 ± 130	500 ± 60	150 ± 40
Plot R1	22-27	65	1.2 ± 0.05	0.40 ± 0.03	0.20 ± 0.02	3400 ± 150	1300 ± 90	690 ± 70
Plot R2	22-27	65	1.0 ± 0.03	0.50 ± 0.04	0.30 ± 0.02	2600 ± 100	1600 ± 100	740 ± 50

These findings demonstrate the utility of the modified custom-built dynamic chambers for accurately capturing N_r fluxes under controlled laboratory settings, but they also highlight the need for more such systems to be implemented across the scientific community to better consider both biogeochemical soil properties and environmental context when interpreting the impacts of N_r fluxes obtained in the lab and scaling them to real soils. There seems to be potential for skewing the atmospheric impacts as a result, in particular for HONO, as the standard approaches have been designed to replicate NO fluxes (Behrendt et al., 2014). Most global models do not consider the effect of soil HONO on air quality through O_3 production and oxidation chemistry (Ha et al., 2023). Several modelling studies like Ha et al. (2023) and Tian et al. (2024) have incorporated the order of magnitude or higher HONO fluxes reported from lab studies, like those by Su et al. (2011), Wang et al. (2021), Oswald et al. (2013), and Meusel et al. (2018). They estimated significant HONO production with maximum flux potentials of 830 μg N m^{-2} hr^{-1}, 95 μg N m^{-2} hr^{-1}, 70 μg N m^{-2} hr^{-1}, 55 μg N m^{-2} hr^{-1}, respectively. In contrast, the field observations that do exist suggest that real HONO fluxes are much smaller at 2-17.5 μg N m^{-2} hr^{-1} (Song et al., 2023; Tang et al., 2019). Similarly, Wu et al. (2022) has used the regional WRF-Chem model to explore the impact of soil HONO emissions on the concentrations of atmospheric HONO, OH, and O_3.

Agricultural soil HONO emissions have been suggested to significantly contribute to OH radical production, accounting for approximately 10% to 60% of total OH formation in rural areas before noon (Oswald et al., 2013; Su et al., 2011), which often exceed the contributions from ozone photolysis. Additionally, high HONO emissions from agricultural soils have been reported to increase local O_3 concentrations by ~0.5 - 1.0 ppb in low-NO_x rural environments where VOCs are not limiting (Zhang et al., 2021), with even greater impacts observed during fertilization periods (Wu et al., 2022). Modelling studies, using GEOS-Chem and CMAQ, for example, claim that incorporating soil HONO emissions improves the agreement between observed and simulated O_3 levels, particularly during the morning (Zhang et al., 2021).

Only a few studies have conducted estimates of soil NO_x emissions under reasonable conditions, like Bao et al. (2022) and Wu et al. (2022), where the researchers tried to mimic field conditions. Even in such an area that has been long studied, large uncertainty still exists around soil sources of NO_x, particularly for agricultural activities where uncertainty is still at least ±30% due to limitations in lab characterizations and field experiments (Gong et al., 2025). It is not surprising,

then, that a similar issue exists for the very recent work on HONO soil emissions. The NO_x uncertainty range results from intricate soil biogeochemical processes and varies with crop types, soil texture, fertilizer types and application rate (Gong et al., 2025). This longstanding and established difficulty in predicting soil NO_x for use in global chemical models means that doing so for HONO without careful ground truthing of real-world emissions could lead to substantial inflation of the impacts on atmospheric chemistry and air quality. Care should be taken in using HONO emissions from lab studies in global models, as it seems they pose a risk of overestimating their atmospheric impacts until a more representative experimental design can be obtained with chamber systems like the one used here.

2.3.5.2 Fluxes of NH_3, N_2O, NO, NO_2, and HONO from fertilized agricultural soil samples

Agricultural soils amended with chemical fertilizers are expected to be hotspots for NH_3, N_2O, HONO, and NO_x emissions. Here, we demonstrate the use of our developed chambers to measure these analytes under controlled lab conditions using our lightly processed pooled soil samples and four fertilizers: urea, ammonium nitrate (AN), ammonium bicarbonate (ABC), and ammonium carbonate (AC) with the temperature maintained at 23 °C, VWC between 25–29%, and headspace RH held at 65% for three days, simulating realistic atmospheric and environmental N_r flux exchange conditions following farm field fertilization (**Figure 3**). In all experiments conducted with the Picarro G2509, the mixing ratio of N_2O began to rise approximately four hours after the experiment started. In the example shown for urea, it peaked at 0.79 ppm after 12 hours, which was followed by a gradual decline (**Figure 3a**). This pattern likely reflects the incubation period of nitrifying and denitrifying bacteria that leads to the subsequent release of gases like HONO, as depicted in Wang et al. (2021), and N_2O in Liu et al. (2022). In contrast, the mixing ratio of NO remained relatively constant throughout the three days (**Figure 3b**), with NO_2 increasing as the N_2O emissions decreased, while NO was emitted constantly throughout (**Figure 3c**). In this example experiment, no measurable emissions of HONO were detected despite the substantial presence of urea and evidence of active microbial nitrification and denitrification from the other emitted gases (**Figure 3d**). Lastly, the urea application example in **Figure 3** shows the expected significant NH_3 emissions, with the integrated amount reaching 22% of the applied N over the three-day incubation period. These findings are consistent with our existing knowledge that NH_3 volatilization as an N loss mechanism dominates early N_r losses from fertilizers.

Volatilization of NH_3 is well-characterized as a major pathway for N loss from fertilizers (Behera et al., 2013; Govoni Brondi et al., 2024; Liu et al., 2020; Moravek et al., 2019; Pan et al., 2016, 2022; Paulot et al., 2014). Besides agronomic concerns due to N loss and reduced fertilizer efficiency related to NH_3 emissions from fertilized soil (Anas et al., 2020), it is a key precursor to secondary inorganic aerosols in the atmosphere with impacts on respiratory and ecosystem health, visibility, and climate (Dennis et al., 2010; Edwards et al., 2024; Fowler et al., 2013; González Ortiz et al., 2020; Jang et al., 2025; Seinfeld and Pandis, 2006).

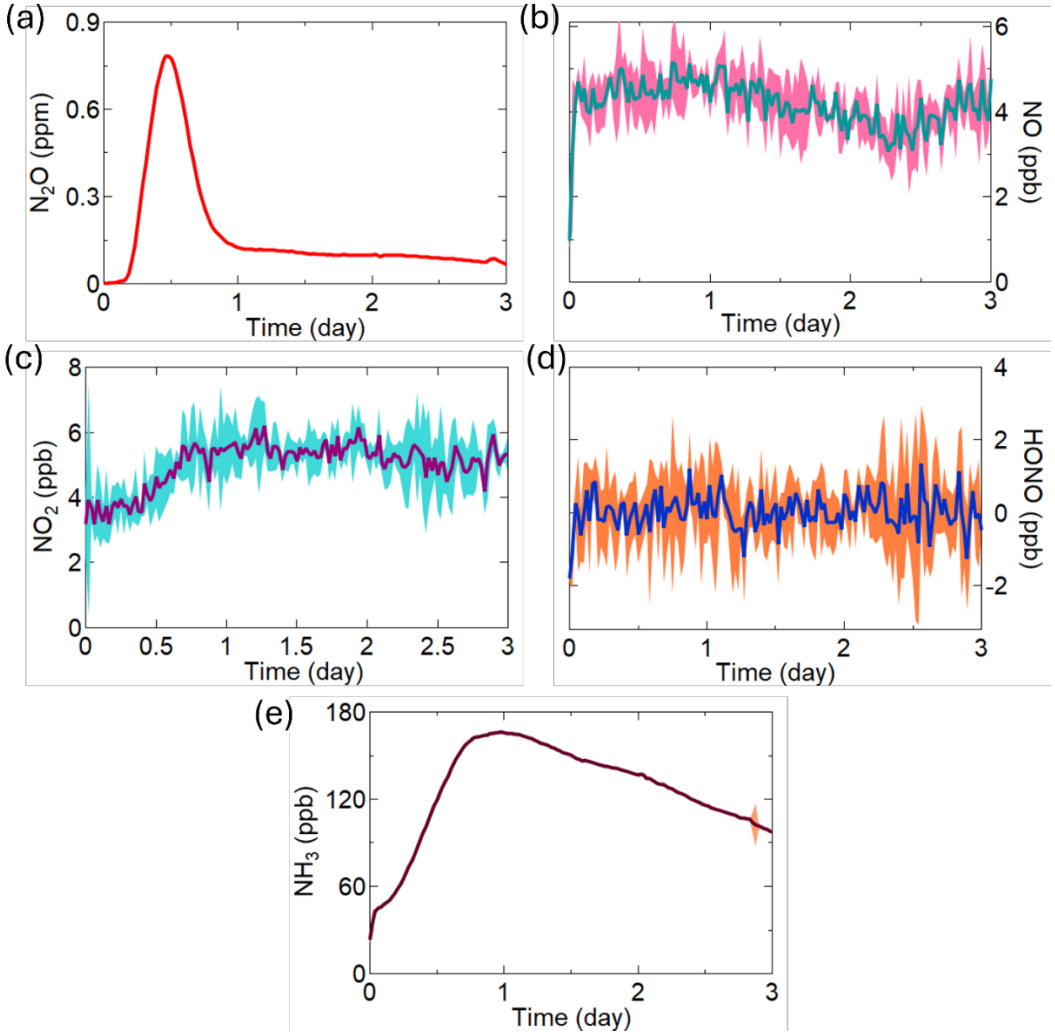

Figure 2.3: Soil emissions of the comprehensive suite gases from soil treated with urea, including (a) N_2O; (b) NO; (c) NO_2; (d) HONO; and (e) NH_3. The NO, NO_2 and HONO emissions were measured at 1-minute resolution and averaged to 30 min. The standard deviation (±1σ) around these averages is shaded with a lighter version of the main trace colour. Similarly, the 2-second resolution of N_2O and NH_3 measurements were also averaged to 30-minute intervals with ±1σ provided in shading.

Emissions of NH_3 and N_2O were observed to be far greater in terms of integrated amounts from the fertilized samples (**Figure 2.4**). Integrated flux for NH_3 produced by soil treated with ABC accounted for 77% of total N_r flux (i.e., 85900 μg N m^{-2}), followed by AC, which was 63700 μg N m^{-2}. This is not surprising, since the use of chemical fertilizers increases the concentration of NH_4^+ in the soil that can deprotonate to emit neutral NH_3 and, in the presence of ammonia-oxidizing microorganisms, increases the production of N_2O (Luo et al., 2025). Nitrous oxide released from the addition of urea accounted for the highest integrated flux of 32400 μg N m^{-2} observed, representing 89% of total N_r released, followed by 25300 μg N m^{-2} and 9600 μg N m^{-2} for ABC and AC, respectively. One way that has been proposed to reduce these large N_2O emissions from inorganic fertilizers is to change the application form to organic fertilizer, as the NH_4^+ in soil is released more slowly (Luo et al., 2025). Due to a limited duration of access to the G2509 to conduct this work, we were unable to measure the N_2O and NH_3 emitted from unamended soils or those treated with AN. Regardless, based on the obtained data, the values found here are similar to those observed under real environmental conditions (**Figure 2.4**). For our sample without N amendment, the integrated flux of NO was the largest (2400 μg N m^{-2}; 87% of total NO_y), followed by comparable levels of NO_2 (160 μg N m^{-2}) and HONO (190 μg N m^{-2}). The fluxes of NO_x and HONO were below 1 μg N m^{-2} hr^{-1} for all the nutrient addition treatments, suggesting a similar trend as those observed under field conditions and from our lab results with unamended soils (**Figure 2.4, Table S1, Section S6**). The exact mechanism behind the HONO release, being due to nitrification and/or denitrification, cannot be definitively assigned based on flux data alone, and many abiotic factors like soil moisture, temperature, and presence of specific microbial communities drive these emissions. There are discrepancies still observed between HONO flux measured from the treated soil samples in the laboratory and similar measurements in literature (Oswald et al., 2013; Su et al., 2011), some of which report fluxes of up to ~3600 μg N m^{-2} hr^{-1} and are likely overestimating the soil N_r fluxes found in the real world. In contrast, our results are in close agreement with the field-based measurements of Tang et al. (2020), which also used a dynamic chamber flux method.

These in-lab experiments show that simultaneous speciated N_r emissions in a controlled environment can be conducted using a single chamber and potentially applied to an array of chambers, as others have done for a subset of gaseous N_r (Scharko et al., 2015; Tang et al., 2019). With even limited replicates we did here, our results raise a question for researchers who have

been using lab studies as a standard to predict and incorporate HONO soil emission values in particular, into regional and global models.

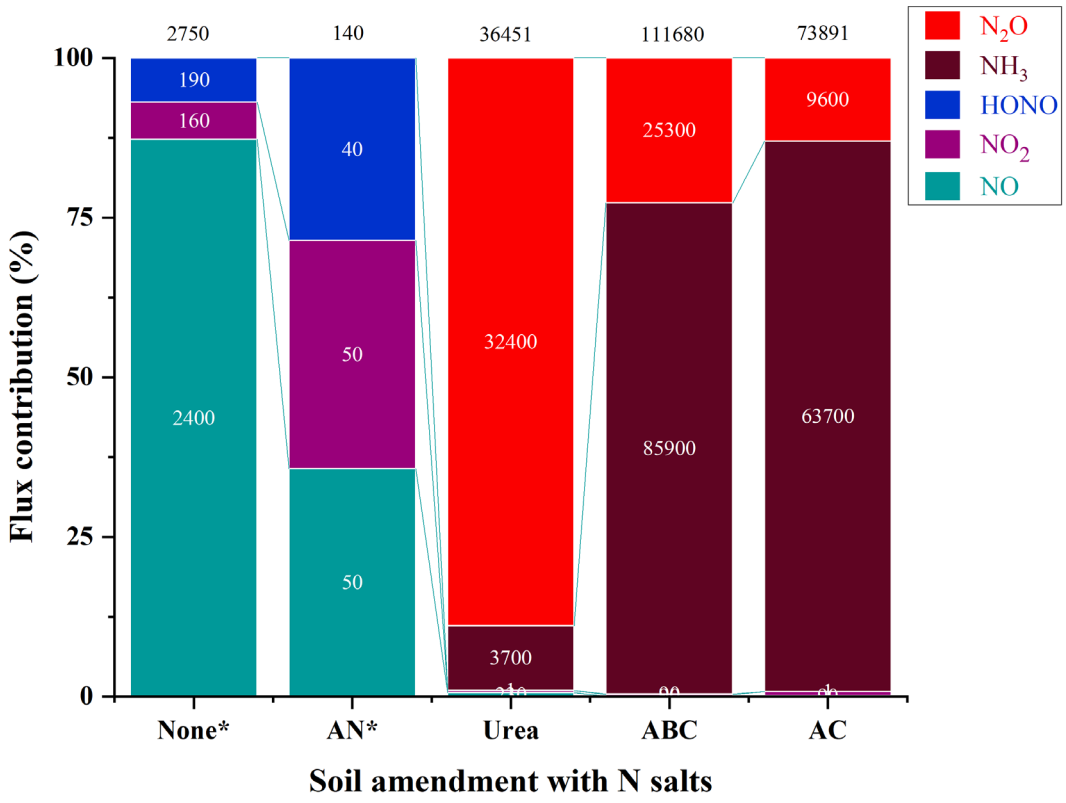

Figure 2.4: Relative flux contribution of soil treated with four different nitrogen-containing fertilizer salts. Each segment shows the proportion of integrated flux of NO (cyan), NO_2 (purple), HONO (blue), NH_3 (brown) and N_2O (red), with discrete flux values presented in white text, and the total flux provided in black text above the column (μg N m^{-2}). Some samples (denoted by *) were only characterized for fluxes of NO, NO_2 and HONO using the modified NO_x analyzer, as the duration of our access to the G2509 for NH_3 and N_2O measurements was limited.

2.3.6 Dual chamber field deployment for automated continuous dynamic fluxes

A pilot scale field campaign was carried out to demonstrate the application of our dual soil flux chambers in capturing N_r gas exchange processes, taking into account the characterized processes presented above that are necessary for accurate determinations. A paired measurement and reference chamber setup was deployed in the same field a year after the soil samples were collected for our lab experiments. During a period of stimulated N_r emission from an experimental application of urea in situ, the mixing ratios of NO, N_2O, and NH_3 were impacted compared to the unfertilized state. The changes within both the measurement and reference chambers were measured and used to calculate fluxes (**Figure 2.5**). The selected data for NH_3 correspond to

measurements taken after the fertilization event, while the selected NO and N_2O data segments are examples prior to the fertilization event so that the mathematical terms in **E6** and **E7** contributing to the net flux can be considered more easily – they are entirely ascribed to the rate term otherwise. Each set of observations span three consecutive hours of dynamic changes in gas concentrations within the chambers which allow fluxes to be calculated.

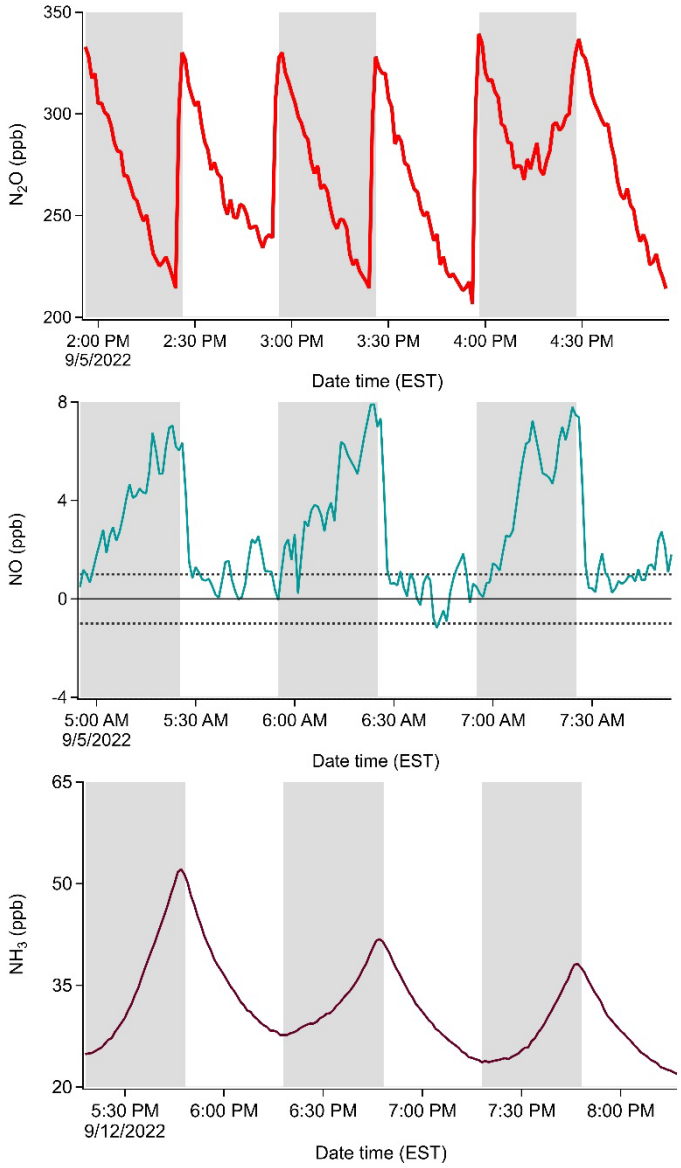

Figure 2.5: Mixing ratios of N_2O (ppb), NO (ppb), and NH_3 (ppb) in the measurement (grey shading) and reference (unshaded) chambers from three consecutive cycles during the pilot field study. The NH_3 cycles correspond to measurements taken after the fertilization perturbation, while the NO and N_2O cycles are from the same period before fertilization. The dashed lines for the NO measurements indicate ±1 ppb (3σ noise), where the positive boundary represents the detection limit of the NO_x analyzer.

The breakdown of the flux components for NH_3, N_2O, and NO can allow the contributions of the experimental setup (e.g. dilution) and environmental factors (e.g. reaction) to be considered independently (**Figure 2.6**). We consider these across three consecutive measurement cycles from the pilot field deployment to provide meaningful examples. The uncertainty in each term is estimated from a triplicate of consecutive reference chamber background measurements. Therefore, the error bars for each term are derived from the variability in the measured slope of the three reference chamber measurements. This error estimate corresponds to that arising only from reference chamber observations used in **E6** or **E7** and assumes that ambient atmospheric composition did not change substantially during this error derivation period.

The rate term (dC/dt) is the dominant contributor to the determined flux for all three gases (**Figure 2.6**), which are all positive and indicate emissions despite their clearly differing temporal trends. Each contribution term is defined and discussed in further detail in **Section S7** of the Supplementary Information. Accurate quantification of trace gas fluxes using dynamic chamber systems requires correction for attenuation caused by surface interactions. These effects can significantly suppress the measured accumulation rate of reactive species within the closed chamber, particularly for compounds with notable surface affinities such as NH_3, NO_2, and HONO (**Figure 2.5**). To account for such losses, an attenuation factor (λ) was introduced in this work **(ES12)**, defined as the ratio of the theoretical concentration signal to the measured signal over the chamber closure period. The value of λ is gas-specific and time-dependent, reflecting wall affinity and kinetics, which are therefore calculated over the first 30 min of chamber closure, as this was the duration of our field measurement closures. This correction reduces bias that would otherwise result in the calculated gas exchange rates, independent of chamber-specific losses. The highest attenuation was observed for NH_3, for which a λ of 5.40 was determined for the corresponding closure period. That is, substantial bias would result without this correction. Comparative values for NO_2 and HONO are also provided in the Supporting Information (**Section 2.S7.3**).

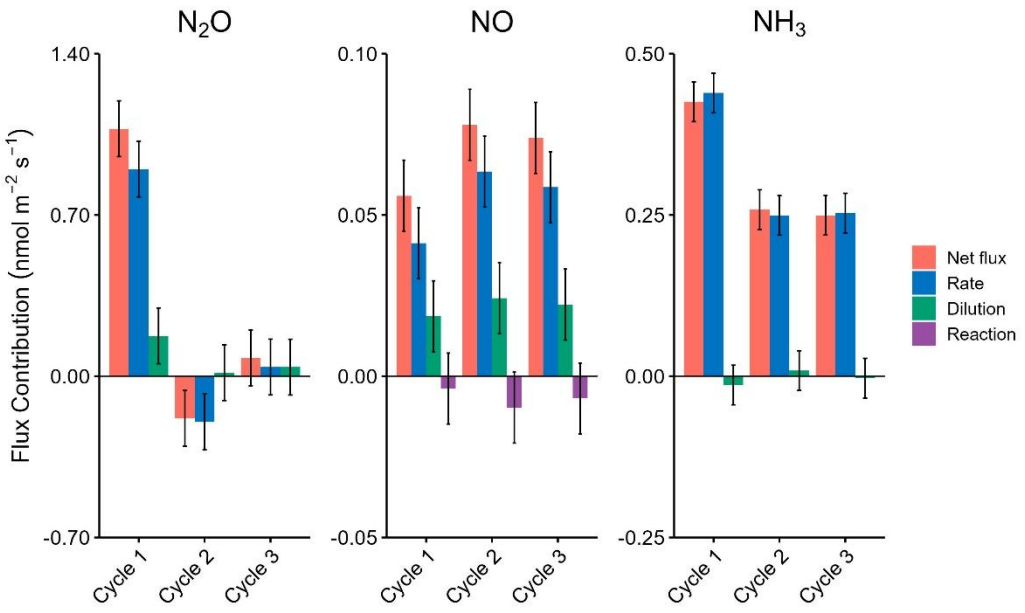

Figure 2.6: Contributions of different terms (rate, dilution, and reaction) to the net flux of NO, NH_3, and N_2O across three consecutive cycles (nmol m^{-2} s^{-1}). The rate represents the change in concentration measured over time, the dilution represents the integrated loss to dilution, and the reaction represents the contribution of known reactions happening inside the chamber. Error bars are calculated using the mean value of the corresponding terms from three reference chambers plus their standard deviation. For visual clarity, the attenuation correction (λ = 5.40) for NH_3 is not applied in this figure, as it constitutes a linear scaling factor across all NH_3 bars (**Section S2.7.3**).

For N_2O, the first cycle exhibits the highest flux (1.07±0.12 nmol m^{-2} s^{-1}), while the second cycle showed uptake by the soil (-0.18±0.12 nmol m^{-2} s^{-1}), and the final cycle showed no net flux within error (0.08±0.12 nmol m^{-2} s^{-1}). This occurs for a non-reactive greenhouse gas like N_2O despite the concentration decreasing with time for both the measurement and reference periods, as the rate of decrease during the measurement cycle is slower than that from dilution alone (**Figure 2.6**). Across the three cycles, the rate of concentration change term contributed 84±15% to the measured flux in the first cycle, 109±98% in the second cycle, and 50±171% in the third cycle. The negative rate of change in all of the observation periods arises due to the use of N_2O-free purge gas delivered to the chamber headspace, which is required for the gas sample to be destructively quantified, while not introducing ambient air into the chamber. This simultaneously prevents sudden changes in local outdoor air composition from making small fluxes difficult to detect, as well as reduces the uncertainty in the fluxes assigned. Here, the dilution terms range from 8 to 50% of the net flux, as would be expected from the N_2O exchange switching from emission to deposition during the three-cycle example (i.e. 3 hours). In the final measurement cycle, the rate of concentration change

transitions from a loss to steady state during the observation period, suggesting that an instant of 'hot spot, hot moment' emission of N_2O was likely occurring. As such, the transition leads to no net flux for the observation period, which is a limitation of our dual-chamber approach compared to one with recirculating headspace, or that of an eddy covariance approach that can capture much higher temporal resolution changes in concentration. The N_2O fluxes observed here are consistent with those reported for European arable soils using both dynamic and static chambers, where event-driven N_2O peaks after fertilization commonly range between 0.2 and 2.4 nmol m^{-2} s^{-1}, and background periods can be as low as 0.08 nmol m^{-2} s^{-1} (Kong et al., 2025, Murphy et al., 2022, Maier et al., 2024). Field-scale eddy covariance studies, such as Maier et al. (2022), have captured post-harvest pulses up to 1.6 nmol m^{-2} s^{-1}, highlighting the capacity of EC to resolve large, rapid emission events that single-point chamber systems may miss. However, dynamic chamber systems provide high-precision, temporally resolved flux data under controlled conditions, enabling direct attribution of emissions to specific soil management or environmental factors (Butterbach-Bahl et al., 2013; Kong et al., 2025). This makes dynamic chambers, like those demonstrated here, especially valuable for mechanistic and process-level studies. For NO, the only gas we consider in the examples here with a reaction term, the reaction contribution is the smallest among the three flux components. Over all three cycles, the reaction term opposed the net flux by less than 13%. The magnitude of the reaction term is always negligible, remaining within the ± 0.01 nmol m^{-2} s^{-1} variability caused by background correction from the reference chamber. Instead, the time rate of change in concentration term drove 74–81% of the total flux for all three cycles and dilution accounted for the remaining 30–33%. The reaction term falling within the uncertainty range of no contribution in all three cycles (e.g. -0.01±0.01 nmol m^{-2} s^{-1} in the second cycle, where it had the greatest potential), indicates that its contribution is less certain than the other flux components as it is driven by the presence of O_3, which is rapidly lost upon chamber closure. Overall, the low contribution of the reaction term suggests this process has a minor role in measured NO fluxes. In other, more polluted regions, such as the North China Plain (NCP) and the Pearl River Delta (PRD), where summertime ambient O_3 concentrations frequently range from 60 to 275 ppbv, and exceedances above 200 ppbv occur during pollution episodes (Wang et al., 2017), this term could become very important to include. As noted above, the PFA film on the chamber surface will change its properties with respect to O_3 transmission over time, highlighting the utility of the

reference chamber, which is designed to accumulate the same atmospheric compounds as the measurement chamber over time on all sampling surfaces.

The resulting emission fluxes of NO observed in these three cycles were 0.056-0.078 nmol m^{-2} s^{-1}, which is well within the range reported for agricultural soils in North America and Europe, such as Taylor et al. (1999) who observed -0.07-4.2 nmol m^{-2} s^{-1} in Canadian fertilized cropland, and Pape et al. (2009) and Almand-Hunter et al. (2014) who reported values of 0.05-4.0 nmol m^{-2} s^{-1}, using dynamic chambers in grass and cropland soils. Therefore, in the case of NO for this example, the variability in the fluxes is largely driven by real fluctuations in the rate term. This highlights the sensitivity of the total flux to changes in the rate of concentration change, and the precision of the method, as the uncertainty in the final fluxes here is on the order of 14%. Compared to the dynamic chambers reported by these prior studies, our reference chamber in our dual-chamber system offers a clear advantage by directly correcting for baseline fluctuations and environmental drift that can confound single-chamber approaches. This is especially important for reactive gases such as NO, which are susceptible to rapid loss to O_3 and short-term background variability (Taylor et al., 1999). The dual-chamber system provides more robust, artifact-free quantification of soil–atmosphere exchange and is less susceptible to interference from transient local emissions (e.g. from nearby traffic or agricultural equipment) than single-chamber systems. In comparison to eddy covariance or flux-gradient techniques, which integrate over larger areas but may underestimate true NO fluxes due to post-emission chemistry (Taylor et al., 1999; Plake et al., 2015), our approach yields high-frequency, process-resolving data ideal for mechanistic and plot-scale studies.

For NH_3, the rate of change term dominates the total flux, contributing 103 ± 10%, 97 ± 16%, and 101 ± 17% of the flux in cycles one, two, and three, respectively, while the dilution term contributes inconsequentially at -3 ± 7%, 3 ± 12%, and -1 ± 12% in the same three cycles, respectively. The resulting emission fluxes of NH_3 observed across these cycles ranged from 0.43 ± 0.03 nmol m^{-2} s^{-1} in cycle one down to 0.25 ± 0.03 nmol m^{-2} s^{-1} in cycle three. The relatively small contribution of the dilution term is consistent with the expectation that the reference and measurement chambers exhibit similar dilution effects. The relative uncertainty in the final NH_3 fluxes is 7% for cycle one, and 12% for cycles two and three. By comparison, relative uncertainties

were 14% for NO and ranged from 15% to 171% for N_2O, reflecting the greater variability and lower precision associated with the smaller flux magnitudes for those gases.

Our observed NH_3 fluxes (0.25–0.43 nmol m^{-2} s^{-1}) are consistent with literature values for managed grass and croplands. For instance, Milford et al. (2009) reported bi-directional background fluxes from –3.8 to 2.5 nmol m^{-2} s^{-1} prior to cutting intensively managed grassland, with larger diurnal emissions up to 42 nmol m^{-2} s^{-1} after cutting and maxima up to 224 nmol m^{-2} s^{-1} following fertilizer application. Abdulwahab et al. (2024) observed highly variable fluxes in intensively grazed French grassland, ranging from –6.6 to 188 nmol m^{-2} s^{-1}, with short-lived maxima above 300 nmol m^{-2} s^{-1} after slurry application, though most measurements were at much lower magnitudes. Notably, accurate quantification of NH_3 fluxes in this system critically depends on the application of the chamber-specific attenuation factor λ (**Section 2.S.7.3**). In our study, λ for NH_3 was 5.40 for the 30-minute closure interval, meaning that without this correction, true NH_3 fluxes would be underestimated by more than fivefold. The necessity of such a large λ correction is due to the strong surface affinity of NH_3 and emphasizes the importance of it for gas- and chamber-specific corrections to obtain high-quality N_r fluxes. While the reference chamber correction plays a role in the flux calculations, its impact on NH_3 is less pronounced than on N_2O, where the correction significantly alters the net flux direction (**Figure 2.5**; first cycle). Chamber-based approaches such as ours provide a key advantage for NH_3 over micrometeorological methods like eddy covariance, which are especially prone to high-frequency attenuation and chemical interferences for reactive gases. As shown in Moravek et al. (2019), even state-of-the-art closed-path EC systems may recover less than half (as little as 46%) of true NH_3 fluxes due to instrument limitations and turbulence losses. Challenges were also evident for relaxed eddy accumulation (REA), where Xu et al. (2010) found that turbulence and surface effects complicated flux interpretation in cropland. Related methodological considerations have also been noted in other contexts. Schlossberg et al. (2017) highlighted how airflow and canopy structure can influence chamber NH_3 fluxes in turf systems, underscoring the need for chamber methods that minimize such artifacts. In contrast, our dynamic chamber system, with a chamber-specific λ correction and reference chamber, enables robust, bias-corrected quantification of both low and episodic NH_3 fluxes, as well as clear partitioning of emission and dilution terms, even under highly variable field conditions. Overall, the combination of dual-chamber design with explicit λ correction in our method provides more

accurate and robust quantification of soil NH_3 emissions than single-chamber, eddy covariance, or relaxed eddy accumulation techniques, particularly for short-term or low-flux events.

2.4 Conclusions

In this work, we presented a dynamic chamber system for reactive nitrogen flux measurements, developed for the first time through the modification of commercially available chambers by implementing two key changes: the use of PTFE fittings instead of original brass fittings and the installation of an inert PFA film, which retains their actinic transparency. These modifications provide a targeted methodology for other researchers to convert commercially available chambers into those capable of measuring N_r. The performance of these modifications was quantified through the rise and fall time constants of target gas concentrations, as well as a reduction in reactive losses. The time constants for the transfer of GHGs were not different from those of a theoretically inert gas and showed no change from the modifications. Improved transmission for the reactive and surface-active N_r species NO_2, HONO, and NH_3 targeted here ranged from 0.8 to 2.6 minutes. Similarly, a commercial chamber multiplexing unit with stainless steel valves and fittings replaced with PTFE and PFA, respectively, resulted in a 9–27% reduction in surface losses of N_r compounds.

Only NO_2 showed reactive loss in the system, and the loss fraction in the chambers in their unmodified configurations was up to ~36%. Losses were reduced to the gas analyzer detection limits (<10%) with the same fluoropolymer modifications when atmospherically relevant NO_2 and RH mixtures were introduced. Lastly, O_3 loss was pervasive within chambers in both their modified and unmodified configurations at 35% and 45% respectively, demonstrating the necessity of the reference chamber. It allows characterization of deposited surface film reactivity for O_3, especially when obtaining quality O_3 measurements is needed to account for the conversion of NO to NO_2 during a sampling period. Taken together, the modified commercial system is capable of measuring dynamic soil fluxes of GHGs and N_r when a measurement and reference chamber are deployed simultaneously.

Proof of concept flux measurements using this N_r dynamic chamber system were conducted using real agricultural soil samples in the lab, with a single chamber, and during a pilot study in the field with a measurement-reference chamber pair. The lab soil emissions were found to be consistent

with prior field reports in the literature for NO and HONO, with unexpected emissions of NO_2 also observed. Substantial variability in NO_2 and HONO emissions between replicates demonstrates the potential heterogeneity of soil emissions that may result from samples kept intact and subject to minimal preparation conditions. Upon the addition of typical fertilizers, like urea, substantial NH_3 and N_2O emissions fluxes matched expectations, with increasing quantities of NO, NO_2, and HONO as the soil water content decreased.

Last, fully automated operation of the chambers was carried out in a field pilot study with the delivery of external fertilizer conducted at the midpoint of the study to stimulate N_r emissions, mainly in the form of NH_3. Continuous flux observations were made by switching sample flows between a paired reference and measurement chambers with a custom-built valve system to obtain continuous N_r fluxes over two weeks. While the details of the entire campaign will be presented in a future manuscript, it was shown here how the methodology developed yields reliable flux determinations by accounting for known reactions and our lab-derived surface effects. The mathematical foundation of each term and its error in a mass balance equation, which are central to reducing flux bias, are fully described. The observed fluxes from our dynamic chambers are simpler to quantify with standard gas analyzers and can be compared readily with prior reports in the literature from other common flux techniques. One key limitation of the dynamic chamber approach is the limited footprint covered in a system that is notoriously heterogeneous, where EC and REA flux approaches are less prone to this effect. Using a multiplexer and a larger array of dynamic chambers, it is possible to reduce the susceptibility of the dynamic chamber approach to this issue.

Through our modifications and validation, this work provides insight into how commercial dynamic chamber options, like those offered by Eosense, can be modified easily for scientists from various disciplines interested in studying N_r exchange at atmospheric interfaces. This is particularly important for research groups which currently do not have the expertise and resources to develop their own N_r flux measurement systems. The modified system utilizes destructive sampling techniques, as opposed to the re-circulation of chamber air, enabling integration of the dynamic chamber approach with various standard gas analysis instruments (e.g., NO_x chemiluminescence) to study their exchange. The large footprint allows gas concentrations to change in easily determined quantities even for very small fluxes. We show here, for the first time,

that such a system can provide simultaneous measurement of NO, NO_2, HONO, NH_3, CO_2, H_2O, CH_4, and N_2O fluxes. In addition, we show fully automated operation of the chambers, switching of sample flows, and data collection workflows for continuous and unattended measurements of fluxes at field sites. Given the pressing need to understand global perturbations to the biogeochemical cycle of N, reduce nitrogen use in agriculture, and gauge the impacts of N status on biodiversity or ecosystem function, wider accessibility of N_r flux techniques for the global research community is needed to increase the pace of research outcomes and improve the capacity for interdisciplinary work between atmospheric and earth system researchers.

2.5 References

Almand-Hunter, B. B., Walker, J. T., Masson, N. P., Hafford, L., & Hannigan, M. P. (2015). Development and validation of inexpensive, automated, dynamic flux chambers. *Atmospheric Measurement Techniques*, *8*(1), 267–280. https://doi.org/10.5194/amt-8-267-2015

Anas, M., Liao, F., Verma, K. K., Sarwar, M. A., Mahmood, A., Chen, Z. L., Li, Q., Zeng, X. P., Liu, Y., & Li, Y. R. (2020). Fate of nitrogen in agriculture and environment: agronomic, eco-physiological and molecular approaches to improve nitrogen use efficiency. In *Biological Research* (Vol. 53, Issue 1). BioMed Central Ltd. https://doi.org/10.1186/s40659-020-00312-4

Aneja, V. P., Blunden, J., Claiborn, C. S., & Rogers, H. H. (2006). Dynamic Chamber System to Measure Gaseous Compounds Emissions and Atmospheric-Biospheric Interactions. *Environmental Simulation Chambers: Application to Atmospheric Chemical Processes*, 97–109. https://doi.org/10.1007/1-4020-4232-9_7

Anthony, T. L., & Silver, W. L. (2024). Hot spots and hot moments of greenhouse gas emissions in agricultural peatlands. *Biogeochemistry*, *167*(4), 461–477. https://doi.org/10.1007/s10533-023-01095-y

Bao, F., Cheng, Y., Kuhn, U., Li, G., Wang, W., Kratz, A. M., Weber, J., Weber, B., Pöschl, U., & Su, H. (2022). Key Role of Equilibrium HONO Concentration over Soil in Quantifying Soil–Atmosphere HONO Fluxes. *Environmental Science & Technology*. https://doi.org/10.1021/acs.est.1c06716

Barney, W. S., & Finlayson-Pitts, B. J. (2000). Enhancement of N2O4 on Porous Glass at Room Temperature: A Key Intermediate in the Heterogeneous Hydrolysis of NO2? *Journal of Physical Chemistry A*, *104*(2), 171–175. https://doi.org/10.1021/jp993169b

Becciolini, V., Leso, L., Fuertes Gimeno, E., Rossi, G., Barbari, M., Dalla Marta, A., Orlandini, S., & Verdi, L. (2024). Nitrogen loss abatement from dairy cow excreta through urine and faeces separation: The effect of temperature and exposure period on NH3 fluxes. *Agricultural Systems*, *216*. https://doi.org/10.1016/j.agsy.2024.103898

Behera, S. N., Sharma, M., Aneja, V. P., & Balasubramanian, R. (2013). Ammonia in the atmosphere: A review on emission sources, atmospheric chemistry and deposition on terrestrial bodies. In *Environmental Science and Pollution Research* (Vol. 20, Issue 11, pp. 8092–8131). https://doi.org/10.1007/s11356-013-2051-9

Behrendt, T., Veres, P. R., Ashuri, F., Song, G., Flanz, M., Mamtimin, B., Bruse, M., Williams, J., & Meixner, F. X. (2014). Characterisation of NO production and consumption: New insights by an improved laboratory dynamic chamber technique. *Biogeosciences*, *11*(19), 5463–5492. https://doi.org/10.5194/bg-11-5463-2014

Benedict, K. B., Prenni, A. J., Carrico, C. M., Sullivan, A. P., Schichtel, B. A., & Collett, J. L. (2017). Enhanced concentrations of reactive nitrogen species in wildfire smoke. *Atmospheric Environment*, *148*, 8–15. https://doi.org/10.1016/j.atmosenv.2016.10.030

Burkholder, J. B., Cox, R. A., & Ravishankara, A. R. (2015). Atmospheric Degradation of Ozone Depleting Substances, Their Substitutes, and Related Species. *Chemical Reviews*, *115*(10), 3704–3759. https://doi.org/10.1021/cr5006759

Butterbach-Bahl, K., & Dannenmann, M. (2011). Denitrification and associated soil N2O emissions due to agricultural activities in a changing climate. *Current Opinion in Environmental Sustainability*, *3*(5), 389–395. https://doi.org/10.1016/j.cosust.2011.08.004

Crilley, L. R., Kramer, L. J., Ouyang, B., Duan, J., Zhang, W., Tong, S., Ge, M., Tang, K., Qin, M., Xe, P., Shaw, M. D., Lewis, A. C., Mehra, A., Bannan, T. J., Worrall, S. D., Priestley, M., Bacak, A., Coe, H., Allan, J., … Bloss, W. J. (2019). *Intercomparison of nitrous acid (HONO) measurement techniques in a megacity (Beijing)*. https://doi.org/10.5194/amt-2019-139

Crilley, L. R., Lao, M., Salehpoor, L., & VandenBoer, T. C. (2023). Emerging investigator series: an instrument to measure and speciate the total reactive nitrogen budget indoors: description and field measurements. *Environmental Science: Processes and Impacts*, *25*(3), 389–404. https://doi.org/10.1039/d2em00446a

Degaspari, I. A. M., Soares, J. R., Montezano, Z. F., Del Grosso, S. J., Vitti, A. C., Rossetto, R., & Cantarella, H. (2020). Nitrogen sources and application rates affect emissions of N2O and NH3 in sugarcane. *Nutrient Cycling in Agroecosystems*, *116*(3), 329–344. https://doi.org/10.1007/s10705-019-10045-w

Delaria, E. R., & Cohen, R. C. (2023). Measurements of Atmosphere-Biosphere Exchange of Oxidized Nitrogen and Implications for the Chemistry of Atmospheric NOx. *Accounts of Chemical Research*, *56*(13), 1720–1730. https://doi.org/10.1021/acs.accounts.3c00090

Dennis, R. L., Mathur, R., Pleim, J. E., & Walker, J. T. (2010). Fate of ammonia emissions at the local to regional scale as simulated by the Community Multiscale Air Quality model. *Atmospheric Pollution Research*, *1*(4), 207–214. https://doi.org/10.5094/APR.2010.027

Ebnesajjad, S. (2017). Introduction to Fluoropolymers. *Applied Plastics Engineering Handbook: Processing, Materials, and Applications: Second Edition*, 55–71. https://doi.org/10.1016/B978-0-323-39040-8.00003-1

Edwards, T. M., Puglis, H. J., Kent, D. B., Durán, J. L., Bradshaw, L. M., & Farag, A. M. (2024). Ammonia and aquatic ecosystems – A review of global sources, biogeochemical cycling, and effects on fish. In *Science of the Total Environment* (Vol. 907). Elsevier B.V. https://doi.org/10.1016/j.scitotenv.2023.167911

Ellis, R. A., Murphy, J. G., Pattey, E., Van Haarlem, R., O'Brien, J. M., & Herndon, S. C. (2010). Characterizing a Quantum Cascade Tunable Infrared Laser Differential Absorption

Spectrometer (QC-TILDAS) for measurements of atmospheric ammonia. *Atmospheric Measurement Techniques*, *3*(2), 397–406. https://doi.org/10.5194/amt-3-397-2010

Finlayson-Pitts, B. J., Wingen, L. M., Sumner, A. L., Syomin, D., & Ramazan, K. A. (2003). The heterogeneous hydrolysis of NO2 in laboratory systems and in outdoor and indoor atmospheres: An integrated mechanism. *Physical Chemistry Chemical Physics*, *5*(2), 223–242. https://doi.org/10.1039/b208564j

Fowler, D., Coyle, M., Skiba, U., Sutton, M. A., Cape, J. N., Reis, S., Sheppard, L. J., Jenkins, A., Grizzetti, B., Galloway, J. N., Vitousek, P., Leach, A., Bouwman, A. F., Butterbach-Bahl, K., Dentener, F., Stevenson, D., Amann, M., & Voss, M. (2013). The global nitrogen cycle in the twenty-first century. *Philosophical Transactions of the Royal Society B: Biological Sciences*, *368*(1621). https://doi.org/10.1098/rstb.2013.0164

Geddes, J. A., & Murphy, J. G. (2014). Observations of reactive nitrogen oxide fluxes by eddy covariance above two midlatitude North American mixed hardwood forests. *Atmospheric Chemistry and Physics*, *14*(6), 2939–2957. https://doi.org/10.5194/acp-14-2939-2014

George, C., Ammann, M., D'Anna, B., Donaldson, D. J., & Nizkorodov, S. A. (2015). Heterogeneous Photochemistry in the Atmosphere. *Chemical Reviews*, *115*(10), 4218–4258. https://doi.org/10.1021/cr500648z

Gong, C., Wang, Y., Tian, H., Kou-Giesbrecht, S., Vuichard, N., & Zaehle, S. (2025). Uncertainties in fertilizer-induced emissions of soil nitrogen oxide and the associated impacts on ground-level ozone and methane. *EGUsphere*. https://doi.org/10.5194/egusphere-2025-1416

González Ortiz, Alberto., Guerreiro, Cristina., & Soares, Joana. (2020). *Air quality in Europe: 2020 report*. European Environment Agency. https://doi.org/10.2800/786656

Govoni Brondi, M., Bortoletto-Santos, R., Farias, J. G., Farinas, C. S., Ammar, M., Ribeiro, C., Williams, C., & Baltrusaitis, J. (2024). Mechanochemically Synthesized Nitrogen-Efficient Mg- and Zn-Ammonium Carbonate Fertilizers. *ACS Sustainable Chemistry and Engineering*, *12*(16), 6182–6193. https://doi.org/10.1021/acssuschemeng.3c07785

Ha, P. T. M., Kanaya, Y., Taketani, F., Andres Hernandez, M. D., Schreiner, B., Pfeilsticker, K., & Sudo, K. (2023). Implementation of HONO into the chemistry-climate model CHASER (V4.0): Roles in tropospheric chemistry. *Geoscientific Model Development*, *16*(3), 927–960. https://doi.org/10.5194/gmd-16-927-2023

He, Y., Zhou, X., Hou, J., Gao, H., & Bertman, S. B. (2006). Importance of dew in controlling the air-surface exchange of HONO in rural forested environments. *Geophysical Research Letters*, *33*(2). https://doi.org/10.1029/2005GL024348

Huang, G., Zhou, X., Deng, G., Qiao, H., & Civerolo, K. (2002). Measurements of atmospheric nitrous acid and nitric acid. *Atmospheric Environment*, *36*(13), 2225–2235. https://doi.org/10.1016/S1352-2310(02)00170-X

Huber, D. E., Kort, E. A., & Steiner, A. L. (2024). Soil Moisture, Soil NOx and Regional Air Quality in the Agricultural Central United States. *Journal of Geophysical Research: Atmospheres*, *129*(12). https://doi.org/10.1029/2024JD041015

IPCC. (2023). Climate Change 2021- The Physical Science Basis. *Cambridge University Press*. https://doi.org/https://doi.org/10.1017/9781009157896

Jang, J.-H., Hong, J., Kim, J. B., Park, S., Hwang, K., Kim, J., Kim, J. Y., Bae, G.-N., Kim, S., & Kim, K. H. (2025). Influence of atmospheric ammonia on secondary inorganic aerosol formation in PM2.5 during spring 2024 in the Hongseong area, Republic of Korea. *Atmospheric Environment*, 121363. https://doi.org/10.1016/j.atmosenv.2025.121363

Kamboures, M. A., Raff, J. D., Miller, Y., Phillips, L. F., Finlayson-Pitts, B. J., & Gerber, R. B. (2008). Complexes of HNO3 and NO3- with NO2 and N2O4, and their potential role in atmospheric HONO formation. *Physical Chemistry Chemical Physics*, *10*(39), 6019–6032. https://doi.org/10.1039/b805330h

Kamp, J. N., Häni, C., Nyord, T., Feilberg, A., & Sørensen, L. L. (2020). The aerodynamic gradient method: Implications of non-simultaneous measurements at alternating heights. *Atmosphere*, *11*(10). https://doi.org/10.3390/atmos11101067

Kleffmann, J., Gavriloaiei, T., Hofzumahaus, A., Holland, F., Koppmann, R., Rupp, L., Schlosser, E., Siese, M., & Wahner, A. (2005). Daytime formation of nitrous acid: A major source of OH radicals in a forest. *Geophysical Research Letters*, *32*(5), 1–4. https://doi.org/10.1029/2005GL022524

Kolari, P., Bäck, J., Taipale, R., Ruuskanen, T. M., Kajos, M. K., Rinne, J., Kulmala, M., & Hari, P. (2012). Evaluation of accuracy in measurements of VOC emissions with dynamic chamber system. *Atmospheric Environment*, *62*, 344–351. https://doi.org/10.1016/j.atmosenv.2012.08.054

Kool, D. M., Wrage, N., Zechmeister-Boltenstern, S., Pfeffer, M., Brus, D., Oenema, O., & Van Groenigen, J. W. (2010). Nitrifier denitrification can be a source of N2O from soil: A revised approach to the dual-isotope labelling method. *European Journal of Soil Science*, *61*(5), 759–772. https://doi.org/10.1111/j.1365-2389.2010.01270.x

Lao, M., Crilley, L. R., Salehpoor, L., Furlani, T. C., Bourgeois, I., Andrew Neuman, J., Rollins, A. W., Veres, P. R., Washenfelder, R. A., Womack, C. C., Young, C. J., & VandenBoer, T. C. (2020). A portable, robust, stable, and tunable calibration source for gas-phase nitrous acid (HONO). *Atmospheric Measurement Techniques*, *13*(11), 5873–5890. https://doi.org/10.5194/amt-13-5873-2020

Laufs, S., Cazaunau, M., Stella, P., Kurtenbach, R., Cellier, P., Mellouki, A., Loubet, B., & Kleffmann, J. (2017). Diurnal fluxes of HONO above a crop rotation. *Atmospheric Chemistry and Physics*, *17*(11), 6907–6923. https://doi.org/10.5194/acp-17-6907-2017

Lee, B. H., Lopez-Hilfiker, F. D., Mohr, C., Kurtén, T., Worsnop, D. R., & Thornton, J. A. (2014). An iodide-adduct high-resolution time-of-flight chemical-ionization mass

spectrometer: Application to atmospheric inorganic and organic compounds. *Environmental Science and Technology*, *48*(11), 6309–6317. https://doi.org/10.1021/es500362a

Lehnert, N., Musselman, B. W., Seefeldt, L. C., & Gutenberg-university, J. (2021). Grand Challenges in the nitrogen cycle. *Chemical Society Reviews*, *50*, 3640–3646. https://doi.org/10.1039/d0cs00923g

Li, L., Fan, W., Kang, X., Wang, Y., Cui, X., Xu, C., Griffin, K. L., & Hao, Y. (2016). Responses of greenhouse gas fluxes to climate extremes in a semiarid grassland. *Atmospheric Environment*, *142*, 32–42. https://doi.org/10.1016/j.atmosenv.2016.07.039

Lipiec, J., Walczak, R., Witkowska-Walczak, B., Nosalewicz, A., Słowińska-Jurkiewicz, A., & Sławiński, C. (2007). The effect of aggregate size on water retention and pore structure of two silt loam soils of different genesis. *Soil and Tillage Research*, *97*(2), 239–246. https://doi.org/10.1016/j.still.2007.10.001

Liu, L., Zhang, X., Xu, W., Liu, X., Li, Y., Wei, J., Wang, Z., & Lu, X. (2020). Ammonia volatilization as the major nitrogen loss pathway in dryland agro-ecosystems. *Environmental Pollution*, *265*. https://doi.org/10.1016/j.envpol.2020.114862

Liu, Zheng, X., Li, Y., Yu, J., Ding, H., Sveen, T. R., & Zhang, Y. (2022). Soil moisture determines nitrous oxide emission and uptake. *Science of the Total Environment*, *822*. https://doi.org/10.1016/j.scitotenv.2022.153566

Ludwig, J., Meixner, F. X., Vogel, B., & Forstner, J. (2001). Soil-air exchange of nitric oxide: An overview of processes, environmental factors, and modeling studies. *Biogeochemistry*, *52*(3), 225–257. https://doi.org/10.1023/A:1006424330555

Luo, X., Zhang, M., Ni, Y., & Shen, G. (2025). Mitigation strategies for NH_3 and N_2O emissions in greenhouse agriculture: Insights into fertilizer management and nitrogen emission mechanisms. *Environmental Technology and Innovation*, *37*. https://doi.org/10.1016/j.eti.2024.103995

Maggiotto, S. R., Webb, J. A., & Thurtell, G. W. (2000). Nitrous and Nitrogen Oxide Emissions from Turfgrass Receiving Different Forms of Nitrogen Fertilizer. *American Society of Agronomy, Crop Science Society of America, and Soil Science Society of America*, *29*, 621–630.

Mangalassery, S., Sjögersten, S., Sparkes, D. L., Sturrock, C. J., & Mooney, S. J. (2013). The effect of soil aggregate size on pore structure and its consequence on emission of greenhouse gases. *Soil and Tillage Research*, *132*, 39–46. https://doi.org/10.1016/j.still.2013.05.003

Meusel, H., Tamm, A., Kuhn, U., Wu, D., Lena Leifke, A., Fiedler, S., Ruckteschler, N., Yordanova, P., Lang-Yona, N., Pöhlker, M., Lelieveld, J., Hoffmann, T., Pöschl, U., Su, H., Weber, B., & Cheng, Y. (2018). Emission of nitrous acid from soil and biological soil crusts represents an important source of HONO in the remote atmosphere in Cyprus. *Atmospheric Chemistry and Physics*, *18*(2), 799–813. https://doi.org/10.5194/acp-18-799-2018

Min, K. E., Pusede, S. E., Browne, E. C., LaFranchi, B. W., & Cohen, R. C. (2014). Eddy covariance fluxes and vertical concentration gradient measurements of NO and NO2 over a ponderosa pine ecosystem: Observational evidence for within-canopy chemical removal of NOx. *Atmospheric Chemistry and Physics*, *14*(11), 5495–5512. https://doi.org/10.5194/acp-14-5495-2014

Mochizuki, T., Amagai, T., & Tani, A. (2018). Effects of soil water content and elevated CO2 concentration on the monoterpene emission rate of Cryptomeria japonica. *Science of the Total Environment*, *634*, 900–908. https://doi.org/10.1016/j.scitotenv.2018.04.025

Moravek, A., Foken, T., & Trebs, I. (2014). Application of a GC-ECD for measurements of biosphere-atmosphere exchange fluxes of peroxyacetyl nitrate using the relaxed eddy accumulation and gradient method. *Atmospheric Measurement Techniques*, *7*(7), 2097–2119. https://doi.org/10.5194/amt-7-2097-2014

Moravek, A., Singh, S., Pattey, E., Pelletier, L., & Murphy, J. G. (2019). Measurements and quality control of ammonia eddy covariance fluxes: A new strategy for high-frequency attenuation correction. *Atmospheric Measurement Techniques*, *12*(11), 6059–6078. https://doi.org/10.5194/amt-12-6059-2019

Mosier, A. R. (2008). Exchange of Gaseous Nitrogen Compounds Between Terrestrial Systems and the Atmosphere. *Nitrogen in the Environment*, 443–462. https://doi.org/10.1016/B978-0-12-374347-3.00013-5

Mushinski, R. M., Phillips, R. P., Payne, Z. C., Abney, R. B., Jo, I., Fei, S., Pusede, S. E., White, J. R., Rusch, D. B., & Raff, J. D. (2019). Microbial mechanisms and ecosystem flux estimation for aerobic NOy emissions from deciduous forest soils. *Proceedings of the National Academy of Sciences of the United States of America*, *116*(6), 2138–2145. https://doi.org/10.1073/pnas.1814632116

Neuman, J. A., Trainer, M., Brown, S. S., Min, K. E., Nowak, J. B., Parrish, D. D., Peischl, J., Pollack, I. B., Roberts, J. M., Ryerson, T. B., & Veres, P. R. (2016). HONO emission and production determined from airborne measurements over the Southeast U.S. *Journal of Geophysical Research*, *121*(15), 9237–9250. https://doi.org/10.1002/2016JD025197

Nodeh-Farahani, D., Bentley, J. N., Crilley, L. R., Caputo, C. B., & VandenBoer, T. C. (2021). A boron dipyrromethene (BODIPY) based probe for selective passive sampling of atmospheric nitrous acid (HONO) indoors. *Analyst*, *146*(18), 5756–5766. https://doi.org/10.1039/d1an01089a

Okiti, I., Efakwu, G., Pindus, M., & Kasak, K. (2025). Environmental and biogeochemical drivers of CH4 and N2O flux variability in treatment wetlands. *Ecological Engineering*, *219*. https://doi.org/10.1016/j.ecoleng.2025.107705

Oswald, R., Behrendt, T., Ermel, M., Wu, D., Su, H., Cheng, Y., Breuninger, C., Moravek, A., Mougin, E., Delon, C., Loubet, B., Pommerening-Röser, A., Sörgel, M., Pöschl, U., Hoffmann, T., Andreae, M. O., Meixner, F. X., & Trebs, I. (2013). HONO emissions from

soil bacteria as a major source of atmospheric reactive nitrogen. *Science*, *341*(6151), 1233–1235. https://doi.org/10.1126/science.1242266

Pan, B., Lam, S. K., Mosier, A., Luo, Y., & Chen, D. (2016). Ammonia volatilization from synthetic fertilizers and its mitigation strategies: A global synthesis. *Agriculture, Ecosystems and Environment*, *232*, 283–289. https://doi.org/10.1016/j.agee.2016.08.019

Pan, B., Xia, L., Lam, S. K., Wang, E., Zhang, Y., Mosier, A., & Chen, D. (2022). A global synthesis of soil denitrification: Driving factors and mitigation strategies. *Agriculture, Ecosystems and Environment*, *327*(September 2021), 107850. https://doi.org/10.1016/j.agee.2021.107850

Pape, L., Ammann, C., Nyfeler-Brunner, A., Spirig, C., Hens, K., & Meixner, F. X. (2009). An automated dynamic chamber system for surface exchange measurement of non-reactive and reactive trace gases of grassland ecosystems. *Biogeosciences*, *6*(3), 405–429. https://doi.org/10.5194/bg-6-405-2009

Paulot, F., Jacob, D. J., Pinder, R. W., Bash, J. O., Travis, K., & Henze, D. K. (2014). Ammonia emissions in the United States, european union, and China derived by high-resolution inversion of ammonium wet deposition data: Interpretation with a new agricultural emissions inventory (MASAGE_NH3). *Journal of Geophysical Research*, *119*(7), 4343–4364. https://doi.org/10.1002/2013JD021130

Plake, D., Sörgel, M., Stella, P., Held, A., & Trebs, I. (2015). Influence of meteorology and anthropogenic pollution on chemical flux divergence of the NO-NO2-O3 triad above and within a natural grassland canopy. *Biogeosciences*, *12*(4), 945–959. https://doi.org/10.5194/bg-12-945-2015

Plake, D., Stella, P., Moravek, A., Mayer, J. C., Ammann, C., Held, A., & Trebs, I. (2015). Comparison of ozone deposition measured with the dynamic chamber and the eddy covariance method. *Agricultural and Forest Meteorology*, *206*, 97–112. https://doi.org/10.1016/j.agrformet.2015.02.014

Possanzini, M., Febo, A., & Liberti, A. (1983). New design of a high-performance denuder for the sampling of atmospheric pollutants. *Atmospheric Environment (1967)*, *17*(12), 2605–2610. https://doi.org/10.1016/0004-6981(83)90089-6

Purchase, M. L., Bending, G. D., & Mushinski, R. M. (2023). Spatiotemporal Variations of Soil Reactive Nitrogen Oxide Fluxes across the Anthropogenic Landscape. *Environmental Science and Technology*, *57*(43), 16348–16360. https://doi.org/10.1021/acs.est.3c05849

Ramazan, K. A., Syomin, D., & Finlayson-Pitts, B. J. (2004). The photochemical production of HONO during the heterogeneous hydrolysis of NO2. *Physical Chemistry Chemical Physics*, *6*(14), 3836–3843. https://doi.org/10.1039/b402195a

Reed, C., Brumby, C. A., Crilley, L. R., Kramer, L. J., Bloss, W. J., Seakins, P. W., Lee, J. D., & Carpenter, L. J. (2016). HONO measurement by differential photolysis. *Atmospheric Measurement Techniques*, *9*(6), 2483–2495. https://doi.org/10.5194/amt-9-2483-2016

Ren, X., Sanders, J. E., Rajendran, A., Weber, R. J., Goldstein, A. H., Pusede, S. E., Browne, E. C., Min, K. E., & Cohen, R. C. (2011). A relaxed eddy accumulation system for measuring vertical fluxes of nitrous acid. *Atmospheric Measurement Techniques*, *4*(10), 2093–2103. https://doi.org/10.5194/amt-4-2093-2011

Ren, Y., Stieger, B., Spindler, G., Grosselin, B., Mellouki, A., Tuch, T., Wiedensohler, A., & Herrmann, H. (2020). Role of the dew water on the ground surface in HONO distribution: A case measurement in Melpitz. *Atmospheric Chemistry and Physics*, *20*(21), 13069–13089. https://doi.org/10.5194/acp-20-13069-2020

Richardson, K., Steffen, W., Lucht, W., Bendtsen, J., Cornell, S. E., Donges, J. F., Drüke, M., Fetzer, I., Bala, G., Von Bloh, W., Feulner, G., Fiedler, S., Gerten, D., Gleeson, T., Hofmann, M., Huiskamp, W., Kummu, M., Mohan, C., Nogués-Bravo, D., … Rockström, J. (2023). *Earth beyond six of nine planetary boundaries*. https://www.science.org

Scharko, N. K., Schu, U. M. E., Berke, A. E., Banina, L., Peel, H. R., Donaldson, M. A., Hemmerich, C., White, R., & Ra, J. D. (2015). *Combined Flux Chamber and Genomics Approach Links Nitrous Acid Emissions to Ammonia Oxidizing Bacteria and Archaea in Urban and Agricultural Soil*. https://doi.org/10.1021/acs.est.5b00838

Schindlbacher, A., Zechmeister-Boltenstern, S., & Jandl, R. (2009). Carbon losses due to soil warming: Do autotrophic and heterotrophic soil respiration respond equally? *Global Change Biology*, *15*(4), 901–913. https://doi.org/10.1111/j.1365-2486.2008.01757.x

Schlesinger, W. H. (2020). *Biogeochemistry: An Analysis of Global Change* (4th ed.). Academic Press. https://doi.org/https://doi.org/10.1016/C2018-0-03255-3

Seinfeld, J. H., & Pandis, S. N. (2006). *Atmospheric chemistry and physics: from air pollution to climate change.* (2nd edition). John Wiley & Sons.

Shah, S. B., Grabow, G. L., & Westerman, P. W. (2006). *Ammonia adsorption in five types of flexible tubing materials*. https://doi.org/10.13031/2013.22253

Song, Y., Xue, C., Zhang, Y., Liu, P., Bao, F., Li, X., & Mu, Y. (2023). *Measurement Report: Exchange Fluxes of HONO over Agricultural Fields in the North China Plain*. *July*, 1–38. https://zenodo.org/record/8115973

Sörgel, M., Trebs, I., Wu, D., & Held, A. (2015). A comparison of measured HONO uptake and release with calculated source strengths in a heterogeneous forest environment. *Atmospheric Chemistry and Physics*, *15*(16), 9237–9251. https://doi.org/10.5194/acp-15-9237-2015

Spataro, F., & Ianniello, A. (2014). Sources of atmospheric nitrous acid: State of the science, current research needs, and future prospects. *Journal of the Air and Waste Management Association*, *64*(11), 1232–1250. https://doi.org/10.1080/10962247.2014.952846

Stepniewski, W., Stepniewska, Z., & Rozej, A. (2015). Gas Exchange in Soils. *Soil Management: Building a Stable Base for Agriculture*, 117–144. https://doi.org/10.2136/2011.soilmanagement.c8

Su, H., Cheng, Y., Oswald, R., Behrendt, T., Trebs, I., Meixner, F. X., Andreae, M. O., Cheng, P., Zhang, Y., & Pöschl, U. (2011). Soil nitrite as a source of atmospheric HONO and OH radicals. *Science*, *333*(6049), 1616–1618. https://doi.org/10.1126/science.1207687

Tang, K., Qin, M., Duan, J., Fang, W., Meng, F., Liang, S., Xie, P., Liu, J., Liu, W., Xue, C., & Mu, Y. (2019). A dual dynamic chamber system based on IBBCEAS for measuring fluxes of nitrous acid in agricultural fields in the North China Plain. *Atmospheric Environment*, *196*(May 2018), 10–19. https://doi.org/10.1016/j.atmosenv.2018.09.059

Tang, K., Qin, M., Fang, W., Duan, J., Meng, F., Ye, K., Zhang, H., Xie, P., Liu, J., Liu, W., Feng, Y., Huang, Y., & Ni, T. (2020). An automated dynamic chamber system for exchange flux measurement of reactive nitrogen oxides (HONO and NOX) in farmland ecosystems of the Huaihe River Basin, China. *Science of the Total Environment*, *745*(X), 140867. https://doi.org/10.1016/j.scitotenv.2020.140867

Tian, H., Pan, N., Thompson, R. L., Canadell, J. G., Suntharalingam, P., Regnier, P., Davidson, E. A., Prather, M., Ciais, P., Muntean, M., Pan, S., Winiwarter, W., Zaehle, S., Zhou, F., Jackson, R. B., Bange, H. W., Berthet, S., Bian, Z., Bianchi, D., … Zhu, Q. (2024). Global nitrous oxide budget (1980-2020). *Earth System Science Data*, *16*(6), 2543–2604. https://doi.org/10.5194/essd-16-2543-2024

Vaittinen, O., Metsälä, M., Persijn, S., Vainio, M., & Halonen, L. (2014). Adsorption of ammonia on treated stainless steel and polymer surfaces. *Applied Physics B: Lasers and Optics*, *115*(2), 185–196. https://doi.org/10.1007/s00340-013-5590-3

VandenBoer, T. C., Brown, S. S., Murphy, J. G., Keene, W. C., Young, C. J., Pszenny, A. A. P. P., Kim, S., Warneke, C., De Gouw, J. A., Maben, J. R., Wagner, N. L., Riedel, T. P., Thornton, J. A., Wolfe, D. E., Dubé, W. P., Öztürk, F., Brock, C. A., Grossberg, N., Lefer, B., … Roberts, J. M. (2013). Understanding the role of the ground surface in HONO vertical structure: High resolution vertical profiles during NACHTT-11. *Journal of Geophysical Research Atmospheres*, *118*(17), 10,155-10,171. https://doi.org/10.1002/jgrd.50721

VandenBoer, T. C., Young, C. J., Talukdar, R. K., Markovic, M. Z., Brown, S. S., Roberts, J. M., & Murphy, J. G. (2015). Nocturnal loss and daytime source of nitrous acid through reactive uptake and displacement. *Nature Geoscience*, *8*(1), 55–60. https://doi.org/10.1038/ngeo2298

Von Der Heyden, L., Wißdorf, W., Kurtenbach, R., & Kleffmann, J. (2022). A relaxed eddy accumulation (REA) LOPAP system for flux measurements of nitrous acid (HONO). *Atmospheric Measurement Techniques*, *15*(6), 1983–2000. https://doi.org/10.5194/amt-15-1983-2022

Wang, Fu, X., Wu, D., Wang, M., Lu, K., Mu, Y., Liu, Z., Zhang, Y., & Wang, T. (2021). Agricultural Fertilization Aggravates Air Pollution by Stimulating Soil Nitrous Acid Emissions at High Soil Moisture. *Environmental Science and Technology*, *55*(21), 14556–14566. https://doi.org/10.1021/acs.est.1c04134

Wang, Y., Fu, X., Wang, T., Ma, J., Gao, H., Wang, X., & Pu, W. (2022). Large Contribution of Nitrous Acid to Soil-Emitted Reactive Oxidized Nitrogen and Its Effect on Air Quality. *Environmental Science and Technology*. https://doi.org/10.1021/acs.est.2c07793

Wolff, V., Trebs, I., Ammann, C., & Meixner, F. X. (2010). Atmospheric Measurement Techniques Aerodynamic gradient measurements of the NH3-HNO3-NH4NO3 triad using a wet chemical instrument: an analysis of precision requirements and flux errors. In *Atmos. Meas. Tech* (Vol. 3). www.atmos-meas-tech.net/3/187/2010/

Wu, D., Deng, L., Liu, Y., Xi, D., Zou, H., Sha, Z., Pan, Y., Hou, L., & Liu, M. (2020). *Comparisons of the effects of different drying methods on soil nitrogen fractions: Insights into emissions of reactive nitrogen gases (HONO and NO)*. https://doi.org/10.1080/16742834.2020.1733388

Wu, D., Horn, M. A., Behrendt, T., Müller, S., Li, J., Cole, J. A., Xie, B., Ju, X., Li, G., Ermel, M., Oswald, R., Fröhlich-Nowoisky, J., Hoor, P., Hu, C., Liu, M., Andreae, M. O., Pöschl, U., Cheng, Y., Su, H., … Sörgel, M. (2019). Soil HONO emissions at high moisture content are driven by microbial nitrate reduction to nitrite: tackling the HONO puzzle. *ISME Journal*, *13*(7), 1688–1699. https://doi.org/10.1038/s41396-019-0379-y

Wu, D., Zhang, J., Wang, M., An, J., Wang, R., Haider, H., Xu-Ri, Huang, Y., Zhang, Q., Zhou, F., Tian, H., Zhang, X., Deng, L., Pan, Y., Chen, X., Yu, Y., Hu, C., Wang, R., Song, Y., … Liu, M. (2022). Global and Regional Patterns of Soil Nitrous Acid Emissions and Their Acceleration of Rural Photochemical Reactions. *Journal of Geophysical Research: Atmospheres*, *127*(6), 1–16. https://doi.org/10.1029/2021JD036379

Yang, J. Y., Drury, C. F., Jiang, R., Worth, D. E., Bittman, S., Grant, B. B., & Smith, W. N. (2024). Reactive nitrogen losses from Canadian agricultural soils over 36 years. *Ecological Modelling*, *495*. https://doi.org/10.1016/j.ecolmodel.2024.110809

Young, C. J., Washenfelder, R. A., Roberts, J. M., Mielke, L. H., Ostho, H. D., Tsai, C., Pikelnaya, O., Stutz, J., Veres, P. R., Cochran, A. K., Vandenboer, T. C., Flynn, J., Grossberg, N., Haman, C. L., Lefer, B., Stark, H., Graus, M., Gouw, J. De, Gilman, J. B., … Brown, S. S. (2012). *Vertically Resolved Measurements of Nighttime Radical Reservoirs in Los Angeles and Their Contribution to the Urban Radical Budget*.

Zhang, S., Sarwar, G., Xing, J., Chu, B., Xue, C., Sarav, A., Ding, D., Zheng, H., Mu, Y., Duan, F., Ma, T., & He, H. (2021). Improving the representation of HONO chemistry in CMAQ and examining its impact on haze over China. *Atmospheric Chemistry and Physics*, *21*(20), 15809–15826. https://doi.org/10.5194/acp-21-15809-2021

Zhou, S., Young, C. J., VandenBoer, T. C., Kowal, S. F., & Kahan, T. F. (2018). Time-Resolved Measurements of Nitric Oxide, Nitrogen Dioxide, and Nitrous Acid in an Occupied New York Home. *Environmental Science and Technology*, *52*(15), 8355–8364. https://doi.org/10.1021/acs.est.8b01792

Zörner, J., Penning De Vries, M., Beirle, S., Sihler, H., Veres, P. R., Williams, J., & Wagner, T. (2016). Multi-satellite sensor study on precipitation-induced emission pulses of NOx from soils in semi-arid ecosystems. *Atmospheric Chemistry and Physics*, *16*(14), 9457–9487. https://doi.org/10.5194/acp-16-9457-2016

Chapter Three: Investigating and understanding the intact agricultural soil N_r emissions in a controlled laboratory environment

Author's Contributions: MS wrote, and TCV edited this work.

3.1 Introduction

Nitrogen is essential for plant growth, but its inefficient and excessive use in the form of fertilizers drives the soil N_r emissions out of control. Soil nitrogen emissions to the atmosphere include several N_r compounds that are NO, NO_2, HONO, and NH_3 due to both current use of fertilizers and the buildup of nitrogen from past applications. These N_r contribute to the formation of tropospheric O_3 and particulate matter, affecting both human health and climate. Agricultural soils are expected to be hotspots as they are intensively managed through external inputs of nitrogenous fertilizers. Agricultural soils in Canada account for approximately 1200 kilotons (kt) of NO_x, 460 kt of NH_3 and 37.6 megatons (mt) of N_2O emissions (Agriculture and Agri-Food Canada, 2023; Ritchie & Roser, 2023). Over the last centuries, people have increasingly used nitrogen fertilizer to increase crop yields. Excess nitrogen can build up in the environment that is not taken up by crops, runs off the land and pollutes rivers, lakes, and the atmosphere for decades later. The amount of nitrogen added to the soils through fertilizers (i.e., 120 Tg N yr^{-1}) far exceeds that added by biological processes that fix nitrogen (60 Tg N yr^{-1}) (Galloway et al., 2008). Crops typically recover up to half of the nitrogen added, but the remaining is lost via various loss pathways like volatilization, leaching or through biological processes like nitrification and denitrification (Osterberg, 2022). Therefore, substantial interest in soil NO_y (i.e. NO + NO_2 + HONO + HNO_3, etc.) fluxes is of growing interest in the global research community.

Research on soil NO and N_2O emissions has been done; however, a comprehensive investigation to measure all N_r species, such as NO_2, and HONO, remain limited. Numerous studies have explored that soil microbial activity leads to the release of NO and N_2O (Butterbach-Bahl & Dannenmann, 2011; Kool et al., 2010; Krichels et al., 2024; M. Tan et al., 2025). This is because non-destructive methods for GHGs like N_2O allow easier flux measurements using spectroscopic techniques. After all, there is no chemical transformation of the analyte (Harris et al., 2020; Rapson & Dacres, 2014). The primary challenge is that these gases (NO_2, HONO) are prone to rapid chemical transformations and interactions with other atmospheric constituents, or by interacting with sampling inlet surfaces, making it difficult to capture their true concentrations and fluxes

accurately (Seinfeld & Pandis, 1998). Limited studies have reported simultaneous measurements of NO, NO_2, and HONO. Scharko et al. (2015) and Tang et al. (2019) were among the first to have highlighted the potential for both HONO and NO_x fluxes from agricultural soils as hotspots impacting atmospheric chemistry. Another reason for focusing on HONO in particular is that, while studies measuring NO, N_2O, and CO_2 show good agreement between laboratory and field observations, the same can not be predicted for HONO, as laboratory observations differ from field measurements. The assumption that biological processes alone govern HONO release, with oversight of the surface chemistry and other abiotic sources, is probably misleading and contributes to the differences between lab and field data.

To address these challenges, dynamic chamber systems integrated with a suite of destructive gas analyzers have been used for measuring localized N_r fluxes such as NO_2 and HONO. Only two studies to date have measured soil NO_2 emissions, making it difficult to infer how much NO_2 might evolve from soils (Pilegaard, 2013; Purchase et al., 2023), let alone any fundamental controls on its production and release within them. The complexity of nitrite (NO_2^-) chemical and biological production and loss in soils, coupled with soil properties facilitating gas exchange of HONO, has led to intense interest and debate around discerning the fundamental controls on its surface-atmosphere exchange (Meusel et al., 2018; Mushinski et al., 2019; Purchase et al., 2023; Song et al., 2023b; Wang et al., 2021). In previous studies significant HONO emissions were estimated from soil samples that reached up to 3000 ng N m^{-2} s^{-1} by Su et al. (2011), but were more typically on the order of 340 ng N m^{-2} s^{-1} as reported by Wang et al. (2021), 250 ng N m^{-2} s^{-1} by Oswald et al. (2013), and 200 ng N m^{-2} s^{-1} by Meusel et al. (2018). Lab experiments have showcased agricultural soils as the strongest HONO emitter, but what has gone relatively unrecognized is how researchers have heavily manipulated their soils. In the case of Su et al. (2011), they had adjusted the soil to a pH by adding dilute HCl, in addition to adding $NaNO_2$ solution to the soil sample, which effectively replicates well-established HONO calibration sources (Lao et al., 2020; Roberts et al., 2010). Lab studies have reported the maximum emission potential of the NO to HONO ratio to be below one (Oswald et al., 2013; Wang et al., 2021; Wu et al., 2019). Whereas field measurements ranged from 4.5 up to more than 100 (like the one in this study) (Meng et al., 2024; Tang et al., 2019). Researchers like Wang et al. (2021), Oswald et al. (2013) and Meusel et al. (2018) all have aggressively dried small amounts (~7-15.5 g) of their soils and used dry zero air to rapidly flush chamber headspace. These sampling disturbances need to be considered, or their

propensity for bias evaluated, as they universally use homogenized, sieved, aggressively dried, and pre-conditioned soils, resulting in soil emission scenarios that may be of limited relatability to the real world. In addition, emission potentials from these experiments with similar soil properties (e.g., soil type, pH, density, etc.) have been another issue, as lab studies usually generalize these as a whole for the production of their respective N_2O species.

In contrast, field measurements retain soils intact and are subject to natural variations in soil properties, microbial activity, and meteorological conditions, which can alter HONO emissions in ways that are difficult to reproduce in the lab (Song et al., 2023b; Tang et al., 2019). To date, field studies that represent direct comparable field measurement for HONO under ambient conditions have reported fluxes to be $\leq$2.5 ng m^{-2} s^{-1}, that is, around two orders of magnitude less than the lab studies (Laufs et al., 2017; X. Ren et al., 2011; Sörgel et al., 2011; Tang et al., 2020). To mimic real-world conditions, environmentally relevant parameters must be considered when designing laboratory experiments to study the release of HONO.

Agricultural fields are assumed to be homogeneous, based on uniform agricultural practices or crop types. This assumption of field homogeneity can lead to substantial uncertainty when interpreting emission data. While fields may appear uniform, soils often differ in texture, organic matter content, pH, the presence of microbial community, and nutrient history, even within the field. Studies have simplified this complexity by treating soils as spatially uniform or by relying on single-point measurements to represent broader land areas, leading to discrepancies between lab and field observations. In this work, an effort has been made to measure soil NO, NO_2 and HONO emissions simultaneously using our modified dynamic chambers. Careful attention was given to the design of soil preparation across all samples to ensure comparability of results across the samples while preserving the soil properties so that experimental samples could behave more like intact samples in the field. By avoiding practices like aggressive drying, grinding, addition of artificial reagents, we aim to ensure that our samples remain comparable not only to each other but to soils as they exist in the field. The heterogeneity is examined from an in-use agricultural field under controlled lab conditions. Comparable results obtained for NO, NO_2 and HONO fluxes would indicate that a typical pooled sample would generate consistent N_r fluxes for application at the landscape scale. If this assumption holds, it will support the use of simplified soil

representations however, if it does not then the assumption of fields being homogeneous becomes problematic.

3.2 Method

3.2.1 Importance of the custom-built automated dynamic chamber for N_r flux measurements

The modifications outlined in Chapter Two bridge this gap by offering a practical solution that allows researchers to deploy field-ready chambers for real-time, accurate measurements. Conventional chambers often had issues like gas adsorption, surface transformations, for reactive species, leading to underestimations of N_r exchange at atmospheric-surface interfaces. Through targeted modifications mentioned in chapter two, such as the use of PTFE fittings and PFA film, helped to reduce gas adsorptions, minimize surface interactions and prevent gas transformations on the chamber surface, enabling measurements for N_r species.

These chambers are compatible with a range of embedded and auxiliary sensors, allowing simultaneous monitoring of multiple environmental parameters, such as air temperature, relative humidity (RH), photosynthetically active radiation (PAR), soil temperature, and volumetric water content (VWC). These features make the custom-built chamber for monitoring the environmental conditions, simultaneously making it an indispensable tool for studying nitrogen cycling. By enabling automated measurements, the custom-built dynamic chamber system reduces labour intensity and potential human error associated with manual sampling.

3.2.2 Experimental site description, soil features, and soil sampling

Soil samples were collected from an agricultural farm in Lambton Shores, Southwestern Ontario (43°09'36.0" N, 81°55'48.0" W). The farm has a clay soil type, consisting of 48.7% clay, 28.0% silt and 23.2% sand. In clay soils, the smaller particle size results in a greater amount of pore space compared to coarser-textured soils like sandy or loam. The bulk density of this soil is 1.12 g cm^{-3}, and the collected soil had a pH of 7.6, indicating a slightly alkaline condition.

Using a random grid sampling technique, 32 soil samples were collected at a depth of 0–6 inches on October 28, 2021. This systematic method is used in agricultural research for its reliability in unbiased sample collection as it minimizes sampling bias, assuming that topographic variations do not affect soil properties and nutrient content within the designated plot area (Baio et al., 2023;

Dinkins et al., 2008; Houlong et al., 2016). In this sampling technique, a grid was superimposed on the field, dividing the total area into eight identical plots (A–H), each covering an area of 10800 m^2 (120 m × 90 m), as shown in **Figure 3.1**. Python, a computer programming language, was used to generate four random coordinates within each plot for soil collection (**Figure 3.1**), with the assumption that samples collected within a 1 m^2 area were homogenous (Appendix B contains the Python code used to generate the coordinates).

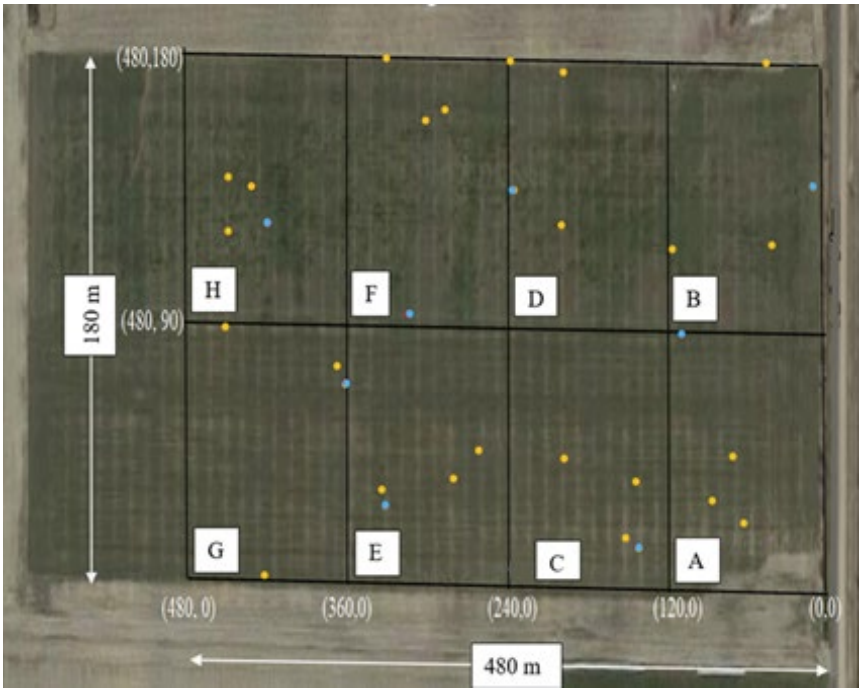

Figure 3.1: Schematic representation of soil sampling from an agricultural field (86,400 m^2, 480 × 180 m) divided into eight plots (A-H) of equal size, with (x,y) coordinates for each grid shown in metres, using a random grid sampling method. Four soil samples were collected per plot: three random samples (yellow dots) representing individual samples (samples A–H) and one pooled sample (blue dots) representing a composite for each plot. The dot locations are approximate, based on algorithmically obtained coordinates from a Python script.

Within each plot, four samples were taken to improve the representation of soil properties and nutrient content for each plot. Of these, three samples represent the plot's characteristics (A–H), and one additional sample from each plot was combined across all plots to create a pooled sample, as detailed in **Table S3.1** (Appendix B). Sampling was conducted following the year's corn harvest using GPS on a smartphone to locate the coordinates. Soil cores were transferred into pre-labelled, clean Ziploc bags at ambient temperatures, stored in the parking garage (~5 °C) and transported to the laboratory within one week of collection for analysis.

3.2.3 Drying of the soil sample

The soil samples were oven-dried after manually removing roots, seeds, worms, debris, and stones to ensure that the measured mass represents only the soil fraction, preventing mass bias from non-soil materials. Drying was carried out by spreading the soil on stainless-steel mesh trays lined with aluminum foil and placing them in an oven at 35 °C for approximately 24–72 hours. The drying temperature of 35 °C was chosen to reflect the natural conditions that soils experience during summer, thereby enhancing the comparability of the laboratory-prepared soils with those in the field (Nodeh-Farahani et al., 2025, in preparation). The temperature was carefully monitored to avoid affecting microbial viability, ensuring that the drying conditions were less extreme than those typically experienced under natural summer conditions. Wang et al. (2021) emphasize the importance of low-temperature drying for preserving soil biological characteristics. Unlike studies that use higher drying temperatures (e.g., >40 °C) to expedite moisture removal (Haney et al., 2004; Jager & Bruins, 1975; Sunil & Deepa, 2016). Higher drying temperatures can compromise microbial activity and alter nutrient content, leading to misrepresentations of soil biogeochemical processes.

During the drying process, the soil was periodically removed and mixed to promote complete drying. Drying was required to eliminate variability from the unknown initial moisture content of soil, while subsequent rehydration to a defined soil VWC allowed accurate control of both soil mass and water content for each experimental run. Drying was considered complete when there was no noticeable change in mass after two consecutive weighing determinations taken 12 hours apart (i.e., reading varied by less than ± 1 g) using an analytical balance (Mettler Toledo, ME103E; 120 ± 0.001 g). Once dried, the soil samples were stored in labelled Ziploc bags at room temperature until further processing or emissions analysis.

3.2.4 Preparation and storage of plot and pooled soil samples prior to laboratory emission analysis

The dried soil was homogenized by breaking aggregates of soil clumps into smaller soil particles 1 cm in diameter and smaller using a mortar and pestle to ensure uniformity (**Appendix B, Figure S3.2**). Representative plot samples (Sample A–H) were prepared by combining equal dry mass from three subsamples collected within each plot. For instance, Sample A was formed by mixing 120 g of soil from three specific points within plot A (coordinates: 21, 57; 77, 58; 83, 29) as

indicated by the yellow dots in **Figure 3.1**. The combined 360 g of soil was then placed into a clean, labelled Ziploc bag. The bag was sealed and shaken vigorously by hand for approximately 30 seconds to thoroughly homogenize the sample. The manual mixing technique was chosen over mechanical mixing to preserve natural soil structure, which could be disrupted by aggressive methods like mechanical stirring and/or ultrasonication treatment (Bao et al., 2022; W. Zhou et al., 2020). The same procedure was followed for plots B through H, ensuring consistency in sample preparation. Detailed subsample coordinates and masses for each plot are provided in Appendix B (**Table S3.1**). Duplicate samples were prepared in the same manner for each plot sample. Consistency was maintained across the preparation process for samples from plots B through H by using identical tools, sample handling techniques, and environmental conditions (i.e. room temperature).

In addition to the individual plot samples, a pooled sample was prepared to represent the entire field. This composite sample was created by taking equal dry masses (~50 g) from one subsample in each plot (A–H), corresponding to the blue points in **Figure 3.1**. These eight contributions were thoroughly mixed following the same steps outlined above to achieve a final mass of approximately 1200 g. The pooled sample was shaken vigorously by inverting the bag by hand for approximately 30 seconds. The homogenized sample was then stored in a clean, labelled Ziploc bag at room temperature for subsequent manipulations and/or emissions analyses. Duplicate pooled samples were prepared in the same manner. This methodology ensures the maximum comparability within and between all samples, that is, both plot-specific and field-representative samples are being consistently prepared to be as individually homogeneous as possible without overly processing them to the point that the soil structure undergoes substantial change.

3.2.5 Calibration of NO_x analyzer prior to soil emission determinations

Calibration ensures accurate and reliable measurements by checking the instrument's response. The NO_x analyzer (Serinus 40, American Ecotech, Warren, RI) was calibrated following a standardized procedure. The instrument is first warmed up for at least two hours, ensuring no error messages are displayed, and so that the catalyst for converting NO_2 to NO has reached its setpoint of 325 °C. Calibration gases are provided using a GasCal (Gascal 1100TS, American Ecotech, Warren, RI), which has mass flow controllers (MFCs) to regulate the flow rates. Before introducing calibration gases, all lines are flushed with ZA (Praxair; Air Ultra Zero, 99.999 %, AI 0.0UZ-K). A known concentration of NO gas (Praxair, NI NO5MC-A3, 4.50 (±5 %) ppmv) was connected to

one channel of the GasCal system, diluted to the desired calibration mixing ratio, and the corresponding instrument response recorded. Span calibration with 80 ppb of NO was delivered for 30 minutes to stabilize prior to confirming if there was drift in the instrument response. If a deviation greater than 1 ppb was detected, a multi-point calibration with additional 60 ppb and 40 ppb NO mixing ratios was performed to redefine the instrument response, and to assess its linearity and precision. For NO_2, calibration was conducted by reacting excess NO with a limited amount of ozone (O_3) generated through gas phase titration within the GasCal to form NO_2. Mixing ratios of 40, 50, and 60 ppb of NO_2 were introduced to the analyzer and allowed to stabilize. The conversion efficiency of NO_2 across this range was assessed to ensure that the value was at least 96%. Before use for experimental measurements, the system was flushed with zero air for 30 minutes to purge residual gases and restore baseline conditions. Upon successful calibration, a slope of 1.00 ± 0.02 and $r^2 > 0.98$ confirmed the analyzer to be properly calibrated and ready for use to collect experimental measurements (**Appendix B, S.3.3**). Span checks were conducted twice in between the soil experiments described below to verify the analyzer performance using 40 ppb of NO. Conversion efficiency of the catalyst was assessed before and after the experiments and found to be unchanged and greater than 96%.

3.2.6 Calibration of the soil moisture sensor

Measurements of soil moisture were performed using a TEROS 11 advanced soil moisture sensor (METER Group, Inc.). The device was calibrated according to the manufacturer's guidelines to ensure accurate measurements of soil volumetric water content (VWC). Calibration was carried out using a representative, pooled soil sample identical to the soil used during experimental measurements, ensuring that the sensor response would accurately reflect the dielectric properties of the target soil matrix.

The soil was packed into a cylindrical flowerpot with a conical frustum shape (height: 11 cm; bottom radius: 7.5 cm; top radius: 11 cm). Its geometry allowed for sufficient soil depth to fully insert the 5.5 cm TEROS 11 prongs vertically into the soil, ensuring full contact and minimizing the presence of air gaps that could affect the dielectric readings.

Calibration involved incremental wetting of the soil, starting with completely dry soil. At each step, deionized water ($\rho \geq 18.2$ MΩ·cm) was added in sequential increments as follows: 100 mL, 100 mL, 80 mL, 50 mL, corresponding to 5 points on the calibration curve (**Appendix S3.4**). After

each addition of DIW, the soil was mixed thoroughly in a larger container to ensure even moisture distribution. The wet soil was transferred back into the flowerpot, and the soil probe was inserted for 5 minutes to stabilize before recording the voltage. The sensor output, including dielectric permittivity and factory-calibrated VWC value, was recorded after each wetting step (**Appendix S3.4**). A calibration curve was developed by plotting the sensor voltage output against the calculated VWC values. The sensor data ranged from 1930 mV (completely dry) to 2635 mV (saturated), and the resulting third-order polynomial equation was determined as directed by the manufacturer (**Appendix B**). The saturated VWC value for this soil type corresponded to a reading of 2635 mV at a value of 35.0% (v/v) (**Appendix B, Table S3.4, Figure S3.4**). This calibration curve allows conversion of the sensor voltage measurements to VWC values for field or lab measurements, so long as the same soil type is being utilized.

3.2.7 Setup of the dynamic chamber system

The fluxes of NO, NO_2, and HONO from soil samples were measured using our dynamic chamber system coupled with a commercial NO_x analyzer (Serinus 40, American Ecotech, Warren, RI) modified with a Na_2CO_3-coated annular denuder and a solenoid valve so that it is capable of measuring HONO (Lao et al., 2020). The chamber is manufactured with a small fan, mounted on an adjustable arm, to ensure that the gases are mixed uniformly within the chamber headspace (Pape et al., 2009; Pavelka et al., 2018) (**Figure 3.2**).

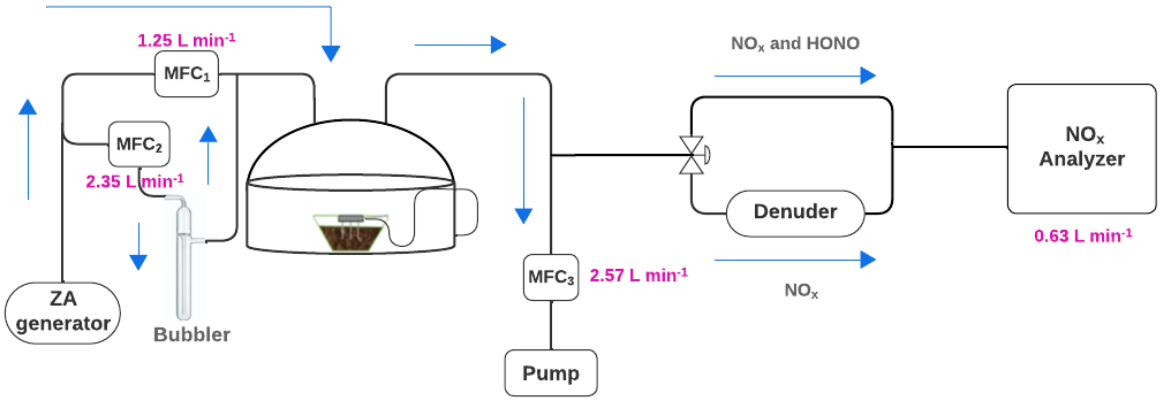

Figure 3.2: Schematic of the dynamic chamber system for measuring NO, NO_2, and HONO fluxes. Soil samples were placed on a stainless-steel mesh tray covered with PFA inside the chamber and flushed with zero air humidified to 65% RH at a constant flow rate of 3.6 L min^{-1}. A small fan ensured uniform gas mixing, and a probe monitored soil moisture level. One pathway directed air to the NO_x analyzer (measuring NO, NO_2, NO_x, and HONO), while another pathway passed air

through a denuder (measuring NO, NO_2, and NO_x). Blue arrows indicate airflow to and from the chamber.

This design feature is crucial for dynamic flux measurements, where accurate detection of gas concentration changes over time depends on the assumption that the sampled air represents the amount present in the entire chamber volume (Pavelka et al., 2018; Themistokleous et al., 2024). Without sufficient mixing, spatial gradients of gas concentration may develop, particularly near the soil surface, leading to biased or unrepresentative flux calculations (Pavelka et al., 2018). Proper mixing ensures that the air sampled at the outlet line reflects the true mean concentration of the chamber atmosphere, thereby enhancing the reliability and reproducibility of flux estimates. Satisfaction of this requirement was obtained from our controlled filling and emptying experiments for all N_r species (see **Section 2.3.1.2**, Chapter 2).

This experimental setup provided precise control over environmental conditions (i.e., humidity, soil and temperature), ensured that the system was leak-free, and allowed robust quantification of gaseous emissions from the soil samples. While temperature was not directly controlled at the chamber level, it was maintained at a constant value by the building HVAC system, which holds room temperature between approximately 20-23 °C. This approach aligns with many previous studies that conduct measurements at ambient room temperature, under the assumption that minor fluctuations do not impact soil emission dynamics (Oswald et al., 2013; Wang et al., 2021). To contextualize the design of this study, it is useful to compare it with experimental setups from existing literature (**Table 3.1**).

Table 3.1: Summarizes the key methodological choices across relevant laboratory studies. Most of these studies use purified air (PA) that is air without hydrocarbons, water vapour, HONO, NO_x, and O_3. Data not available in the report is represented by (-).

Study	Headspace gas	Head-space gas RH (%)	Temp. (°C)	Soil type	Soil prep	Analytes	Analyzer
This study	ZA	65	20-23	Agricultural soil (Soybean and corn; Ag)	Section 3.2.2/3	NO, NO_2, HONO	Modified NO_x
Bao et al. (2022)	PA	46	22	Ag (wheat)	Air-dried, ground, and sieved. Soil wet with DIW by mechanical stirring	HONO	LOPAP
Oswald et al. (2013)	PA	-	25	One of each from forest (Eucalyptus, tropical rain, coniferous), grassland, desert, Ag (corn, wheat, cotton)	Dried, ground, sieved and stored in an open plastic bag (4 °C)	NO; HONO	Chemiluminescence detector (CLD); LOPAP
Scharko et al. (2015)	ZA	50	22	Two samples: Ag (soybean), municipal park	Air-dried, sieved, stored in plastic containers	HONO or $HO^{15}NO$	CIMS
Wang et al. (2022)	PA	0	25	24 cropland and 24 forest	Fertilized soil (urea, NH_4HCO_3, NH_4NO_3)	HONO	LOPAP
Weber et al. (2015)	PA	0	25	Desert soil	Air-dried and stored at 5 °C	NO, NO_2; HONO	CLD; LOPAP
Wu, Deng, Liu, Xi, Zou, Wang, et al. (2020)	PA	-	-	Farmland, grassland, forest, grassland	Sieved soil was divided into four parts: air, freeze, oven-dried, and fresh soil	HONO, NO_x; O_3; CO_2, and H_2O	Stripe coil coupled with high-performance liquid chromatography (SC-HPLC), CLD; O_3 analyzer; LI-COR

The flow through the soil flux experimental setup was held constant at 3.60 L min^{-1}, which produces a residence time of 20 minutes for air inside the chamber. The chamber was sealed, using the reference chamber rings and PFA film during all measurements (see **Section 2.S1, Appendix A**). The gas flow to the chamber headspace consisted of zero air supplied via a pump connected to a mass flow controller (MFC 1), which maintained a flow rate of 1.25 L min^{-1} (**Figure 3.2**). The zero-air generator was custom-built, consisting of a pump, water filter (0.25" NPT, AFR-2000, SPK603, Thailand), membrane air dryer (IDG1-N02, Proax Technologies Ltd, Oakville, ON, Canada), and empty tube cartridges (400 cm^3, 0.25" Swagelok tube fittings, Chromatographic Specialties Inc.) filled with a mixture of molecular purification media (CP Blend, Purakol, Purafil Inc., Doraville, GA, U.S.A) to remove trace gases like NO_x, ammonia (NH_3), ozone (O_3), water, and volatile organic compounds (VOCs). Humidification of the air to 65% RH mimicked the atmospheric humidity observed over this soil from field campaigns conducted by the group, so that drying was representative of typical environmental conditions. This was achieved using a bubbler connected to MFC 2, operated at a flow rate of 2.35 L min^{-1} (**Figure 3.2**), which generated an airflow saturated with water vapour. The flow rate exiting the chamber was controlled at ~2.57 L min^{-1} using MFC 3, while the NO_x analyzer sampling flow is an additional ~0.63 L min^{-1}, resulting in a total outflow of approximately 3.20 L min^{-1}. The difference between the inflow and outflow (~0.4 L min^{-1}) was released through a vent installed in the side of the dynamic chamber, which is designed to maintain atmospheric pressure within. This serves as our point of atmospheric overflow in all experiments, much like any standard gas calibration setup (see Section 3.2.4).

Before introducing soil samples, a blank experiment was conducted using the same experimental setup. The chamber was flushed with ZA at 65% RH for 20 mins, with only the stainless-steel mesh tray and soil VWC probe inside, to establish baseline conditions. Baseline stability was verified by monitoring NO and NO_2 concentrations, which were to remain at ~0 ppbv and ≤2 ppbv, respectively. Between duplicate analyses for each plot, the chamber was also flushed for 20 minutes with 65% humidified ZA. Once the NO and NO_2 signals were confirmed to have returned to baseline levels consistent with prior blank measurements within this period, it confirmed there were no leaks in the system, and it also prevented any potential emission carryover between experiments.

For each experimental soil run, duplicate samples from plots A-H and triplicates from the pooled sample, 350 g of soil was weighed using a calibrated analytical balance and transferred into a mortar. A precise volume of 280 mL of DIW measured using a graduated measuring cylinder (500 ±1.30 mL) was poured into the mortar, and the soil was thoroughly mixed for 2 minutes using a stainless-steel laboratory spatula to obtain uniform hydration between 25-27% VWC. The prepared wetted soil was then gathered as a single lump onto a stainless-steel mesh tray lined with PFA film. The soil VWC probe was inserted vertically into the soil to continuously monitor the moisture level throughout the experiment, instead of using the headspace water content from flowing completely dry air over the sample, as has been done in other reports (**Table 3.1**). Following the probe insertion, the tray was placed into the chamber, and the chamber was closed using the Eosense software (eosAnalyze-AC, Eosense Inc., Dartmouth, NS) to initiate the measurement cycle. The time required for each sample, from the initial soil sample drying to a hydrated state ready for analysis, took approximately 50 hours.

A solenoid valve was then used to alternate headspace air sampling between two pathways: one for the direct measurement of the sum of NO_x (NO + NO_2) and HONO concentrations, and the other for measuring NO_x after selectively removing HONO. The valve was controlled via LabJack software to switch between pathways at regular intervals of 5 minutes to obtain reliable measurements, when post-processing the observations (see Section 3.2.7) (Lao, 2022; Lao et al., 2020). The program logs the date and time, elapsed time, and the switching of solenoid valves. The program logs the valve state of the initial position as '0' (NO_x + HONO) and when it switches as '1' (NO_x) for easy flagging and post-processing of the data. The mixing ratio of HONO (in parts per billion by volume, ppbv) was calculated as the difference between the NO_2 and the sum of NO_2 and HONO obtained from the two pathways.

3.2.8 Data processing for NO, NO_2 and HONO flux calculations

The data processing workflow began by collecting measurements from multiple instruments operating at different time resolutions. Soil probe data were recorded every 10 seconds, while the NO_x analyzer provides measurements for NO, NO_2 or the combined NO_2 + HONO signal at one-minute intervals. Valve data, recorded at a much higher frequency (60 data points per minute), were essential for distinguishing HONO from the NO_2 + HONO signal. The valve switch interval was set to 5 minutes, sampling between the two pathways (**Figure 3.2**). Due to the switching

mechanism, it was observed that the first measurement immediately after each valve switch could be contaminated by residual air from the previous sampling channel. These measurements were systematically removed in each valve cycle to ensure the instrument was fully sampling from the correct line when including data for analysis. No additional steps were performed beyond the removal of these data points for each cycle. The HONO values were then interpolated to achieve one-minute time resolution across the dataset. After interpolation, all datasets (NO, NO_2, HONO, valve state, and soil probe readings) were synchronized to one-minute intervals, producing a unified dataset on the same time base. The data were subsequently averaged to 10-minute intervals, smoothing short-term variability and enabling clearer interpretation of gas fluxes to soil VWC (%). Atmospheric gas flux from the soil sample within the dynamic chamber was then calculated using the change in respective gas concentration over time, the chamber volume, and the soil surface area occupied in the chamber. The fluxes of HONO, NO, and NO_2 were calculated based on the difference in concentration when the soil sample was placed in the chamber (C_{sample}) versus the background concentration in zero air measured in the absence of a soil sample ($C_{background}$) using Equation 5. To compare the replicates within the sample plot and/or with the pooled sample, the fluxes within a specific binned soil VWC range were examined.

$$F_N = \frac{Q}{A} \times \frac{M_N}{V_m} \times \left[C_{sample} - C_{background}\right] \qquad \text{(E5)}$$

Where F_N is the measured flux (μg N m^{-2} hr^{-1}), Q is the flow rate (3.60 L min^{-1}), A is the soil area covered by the dynamic chamber (0.021 m^2), M_N is the molar mass of nitrogen (14.007 g mol^{-1}), V_m is the molar volume of air (22.4 L mol^{-1}), and C_{sample} and $C_{background}$ are the respective analyte mixing ratios (ppb).

3.3 Results and Discussion

3.3.1 Rationale for sampling and preparation strategy

The soil handling methods in this study were chosen to preserve the integrity of soil properties and also minimize inter-experimental variability, thereby ensuring the reliability of analyses. Our soil handling (drying at 35 °C, which is summer-relevant temperatures, removing non-soil material, and rehydrating to field-relevant VWC) ensured that the laboratory experiments remained transferable to field conditions. Our approach, therefore, provides a greater confidence that the processes observed in these controlled experiments capture the soil dynamics that are transferable

to real environmental conditions. The overarching goal of these experiments was to ascertain the reliability of a single pooled soil sample in ascribing representative field-scale fluxes of N_r.

The random grid sampling technique was selected in particular to ensure comparability of results across the samples while preserving soil properties. It reduces sampling bias in the measurement of soil properties like soil N content, pH, and microbial community by providing a representative distribution of soil samples across the field, a method used in agricultural research to minimize the influence of localized variability (Dinkins et al., 2008; Mallarino & Wittry, 2004). This approach assumes homogeneity within designated grid areas and systematically accounts for potential differences in soil composition and nutrient content across the system under study. In contrast, other commonly used methods, such as transect sampling, convenience sampling, stratified random sampling, and composite sampling, each have specific applications depending on the research objectives and field conditions (Dinkins et al., 2008). Transect sampling captures linear variability but may miss out on the heterogeneous patches across the field, while randomly selected samples would have accounted for it. Convenience sampling risks over-representing easily accessible areas, leading to skewed results (Carter & Gregorich, 2007). It is also prone to bias, as it often over-represents accessible areas and under-represents difficult-to-access areas. However, the random grid sampling technique ensures that all locations within the site have an equal probability of selection. Stratified sampling is a more complex, time-consuming technique, and researchers require prior knowledge of field variability to define strata accurately, information which was not available for this field beforehand.

Following soil collection, sample preparation was carried out with utmost care. Homogenization of soil samples by combining equal dry mass from subsamples ensured uniformity and reproducibility in measurements, while preserving soil functionality and structure so that sample fluxes could reflect the true heterogeneity for exchange processes within an agricultural field. Both random grid sampling and the sample preparation method that was developed overcome the drawbacks of the other mentioned sampling techniques. A paired t-test was performed between the average fluxes of duplicate measurements across the eight plots. The results for NO, NO_2, and HONO revealed that only three out of eight plots (B, E, H) were statistically similar (i.e., $p \geq 0.5$) while the remaining five out of eight plots were different (i.e., $p < 0.5$ for plots A, C, D, F, G), indicating heterogeneity (**Appendix B, Table S3.6**). The observed variability within the duplicate

measurements of NO_y fluxes across the eight plots suggests that the assumption of spatial homogeneity is not valid for this study site.

The method implemented in this study reflects best practices in soil sampling and preparation amongst all the techniques mentioned in **Table 3.1**. Despite the limitations of the very few studies that have examined soil NO, NO_2 and HONO simultaneously (i.e., Scharko et al. (2015) and Tang et al. (2019). This approach ensured obtaining a more accurate picture of soil NO_y fluxes and their field-scale heterogeneity. Laboratory studies often simplify field complexity by using a single soil sample assumed to represent the entire field. The assumption that fields would have uniform emissions may lead to overestimation of fluxes when upscaling from plot to field level. Moving forward, stratified sampling strategies, spatial mapping, or targeted sampling around known hotspots could be used to improve the representation of field-scale emissions.

3.3.2 Soil NO, NO_2, and HONO fluxes from one of the pooled replicates

Soil NO, NO_2, and HONO emissions from one of the pooled agricultural soil sample replicates are provided as an example of the flux results obtained over a 3-day drying period, where soil VWC was reduced from 22% to 13% (**Figure 3.3)**. The measured fluxes of NO, NO_2, and HONO are consistent with trends reported in the literature, where a decrease in soil VWC leads to a rise in NO and HONO emissions. For all the samples, plot and the pooled one, NO is the dominant species emitted with fluxes ranging from approximately 0.4 to 2.5 μg N m^{-2} hr^{-1}. Previous studies that have analyzed soil types similar to the ones used in this study (i.e. clay), reported NO flux to be between 0.1 and 1.5 μg N m^{-2} hr^{-1} (Butterbach-Bahl et al., 2002; Oswald et al., 2013), showing good consistency observed to originate only from the residual nitrogen present in the agricultural soil studied here. The emitted NO from the soil could be attributed to microbial nitrification under moist conditions, or post-wetting pulses common in fine-textured soils with high water retention capacity, which is a particular characteristic of clay soils (Butterbach-Bahl et al., 2002). The pooled soil sample NO_2 fluxes obtained across the replicates ranged between 0.1-0.8 μg N m^{-2} hr^{-1}, with a standard error of 0.06 μg N m^{-2} hr^{-1}. Soil HONO fluxes were found to be <1.5 μg N m^{-2} hr^{-1} as depicted in **Figure 3.3**, similar to the ones reported for intact soils in the literature (Bao et al., 2022; Weber et al., 2015; Wu et al., 2022b).

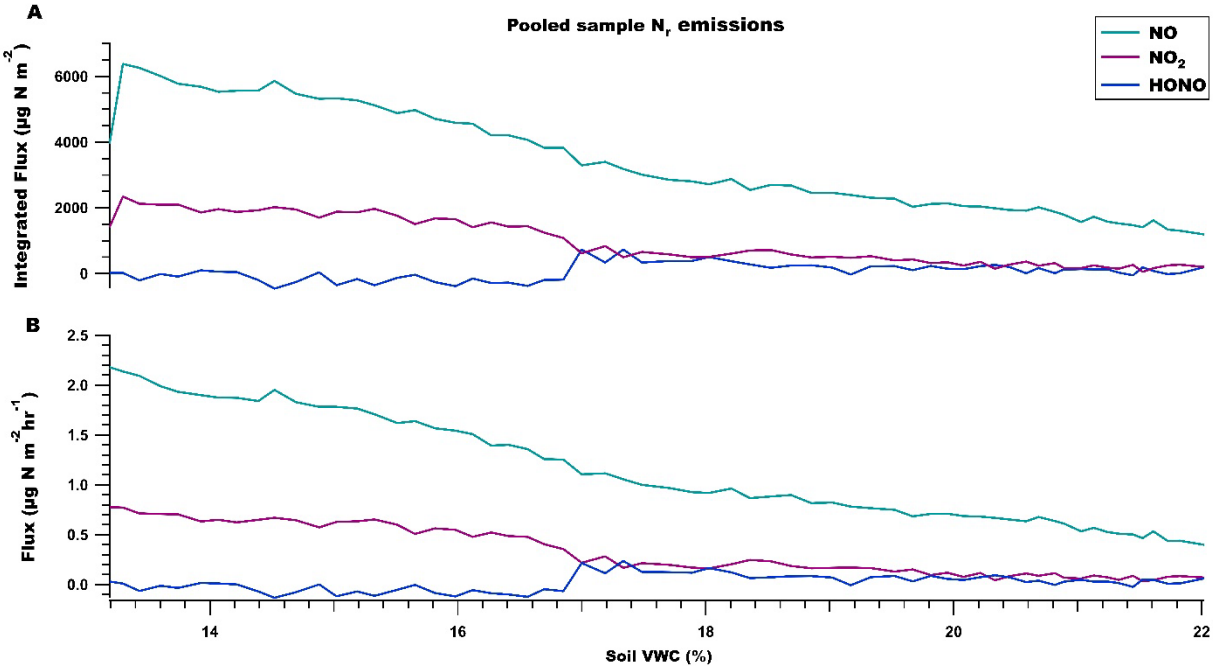

Figure 3.3: (A) Integrated flux of NO, NO_2, and HONO depicted in cyan, purple and blue respectively as a function of soil VWC (%). **(B)** Average hourly flux of NO (cyan), NO_2 (purple), and HONO (blue) when the soil VWC is between 13-22%.

3.3.3 Paired t-test analysis to assess the duplicate sample agreement within plots for NO, NO_2, and HONO fluxes

Triplicate analysis of the pooled and duplicate assessment for the respective plot samples was carried out, where average NO, NO_2 and HONO fluxes were compared using a paired t-test. All the replicate measurements were binned into soil VWC ranging between 20-24% for a comparable analysis. The composite pooled sample was obtained by averaging the fluxes of eight plot samples. Replicate sample fluxes of NO, NO_2, and HONO were statistically similar to each other (i.e., p value $\geq$0.5) for plots B, E and H. In contrast, plots A, C, D, F, and G replicates were statistically different (**Appendix B, Table S3.5).** The replicates within each plot were treated the same way in terms of sample preparation, wetting, and headspace gas analysis, but the differences in terms of fluxes suggest emission heterogeneity within the agricultural field. Average soil NO emissions were higher compared to NO_2 and HONO for all the samples, and a general trend was observed for soils (**Figure 3.4**).

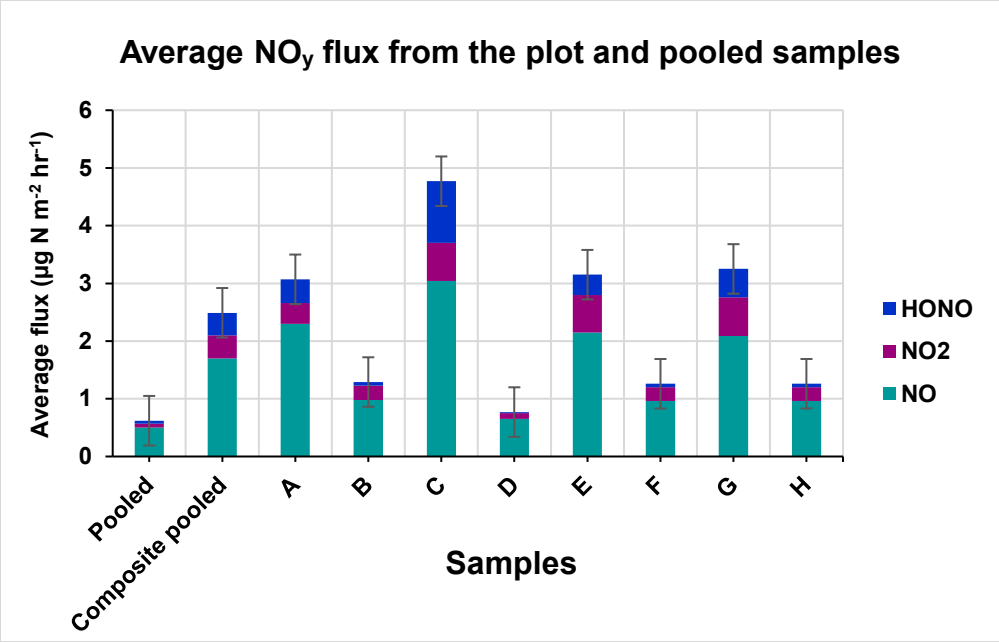

Figure 3.4: Average fluxes of NO, NO_2 and HONO for pooled and plot samples represented in cyan, purple and blue, respectively. Composite pooled flux is calculated by taking the average of plots A-H.

The plot sample replicates had a higher NO flux, compared to the pooled replicates, likely indicating the preserved microbial hotspots, intact plot-level soil aggregate and spatial variability (**Appendix B, Table S3.6**). Soil NO flux was highest for sample C (3 ± 0.05 µg N m^{-2} hr^{-1}) followed by similar NO flux for samples A, E, and G (~2 µg N m^{-2} hr^{-1}) (**Figure 3.4**). This could suggest that the soil texture and aggregate size play an important role in building the porous structure of soil, which affects the release of gases from soil (Mangalassery et al., 2013). Soil aggregates regulate the release of specific gases based on the aerobic or anaerobic state of the soil (Lipiec et al., 2007).

To assess the variability, each plot was sampled twice to obtain duplicate measurements. Even these duplicate measurements from the same land plot revealed heterogeneity, highlighting the spatial variability that may be overlooked when relying on a single sample. When single-sample measurements from laboratory studies are incorporated into regional and global models, they are unlikely to accurately reflect field-relevant NO_x and HONO. Studies that predict NO_x have large uncertainty, and only a few lab-based experiments have attempted to mimic field conditions (e.g., Bao et al. (2022); Wu et al. (2022b), limiting our ability to narrow this uncertainty range until representative conditions can be established for lab samples (Gong et al., 2025).

3.3.4 Variability in NO_y fluxes across the plots

Our measurements across eight field plots, each with two replicates, demonstrate notable variability both within (i.e., using p-value) and between plots (**Figure 3.5**).

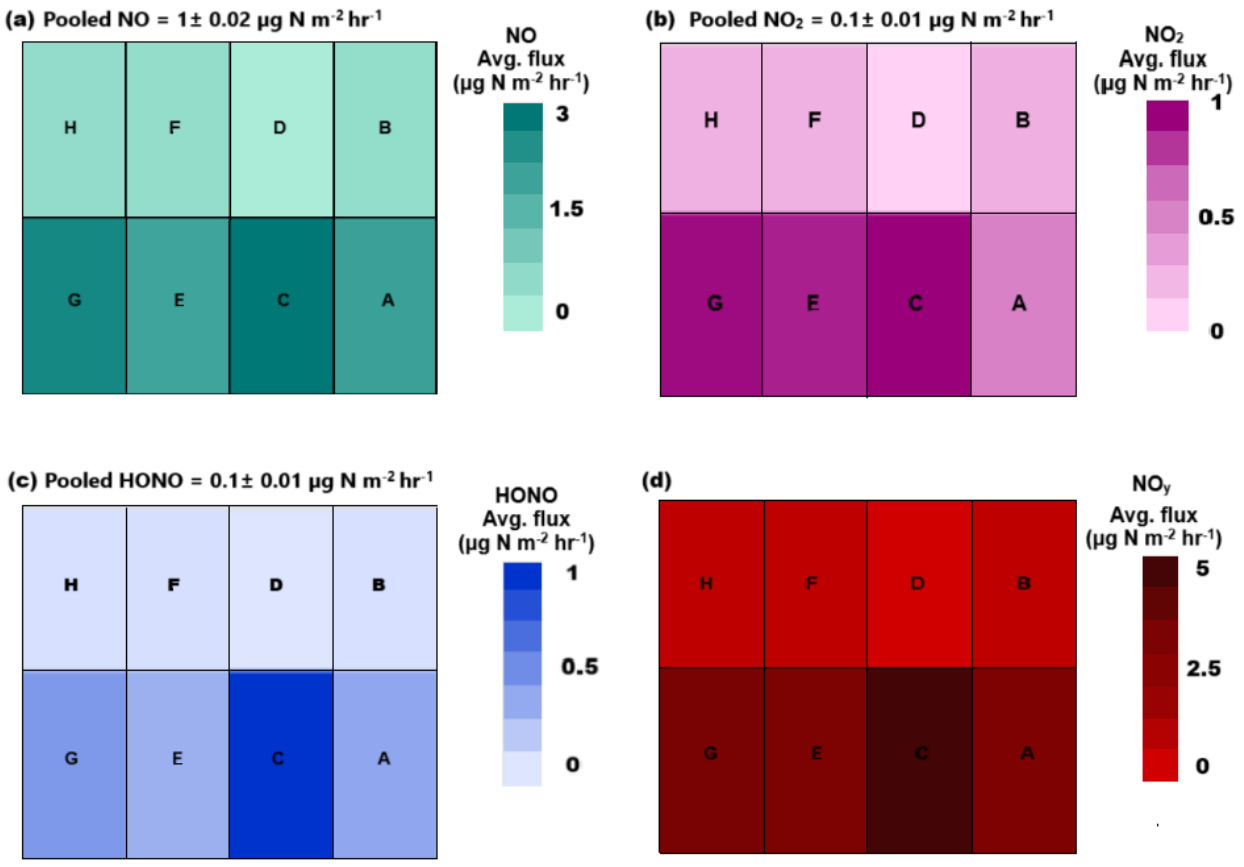

Figure 3.5: Heat map of NO_y fluxes across the managed agricultural field. Panel (a) NO (cyan) (b) NO_2 (pink) (c) HONO (blue) (d) NO_y (NO + NO_2 + HONO; red) fluxes. Deeper colour indicates higher emission flux (µg N m^{-2} hr^{-1}).

Fluxes of NO, NO_2, and HONO showed spatial variability across the eight plots with hotspots (i.e., plot C and G) (**Figure 3.5**). Plots C and G exhibited elevated fluxes for all three species, suggesting localized conditions that favoured the release of N_r, such as higher microbial activity or residual fertilizer presence in the soil collected. Among the three, NO fluxes were higher, followed by a similar pattern for NO_2 and HONO. When compared to the pooled sample across all plots, it is clear that individual plot samples differ from one another, highlighting that spatial variability would be masked if only a pooled sample were analyzed (**Figure 3.5**).

Studies have shown soils to be a major HONO source; however, our measurements did not support it (**Figure 3.5**). Lab study by Su et al. (2011), Wang et al. (2021), Oswald et al. (2013), Meusel et al. (2018) have estimated significant HONO production up to 3000 ng m^{-2} s^{-1}, 340 ng m^{-2} s^{-1}, 250 ng m^{-2} s^{-1}, 200 ng m^{-2} s^{-1} respectively which was not observed in this study. In contrast, field observations that do exist suggest that real HONO fluxes are indeed much smaller at 2-17.5 µg N m^{-2} hr^{-1} (Song et al., 2023; Tang et al., 2019). When the HONO emission potential curve is misrepresented, that is measured HONO is high in the lab versus low under real soil conditions, then the NO to HONO ratio derived from lab settings will be low compared to field work. This leads to a critical issue when global models use this lab-derived ratio to estimate HONO based on simulated NO emissions. Due to the limited in-situ field flux observations, lab-derived HONO emissions potentials have been implemented in global models. Lab studies have reported the maximum emission potential of the NO to HONO ratio being below one (Oswald et al., 2013; Wang et al., 2021; Wu et al., 2019). Whereas field measurements ranged from 4.5 up to more than 100 (like the one in this study) (Meng et al., 2024; Tang et al., 2019). For example, Wu et al. (2022b) used the regional WRF-Chem model to quantify the soil HONO emissions on the concentrations of atmospheric HONO, OH, and O_3, indicating the impact of soil HONO emissions being overlooked. Global models do not consider that the effect of HONO in remote or polluted areas can impact the NO_x-O_3 chemistry (Ha et al., 2023). This would have direct consequences for key processes such as radical generation, NO_x cycling, and O_3 formation. If the HONO emission is overestimated (as happens with a 1:1 NO: HONO ratio instead of a realistic 100:1), the model will enhance the morning OH concentration, which would initiate a cascade of other atmospheric reactions. Therefore, researchers need to be cautious when stating lab data to represent real-world data.

3.4 Conclusion

This chapter assessed the effectiveness of the modified chamber system for measuring N_r fluxes in the lab under controlled conditions. It showcased the heterogeneity of NO, NO_2 and HONO emissions still exists within the managed agricultural field. The obtained p-value for the NO, NO_2 and HONO using the paired t-test indicated the heterogeneity across the plot within the field. Variation among the samples led to exploring the conditions within a specific soil VWC range (20-24%), however, even within that, more than half of the samples were statistically different. This

work highlights the importance of the spatial variability of soil samples and soil properties within each plot. To improve the reliability of laboratory findings, future studies should adopt a stratified sampling approach in which soil variability is explicitly accounted for, especially now that field-scale information is available. This will allow laboratory experiments to better reflect the heterogeneity observed in real agricultural fields.

Soil NO was the dominant species among the NO_y and measured fluxes for all the plots, and the pooled sample ranged between 0.4 to 2.5 μg N m^{-2} hr^{-1}. Pooled NO_2 fluxes were determined to be 0.1-0.8 μg N m^{-2} hr^{-1}, and HONO fluxes were found to be <1.5 μg N m^{-2} hr^{-1} for all the samples, indicating that soil, when treated similarly as in the field, does not emit HONO, unlike studies that have manipulated them. Considering the urgent need to address the fact that soils exclusively emit HONO, the results suggest an opportunity to reflect on the soil sampling and handling techniques when working in the laboratory. This raises a major concern when global models use the obtained values of NO_y, particularly HONO, to determine the NO_x-O_3 chemistry.

3.5 References

Agriculture and Agri-Food Canada. (2023). *Sustainable Agriculture Strategy: Discussion Document*. *4*(1), 88–100. https://agriculture.canada.ca/en/department/transparency/public-opinion-research-consultations/sustainable-agriculture-strategy/document

Baio, F. H. R., Alixame, D., Neves, D. C., Teodoro, L. P. R., da Silva Júnior, C. A., Shiratsuchi, L. S., de Oliveira, J. T., & Teodoro, P. E. (2023). Adding random points to sampling grids to improve the quality of soil fertility maps. *Precision Agriculture*, *24*(5), 2081–2097. https://doi.org/10.1007/s11119-023-10031-x

Bao, F., Cheng, Y., Kuhn, U., Li, G., Wang, W., Kratz, A. M., Weber, J., Weber, B., Pöschl, U., & Su, H. (2022). Key Role of Equilibrium HONO Concentration over Soil in Quantifying Soil–Atmosphere HONO Fluxes. *Environmental Science & Technology*. https://doi.org/10.1021/acs.est.1c06716

Butterbach-Bahl, K., Breuer, L., Gasche, R., Willibald, G., & Papen, H. (2002). Exchange of trace gases between soils and the atmosphere in Scots pine forest ecosystems of the northeastern German lowlands: 1. Fluxes of N2O, NO/NO2 and CH4 at forest sites with different N-deposition. *Forest Ecology and Management*, *167*(1–3), 123–134. https://doi.org/10.1016/S0378-1127(01)00725-3

Butterbach-Bahl, K., & Dannenmann, M. (2011). Denitrification and associated soil N2O emissions due to agricultural activities in a changing climate. *Current Opinion in Environmental Sustainability*, *3*(5), 389–395. https://doi.org/10.1016/j.cosust.2011.08.004

Carter, M. R., & Gregorich, E. G. (2007). *Soil Sampling and Methods of Analysis (2nd ed.)*. CRC Press. https://doi.org/10.1201/9781420005271

Dinkins, C. P., Jones, C. D., & Olson-Rutz, K. (2008). Soil Sampling Strategies. *Environmental Sciences*, *C*, 1–4. http://msuextension.org/publications/AgandNaturalResources/MT200803AG.pdf

Galloway, J. N., Townsend, A. R., Erisman, J. W., Bekunda, M., Cai, Z., Freney, J. R., Martinelli, L. A., Seitzinger, S. P., & Sutton, M. A. (2008). Transformation of the nitrogen cycle: Recent trends, questions, and potential solutions. *Science*, *320*(5878), 889–892. https://doi.org/10.1126/science.1136674

Gong, C., Wang, Y., Tian, H., Kou-Giesbrecht, S., Vuichard, N., & Zaehle, S. (2025). Uncertainties in fertilizer-induced emissions of soil nitrogen oxide and the associated impacts on ground-level ozone and methane. *EGUsphere*. https://doi.org/10.5194/egusphere-2025-1416

Ha, P. T. M., Kanaya, Y., Taketani, F., Andres Hernandez, M. D., Schreiner, B., Pfeilsticker, K., & Sudo, K. (2023). Implementation of HONO into the chemistry-climate model CHASER (V4.0): Roles in tropospheric chemistry. *Geoscientific Model Development*, *16*(3), 927–960. https://doi.org/10.5194/gmd-16-927-2023

Haney, R. L., Franzluebbers, A. J., Porter, E. B., Hons, F. M., & Zuberer, D. A. (2004). Soil Carbon and Nitrogen Mineralization. *Soil Science Society of America Journal*, *68*(2), 489–492. https://doi.org/10.2136/sssaj2004.4890

Harris, S. J., Liisberg, J., Xia, L., Wei, J., Zeyer, K., Yu, L., Barthel, M., Wolf, B., Kelly, B. F. J., Cendón, D. I., Blunier, T., Six, J., & Mohn, J. (2020). N2O isotopocule measurements using laser spectroscopy: Analyzer characterization and intercomparison. *Atmospheric Measurement Techniques*, *13*(5), 2797–2831. https://doi.org/10.5194/amt-13-2797-2020

Houlong, J., Daibin, W., Chen, X., Shuduan, L., Hongfeng, W., Chao, Y., Najia, L., Yiyin, C., & Lina, G. (2016). Comparison of kriging interpolation precision between grid sampling scheme and simple random sampling scheme for precision agriculture. *EURASIAN JOURNAL OF SOIL SCIENCE (EJSS)*, *5*(1), 62. https://doi.org/10.18393/ejss.2016.1.062-073

Jager, G., & Bruins, E. H. (1975). Effect of repeated drying at different temperatures on soil organic matter decomposition and characteristics, and on the soil microflora. *Soil Biology and Biochemistry*, *7*(2), 153–159. https://doi.org/10.1016/0038-0717(75)90013-9

Kool, D. M., Wrage, N., Zechmeister-Boltenstern, S., Pfeffer, M., Brus, D., Oenema, O., & Van Groenigen, J. W. (2010). Nitrifier denitrification can be a source of N2O from soil: A revised approach to the dual-isotope labelling method. *European Journal of Soil Science*, *61*(5), 759–772. https://doi.org/10.1111/j.1365-2389.2010.01270.x

Krichels, A. H., Greene, A. C., Stephens, E. Z., Zhao, S., Schimel, J. P., Aronson, E. L., Hanan, E. J., & Homyak, P. M. (2024). Nitrifier controls on soil NO and N2O emissions in three chaparral ecosystems under contrasting atmospheric N inputs. *Soil Biology and Biochemistry*, *196*(May), 109482. https://doi.org/10.1016/j.soilbio.2024.109482

Lao, M. (2022). Developing an Automated Nitrous Acid (HONO) Platform to Detect Emerging Pollutants in a Commercial and Domestic Environment. *York University*, 187.

Lao, M., Crilley, L. R., Salehpoor, L., Furlani, T. C., Bourgeois, I., Andrew Neuman, J., Rollins, A. W., Veres, P. R., Washenfelder, R. A., Womack, C. C., Young, C. J., & VandenBoer, T. C. (2020). A portable, robust, stable, and tunable calibration source for gas-phase nitrous acid (HONO). *Atmospheric Measurement Techniques*, *13*(11), 5873–5890. https://doi.org/10.5194/amt-13-5873-2020

Laufs, S., Cazaunau, M., Stella, P., Kurtenbach, R., Cellier, P., Mellouki, A., Loubet, B., & Kleffmann, J. (2017). Diurnal fluxes of HONO above a crop rotation. *Atmospheric Chemistry and Physics*, *17*(11), 6907–6923. https://doi.org/10.5194/acp-17-6907-2017

Lipiec, J., Walczak, R., Witkowska-Walczak, B., Nosalewicz, A., Słowińska-Jurkiewicz, A., & Sławiński, C. (2007). The effect of aggregate size on water retention and pore structure of two silt loam soils of different genesis. *Soil and Tillage Research*, *97*(2), 239–246. https://doi.org/10.1016/j.still.2007.10.001

Mallarino, A. P., & Wittry, D. J. (2004). *Efficacy of Grid and Zone Soil Sampling Approaches for Site-Specific Assessment of Phosphorus, Potassium, pH, and Organic Matter*. 131–144.

Mangalassery, S., Sjögersten, S., Sparkes, D. L., Sturrock, C. J., & Mooney, S. J. (2013). The effect of soil aggregate size on pore structure and its consequence on emission of greenhouse gases. *Soil and Tillage Research*, *132*, 39–46. https://doi.org/10.1016/j.still.2013.05.003

Meng, F., Han, B., Qin, M., Fang, W., Tang, K., Shao, D., Liao, Z., Duan, J., Feng, Y., Huang, Y., Ni, T., & Xie, P. (2024). Measurement report: Surface exchange fluxes of HONO during the growth process of paddy fields in the Huaihe River Basin, China. In *EGUsphere*. https://doi.org/10.5194/egusphere-2024-2127

Meusel, H., Tamm, A., Kuhn, U., Wu, D., Lena Leifke, A., Fiedler, S., Ruckteschler, N., Yordanova, P., Lang-Yona, N., Pöhlker, M., Lelieveld, J., Hoffmann, T., Pöschl, U., Su, H., Weber, B., & Cheng, Y. (2018). Emission of nitrous acid from soil and biological soil crusts represents an important source of HONO in the remote atmosphere in Cyprus. *Atmospheric Chemistry and Physics*, *18*(2), 799–813. https://doi.org/10.5194/acp-18-799-2018

Mushinski, R. M., Phillips, R. P., Payne, Z. C., Abney, R. B., Jo, I., Fei, S., Pusede, S. E., White, J. R., Rusch, D. B., & Raff, J. D. (2019). Microbial mechanisms and ecosystem flux estimation for aerobic NOy emissions from deciduous forest soils. *Proceedings of the National Academy of Sciences of the United States of America*, *116*(6), 2138–2145. https://doi.org/10.1073/pnas.1814632116

Osterberg, D. (2022, May 3). Index suggests that half of nitrogen applied to crops is lost. *Eos*. https://eos.org/articles/index-suggests-that-half-of-nitrogen-applied-to-crops-is-lost

Oswald, R., Behrendt, T., Ermel, M., Wu, D., Su, H., Cheng, Y., Breuninger, C., Moravek, A., Mougin, E., Delon, C., Loubet, B., Pommerening-Röser, A., Sörgel, M., Pöschl, U., Hoffmann, T., Andreae, M. O., Meixner, F. X., & Trebs, I. (2013). HONO emissions from soil bacteria as a major source of atmospheric reactive nitrogen. *Science*, *341*(6151), 1233–1235. https://doi.org/10.1126/science.1242266

Pape, L., Ammann, C., Nyfeler-Brunner, A., Spirig, C., Hens, K., & Meixner, F. X. (2009). An automated dynamic chamber system for surface exchange measurement of non-reactive and reactive trace gases of grassland ecosystems. *Biogeosciences*, *6*(3), 405–429. https://doi.org/10.5194/bg-6-405-2009

Pavelka, M., Acosta, M., Kiese, R., Altimir, N., Brümmer, C., Crill, P., Darenova, E., Fuß, R., Gielen, B., Graf, A., Klemedtsson, L., Lohila, A., Longdoz, B., Lindroth, A., Nilsson, M., Jiménez, S. M., Merbold, L., Montagnani, L., Peichl, M., … Kutsch, W. (2018). Standardisation of chamber technique for CO2, N2O and CH4 fluxes measurements from terrestrial ecosystems. *International Agrophysics*, *32*(4), 569–587. https://doi.org/10.1515/intag-2017-0045

Pilegaard, K. (2013). Processes regulating nitric oxide emissions from soils. *Philosophical Transactions of the Royal Society B: Biological Sciences*, *368*(1621). https://doi.org/10.1098/rstb.2013.0126

Purchase, M. L., Bending, G. D., & Mushinski, R. M. (2023). Spatiotemporal Variations of Soil Reactive Nitrogen Oxide Fluxes across the Anthropogenic Landscape. *Environmental Science and Technology*, *57*(43), 16348–16360. https://doi.org/10.1021/acs.est.3c05849

Rapson, T. D., & Dacres, H. (2014). Analytical techniques for measuring nitrous oxide. In *TrAC - Trends in Analytical Chemistry* (Vol. 54, pp. 65–74). Elsevier B.V. https://doi.org/10.1016/j.trac.2013.11.004

Ren, X., Sanders, J. E., Rajendran, A., Weber, R. J., Goldstein, A. H., Pusede, S. E., Browne, E. C., Min, K. E., & Cohen, R. C. (2011). A relaxed eddy accumulation system for measuring vertical fluxes of nitrous acid. *Atmospheric Measurement Techniques*, *4*(10), 2093–2103. https://doi.org/10.5194/amt-4-2093-2011

Ritchie, H., & Roser, M. (2023). *Nitrous oxide emissions from agriculture*. Our World in Data. https://ourworldindata.org/grapher/nitrous-oxide-agriculture?mapSelect=~CAN

Roberts, J. M., Veres, P., Warneke, C., Neuman, J. A., Washenfelder, R. A., Brown, S. S., Baasandorj, M., Burkholder, J. B., Burling, I. R., Johnson, T. J., Yokelson, R. J., & De Gouw, J. (2010). Measurement of HONO, HNCO, and other inorganic acids by negative-ion proton-transfer chemical-ionization mass spectrometry (NI-PT-CIMS): Application to biomass burning emissions. *Atmospheric Measurement Techniques*, *3*(4), 981–990. https://doi.org/10.5194/amt-3-981-2010

Scharko, N. K., Schu, U. M. E., Berke, A. E., Banina, L., Peel, H. R., Donaldson, M. A., Hemmerich, C., White, R., & Ra, J. D. (2015). *Combined Flux Chamber and Genomics Approach Links Nitrous Acid Emissions to Ammonia Oxidizing Bacteria and Archaea in Urban and Agricultural Soil*. https://doi.org/10.1021/acs.est.5b00838

Seinfeld, J. H., & Pandis, S. N. (1998). *From Air Pollution to Climate Change* (2nd ed.). Wiley.

Song, Y., Xue, C., Zhang, Y., Liu, P., Bao, F., Li, X., & Mu, Y. (2023). *Measurement Report: Exchange Fluxes of HONO over Agricultural Fields in the North China Plain*. *July*, 1–38. https://zenodo.org/record/8115973

Sörgel, M., Regelin, E., Bozem, H., Diesch, J. M., Drewnick, F., Fischer, H., Harder, H., Held, A., Hosaynali-Beygi, Z., Martinez, M., & Zetzsch, C. (2011). Quantification of the unknown HONO daytime source and its relation to NO2. In *Atmospheric Chemistry and Physics* (Vol. 11, Issue 20, pp. 10433–10447). https://doi.org/10.5194/acp-11-10433-2011

Su, H., Cheng, Y., Oswald, R., Behrendt, T., Trebs, I., Meixner, F. X., Andreae, M. O., Cheng, P., Zhang, Y., & Pöschl, U. (2011). Soil nitrite as a source of atmospheric HONO and OH radicals. *Science*, *333*(6049), 1616–1618. https://doi.org/10.1126/science.1207687

Sunil, B. M., & Deepa, A. V. (2016). Influence of Drying Temperature on Three Soils Physical Properties. *Geotechnical and Geological Engineering*, *34*(3), 777–788. https://doi.org/10.1007/s10706-016-0001-2

Tan, M., Hu, Y., Song, Y., Huang, Z., Mu, Y., Liu, J., Zhang, C., Liu, P., & Zhang, Y. (2025). An improved open-top dynamic chambers method for measuring the exchange fluxes of N2O, NO and NH3 from farmland. *Journal of Environmental Sciences*. https://doi.org/10.1016/j.jes.2025.03.021

Tang, K., Qin, M., Duan, J., Fang, W., Meng, F., Liang, S., Xie, P., Liu, J., Liu, W., Xue, C., & Mu, Y. (2019). A dual dynamic chamber system based on IBBCEAS for measuring fluxes of nitrous acid in agricultural fields in the North China Plain. *Atmospheric Environment*, *196*(May 2018), 10–19. https://doi.org/10.1016/j.atmosenv.2018.09.059

Tang, K., Qin, M., Fang, W., Duan, J., Meng, F., Ye, K., Zhang, H., Xie, P., Liu, J., Liu, W., Feng, Y., Huang, Y., & Ni, T. (2020). An automated dynamic chamber system for exchange flux measurement of reactive nitrogen oxides (HONO and NOX) in farmland ecosystems of the Huaihe River Basin, China. *Science of the Total Environment*, *745*(X), 140867. https://doi.org/10.1016/j.scitotenv.2020.140867

Themistokleous, G., Savvides, A. M., Philippou, K., Ioannides, I. M., & Omirou, M. (2024). A high-frequency greenhouse gas flux analysis tool: Insights from automated non-steady-state transparent soil chambers. *European Journal of Soil Science*, *75*(5). https://doi.org/10.1111/ejss.13560

Wang, F., Che, R., Deng, Y., Wu, Y., Tang, L., Xu, Z., Wang, W., Liu, H., & Cui, X. (2021). Air-drying and long time preservation of soil do not significantly impact microbial community composition and structure. *Soil Biology and Biochemistry*, *157*, 108238. https://doi.org/10.1016/J.SOILBIO.2021.108238

Wang, Fu, X., Wu, D., Wang, M., Lu, K., Mu, Y., Liu, Z., Zhang, Y., & Wang, T. (2021). Agricultural Fertilization Aggravates Air Pollution by Stimulating Soil Nitrous Acid Emissions at High Soil Moisture. *Environmental Science and Technology*, *55*(21), 14556–14566. https://doi.org/10.1021/acs.est.1c04134

Wang, Y., Fu, X., Wang, T., Ma, J., Gao, H., Wang, X., & Pu, W. (2022). Large Contribution of Nitrous Acid to Soil-Emitted Reactive Oxidized Nitrogen and Its Effect on Air Quality. *Environmental Science and Technology*. https://doi.org/10.1021/acs.est.2c07793

Weber, B., Wu, D., Tamm, A., Ruckteschler, N., Rodríguez-Caballero, E., Steinkamp, J., Meusel, H., Elbert, W., Behrendt, T., Sörgel, M., Cheng, Y., Crutzen, P. J., Su, H., Pöschl, U., & Wofsy, S. C. (2015). Biological soil crusts accelerate the nitrogen cycle through large NO and HONO emissions in drylands. *Proceedings of the National Academy of Sciences of the United States of America*, *112*(50), 15384–15389. https://doi.org/10.1073/pnas.1515818112

Wu, D., Deng, L., Liu, Y., Xi, D., Zou, H., Wang, R., Sha, Z., Pan, Y., Hou, L., & Liu, M. (2020). Comparisons of the effects of different drying methods on soil nitrogen fractions: Insights

into emissions of reactive nitrogen gases (HONO and NO). *Atmospheric and Oceanic Science Letters*, *13*(3), 224–231. https://doi.org/10.1080/16742834.2020.1733388

Wu, D., Horn, M. A., Behrendt, T., Müller, S., Li, J., Cole, J. A., Xie, B., Ju, X., Li, G., Ermel, M., Oswald, R., Fröhlich-Nowoisky, J., Hoor, P., Hu, C., Liu, M., Andreae, M. O., Pöschl, U., Cheng, Y., Su, H., … Sörgel, M. (2019). Soil HONO emissions at high moisture content are driven by microbial nitrate reduction to nitrite: tackling the HONO puzzle. *ISME Journal*, *13*(7), 1688–1699. https://doi.org/10.1038/s41396-019-0379-y

Wu, D., Zhang, J., Wang, M., An, J., Wang, R., Haider, H., Xu-Ri, Huang, Y., Zhang, Q., Zhou, F., Tian, H., Zhang, X., Deng, L., Pan, Y., Chen, X., Yu, Y., Hu, C., Wang, R., Song, Y., … Liu, M. (2022). Global and Regional Patterns of Soil Nitrous Acid Emissions and Their Acceleration of Rural Photochemical Reactions. *Journal of Geophysical Research: Atmospheres*, *127*(6). https://doi.org/10.1029/2021JD036379

Zhou, W., Lu, X., Qi, C., & Yang, M. (2020). Utilisation of ultrasonic treatment to improve the soil amelioration property of coal fly ash. *Journal of Environmental Management*, *276*. https://doi.org/10.1016/j.jenvman.2020.111311

Chapter four: Understanding soil N_r and GHG emissions from fertilization in a controlled laboratory environment

Author contributions: MS wrote, KZA processed the soil data, and TCV edited the work.

4.1 Introduction

Sustainable agriculture is envisioned as a system where food is both nutritious and accessible to all, while natural resources are managed in a way that preserves the ecosystem to meet the needs of present and future generations. With the global population projected to reach around 9.7 billion by 2050, ensuring Canada's ability to support food security will remain critical (Agriculture and Agri-Food Canada, 2023). However, achieving sustainable agriculture presents challenges, particularly the pressure to increase food production to meet the demands of a rapidly growing population. Soil serves as a major N_r source and is often an overlooked contributor to climate change and environmental degradation (Schlesinger, 2020). Agricultural soils are particularly hotspots for NO_y, and GHGs including CO_2, CH_4, and N_2O, largely due to the increased use of synthetic fertilizer. Fertilizer application has surged from 11.3 teragrams of nitrogen per year (Tg N yr^{-1}) in 1961 to 107.6 Tg N yr^{-1} in 2017 (Lu and Tian, 2017). This sharp rise in fertilizer use has contributed to elevated N_r emissions, which is an increasing concern for both human health and the climate.

Despite the growing concern over N_r emissions, less attention has been directed toward the use of mineral fertilizers like urea, ammonium bicarbonate (ABC), and ammonium nitrate (AN). The two common nitrogen-consuming fertilizers are ammonium bicarbonate (ABC, NH_4HCO_3) and urea (NH_2CONH_2). Globally, these fertilizers have been used extensively to meet the agricultural demand of the growing population, with China being one of the top users (Brondi et al., 2023; Priya et al., 2024). Ammonium bicarbonate was used by many countries 20 years ago until the emergence of urea. The use of ABC is excluded from the organic fertilizer register in the US and is not allowed as a standalone fertilizer due to its poor environmental stability (Environmental Protection Agency, 2004). Ammonium bicarbonate readily decomposes into NH_3 and CO_2 at room temperature. The most recently used synthetic form of fertilizer is urea. Urea is a stable, highly soluble molecule containing 46% nitrogen (N). When a dissolved urea solution is poured onto the ground surface, the soil bacteria release the enzyme urease to unlock NH_4^+ from urea through

mineralization (**R4.1**). The process is known as ammonification, where plants can then use this NH_4^+ ion (**Refer to Figure 1.4, R4.2**).

$$NH_2CONH_2 + 2H_2O \rightarrow (NH_4)_2CO_3 \qquad \text{R4.1}$$

$$(NH_4)_2CO_3 + 2H^+ \rightarrow 2NH_4^+ + CO_2 + H_2O \qquad \text{R4.2}$$

Chemical fertilizers like urea, which have high water solubility, are considered quick-release fertilizers. Out of all chemical fertilizers, urea is considered a poor fertilizer as it is highly water-soluble. Water-soluble fertilizers tend not to be available for later development of plants, and the nitrogen not absorbed by crops is prone to run off. Therefore, in recent years, scientists have shifted their attention to finding ways to synthesize slow-release fertilizers (SRF) to control the release of nitrogen from the soils.

Compared to conventional and quick-release fertilizers like urea and AN, SRFs are an effective way to either limit the fertilizers' availability for absorption by the plant or delay the nitrogen release to the plant. Slow-release fertilizers have a lower environmental effect and are designed to gradually release nutrients to the plant over an extended period. Slow release refers to controlled nutrient release to the plants and must not be confused with slow release to the atmosphere, as the release depends on several environmental factors such as soil moisture, temperature, aeration, and pH (Ni et al., 2011). Commercial controlled-release fertilizers rely on strategies such as coating technologies (polymer-, sulphur-, or resin-coated urea) or chemically modification of urea into less soluble forms (e.g., urea-formaldehyde, isobutylidenediurea) to regulate nutrient release. (Priya et al., 2024). This controlled release can be accomplished through several mechanisms. In coated fertilizers, water penetrates the coatings, and the dissolved nutrient diffuses outward at a rate governed by coating thickness, permeability, and degradation of the coating material (Priya et al., 2024). In chemically slow-release forms, nitrogen is bound in long-chain polymers or less soluble compounds that require microbial breakdown or hydrolysis before becoming plant-available NH_4^+ or NO_3^-. Low-solubility mineral forms rely on inherently slow dissolution rates, with nutrient release influenced by soil pH, root activity, and moisture (Ni et al., 2011). The path in physicochemical stabilization of quick-release fertilizers like ABC lies in synthesizing SRF, usually through mechanochemical stabilization technologies (Govoni Brondi et al., 2024). Mechanochemical method has been an excellent choice where the synthesis of new compounds is achieved by co-grinding two or more elements or compounds using mechanical force, like milling,

to obtain a new crystalline compound (AlShamaileh et al., 2018; Brondi et al., 2023). Two examples of such recently available low solubility mineral-based SRFs are magnesium ammonium carbonate (MAC) and zinc ammonium carbonate (ZAC).

Here, we quantify the effects of different nitrogen fertilizers on N_r fluxes by comparing emissions from soils treated with conventional fertilizers like urea versus mechanochemically synthesized magnesium and zinc ammonium carbonate fertilizers. The study evaluates temporally resolved gaseous emissions of NO, NO_2, HONO, NH_3, and N_2O following the application of these fertilizers, with the amount of total nitrogen volatilized for these double salts.

4.2 Method

Refer to the Chapter 3 method section for in-depth collection and preparation of the pooled sample.

4.2.1 Treating soil samples with nitrogen salts

Urea, ABC and double salts of magnesium ammonium carbonate tetrahydrate (MAC, $Mg(NH_4)_2(CO_3)_2 \cdot 4H_2O$) and zinc ammonium carbonates (ZAC, $Zn(NH_3)CO_3$) were provided from Govoni Brondi et al. (2024) group to analyze soil fluxes. For each experiment, 350 g of soil from pooled samples was used, and the corresponding fertilizer solution equivalent to 1 g N per kg of soil was added. A sterile 15 mL Falcon conical centrifuge tube (Corning, PN: 352096) was rinsed three times with deionized water (DIW, $\rho \geq 18.2$ MΩ·cm) before use. The measured amount of salt was first added to a clean tube, followed by the addition of approximately 7 mL of DIW. The mixture was thoroughly stirred to dissolve the salt, and then additional deionized water was added to bring the final volume up to the 15 mL mark. This solution was then used to measure an additional 75 mL of DIW, which was combined and thoroughly mixed with the soil in a beaker. The complete salt solution was then added to the soil in a mortar and mixed thoroughly. The treated, wet soil was transferred onto PFA-lined mesh trays for flux measurements. Gas fluxes from the soil samples were measured immediately after treatment using NO_x and G2509 analyzers.

4.2.2 Quality control checks for G2509 analyzer

This analyzer enables the simultaneous measurement of NH_3 at ppbv levels, and N_2O, CH_4, and CO_2 at parts-per-million by volume (ppmv). The analyzer offers a fast time response of approximately 8 seconds for N_2O, CH_4, CO_2, and H_2O (%), and less than two minutes for NH_3. Although full-span calibrations are not required regularly for CRDS-based instruments, the

analyzer's performance was validated in the laboratory through zero checks. This was conducted by directly feeding ZA into the analyzer and recording the instrument's response, serving as a reference for ensuring LOD limits. The LODs for the N_2O, NH_3, CO_2, and CH_4 were 0.07 ppmv, 4.46 ppbv, 19.75 ppmv, and 0.02 ppmv, respectively.

4.2.3 Setup of the dynamic chamber

The experimental setup used for measuring gas fluxes was similar to the configuration described in **Section 3.2.7**, with the exception that a G2509 analyzer was installed in-line to measure N_2O, NH_3, along NO_y. The total flow through the soil flux experimental setup was maintained at a constant flow of 3.60 L min^{-1}, regulated by MFCs (**Figure 4.1**). Specifically, MFC 3 was set to 2.4 L min^{-1} to accommodate the sampling flow of the G2509 analyzer (0.25 L min^{-1}).

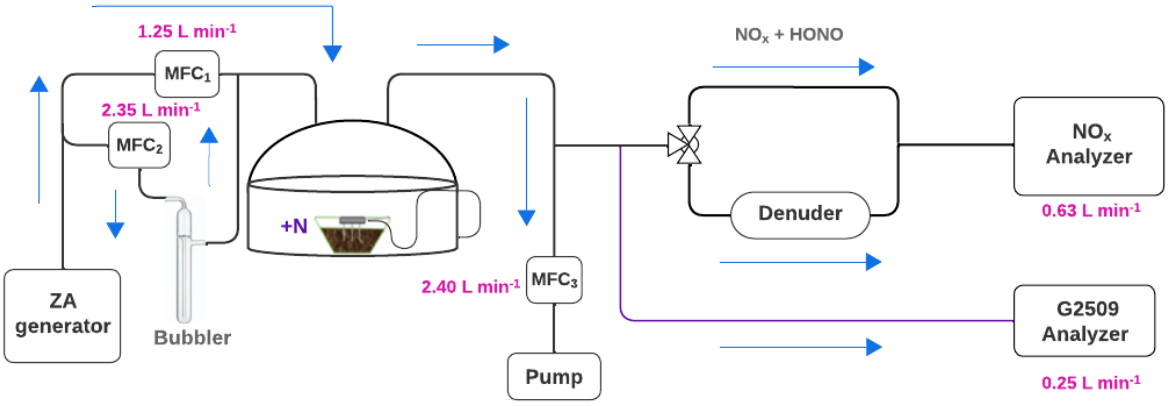

Figure 4.1: Schematic of the dynamic chamber system for measuring NO, NO_2, HONO, N_2O, and NH_3 fluxes. Pooled samples amended with fertilizer were placed on a stainless-steel mesh tray covered with PFA inside the chamber and flushed with zero air humidified to 65% RH. Blue arrows indicate the airflow to and from the chamber.

4.2.4 Data processing for N_2O, NH_3 flux

To process the data, the macros 2010 were loaded on Igor. Macros 2010 was used to average the data to one minute. Averaging the data set to standardized 60-second intervals into one-minute intervals ensured a similar time resolution as the NO_x and chamber data. Following the average flux was calculated similarly to that discussed in Chapter 3.

4.3 Results

4.3.1 Soil fluxes of NH_3, N_2O, NO, NO_2, and HONO from urea treatment

Agricultural soil amended with chemical fertilizers is expected to be a hotspot for NH_3, N_2O, HONO, and NO_x emissions. The temperature was maintained at 23 °C, the soil VWC ranged between 25–29%, and the headspace relative humidity (RH) at 65% for three days, simulating realistic atmospheric and environmental conditions for quantifying the N_r flux from soil treated with urea.

In all experiments conducted with the Picarro G2509, the mixing ratio of N_2O began to rise approximately four hours after the start of the experiment. In this particular example for soil treated with urea, N_2O peaked at 0.79 ppm after 12 hours, which was followed by a gradual decline (**Figure 4.2**). This pattern likely reflects the incubation period of nitrifying and denitrifying bacteria and the subsequent release of gases like HONO, depicted in Wang et al. (2021), and N_2O in Liu et al. (2022).

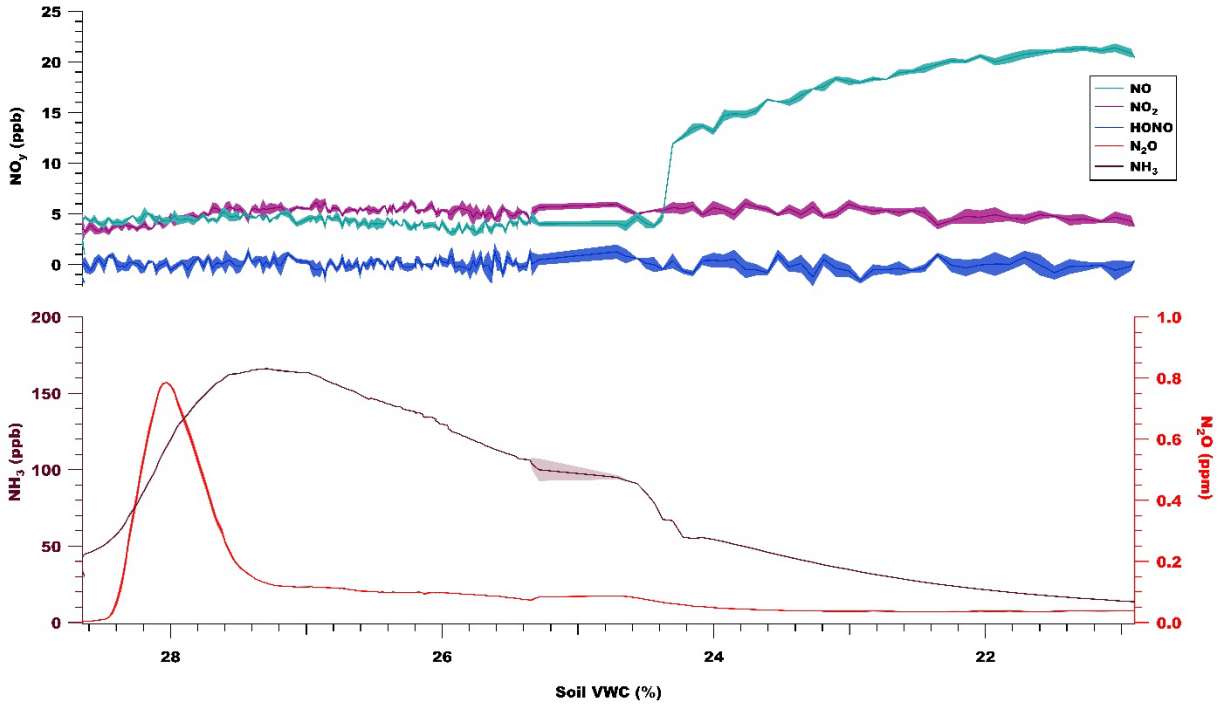

Figure 4.2: Soil emissions of the comprehensive suite gases from soil treated with urea, including NO (cyan), NO_2 (purple), HONO (blue), N_2O (red), and NH_3 (brown). The NO, NO_2 and HONO emissions were measured at 1-minute resolution and averaged over 30 minutes at the respective soil VWC (%). Similarly, the 2-second resolution of N_2O (plotted using the right Y-axis) and NH_3 measurements were also averaged to 30-minute intervals. The standard deviation (±1σ) around these averages is shaded with a lighter version of the main trace colour.

Volatilization of NH_3 is a major pathway for nitrogen loss from fertilizers (Behera et al., 2013; Govoni Brondi et al., 2024; Liu, Zhang, Xu, Liu, Li, et al., 2020; Moravek et al., 2019; B. Pan et al., 2016, 2022; Paulot et al., 2014). The urea application example in **Figure 4.2** shows the expected NH_3 emissions, with the integrated amount reaching 22% of the applied nitrogen over the three-day incubation period. These findings are consistent with our existing knowledge that NH_3 volatilization as a nitrogen loss mechanism dominates early N_r losses from fertilizers (Anas et al., 2020). It is the key precursor to secondary inorganic aerosols in the atmosphere (Fowler et al., 2013; Jang et al., 2025).

The mixing ratio of NO remained relatively constant throughout the three days, with NO_2 increasing as the N_2O emissions decreased, followed by a similar period of stability to NO (**Figure 4.2**). Throughout this experiment, no measurable emissions of HONO were detected despite the substantial presence of urea (**Figure 4.2)**. The step increase of NO likely originated from the microbial processes in the soil rather than from any issues with the instrumental setup. Instrumental artifacts can be ruled out because zero checks were performed before each run, and span checks conducted twice during the experiment confirmed that the measurement system was functioning properly. Consistent with moisture-controlled nitrification/denitrification dynamics, NO emissions increased as soils dried. As the soil dries, oxygen can diffuse more readily into the pore spaces, stimulating nitrification. This process consumes NH_4^+/NH_3 (i.e., reducing its volatilization) and produces NO, which is consistent with our observations that reflect this soil-specific response to decreasing water content. The high clay content and slightly alkaline pH of this soil favour sustained NO production over a broader range of VWC. Soil pH influences microbial pathways: acidic soils tend to favour nitrification suppression, while neutral to alkaline soils can sustain greater NO fluxes (Pilegaard, 2013). Similarly, the availability and form of nitrogen substrates dictate which microbial processes dominate, like with urea. Urea addition provides nitrogen in the form of NH_4^+, which is volatilized as NH_3 or is consumed through nitrification, consistent with the trend observed in the literature (Akiyama et al., 2004). Several modelling studies, like Ha et al. (2023) and Tian et al. (2024),, have incorporated an order of magnitude or higher HONO fluxes from lab studies than the one obtained in this study (< 1 μg N m^{-2} hr^{-1}). The HONO produced from treated soil is less than that of the manipulated ones from lab studies by Su et al. (2011), Wang et al. (2021), Oswald et al. (2013), and Meusel et al. (2018), indicating a major issue when incorporating these values into regional and global models.

4.3.2 Quantifying NH_3, N_2O, NO, NO_2, and HONO fluxes from mechanically synthesized magnesium ammonium carbonate (MAC)

For soil treated with MAC, all the conditions were similar to those of urea. Among the individual N species, NH_3 emissions (~6000 ppb) kick in right from the start of the experiment, followed by N_2O (0.55 ppm) approximately four hours later, which was followed by a gradual decline a day after (**Figure 4.3**). With the drop in soil VWC, NH_3 and N_2O emissions, NO and HONO increased, similar to that obtained for Oswald et al. (2013) (**Figure 4.3**).

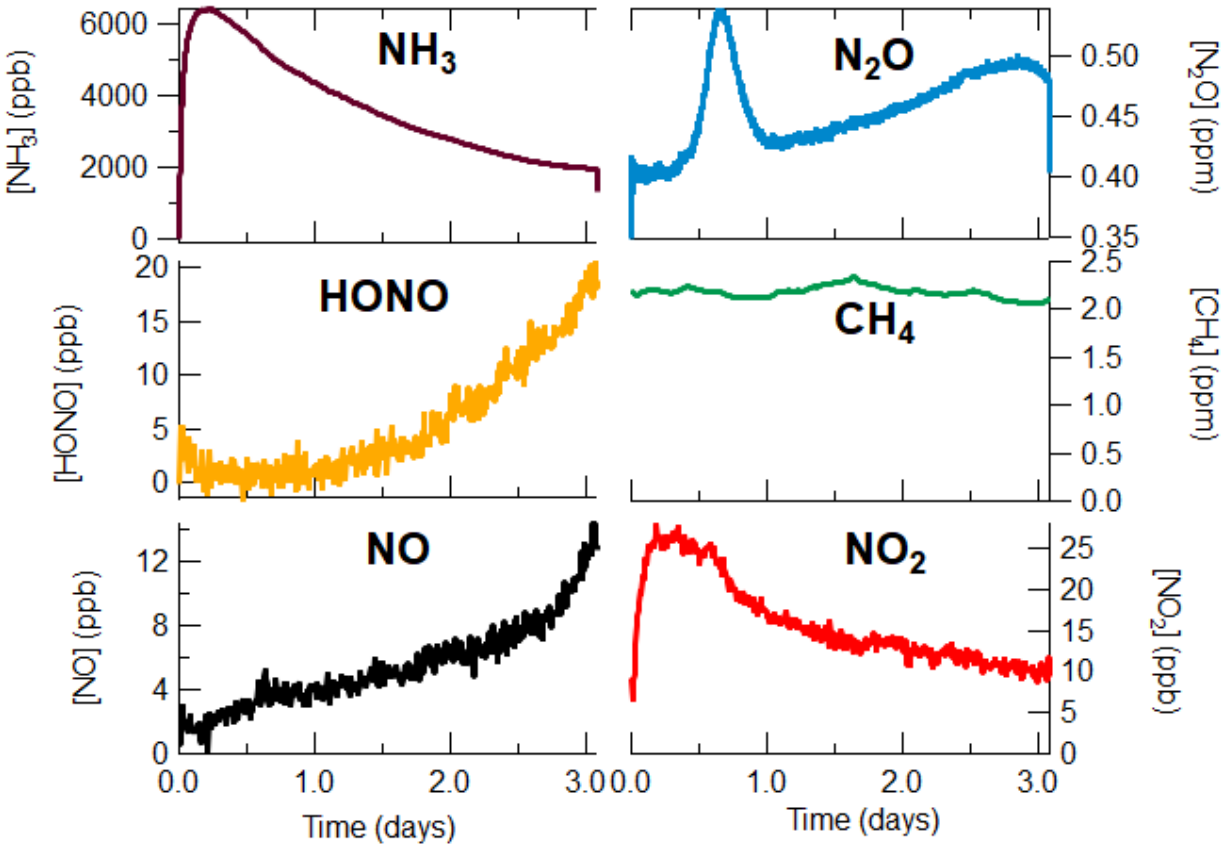

Figure 4.3: Soil emissions of the comprehensive suite of N_r gases from soil treated with MAC, including NH_3, N_2O, HONO, CH_4, NO, and NO_2. The NO, NO_2 and HONO emissions were measured at 1-minute resolution and averaged to an hour. Similarly, the 2-second resolution of N_2O and NH_3 measurements was also averaged to hour intervals.

The interaction between NH_4^+ ions and Mg^{2+}/Zn^{2+} in a double salt structure effectively reduced nitrogen (N) losses through volatilization in the form of NH_3 (Govoni Brondi et al., 2024). However, in this study, MAC did not suppress NH_3 loss by retaining the NH_4^+ in the soil, but rather was higher than that observed by urea. These findings challenge the use of these double salts as an

N stabilizer, highlighting the need for further investigation. To assess the efficiency of MAC and ZAC compared to urea, it is necessary to integrate the fluxes of all nitrogen-containing species into a single metric of total nitrogen volatilized. The following section presents this cumulative assessment, enabling direct comparison of overall nitrogen losses from SRF and urea.

4.3.3 Total nitrogen volatilized from the fertilized soil

The total N volatilized from the soils treated with urea and the double salts MAC and ZAC is shown in **Figure 4.4**. Among the individual N species, NH_3 volatilization accounted for the largest fraction of the total N loss from the soil. It was released shortly after the start of the experiment, followed by N_2O and NO_y. One of the main losses of N from fertilizers is through NH_3 volatilization. The volatilization losses for soil treated with urea (~21% N) are consistent with previous studies reporting 20–30% N loss from surface-applied urea (Jadon et al., 2018; Sunderlage and Cook, 2018).

Soil treated with MAC and ZAC showed higher N volatilization than urea (**Figure 4.4**). Govoni Brondi et al. (2024), who synthesized these salts have claimed that the double salt interaction allowed N stabilization in the NH_4^+ form in the soil, reducing its conversion/transformation to NH_3. However, this was not the case for soil treated with MAC (**Figure 4.3**), where NH_3 was emitted at the highest (~5000 ppb, peaking at ~6000 ppb) during day one. Whether the use of mechanically synthesized double salts (i.e., MAC and ZAC) is advantageous remains uncertain, as the total nitrogen volatilized from these salts exceeded that from urea in this study. Further investigation is needed to assess their effectiveness in minimizing nitrogen losses. Please note that only one replicate was carried out for each salt due to the time constraints of the G2509 analyzer. As a result, it is worth acknowledging that the observed emissions pattern might deviate upon considering additional replicates.

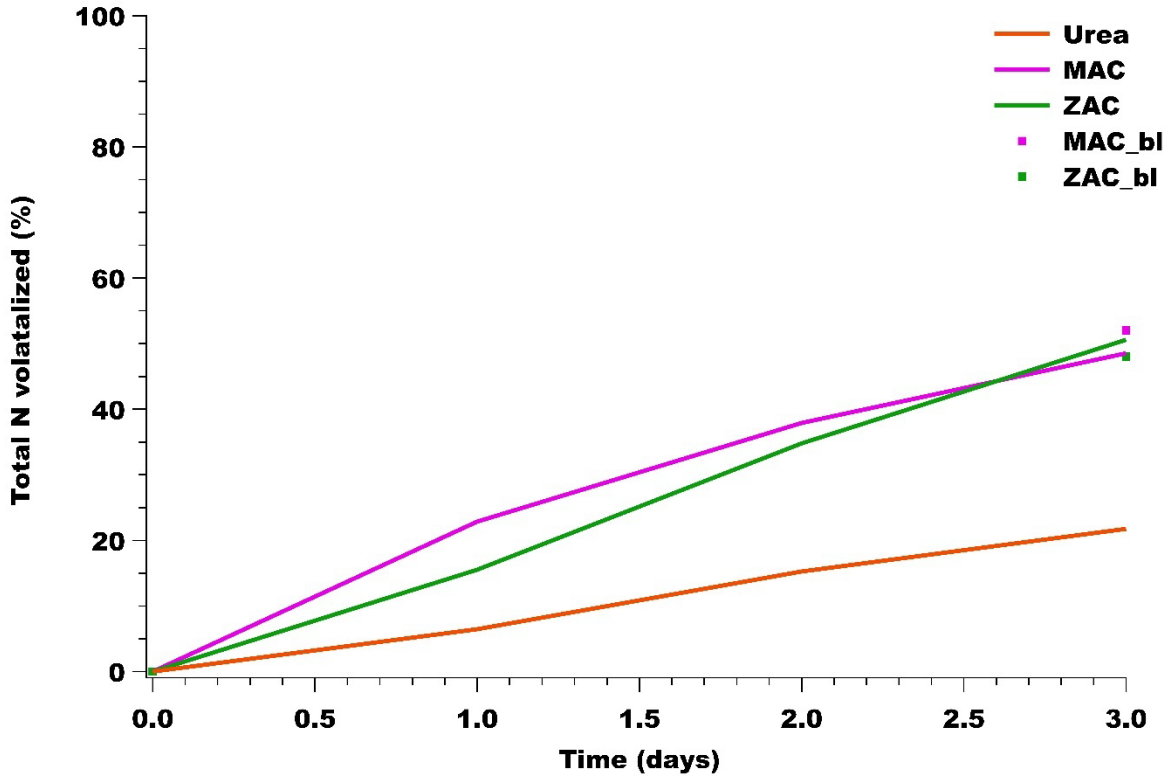

Figure 4.4: Total N volatilized per day from soils treated with urea (orange), MAC (pink) and ZAC (green). Results obtained from the Baltrusaitis laboratory (bl) experiments are represented using dots (i.e., MAC (pink), ZAC (green)).

4.4 Conclusions

In this work, the effects of different nitrogen fertilizers were analyzed by comparing N_r fluxes from soils treated with conventional fertilizers like urea versus mechanochemically synthesized magnesium and zinc ammonium carbonate fertilizers. It evaluated temporally resolved gaseous emissions of NO, NO_2, HONO, NH_3, and N_2O at field-like conditions, that is, at 23 °C and soil VWC between 25–29%. The emissions of N_2O (0.8 ppm) and NH_3 (160 ppb) for soil treated with urea began to rise approximately four hours after the experiment started, peaking at between 10–12-hour marks. Once the N_2O emissions dropped, NO_y (30 ppb) kicked in with NO being the highest (~20 ppb). For the soil treated with MAC, similar to the urea experiment, N_2O began to rise approximately four hours after the experiment started, peaking at 0.55 ppm after 12 hours, which was followed by a gradual decline with the decrease in soil VWC. The mixing ratio of NO (~8 ppb) remained relatively constant throughout the three-day period with a similar HONO emission trend.

Lastly, total nitrogen volatilization was evaluated for soil treated with urea, MAC and ZAC. Despite the application of an equal nitrogen amount to the soil, mechanically synthesized double salts resulted in higher total gaseous N loss. It accounted for up to 50% total N, whereas urea represented less than half of the double salts, at 21%. Due to time constraints, only one replicate was performed per treatment, increasing the chance of uncertainty in results. However, the observed emission trends provide valuable preliminary insight into the different nitrogen gases evolved from fertilized soils.

4.5 References

Agriculture and Agri-Food Canada. (2023). *Sustainable Agriculture Strategy: Discussion Document*. *4*(1), 88–100. https://agriculture.canada.ca/en/department/transparency/public-opinion-research-consultations/sustainable-agriculture-strategy/document

Akiyama, H., Mctaggart, I. P., Ball, B. C., & Scott, A. (2004). N2O, NO, and NH3 emissions from soil after the application of organic fertilizers, urea and water.

AlShamaileh, E., Al-Rawajfeh, A. E., & Alrbaihat, M. (2018). Mechanochemical Synthesis of Slow-release Fertilizers: A Review. *The Open Agriculture Journal*, *12*(1), 11–19. https://doi.org/10.2174/1874331501812010011

Anas, M., Liao, F., Verma, K. K., Sarwar, M. A., Mahmood, A., Chen, Z. L., Li, Q., Zeng, X. P., Liu, Y., & Li, Y. R. (2020). Fate of nitrogen in agriculture and environment: agronomic, eco-physiological and molecular approaches to improve nitrogen use efficiency. In *Biological Research* (Vol. 53, Issue 1). BioMed Central Ltd. https://doi.org/10.1186/s40659-020-00312-4

Behera, S. N., Sharma, M., Aneja, V. P., & Balasubramanian, R. (2013). Ammonia in the atmosphere: A review on emission sources, atmospheric chemistry and deposition on terrestrial bodies. In *Environmental Science and Pollution Research* (Vol. 20, Issue 11, pp. 8092–8131). https://doi.org/10.1007/s11356-013-2051-9

Brondi, M., Eisa, M., Bortoletto-Santos, R., Drapanauskaite, D., Reddington, T., Williams, C., Ribeiro, C., & Baltrusaitis, J. (2023). Recovering, Stabilizing, and Reusing Nitrogen and Carbon from Nutrient-Containing Liquid Waste as Ammonium Carbonate Fertilizer. In *Agriculture (Switzerland)* (Vol. 13, Issue 4). MDPI. https://doi.org/10.3390/agriculture13040909

Environmental Protection Agency. (2004). *Ammonium Bicarbonate; Exemption from the Requirement of a Tolerance*.

Fowler, D., Coyle, M., Skiba, U., Sutton, M. A., Cape, J. N., Reis, S., Sheppard, L. J., Jenkins, A., Grizzetti, B., Galloway, J. N., Vitousek, P., Leach, A., Bouwman, A. F., Butterbach-Bahl, K., Dentener, F., Stevenson, D., Amann, M., & Voss, M. (2013). The global nitrogen cycle in the twenty-first century. *Philosophical Transactions of the Royal Society B: Biological Sciences*, *368*(1621). https://doi.org/10.1098/rstb.2013.0164

Govoni Brondi, M., Bortoletto-Santos, R., Farias, J. G., Farinas, C. S., Ammar, M., Ribeiro, C., Williams, C., & Baltrusaitis, J. (2024). Mechanochemically Synthesized Nitrogen-Efficient Mg- and Zn-Ammonium Carbonate Fertilizers. *ACS Sustainable Chemistry and Engineering*, *12*(16), 6182–6193. https://doi.org/10.1021/acssuschemeng.3c07785

Ha, P. T. M., Kanaya, Y., Taketani, F., Andres Hernandez, M. D., Schreiner, B., Pfeilsticker, K., & Sudo, K. (2023). Implementation of HONO into the chemistry-climate model CHASER (V4.0): Roles in tropospheric chemistry. *Geoscientific Model Development*, *16*(3), 927–960. https://doi.org/10.5194/gmd-16-927-2023

Jadon, P., Selladurai, R., Singh Yadav, S., Vassanda Coumar, M., Lal Dotaniya, M., Kumar Singh, A., & Bhadouriya, J. (2018). Volatilization and leaching losses of nitrogen from different coated urea fertilizers. *Soil Science and Plant Nutrition*, *18 (4)*, 1036–1047.

Jang, J.-H., Hong, J., Kim, J. B., Park, S., Hwang, K., Kim, J., Kim, J. Y., Bae, G.-N., Kim, S., & Kim, K. H. (2025). Influence of atmospheric ammonia on secondary inorganic aerosol formation in PM2.5 during spring 2024 in the Hongseong area, Republic of Korea. *Atmospheric Environment*, 121363. https://doi.org/10.1016/j.atmosenv.2025.121363

Liu, L., Zhang, X., Xu, W., Liu, X., Li, Y., Wei, J., Wang, Z., & Lu, X. (2020). Ammonia volatilization as the major nitrogen loss pathway in dryland agro-ecosystems. *Environmental Pollution*, *265*. https://doi.org/10.1016/j.envpol.2020.114862

Liu, Zheng, X., Li, Y., Yu, J., Ding, H., Sveen, T. R., & Zhang, Y. (2022). Soil moisture determines nitrous oxide emission and uptake. *Science of the Total Environment*, *822*. https://doi.org/10.1016/j.scitotenv.2022.153566

Lu, C., & Tian, H. (2017). Global nitrogen and phosphorus fertilizer use for agriculture production in the past half century: Shifted hot spots and nutrient imbalance. *Earth System Science Data*, *9*(1), 181–192. https://doi.org/10.5194/essd-9-181-2017

Meusel, H., Tamm, A., Kuhn, U., Wu, D., Lena Leifke, A., Fiedler, S., Ruckteschler, N., Yordanova, P., Lang-Yona, N., Pöhlker, M., Lelieveld, J., Hoffmann, T., Pöschl, U., Su, H., Weber, B., & Cheng, Y. (2018). Emission of nitrous acid from soil and biological soil crusts represents an important source of HONO in the remote atmosphere in Cyprus. *Atmospheric Chemistry and Physics*, *18*(2), 799–813. https://doi.org/10.5194/acp-18-799-2018

Moravek, A., Singh, S., Pattey, E., Pelletier, L., & Murphy, J. G. (2019). Measurements and quality control of ammonia eddy covariance fluxes: A new strategy for high-frequency attenuation correction. *Atmospheric Measurement Techniques*, *12*(11), 6059–6078. https://doi.org/10.5194/amt-12-6059-2019

Ni, B., Liu, M., Lü, S., Xie, L., & Wang, Y. (2011). Environmentally friendly slow-release nitrogen fertilizer. *Journal of Agricultural and Food Chemistry*, *59*(18), 10169–10175. https://doi.org/10.1021/jf202131z

Oswald, R., Behrendt, T., Ermel, M., Wu, D., Su, H., Cheng, Y., Breuninger, C., Moravek, A., Mougin, E., Delon, C., Loubet, B., Pommerening-Röser, A., Sörgel, M., Pöschl, U., Hoffmann, T., Andreae, M. O., Meixner, F. X., & Trebs, I. (2013). HONO emissions from soil bacteria as a major source of atmospheric reactive nitrogen. *Science*, *341*(6151), 1233–1235. https://doi.org/10.1126/science.1242266

Pan, B., Lam, S. K., Mosier, A., Luo, Y., & Chen, D. (2016). Ammonia volatilization from synthetic fertilizers and its mitigation strategies: A global synthesis. *Agriculture, Ecosystems and Environment*, *232*, 283–289. https://doi.org/10.1016/j.agee.2016.08.019

Pan, B., Xia, L., Lam, S. K., Wang, E., Zhang, Y., Mosier, A., & Chen, D. (2022). A global synthesis of soil denitrification: Driving factors and mitigation strategies. *Agriculture,*

Ecosystems and Environment, *327*(September 2021), 107850. https://doi.org/10.1016/j.agee.2021.107850

Paulot, F., Jacob, D. J., Pinder, R. W., Bash, J. O., Travis, K., & Henze, D. K. (2014). Ammonia emissions in the United States, european union, and China derived by high-resolution inversion of ammonium wet deposition data: Interpretation with a new agricultural emissions inventory (MASAGE_NH3). *Journal of Geophysical Research*, *119*(7), 4343–4364. https://doi.org/10.1002/2013JD021130

Pilegaard, K. (2013). Processes regulating nitric oxide emissions from soils. *Philosophical Transactions of the Royal Society B: Biological Sciences*, *368*(1621). https://doi.org/10.1098/rstb.2013.0126

Priya, E., Sarkar, S., & Maji, P. K. (2024). A review on slow-release fertilizer: Nutrient release mechanism and agricultural sustainability. In *Journal of Environmental Chemical Engineering* (Vol. 12, Issue 4). Elsevier Ltd. https://doi.org/10.1016/j.jece.2024.113211

Schlesinger, W. H. (2020). *Biogeochemistry: An Analysis of Global Change* (4th ed.). Academic Press. https://doi.org/https://doi.org/10.1016/C2018-0-03255-3

Su, H., Cheng, Y., Oswald, R., Behrendt, T., Trebs, I., Meixner, F. X., Andreae, M. O., Cheng, P., Zhang, Y., & Pöschl, U. (2011). Soil nitrite as a source of atmospheric HONO and OH radicals. *Science*, *333*(6049), 1616–1618. https://doi.org/10.1126/science.1207687

Sunderlage, B., & Cook, R. L. (2018). Soil Property and Fertilizer Additive Effects on Ammonia Volatilization from Urea. *Soil Science Society of America Journal*, *82*(1), 253–259. https://doi.org/10.2136/sssaj2017.05.0151

Tian, H., Pan, N., Thompson, R. L., Canadell, J. G., Suntharalingam, P., Regnier, P., Davidson, E. A., Prather, M., Ciais, P., Muntean, M., Pan, S., Winiwarter, W., Zaehle, S., Zhou, F., Jackson, R. B., Bange, H. W., Berthet, S., Bian, Z., Bianchi, D., … Zhu, Q. (2024). Global nitrous oxide budget (1980-2020). *Earth System Science Data*, *16*(6), 2543–2604. https://doi.org/10.5194/essd-16-2543-2024

Wang, Fu, X., Wu, D., Wang, M., Lu, K., Mu, Y., Liu, Z., Zhang, Y., & Wang, T. (2021). Agricultural Fertilization Aggravates Air Pollution by Stimulating Soil Nitrous Acid Emissions at High Soil Moisture. *Environmental Science and Technology*, *55*(21), 14556–14566. https://doi.org/10.1021/acs.est.1c04134

5.0 Conclusion and Future Work

5.1 Conclusions

In chapter **two**, we present a dynamic chamber for N_r measurements, developed for the first time through the necessary hardware modification of commercially available chambers to optimize the transfer of N_r species like NO_2, HONO, NH_3 and O_3 while minimizing gas losses. Two key changes were made: the use of PTFE fittings instead of original brass fittings and the installation of an inert PFA film. The performance of these modifications was quantified through the rise and fall time constants of target gas concentrations. The time constants for the transfer of GHGs were similar to those of a theoretically inert gas and showed no change from the modifications. The improved transmission for reactive and surface-active N_r species (i.e., NO_2, HONO and NH_3) targeted here ranged from 0.8 to 2.6 minutes. Reactive loss for NO_2 in unmodified configurations was up to ~36% and reduced to the gas analyzer detection limits (<10%) with the modifications when atmospherically relevant NO_2 and RH mixtures were introduced. Ozone loss was prevalent within chambers in both their modified and unmodified configurations at 45% and 35% respectively, demonstrating the necessity of the reference chamber characterization of deposited surface film reactivity for O_3. Taken together, the modified commercial chamber can measure dynamic soil fluxes of GHGs and N_r when a measurement and reference chamber are deployed simultaneously. Proof of concept flux measurements using this N_r dynamic chamber system were conducted using real agricultural soil samples in the lab, where soil NO_y emissions were found to be consistent with prior field reports in the literature for NO, and HONO. Variability in NO_2 and HONO emissions between replicates demonstrates the potential heterogeneity of soil emissions that may result from samples kept intact and subject to minimal preparation conditions. Upon the addition of typical fertilizers, like urea, ABC, AC and AN, substantial NH_3 and N_2O emissions fluxes matched expectations, with increasing quantities of NO, NO_2, and HONO as soil water content decreased.

In chapter **three**, the heterogeneity of NO, NO_2 and HONO emissions within a managed agricultural field was investigated using a paired t-test. The obtained p-value for the NO, NO_2 and HONO within a specific soil VWC range (20-24%) indicated the heterogeneity as five out of eight plots were statistically different (p-value < 0.5). Soil NO was the dominant species among the NO_y, and measured fluxes for all the plots ranged between 0.4 to 2.5 μg N m^{-2} hr^{-1}. The NO_2 fluxes were determined to be 0.1-0.8 μg N m^{-2} hr^{-1}, and HONO fluxes were determined to be <1.5 μg N m^{-2}

hr^{-1} for all the samples, indicating that soil, when treated in a similar manner as in the field, does not emit HONO, unlike studies that have manipulated it. Studying these emissions from unamended agricultural soil gave an insight into how sampling and handling techniques used in the laboratory can have an impact on the NO_y.

In chapter **four**, the effects of different nitrogen fertilizers on N_r fluxes were analyzed by comparing emissions from soils treated with urea versus mechanochemically synthesized MAC and ZAC. It evaluated gaseous emissions of NO, NO_2, HONO, NH_3, and N_2O at field-like conditions, that is, at 23 °C, soil VWC between 25–29% where N_2O (0.8 ppm) and NH_3 (160 ppb) began to rise approximately four hours after the experiment started, peaking at between 10–12-hour marks. The NO_y (30 ppb) kicked once the N_2O and NH_3 declined, with NO being the highest (~20 ppb). For the soil treated with MAC, NH_3 (6000 ppb) and N_2O (0.55 ppm) were the first gases to be produced, similar to urea, but to a greater extent. The mixing ratio of NO (<8 ppb) remained constant throughout the two days, with an increase upon the drop of N_2O and NH_3. Likewise, for HONO, it peaked at day three with the drop in soil VWC, N_2O and NH_3 emissions. Lastly, total nitrogen volatilization was evaluated for soil treated with urea, MAC and ZAC. Despite the application of an equal nitrogen amount to the soil, double salts resulted in higher total gaseous N loss than that of urea. The observed emission trends and the nitrogen loss provide a valuable preliminary insight into the different nitrogen gases released from fertilized soils.

5.2 Future work

The presented modified chamber system addressed key design improvements for measuring reactive nitrogen fluxes. Future work will want to include quantification of HONO to check the heterogeneous surface interaction of NO_2 forming HONO with an instrument that has a lower detection limit than that of the NO_x analyzer. This modified dynamic chamber system (MC and RC) was successfully deployed during our field campaign named MAANURE–Measurements of Agricultural Atmospheric Nitrogen: Understanding Realistic Emissions to capture reactive nitrogen fluxes. Deploying multiple chambers across a study site in future studies would allow for the characterization of spatial heterogeneity in fluxes at the ground–atmosphere interface. As the full dataset is still being processed and analyzed for the MAANURE campaign, future work will involve evaluating the system's performance in terms of data quality at a range of environmental conditions. This includes identifying any pressure artifacts, condensation issues, or response delays under varying temperature and humidity. Beyond the current campaign, future work should focus on extending the chamber's application across different soil types to assess its robustness and adaptability in varying agricultural contexts.

The soil experiments provided important insight into the inherent spatial heterogeneity of reactive nitrogen emissions in the absence of fertilizer additions. To improve the reliability of laboratory findings, future studies should implement a stratified sampling approach in which soil variability is explicitly accounted for, especially now that field-scale information is available. Following this, incorporating this knowledge into modelling frameworks may increase the precision of nitrogen flux estimations at broader regional scales.

The current laboratory experiments highlight the complexity of reactive nitrogen emissions from soils treated with various fertilizers, including urea and double salts such as MAC and ZAC. Due to time constraints, only one replicate was performed per treatment; therefore, future experiments should include several replicates at a wider range of environmental conditions, such as varying temperature, moisture, and pH, to evaluate the stability and effectiveness of the salts. Ion chromatography work also needs to be carried out to examine the stability of double salts.

6.0 References:

Agriculture and Agri-Food Canada. (2023). *Sustainable Agriculture Strategy: Discussion Document*. *4*(1), 88–100. https://agriculture.canada.ca/en/department/transparency/public-opinion-research-consultations/sustainable-agriculture-strategy/document

Akiyama, H., Mctaggart, I. P., Ball, B. C., & Scott, A. (2004). N2O, NO, and NH3 emissions from soil after the application of organic fertilizers, urea and water.

AlShamaileh, E., Al-Rawajfeh, A. E., & Alrbaihat, M. (2018). Mechanochemical Synthesis of Slow-release Fertilizers: A Review. *The Open Agriculture Journal*, *12*(1), 11–19. https://doi.org/10.2174/1874331501812010011

Anas, M., Liao, F., Verma, K. K., Sarwar, M. A., Mahmood, A., Chen, Z. L., Li, Q., Zeng, X. P., Liu, Y., & Li, Y. R. (2020). Fate of nitrogen in agriculture and environment: agronomic, eco-physiological and molecular approaches to improve nitrogen use efficiency. In *Biological Research* (Vol. 53, Issue 1). BioMed Central Ltd. https://doi.org/10.1186/s40659-020-00312-4

Behera, S. N., Sharma, M., Aneja, V. P., & Balasubramanian, R. (2013). Ammonia in the atmosphere: A review on emission sources, atmospheric chemistry and deposition on terrestrial bodies. In *Environmental Science and Pollution Research* (Vol. 20, Issue 11, pp. 8092–8131). https://doi.org/10.1007/s11356-013-2051-9

Brondi, M., Eisa, M., Bortoletto-Santos, R., Drapanauskaite, D., Reddington, T., Williams, C., Ribeiro, C., & Baltrusaitis, J. (2023). Recovering, Stabilizing, and Reusing Nitrogen and Carbon from Nutrient-Containing Liquid Waste as Ammonium Carbonate Fertilizer. In *Agriculture (Switzerland)* (Vol. 13, Issue 4). MDPI. https://doi.org/10.3390/agriculture13040909

Environmental Protection Agency. (2004). *Ammonium Bicarbonate; Exemption from the Requirement of a Tolerance*.

Fowler, D., Coyle, M., Skiba, U., Sutton, M. A., Cape, J. N., Reis, S., Sheppard, L. J., Jenkins, A., Grizzetti, B., Galloway, J. N., Vitousek, P., Leach, A., Bouwman, A. F., Butterbach-Bahl, K., Dentener, F., Stevenson, D., Amann, M., & Voss, M. (2013). The global nitrogen cycle in the twenty-first century. *Philosophical Transactions of the Royal Society B: Biological Sciences*, *368*(1621). https://doi.org/10.1098/rstb.2013.0164

Govoni Brondi, M., Bortoletto-Santos, R., Farias, J. G., Farinas, C. S., Ammar, M., Ribeiro, C., Williams, C., & Baltrusaitis, J. (2024). Mechanochemically Synthesized Nitrogen-Efficient Mg- and Zn-Ammonium Carbonate Fertilizers. *ACS Sustainable Chemistry and Engineering*, *12*(16), 6182–6193. https://doi.org/10.1021/acssuschemeng.3c07785

Ha, P. T. M., Kanaya, Y., Taketani, F., Andres Hernandez, M. D., Schreiner, B., Pfeilsticker, K., & Sudo, K. (2023). Implementation of HONO into the chemistry-climate model CHASER

(V4.0): Roles in tropospheric chemistry. *Geoscientific Model Development*, *16*(3), 927–960. https://doi.org/10.5194/gmd-16-927-2023

Jadon, P., Selladurai, R., Singh Yadav, S., Vassanda Coumar, M., Lal Dotaniya, M., Kumar Singh, A., & Bhadouriya, J. (2018). Volatilization and leaching losses of nitrogen from different coated urea fertilizers. *Soil Science and Plant Nutrition*, *18 (4)*, 1036–1047.

Jang, J.-H., Hong, J., Kim, J. B., Park, S., Hwang, K., Kim, J., Kim, J. Y., Bae, G.-N., Kim, S., & Kim, K. H. (2025). Influence of atmospheric ammonia on secondary inorganic aerosol formation in PM2.5 during spring 2024 in the Hongseong area, Republic of Korea. *Atmospheric Environment*, 121363. https://doi.org/10.1016/j.atmosenv.2025.121363

Liu, L., Zhang, X., Xu, W., Liu, X., Li, Y., Wei, J., Wang, Z., & Lu, X. (2020). Ammonia volatilization as the major nitrogen loss pathway in dryland agro-ecosystems. *Environmental Pollution*, *265*. https://doi.org/10.1016/j.envpol.2020.114862

Liu, Zheng, X., Li, Y., Yu, J., Ding, H., Sveen, T. R., & Zhang, Y. (2022). Soil moisture determines nitrous oxide emission and uptake. *Science of the Total Environment*, *822*. https://doi.org/10.1016/j.scitotenv.2022.153566

Lu, C., & Tian, H. (2017). Global nitrogen and phosphorus fertilizer use for agriculture production in the past half century: Shifted hot spots and nutrient imbalance. *Earth System Science Data*, *9*(1), 181–192. https://doi.org/10.5194/essd-9-181-2017

Meusel, H., Tamm, A., Kuhn, U., Wu, D., Lena Leifke, A., Fiedler, S., Ruckteschler, N., Yordanova, P., Lang-Yona, N., Pöhlker, M., Lelieveld, J., Hoffmann, T., Pöschl, U., Su, H., Weber, B., & Cheng, Y. (2018). Emission of nitrous acid from soil and biological soil crusts represents an important source of HONO in the remote atmosphere in Cyprus. *Atmospheric Chemistry and Physics*, *18*(2), 799–813. https://doi.org/10.5194/acp-18-799-2018

Moravek, A., Singh, S., Pattey, E., Pelletier, L., & Murphy, J. G. (2019). Measurements and quality control of ammonia eddy covariance fluxes: A new strategy for high-frequency attenuation correction. *Atmospheric Measurement Techniques*, *12*(11), 6059–6078. https://doi.org/10.5194/amt-12-6059-2019

Ni, B., Liu, M., Lü, S., Xie, L., & Wang, Y. (2011). Environmentally friendly slow-release nitrogen fertilizer. *Journal of Agricultural and Food Chemistry*, *59*(18), 10169–10175. https://doi.org/10.1021/jf202131z

Oswald, R., Behrendt, T., Ermel, M., Wu, D., Su, H., Cheng, Y., Breuninger, C., Moravek, A., Mougin, E., Delon, C., Loubet, B., Pommerening-Röser, A., Sörgel, M., Pöschl, U., Hoffmann, T., Andreae, M. O., Meixner, F. X., & Trebs, I. (2013). HONO emissions from soil bacteria as a major source of atmospheric reactive nitrogen. *Science*, *341*(6151), 1233–1235. https://doi.org/10.1126/science.1242266

Pan, B., Lam, S. K., Mosier, A., Luo, Y., & Chen, D. (2016). Ammonia volatilization from synthetic fertilizers and its mitigation strategies: A global synthesis. *Agriculture, Ecosystems and Environment*, *232*, 283–289. https://doi.org/10.1016/j.agee.2016.08.019

Pan, B., Xia, L., Lam, S. K., Wang, E., Zhang, Y., Mosier, A., & Chen, D. (2022). A global synthesis of soil denitrification: Driving factors and mitigation strategies. *Agriculture, Ecosystems and Environment*, *327*(September 2021), 107850. https://doi.org/10.1016/j.agee.2021.107850

Paulot, F., Jacob, D. J., Pinder, R. W., Bash, J. O., Travis, K., & Henze, D. K. (2014). Ammonia emissions in the United States, european union, and China derived by high-resolution inversion of ammonium wet deposition data: Interpretation with a new agricultural emissions inventory (MASAGE_NH3). *Journal of Geophysical Research*, *119*(7), 4343–4364. https://doi.org/10.1002/2013JD021130

Pilegaard, K. (2013). Processes regulating nitric oxide emissions from soils. *Philosophical Transactions of the Royal Society B: Biological Sciences*, *368*(1621). https://doi.org/10.1098/rstb.2013.0126

Priya, E., Sarkar, S., & Maji, P. K. (2024). A review on slow-release fertilizer: Nutrient release mechanism and agricultural sustainability. In *Journal of Environmental Chemical Engineering* (Vol. 12, Issue 4). Elsevier Ltd. https://doi.org/10.1016/j.jece.2024.113211

Schlesinger, W. H. (2020). *Biogeochemistry: An Analysis of Global Change* (4th ed.). Academic Press. https://doi.org/https://doi.org/10.1016/C2018-0-03255-3

Su, H., Cheng, Y., Oswald, R., Behrendt, T., Trebs, I., Meixner, F. X., Andreae, M. O., Cheng, P., Zhang, Y., & Pöschl, U. (2011). Soil nitrite as a source of atmospheric HONO and OH radicals. *Science*, *333*(6049), 1616–1618. https://doi.org/10.1126/science.1207687

Sunderlage, B., & Cook, R. L. (2018). Soil Property and Fertilizer Additive Effects on Ammonia Volatilization from Urea. *Soil Science Society of America Journal*, *82*(1), 253–259. https://doi.org/10.2136/sssaj2017.05.0151

Tian, H., Pan, N., Thompson, R. L., Canadell, J. G., Suntharalingam, P., Regnier, P., Davidson, E. A., Prather, M., Ciais, P., Muntean, M., Pan, S., Winiwarter, W., Zaehle, S., Zhou, F., Jackson, R. B., Bange, H. W., Berthet, S., Bian, Z., Bianchi, D., … Zhu, Q. (2024). Global nitrous oxide budget (1980-2020). *Earth System Science Data*, *16*(6), 2543–2604. https://doi.org/10.5194/essd-16-2543-2024

Wang, Fu, X., Wu, D., Wang, M., Lu, K., Mu, Y., Liu, Z., Zhang, Y., & Wang, T. (2021). Agricultural Fertilization Aggravates Air Pollution by Stimulating Soil Nitrous Acid Emissions at High Soil Moisture. *Environmental Science and Technology*, *55*(21), 14556–14566. https://doi.org/10.1021/acs.est.1c04134

Appendices

Appendix A: Supporting information for Chapter Two

Modification and validation of a commercial dynamic chamber for reactive nitrogen and greenhouse gas flux measurements

Moxy Shah[1], Kifle Z. Aregahegn[1], Danial Nodeh-Farahani[1], Leigh R. Crilley[1,ǂ], Tasnia Hasan[1], Yashar Ebrahimi-Iranpour[1], Fahim Sarker[1], Nick Nickerson[2], Chance Creelman[2], Sarah Morrison[2], Alexander Moravek[1,§] , Trevor C. VandenBoer[1,*]

[1] Department of Chemistry, York University, Toronto, Ontario, Canada

[2] Eosense Inc., Dartmouth, Nova Scotia, Canada

[ǂ] Now at: Atmospheric Services, WSP Australia, Brisbane, QLD, Australia

[§] Now at: German Environment Agency, Department of Air Quality, Dessau-Rosslau, Germany

[*]Communicating author: tvandenb@yorku.ca

The material presented in the SI has been submitted to *Atmospheric Measurement Techniques* (AMT; egusphere-2025-4662) for peer review on 22 September 2025.

2.S1. Chamber customized components and LabVIEW software

To meet the performance requirements for measuring N_r gases, chamber modifications were implemented to create inert surfaces that transmit them effectively to downstream gas analyzers. In addition, a reference chamber with an inert surface at the bottom (**Figure 2.S1**) was required to benchmark the performance of a modified chamber (**Figure 2.S2**) where fittings and surfaces identified to be reactive or to facilitate stronger surface interactions were replaced with more inert components.

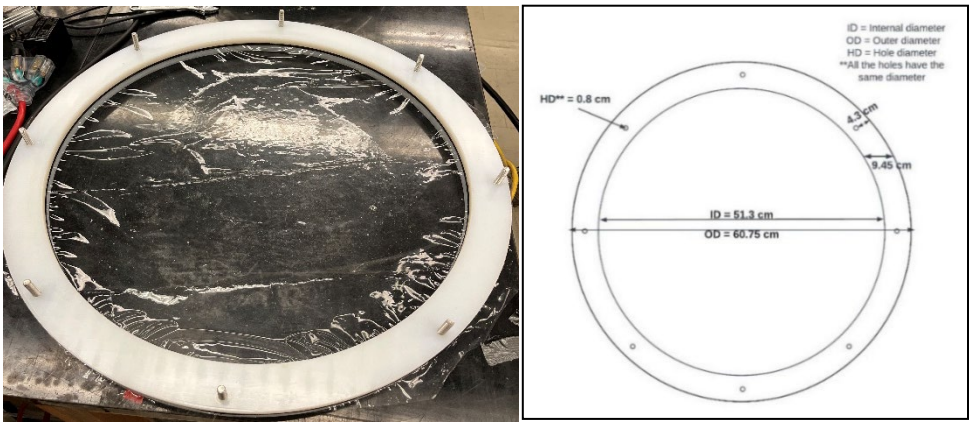

Figure 2.S1: (left) Image of the custom-made base rings made from 1.2 cm thick PTFE with a PFA film pinned between them; all the holes have identical diameters, are located equidistant from the edges of the plate and can fit M8 bolts secured with corresponding nuts (McMasterr-Carr®, PN: 90591A161 and 91263A918). (right) Technical scale drawing of a custom-made ring for the chambers with the inner diameter, outer diameter, ring width, and diameter of holes and their distance from the outer edges denoted.

A custom LabVIEW program was created to automate control of the solenoid valves and mass flow controller in the measurement setup using the microcontroller. The front panel of the LabVIEW program (Figure S3a) allows for the timings of the solenoid valve changes to be manually set, along with the log intervals. A graphical representation of the valve states in real time is also included on the front window to allow the user to assess the measurement state. In the back window (Figure S3b), the valve timings are controlled within a state machine to allow for continuous valve switching at the time interval selected on the front window. The MFC flow rate is controlled by sending the required voltage to the MFC based on the selected flow rate. The data logging of the valve switching timings and MFC flow is handled as well within a state machine to ensure continuous logging to a CSV file. The LabVIEW VI is available on the GitHub repository (https://github.com/fjs-vdblab/fluxchamber.git).

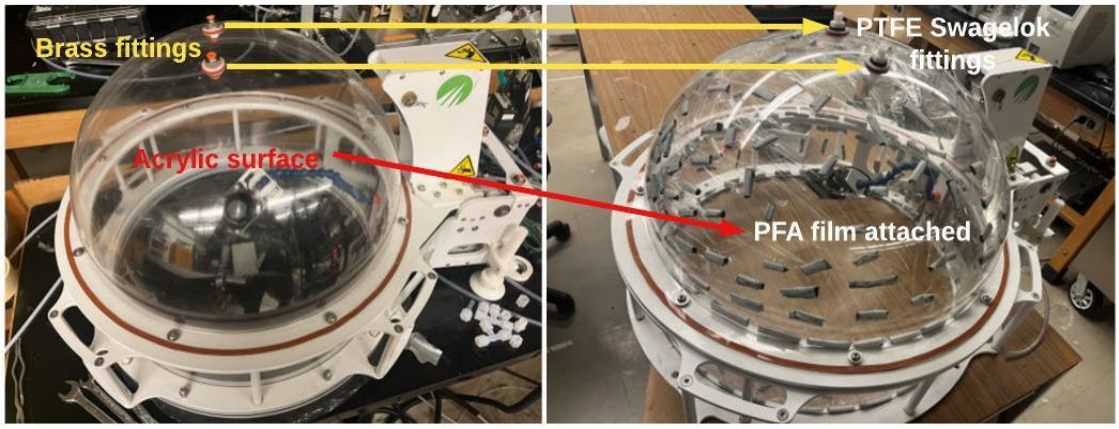

Figure 2.S2: (left) The chamber is in its original configuration from the manufacturer, with brass push-connect inlet and outlet fittings and an acrylic dome. (right) The modified chamber has 1/4" PTFE Swagelok bulkhead fittings and an attached film of PFA on the interior of the acrylic dome and all chamber sidewalls using adhesive tape.

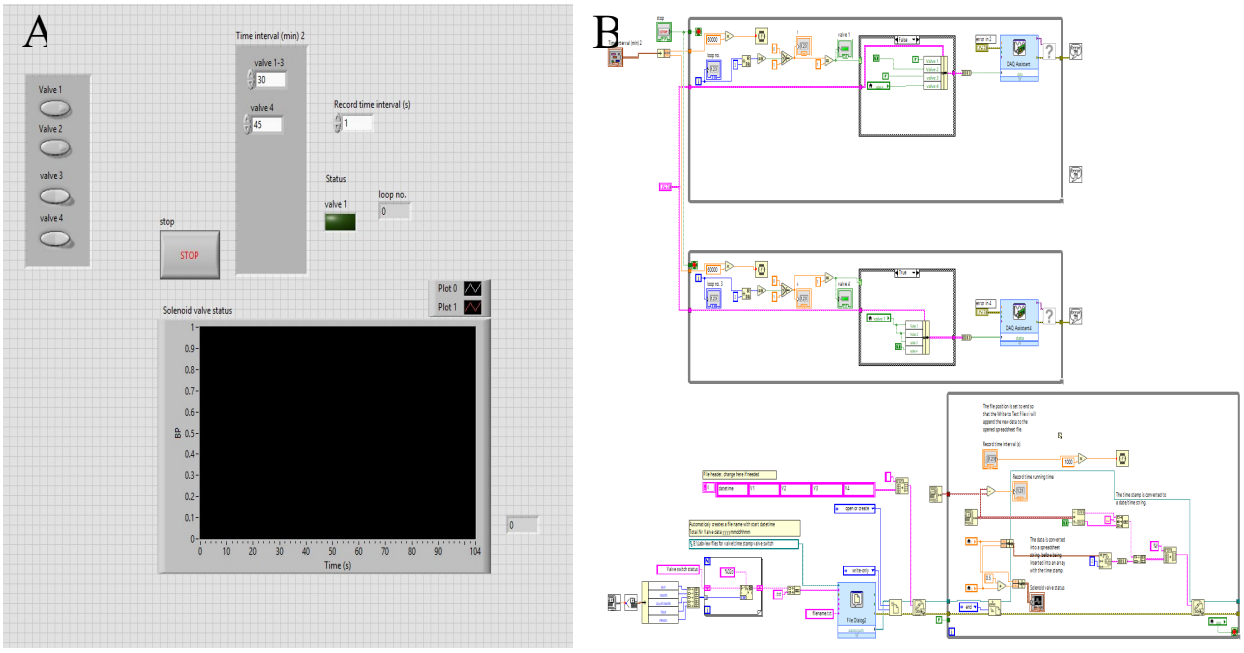

Figure 2.S3: The custom LabVIEW VI for controlling the reference and measurement chambers (A) flows, valve states, timing for lid closures, and rate of datalogging through a graphical user interface front window, and (B) the back window virtual machines controlling the objects, voltages, and data flows.

2.S2. Gas analyzer quality control procedures

The NO_x analyzer is calibrated with multipoint NO and NO_2 mixing ratios to generate calibration curves on at least an annual basis, with span checks and blanks performed regularly before the collection of experimental data. For field use, a full calibration is performed before relocation of

the system to the deployment site, a span check on site, and again at the end of the deployment period to account for any instrumental drift. Zero air from a gas-calibration instrument (Gascal 1100TS, American Ecotech, Warren, RI) is introduced to the analyzer through the sampling inlet to set the zero point. If the NO, NO_2 and NO_x readings are within ±0.5 ppbv of one another, the zero offset is calculated and applied. Then, an NO span check is performed using a known mixing ratio from a certified cylinder (e.g. Praxair, NI NO5MC-A3, 4.88 (±5 %) ppmv, Toronto, ON) to ensure the NO and NO_x readings are within ±1 ppbv of the true value. Next, a multi-point precision check of NO is performed at 40 ppbv, 60 ppbv, and 80 ppbv for 30 min, ensuring a stable signal has been achieved. The calibration is considered successful when the analyzer's response to changes in NO mixing ratio is linear, with a slope of 1.00 ± 0.02 and R^2>0.98. For multi-point precision checks of NO_2, 40 ppbv, 60 ppbv, and 80 ppbv were produced using gas-phase titration of excess NO with O_3, again using the GasCal. The criteria for a successful calibration are the same as described for NO. Conversion efficiency (CE) of NO_2 to NO in the analyzer is the final parameter to be quantified, and a CE > 96% indicates that the molybdenum catalyst in the analyzer is operating reliably.

Calibration for the O_3 analyzer involves a multipoint check, after one hour of warmup time to ensure lamp stability, using 100, 200, 300, and 400 ppbv mixing ratios. The procedure is considered successful if the slope falls between 0.98 and 1.02, the y-intercept is between -2 and 2 ppb, and an overall $R^2 > 0.99$.

The calibration and precision check procedure for the Picarro G2509 involved measuring multiple known concentrations of GHGs from a calibration cylinder. The calibration cylinder contained a custom blend of GHGs (4.30 ppm (+/- 5%) N_2O, 24.8 ppm (+/- 5%) CH_4, 3587 ppm (+/- 2%) CO_2), which was a certified standard grade in an air matrix (Linde Canada Plc; PN: AI CD.4MN1C-A3; CGA-590). Pure nitrogen and three calibration points at none, 4.5, and 10-times dilution of the original GHG mixing ratios in the cylinder were delivered to the Picarro analyzer until stable responses were achieved, in triplicate. The dilution of gases was achieved by combining the flow from a liquid N_2 dewar (Linde Canada Plc, PN: NI LC250-230). The observed versus returned slopes of 0.99 for N_2O, 0.99 for CH_4, and 0.98 for CO_2 when compared to the known concentrations delivered, thereby demonstrating suitable and stable calibration of the instrument, as these slopes are within the cylinder mixing ratio uncertainties.

2.S3. Gas handling for chamber filling and emptying challenge experiments

Dilution and analyte gas flow rates were controlled using MFCs (10 L min^{-1}, PN: 1179C01314CR1BV, MKS Instruments Inc., Andover, MA, US). Mixing ratios of CO_2, CH_4 and N_2O were controlled by dilution of a calibration gas cylinder containing a custom blend of the three gases (4000 ppm CO_2, 20 ppm CH_4, 3.3 ppm N_2O in zero air from Linde Canada). Known concentrations of NO and NO_2 were added from their respective calibration gas cylinders (5.9 (±5 %) ppmv of NO in air, PN: NI NO5MC-A3; 4.5 (±5 %) ppmv NO_2 in air, PN: NI NX5MC-AQ; Linde Canada plc, Toronto, ON). Production of known mixing ratios of O_3 to the chamber was achieved by combining output from the built-in ozone generator and photometer of the GasCal into dilution gas at 2 L min^{-1}.

Nitrous acid (HONO) was generated using our in-house calibration source based on the reaction between gas-phase hydrochloric acid (HCl) and a $NaNO_2$ crystalline film on the surface of PFA tubing (**RS-1**) at 50% RH to generate gas-phase HONO (Lao et al., 2020).

$$NaNO_{2(s)} + HCl_{(g)} \rightarrow HONO_{(g)} + NaCl_{(s)} \qquad \textbf{RS-1}$$

In the HONO calibration source, a flow of dry carrier gas (Air Ultra Zero, 99.999%, AI 0.0UZ-K, Praxair) at 50 cm^3 min^{-1} passes through a permeation device (PD) containing HCl solution, heated to 30-40 °C. Another 50 cm^3 min^{-1} passes through a glass impinger containing deionized water to become saturated with water vapour, so the flow obtains an RH of 50% when combined with that of the HCl. This HCl-water vapour mixture enters a $NaNO_2$-coated PFA reaction device, and HONO is released by acid displacement. The 100 cm^3 min^{-1} flow of HONO exiting the calibration source was diluted using ZA at 2 L min^{-1}, and a mixing ratio of 10-100 ppbv was obtained.

The custom-built permeation oven was also used to generate known mixing ratios of NH_3 by quantification of bubbler-scrubbed NH_3 using ion chromatography (Salehpoor and VandenBoer, 2023). A dry 90 cm^3 min^{-1} zero air flow was passed over a PD containing NH_4OH (30% v/v in 1/8" OD tubing with a 9 cm length). The output was diluted with 2 L min^{-1} of zero air to generate NH_3 mixing ratios on the order of 30 ppbv.

The time response of gases for the fill and empty process was calculated from the time required to fill the chamber and empty the chamber (**Figure S4**). It can be described by a single exponential function for non-reactive gases such as N_2O, CH_4, CO_2, and NO and thus the time response, τ, for

the exchange of sample gases volume (**Section 2.1; E1-4**). The double exponential function was used for surface-sensitive and reactive gases, such as NO_2, HONO, and NH_3 to yield two time constants, τ_1 and τ_2, the time response towards the exchange of the sample air volume and wall interactions (**ES-1**), respectively (Ellis, Murphy, Pattey, Van Haarlem, O'brien, et al., 2010).

$$f(t) = y_0 + A_1 \times \exp\left(\frac{-(t-t_0)}{\tau_1}\right) + A_2 \times \exp\left(\frac{-(t-t_0)}{\tau_2}\right) \qquad \textbf{ES-1}$$

Where t_0 is the start time and y_0 is the offset that represents the measurement baseline level; A_1 and A_2 are proportionality coefficients from the contribution of the physical processes of sample volume exchange in the chamber, and reaction and wall interactions, respectively. The relative role of wall interactions or reactions, D, to the overall transfer of gases through a handling system is determined by the contribution of the A_2 term to the sum of both A terms (**ES-2**).

$$D = \left(\frac{A_2}{A_1+A_2}\right) \times 100\% \qquad \textbf{ES-2}$$

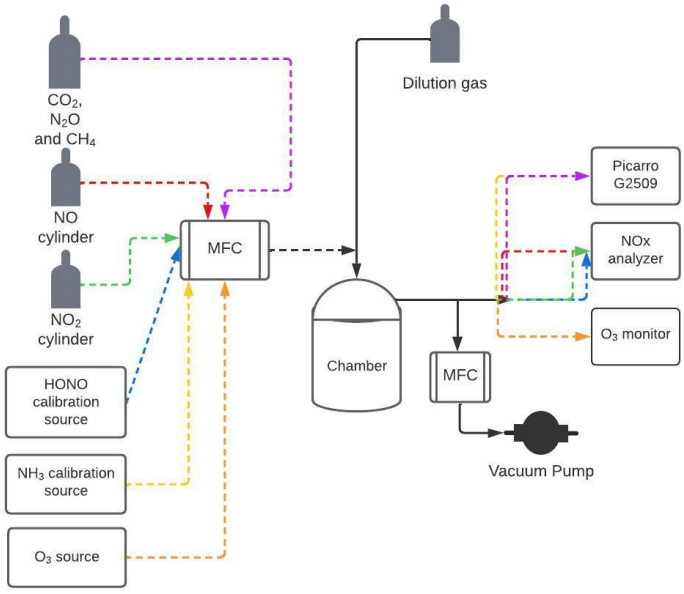

Figure 2.S4: Experimental setup to perform fill/empty experiments in the chambers with greenhouse gases: CH_4, CO_2 and N_2O (purple); N_r gases NO (red), NO_2 (green), HONO (blue), NH_3 (yellow), and O_3 (orange); and dilution gas (black). Dashed arrows show the flow of gases from their respective sources for filling experiments to their respective gas analyzers. Emptying experiments use dilution gas alone once a steady state of the challenge gas has been obtained in the chamber.

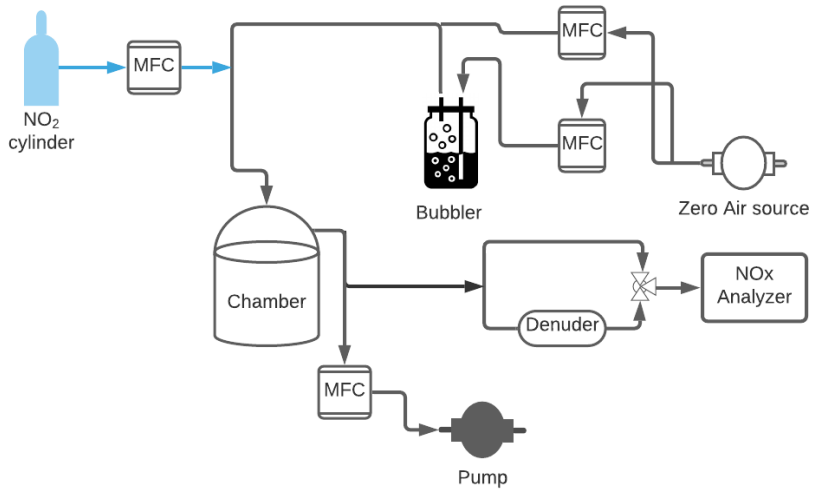

Figure 2.S5: Experimental setup for NO_2 surface loss characterization, where arrows indicate direction of gas flows. Characterization of losses or transformation to HONO was made by a modified NO_x analyzer with an experimental flow balance with an added MFC and pump.

2.S4. Multiplexer modification tests on gas transfer of N_r and GHGs

A 2 L min^{-1} flow of dry zero air containing 0.058 ppm of N_2O, 0.57 ppm of CH_4, and 81.5 ppm of CO_2, was passed through a multiplexer equipped with either PTFE or stainless-steel (SS) valves and fittings for 30 min to access relative losses. A separate experiment was performed with 2 L min^{-1} zero air containing a known concentration of NH_3 (0.41 ppm), which was generated based on the method described in Crilley et al. (2023) from a permeation tube containing NH_4OH. Similarly, the transfer efficiency of NO_2 was determined using a calibration cylinder (Linde Canada; PN: NI NX5MC-AQ; 5.9 (±5%) ppm) which was combined with a 2 L min^{-1} dilution flow of dry ZA to achieve a mixing ratio of 54 ppb. All challenge gases were passed through the multiplexer equipped with either PTFE or SS valves and PFA or SS fittings, respectively, to assess relative losses. All delivered and exiting flows were confirmed to be equal during these tests, ensuring no leaks led to a measured loss. The loss percentage in SS fittings and gas handling valves was measurable but generally remained below 20%, except for NH_3, which exhibited a 38% reduction. With the modifications, minimal surface loss of GHGs and NO_2 (<1%) was observed when using the PFA fittings and PTFE valves, whereas NH_3 exhibited a reduced 11% loss (**Figure 2.S6**).

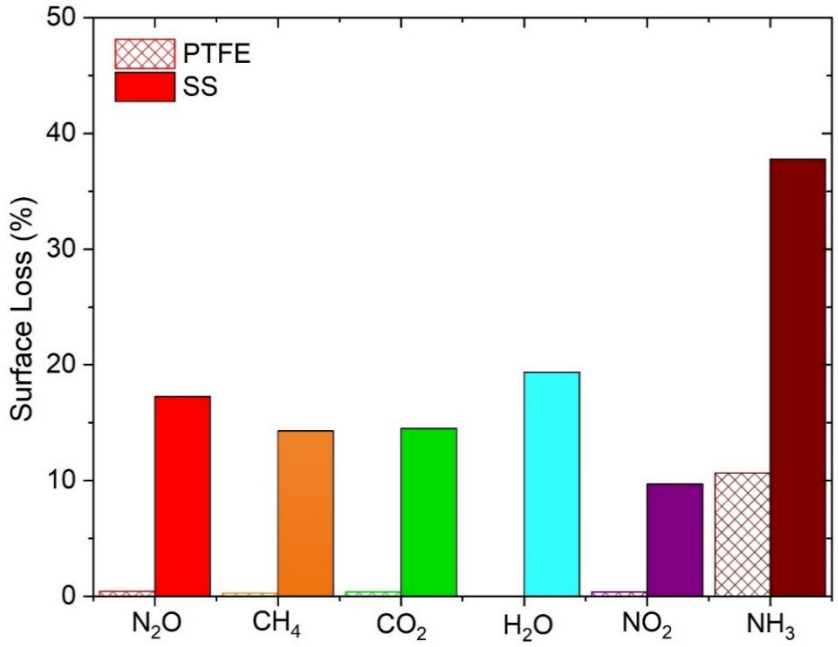

Figure 2.S6: Loss percentage of GHGs (N_2O, CH_4, and CO_2) and N_r (NO_2, NH_3) gases on stainless steel fittings is higher than that of a PTFE valve and unions.

The surface porosity of SS can influence its adsorption capacity for CH_4 through van der Waals interaction potentials (Sapag et al., 2010). Previous studies have shown that passivation of the SS surface via NO treatment can remove surface iron and promote the formation of chromium-enriched oxide films, which in turn govern the surface chemical reactivity toward NO (Ma et al., 2020). Furthermore, thin layers of iron oxides formed on SS surfaces can affect the interaction with N_2O and alter its decomposition pathways. Consequently, the combined effects of SS surface porosity on CH_4 van der Waals interactions, chromium-oxide passive films influencing NO reactivity, and iron-oxide layers acting as active adsorption sites for N_2O may contribute to up to a 20 % loss of these gases on SS surfaces. Likely, the surface losses observed here for very clean SS purged extensively with dry zero air before these experiments are passivated over time when exposed to ambient air continuously, where the surface adsorption sites are fully occupied and losses no longer occur.

2.S5. Chamber modification impacts on gas transfer of NO_2

Gas interactions on chamber surfaces during challenge experiments were reversible for all N_r and GHGs tested, except NO_2, which showed reactive losses. These were characterized by calculating the lost fraction from a small 5 ppb mixing ratio delivered into an unmodified chamber at a high

relative humidity of 83%, followed by modifications to reduce this outcome under these challenging simulated environmental conditions (**Figure 2.S5**). Replacement of the brass push-to-connect fittings delivered the greatest reduction in reactive losses of NO_2, with modest gains obtained from covering chamber surfaces with the PFA film (**Figure 2.S7**). The final lost fraction of NO_2 in the modified system reported here is technically at the modified NO_x analyzer detection limit and therefore represents a conservative upper limit estimate.

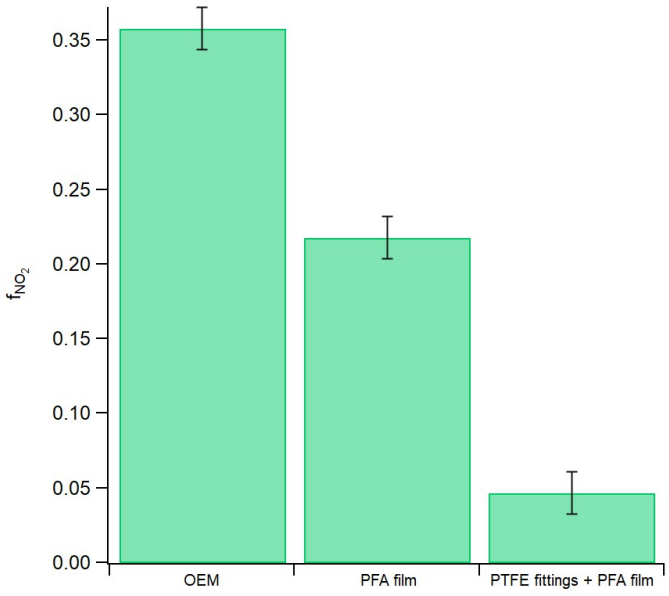

Figure 2.S7: Average NO_2 loss fraction observed upon addition of 5 ppbv of NO_2 at 83% RH to an eosAC-LT® chamber (n = 3 each). These trials were conducted in chambers sequentially: without any modifications (original equipment manufacturer; OEM), following attachment of a PFA film to the inner surface (PFA film), and replacing brass-lined push-to-connect fittings with ¼" PTFE Swagelok bulkhead (PTFE fittings + PFA film).

2.S6. Agricultural soil samples used for laboratory N_r emission measurements

A systematic method was used to collect soil samples from an agricultural field to avoid sampling bias, assuming there is no topographic reason for differences in soil properties and nutrient content within the specified plot area. The total field area was divided into eight identical plots (A-H) of 10,800 m^2 (120 m × 90 m). Soil samples were collected from four random coordinates within each plot, assuming that samples collected within 1 m^2 were homogeneous. An approximate 1 L soil core ~15 cm deep was collected with a clean shovel into a pre-labelled clean Ziploc bag. All soil samples were stored below 10 °C and transported to the laboratory within a week.

Four within-plot samples were collected to better approximate soil properties and nutrient content across the entire field. A total of 32 soil samples were collected from the field, where three of the randomly collected within-plot samples were combined to generate a plot-scale sample, and one sample within each plot was randomly selected to be combined into a pooled sample representative of the field scale. For this work, we assessed the emissions of NO, NO_2, and HONO from duplicate pooled samples and from Plot D within this sampling experiment (**Figure 2.S8**).

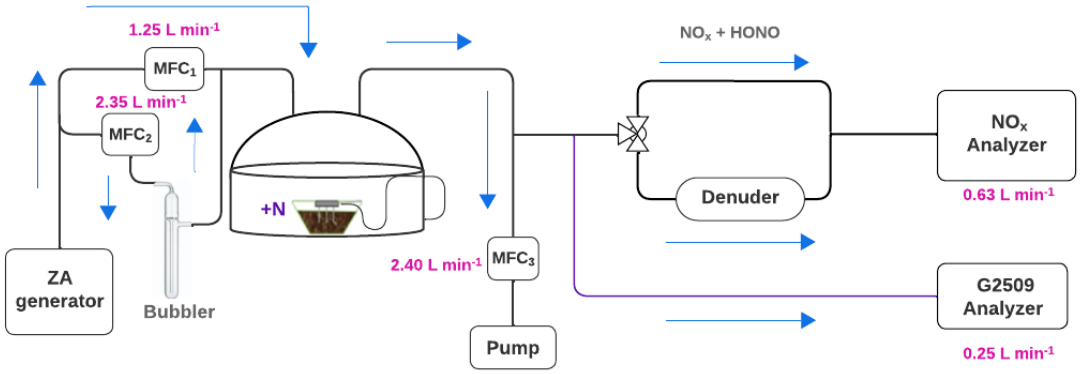

Figure 2.S8: Schematic representation of a dynamic chamber system to measure NO, NO_2, and HONO fluxes with a modified NO_x analyzer (black lines) and NH_3 and N_2O for soil amended with fertilizer using G2509 (purple line). Zero air and humid airflow rates were set using MFC 1 and MFC 2, for a total of 3.6 L min^{-1} going into the chamber. The three-way valve either sends headspace air directly to the NO_x analyzer (measures NO and NO_2+HONO) or via the Na_2CO_3-coated denuder (measures NO and NO_2). Blue arrows indicate the flows throughout the experimental setup, with flow rates provided in pink text.

Soil NH_3 and N_2O, along with NO, NO_2, and HONO, were measured when the pooled soil sample was amended with four different nitrogen salts (i.e., AN, urea, ABC, AC; **Table S1, Figure 2.4**). For each experiment, 350 g of soil was used, and a corresponding fertilizer solution equivalent to 100 kg N ha^{-1} was added. Additional experimental details are provided in **Section 2.6.1** of the main manuscript. The interpretation of the full set of experimental results will be presented in a forthcoming publication on field-scale heterogeneity of N_r emissions and comments on the assumption that individual samples represent these processes across fields with similar physicochemical properties.

Table 2.S1. The average and integrated flux for soil treated with 4 different nitrogen salts (urea, ammonium bicarbonate (ABC), ammonium carbonate (AC), and ammonium nitrate (AN)). Average fluxes were calculated over the entire experimental cycle. Integrated fluxes were obtained using the trapezoidal rule. Standard deviations reflect the variability in fluxes measured across the time points for the single sample analyzed per treatment. Replicates of urea (~40 hours) and AN (~5 hours) were analyzed with only the modified NO_x analyzer, thus lacking data for N_2O and NH_3 (represented by -).

Soil sample	Avg Flux (μg N m^{-2} hr^{-1})					Integrated flux (μg N m^{-2})				
	NO	NO_2	HONO	N_2O	NH_3	NO	NO_2	HONO	N_2O	NH_3
Urea	0.1 ± 0.06	0.03 ± 0.01	0.002 ± 0.004	9 ± 3	1 ± 0.5	230	120	1	32400	3700
ABC	0.03 ± 0.01	0.1 ± 0.01	0.03 ± 0.02	7 ± 6	20 ± 7	90	300	90	25300	85900
AC	0.03 ± 0.004	0.2 ± 0.03	0.01 ± 0.01	3 ± 2	20 ± 3	90	500	1	9600	63700
*AN	1 ± 0.1	1 ± 0.1	1 ± 0.02	-	-	50	50	40	-	-

2.S7. Analytical solutions to soil reactive gas flux determination with a two-chamber setup

For a single chamber system, **ES1** can be used to calculate the flux of gases to and from an enclosed surface. Each of these terms and their units are provided in **Section 2.7** of the main manuscript.

$$V\frac{dC_{\text{cham}}(t)}{dt} = (A \cdot F_{\text{soil}}(t)) + (Q_{\text{in}} \cdot c_{\text{in}}(t)) - (Q_{\text{out}} \cdot c_{\text{out}}(t)) + (V \cdot R(t)) \qquad \textbf{ES1}$$

In our field pilot study, the measurement and reference chambers were installed on clay soil using serrated collars inserted about 10 cm deep into pre-dug circles (30 cm diameter, 20 cm depth) between crop rows of senescing soybeans after removing debris. Collars were left to settle for over 24 h before the chambers were bolted securely to ensure a gas-tight seal. Flux observations were made for two weeks from 02-16 September 2022, during a period when daytime air temperatures were regularly over 25 °C and there were no instances of rain. During the second week of observations, a fertilizer addition of 25 kg N ha^{-1} was made by broadcasting urea in the chamber, followed by applying clean water to simulate 2.5 cm (1") of rainfall.

In our sampling setup, there is a negligible concentration of any target gas in the inflow ($c_{\text{in}}(t) \approx 0$) due to the use of ultra-pure zero air or nitrogen, and the air is actively mixed inside the chamber with its fan, such that $c_{\text{chamb}} = c_{\text{out}}$, so the equation simplifies to **ES2**. For non-steady-state conditions, where the concentration inside the chamber is changing over time, the time-varying nature of the sources and sinks needs to be accounted for. The instantaneous equation that describes the behaviour over an interval [t_1, t_2] is the integral in **ES3**.

$$V\frac{dC_{\text{cham}}(t)}{dt} = (A \cdot F_{\text{soil}}(t)) - (Q_{\text{out}} \cdot c_{\text{cham}}(t)) + (V \cdot R(t)) \qquad \textbf{ES2}$$

$$\int_{t_1}^{t_2} V\frac{dC_{\text{cham}}(t)}{dt}\,dt = \int_{t_1}^{t_2}[(A \cdot F_{\text{soil}}(t)) - (Q_{\text{out}} \cdot c_{\text{cham}}(t)) + (V \cdot R(t))]\,dt \qquad \textbf{ES3}$$

Assuming the soil flux, $F_{\text{soil}}(t)$ (mol m^{-2} s^{-1}), is constant over the time interval [t_1, t_2] is a reasonable assumption for experimental setups where the environmental conditions and, where relevant, soil-plant activity, do not change substantially over short periods of a few to tens of minutes (Pape et al., 2009). Rearranging the **ES3** expression, a flux can be calculated using **ES4**.

$$F_{soil} = \frac{V\Delta C_{\text{cham}} + Q_{\text{out}}\int_{t_1}^{t_2} c_{\text{cham}}(t)\,dt - V\int_{t_1}^{t_2} R(t)\,dt}{A(t_2 - t_1)} \qquad \textbf{ES4}$$

The volumetric mixing ratio (**ES5**) is often the unit of measurement for many gas analyzers and defined as the number of moles of the gas divided by the number of moles of dry air. The mixing ratio X is dimensionless and provides a way to express gas concentrations independently of changes in temperature or pressure.

$$X = \frac{n_{\text{gas}}}{n_{\text{air}}} \quad \textbf{ES5}$$

We can then write the molar concentration, c (mol m^{-3}), in the form of volumetric mixing ratio using **ES6**:

$$c_{\text{chamber}} = X_{\text{out}} \times \rho_d \quad \textbf{ES6}$$

Here, ρ_d (mol m^{-3}) is the molar density of the air. The total pressure P is equal to atmospheric pressure, such that by using the ideal gas law, we can define the density of air using **ES7**:

$$\rho_d = \frac{P}{R \cdot T} \quad \textbf{ES7}$$

Where, P (Pa) is the pressure, R (J mol^{-1} K^{-1}) is the universal gas constant, and T (K) is the absolute temperature. In **ES7** it is assumed that atmospheric air behaves as an ideal gas, which is a reasonable approximation under typical environmental conditions, even at the Earth's surface. The resulting molar concentrations can then be calculated and used in the flux determinations as presented in **E6** and **E7** in the main manuscript.

2.S7.1 Dynamics and physical corrections from reference and measurement chambers

In environmental and experimental settings where gas flux is measured, it is important to capture the rate at which gas concentrations change over time. This rate reflects the net outcome from both gas emission and deposition occurring simultaneously, influenced by the surface under study, temperature, pressure, flow, and surface interactions (**ES8**). The RC (r), which operates under identical conditions to the MC (m) but excludes the surface under study by isolating it beneath the PFA film, takes into account the environmental and surface effects, such that its observed flux rate is described by (**ES9**). To isolate the effects of the surface under study from reactions taking place

in the atmospheric sample and on the chamber surfaces, the rate of change in the RC is subtracted from that in the MC, yielding the net flux through **ES10**.

$F_{\mathrm{m}} =$ surface under study + environmental and chamber effects **ES8**

$F_{\mathrm{r}} =$ environmental and chamber effects **ES9**

$$F_{\mathrm{net}} = F_{\mathrm{m}} - F_{\mathrm{r}} \quad \textbf{ES10}$$

The net rate of change can now be used to calculate the molar flux by substituting it into **ES4** to arrive at **ES11**, which is the core of **E6**.

$$F_{\mathrm{net}} = \frac{V}{A}\left(\frac{\Delta C_m}{\Delta t_m} - \frac{\Delta C_r}{\Delta t_r}\right) + \frac{Q_{\mathrm{out}}}{A}\left(\frac{\int_{t_{1m}}^{t_{2m}} c_m(t)\ dt}{\Delta t_m} - \frac{\int_{t_{1r}}^{t_{2r}} c_r(t)\ dt}{\Delta t_r}\right) - \frac{V}{A}\left(\frac{\int_{t_{1m}}^{t_{2m}} R_m(t)\ dt}{\Delta t_m} - \frac{\int_{t_{1r}}^{t_{2r}} R_r(t)\ dt}{\Delta t_r}\right) \quad \textbf{ES11}$$

The closure period of the two chambers is matched to facilitate an accurate correction of the kinetics and surface interactions. The calculated flux from the surface under study is therefore corrected for background and environmental effects, reducing systematic bias from gas reactivity.

Last, we introduce a flux loss factor (λ; **ES12**) to correct for partial transmission of a targeted reactive gas due to adsorption to chamber walls and gas handling lines during a measurement cycle (t_1-t_2). This factor needs to be determined empirically through calibration experiments, like those presented in **Figure 2.2**, where the loss is quantified relative to theoretical expectations for each gas of interest during both filling and emptying processes.

$$\lambda = \frac{\int_{t_1}^{t_2}\left(\frac{\mathrm{dX}}{\mathrm{dt}}\right)_{\mathrm{theoretical}}\mathrm{dt}}{\int_{t_1}^{t_2}\left(\frac{\mathrm{dX}}{\mathrm{dt}}\right)_{\mathrm{measured}}\mathrm{dt}} \quad \textbf{ES12}$$

We can account for λ in **ES11,** to get the molar flux of gas inside the chamber, which accounts for flux loss (**ES13**) by scaling the equation directly to arrive at the full form presented as **E6** in the main manuscript.

$$F_{\text{net}} = (\lambda).\left(\frac{V}{A}\left(\frac{\Delta C_m}{\Delta t_m} - \frac{\Delta C_r}{\Delta t_r}\right) + \frac{Q_{\text{out}}}{A}\left(\frac{\int_{t_{1m}}^{t_{2m}} c_m(t)\ dt}{\Delta t_m} - \frac{\int_{t_{1r}}^{t_{2r}} c_r(t)\ dt}{\Delta t_r}\right)\right. \quad \textbf{ES13}$$

$$\left. - \frac{V}{A}\left(\frac{\int_{t_{1m}}^{t_{2m}} R_m(t)\ dt}{\Delta t_m} - \frac{\int_{t_{1r}}^{t_{2r}} R_r(t)\ dt}{\Delta t_r}\right)\right)$$

2.S7.2 Chemical corrections from reference and measurement chambers

For reactive species impacting our N_r suite – mainly NO, O_3, and NO_2 – flux values can be attenuated or enhanced due to the reaction of NO with O_3 (**RS-2**). We show below (**Figure 2.S9**) that the photolysis of NO_2 and HONO is negligible due to the high-energy photon cut-off of acrylic (<400 nm threshold) (RS-3). Nevertheless, we include the photolysis term in the rate expression for completeness, noting that under our field conditions its contribution (**S7.2.1**) is within the noise of the NO_2 fluxes. The rate of RS-2 and RS-3 for NO_2, therefore, can be expressed by **ES14**.

$$NO + O_3 \rightarrow NO_2 + O_2 \quad \textbf{RS-2}$$

$$NO_2 + h\nu \rightarrow NO + O \quad \textbf{RS-3}$$

$$\frac{d[NO_2]}{dt} = k_{NO+O_3}[NO][O_3] - J_{NO_2}[NO_2] \quad \textbf{ES14}$$

The total change in the concentration due to reaction over a cycle can be expressed by integrating the rate equation over the cycle duration, as the start time (t_0) and end time (t) are known, therefore replacing the term *R* in **ES13** (and **E6**) with the expression in **ES15**. Under our chamber conditions, the integrated photolysis contribution was smaller than the measurement uncertainty of the NO_2 fluxes (**S7.2.1**), and therefore it was not included as an explicit term in **ES15**.

$$\int_{t_0}^{t} R\ d\text{t} = \Delta[\text{NO}] = \Delta[O_3] = -\Delta[NO_2] = -\int_{t_0}^{t} k\,[\text{NO(t)}][O_3(\text{t})]\,d\text{t} \quad \textbf{ES15}$$

Where the R is the loss rate due to the reaction for NO and O_3 ($R \leq 0$) and the simultaneous production rate for NO_2 ($R \geq 0$). For the kinetic determination, the number density of the gases (molec cm^{-3}) is used to track the chemical transformations over time, but instrumentation typically measures mixing ratios. If temperature and pressure are measured alongside target gases in the dynamic chambers, then using ES6 and ES7, the reaction-corrected flux based on measured mixing ratios can be calculated using **ES16**.

$$F_{\text{net}} = \lambda \cdot \frac{P_{\text{air}}}{R \cdot T} \cdot \left(\frac{V}{A}\left(\frac{\Delta X_m}{\Delta t_m} - \frac{\Delta X_r}{\Delta t_r}\right) + \frac{Q_{\text{out}}}{A}\left(\frac{\int_{t_{1m}}^{t_{2m}} X_m(t)\ dt}{\Delta t_m} - \frac{\int_{t_{1r}}^{t_{2r}} X_r(t)\ dt}{\Delta t_r} \right) \right.$$
$$\left. - \frac{V}{A}\left(\frac{P_{\text{air}}}{R \cdot T}\right)\left(\frac{\int_{t_{1m}}^{t_{2m}} k \cdot X_{\text{NO}_m}(t) \cdot X_{\text{O3}_m}(t)\, dt}{\Delta t_m} - \frac{\int_{t_{1r}}^{t_{2r}} k \cdot X_{\text{NO}_r}(t) \cdot X_{\text{O3}_r}(t)\, dt}{\Delta t_r} \right) \right) \qquad \textbf{ES16}$$

Where, again, P_{air} (Pa) is the atmospheric pressure inside the measurement and reference chambers, R (J mol^{-1} K^{-1}) is the gas constant, and T (K) is the temperature inside the RC and MC. For non-reactive gases like CO_2, CH_4, and N_2O, there is no reaction term, and the flux can be described simply using **ES17** as below, which is presented as **E7** in the main manuscript.

$$F_{\text{net}} = \lambda \cdot \frac{P_{\text{air}}}{R \cdot T} \cdot \left(\frac{V}{A}\left(\frac{\Delta X_m}{\Delta t_m} - \frac{\Delta X_r}{\Delta t_r}\right) + \frac{Q_{\text{out}}}{A}\left(\frac{\int_{t_{1m}}^{t_{2m}} X_m(t)\, dt}{\Delta t_m} - \frac{\int_{t_{1r}}^{t_{2r}} X_r(t)\, dt}{\Delta t_r} \right) \right) \qquad \textbf{ES17}$$

S7.2.1 Losses of NO_2 or HONO due to photolysis within transparent chambers

The fraction of NO_2 or HONO lost due to photolysis depends on the photons transmitted through the chamber material (**Figure S9**). The photolysis rate is estimated here under a worst-case scenario with respect to our field observations, using actinic flux data collected for Lambton County, Ontario, Canada, at 12:00 PM local time on September 10, 2022, under clear sky conditions. The effective photolysis rate constant within the chamber was calculated to be 2.62 x 10^{-4} s^{-1}, using **ES18**.

$$J = \int [\sigma(\lambda) \cdot \phi(\lambda) \cdot F(\lambda) \cdot T(\lambda)]\, d\lambda \qquad \textbf{ES18}$$

Where $\sigma(\lambda)$ is the absorption cross-section of NO_2 (cm^2 $molecule^{-1}$), $\Phi(\lambda)$ is the quantum yield (dimensionless; 0-1), $F(\lambda)$ is the actinic flux (photons cm^{-2} s^{-1} nm^{-1}), and $T(\lambda)$ is the transmission of the acrylic chamber material (dimensionless) at wavelength λ (dimensionless; 0-1).

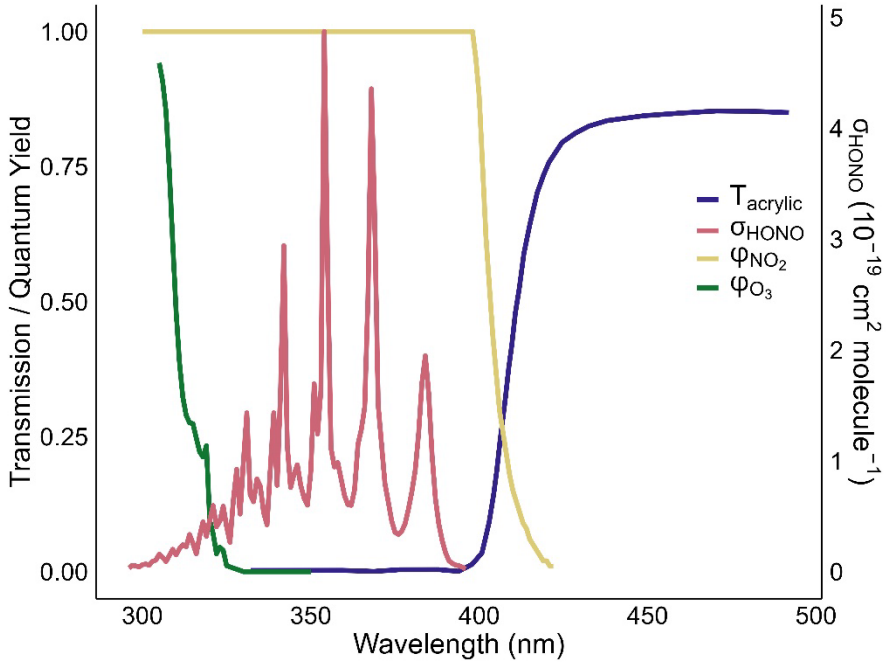

Figure 2.S9: Transmission of light through the chamber and quantum yields for photolysis of O_3 and NO_2, along with the absorption cross section of HONO, as a function of wavelength. Note the negligible overlap for photodissociation. The acrylic effectively blocks wavelengths below approximately 400 nm, meaning the photolysis rate of NO_2 is the only one impacted by a chamber constructed from this material.

Using this attenuated loss rate in a kinetic model, we find that at most 14% of the initial NO_2 concentration is lost due to photolysis within the chamber in the first 10 minutes, and 37% within 30 minutes (**Figure 2.S10, blue trace**). This rate of photolysis significantly reduces the NO_2 mixing ratio within the chamber environment. The wavelength cut-off of polyacrylate limits the penetration of shorter wavelengths, which are more effective in driving NO_2 photolysis, so the overall rate is slowed inside the chamber compared to ambient conditions (**Figure 2.S10, red trace**). Despite this, within the initial 30-minute timeframe (**Figure 2.S10, vertical dashed line**), the change in the fraction of NO_2 lost is relatively small due to the dynamic nature of the chamber headspace (i.e. due to continuous sampling and dilution flows), allowing for a reasonable linear approximation of the curve. The photolytic loss of HONO is much more impacted by the cutoff

wavelength of the polyacrylate chamber lid, to the point where it is not substantially lost due to photolysis. As shown in **Figure 2.S9**, the HONO absorption cross-section lies almost entirely below the ~400 nm transmission cutoff of the chamber lid. This spectral mismatch means that HONO photolysis is effectively suppressed inside the chamber, unlike NO_2, which still absorbs within the transmitted range. Consequently, chamber-derived HONO fluxes are not biased by photolytic loss, making their interpretation simpler than NO_2.

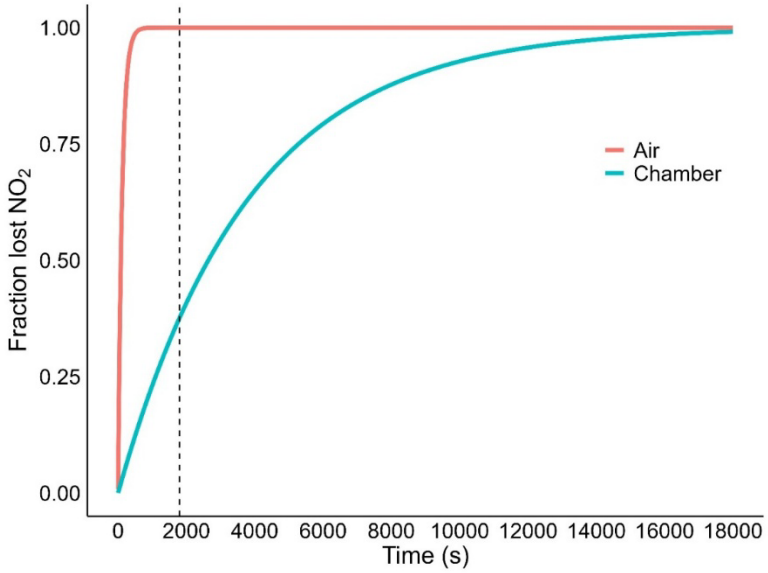

Figure 2.S10: Fraction of NO_2 lost due to photolysis over time, both inside the chamber (blue line) and in ambient air (red line). The vertical dashed line indicates the 30-minute mark, where an initial linear approximation of the loss rate can be applied.

This simplification yields an estimated initial photolysis rate loss of approximately 1% per minute for NO_2 over the initial 30-minute measurement cycle and effectively 0% per minute for HONO under chamber conditions due to the cutoff wavelength. This linear approximation is only valid for this kind of short initial period. Beyond 30 minutes, the overall trend exhibits a steeper exponential decay, characteristic of the NO_2 photolysis process. This photolysis contribution is included within the reaction term (**ES14**). Its effect (~1% min^{-1} maximum at noon under clear-sky conditions) is smaller than the uncertainties of the NO_2 flux measurements, so it is not explicitly propagated into the flux equations in this work.

2.S7.3 Surface interaction correction using the attenuation factor (λ)

Accurate quantification of trace gas fluxes using dynamic chamber systems also requires correction for attenuation caused by gas-wall interactions and the associated sensor response

delays. These effects can significantly suppress the measured accumulation rate of reactive species within the closed chamber, particularly for compounds with strong surface affinity, such as NH_3, NO_2, and HONO, requiring the use of the attenuation factor (λ; **ES12**).

The attenuation factor is derived from our controlled delivery experiments that simulated two sequential measurement scenarios: a filling phase, where gas is introduced and accumulates within the chamber, and an emptying phase, where the chamber is flushed and the gas signal declines (**Figure 2.4**). In an ideal system without wall interactions, the integrated difference between theoretical and observed concentrations within a single chamber should approach zero, and λ would be approximately one. However, as shown in **Figure 2.S11**, all three gases exhibited surface interactions, with NH_3 showing the largest deviation from theoretical predictions.

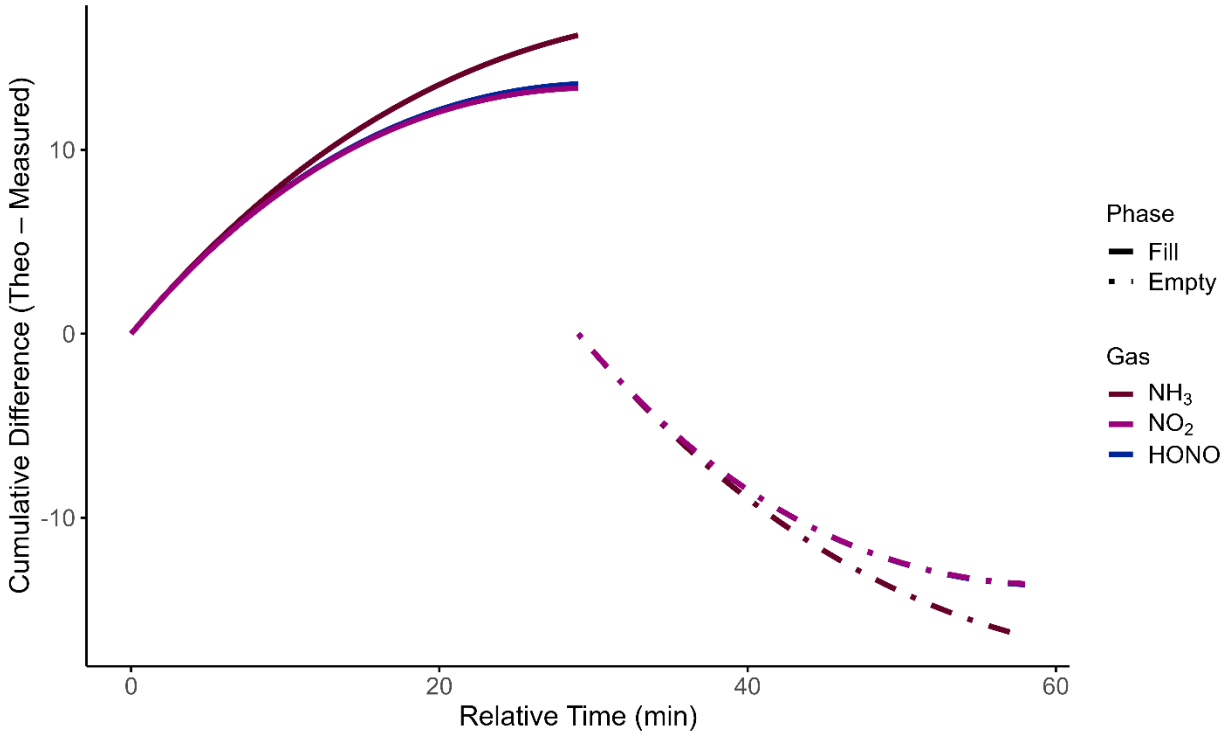

Figure 2.S11: Cumulative integration of the difference between theoretical and measured gas concentrations for NH_3, NO_2, and HONO over a 30-minute filling and emptying period. Theoretical concentrations represent expected values without attenuation, while measured values reflect signal loss due to gas–wall interactions. Solid lines correspond to the filling phase; dashed lines represent the emptying phase, together representing a full in situ measurement cycle. These integrals illustrate the time-dependent and nonlinear attenuation that underlies the empirical calculation of λ.

When filling, the gas accumulates in the chamber, with a strong initial attenuation that diminishes over time as the surfaces passivate. Conversely, adsorbed gases from surface passivation may

partially desorb during emptying, offsetting some of the losses observed during filling. Two respective λ values can be derived and considered separately by integrating the filling and emptying concentration-time series independently.

Where a single-chamber is used to study an experimental system, the filling- and emptying-phase effects offset one another, masking the attenuation as all the surface-interacting molecules are eventually transferred to the gas analyzer. In field applications with a dual chamber approach in use, this symmetry is lost because the measurement chamber accumulates a real emission flux during a defined closure period, while the reference chamber does not. Hence, an empirical calculation of λ is needed, which compensates for the attenuation in both the accumulation and depletion of the target gas (**Table 2.S7**). For NH_3, the fill-phase difference was 16.23, dividing the expected theoretical accumulation by this measured accumulation yields a λ_{fill} of 5.40, while the empty-phase difference was −16.44, with a λ_{empty} of 0.36. Unsurprisingly, NO_2 and HONO followed a similar trend as we also noted their surface interactions, with λ_{fill} values of 3.04 and 3.14 resulting from our characterizations, respectively, and λ_{empty} values near 0.40.

From a physical and mathematical standpoint, attenuation reduces all concentration-dependent components of the flux (accumulation/depletion, dilution, and reaction) by the same factor. As a result, the attenuation factor λ scales the entire net-flux expression rather than only the accumulation term.

Table 2.S7. The cumulative integrated differences between theoretical and measured values from **Figure 2.S11** for both the filling and emptying phases, and the resulting λ values. While the signed fill and empty values appear approximately balanced, their directional impact differs, and the underlying asymmetry becomes critical in real measurements.

Gas	$\int$ (Theo – Meas)$_{fill}$	$\int$ (Theo – Meas)$_{empty}$	difference	λ_{fill}	λ_{empty}
NH_3	16.23	-16.33	-0.20	5.40	0.36
NO_2	13.40	-13.64	-0.23	3.04	0.40
HONO	13.57	-13.65	-0.05	3.14	0.40

S8. References

Crilley, L. R., Lao, M., Salehpoor, L., & VandenBoer, T. C. (2023). Emerging investigator series: an instrument to measure and speciate the total reactive nitrogen budget indoors: description and field measurements. *Environmental Science: Processes and Impacts*, *25*(3), 389–404. https://doi.org/10.1039/d2em00446a

Ellis, R. A., Murphy, J. G., Pattey, E., Van Haarlem, R., O'brien, J. M., & Herndon, S. C. (2010). Characterizing a Quantum Cascade Tunable Infrared Laser Differential Absorption Spectrometer (QC-TILDAS) for measurements of atmospheric ammonia. *Atmos. Meas. Tech*, *3*, 397–406.

Lao, M., Crilley, L. R., Salehpoor, L., Furlani, T. C., Bourgeois, I., Andrew Neuman, J., Rollins, A. W., Veres, P. R., Washenfelder, R. A., Womack, C. C., Young, C. J., & VandenBoer, T. C. (2020). A portable, robust, stable, and tunable calibration source for gas-phase nitrous acid (HONO). *Atmospheric Measurement Techniques*, *13*(11), 5873–5890. https://doi.org/10.5194/amt-13-5873-2020

Ma, L., Pascalidou, E. M., Wiame, F., Zanna, S., Maurice, V., & Marcus, P. (2020). Passivation mechanisms and pre-oxidation effects on model surfaces of FeCrNi austenitic stainless steel. *Corrosion Science*, *167*, 108483. https://doi.org/10.1016/J.CORSCI.2020.108483

Pape, L., Ammann, C., Nyfeler-Brunner, A., Spirig, C., Hens, K., & Meixner, F. X. (2009). An automated dynamic chamber system for surface exchange measurement of non-reactive and reactive trace gases of grassland ecosystems. *Biogeosciences*, *6*(3), 405–429. https://doi.org/10.5194/bg-6-405-2009

Salehpoor, L., & VandenBoer, T. C. (2023). Suppressor and calibration standard limitations in cation chromatography of ammonium and 10 alkylamines in atmospheric samples. *Analytical Methods*, *15*(31), 3822–3842. https://doi.org/10.1039/d3ay01158e

Sapag, K., Vallone, A., Blanco, A. A. G., & Solar, C. (2010). Adsorption of Methane in Porous Materials as the Basis for the Storage of Natural Gas. *Natural Gas*. https://doi.org/10.5772/9846

Appendix B: Supporting information for Chapter Three

S3.1: Python script to generate coordinates for soil sample collection using the random grid sampling technique.

This Python script was made to generate coordinates for soil sample collection across an agricultural field using a random sampling technique. Full details of the code are open-sourced and available in the GitHub repository (https://github.com/moxy29/Soil-Data-Analyzer). The agricultural field (43°09'36.0"N, 81°55'48.0"W; 180 m × 480 m) was divided into 8 grids (each of 120 m × 90 m) based on user-defined dimensions. Random 4 coordinates were generated within each grid, and the resulting coordinates are shown in **Table S3.1**.

Table S3.1: Randomly obtained coordinates using Python for each plot. Four soil samples from plots A through H were collected, out of which three correspond to the individual sample denoted in black, whereas the pooled samples are shown in blue.

	Coordinates (x,y)			
	Sample (i)	Sample (ii)	Sample (iii)	Sample (iv)
Plot A	(21, 57)	(77, 58)	(83, 29)	(97, 88)
Plot B	(6, 140)	(45, 180)	(25, 114)	(107, 105)
Plot C	(131, 36)	(127, 10)	(137, 17)	(218, 43)
Plot D	(236, 180)	(230, 138)	(197, 169)	(196, 112)
Plot E	(348, 28)	(261, 55)	(275, 40)	(341, 24)
Plot F	(276, 160)	(295, 149)	(347, 180)	(316, 95)
Plot G	(362, 68)	(462, 89)	(423, 1)	(374, 7)
Plot H	(456, 141)	(436, 138)	(453, 112)	(405, 119)

S3.2: Preparation of dried soil for lab analysis

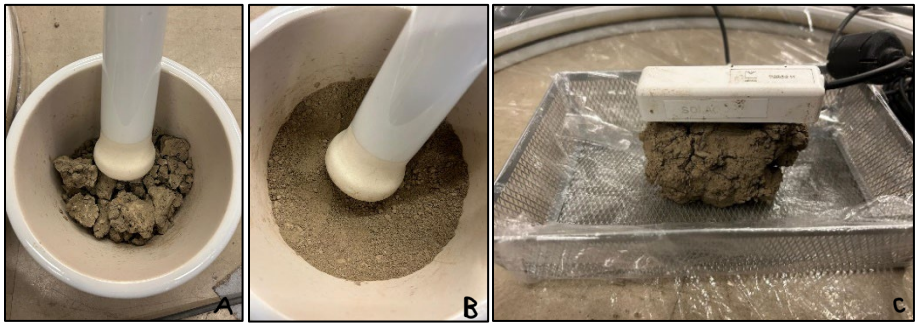

Figure S3.2: Soil sample before and after processing with a mortar and pestle. A) The initial sample cohesive clumps of soil. B) After finely grinding with a clump size less than 1 cm in diameter. C) After wetting the soil with DIW and soil probe insertion for analysis.

S3.3: Calibration of NO_x analyzer

Using the Gascal, zero air, 40, 60, and 80 ppbv are added to the analyzer for 30 mins, where a stable signal is typically achieved. The average NO concentration measured during this period is then calculated, and a calibration curve of average NO response vs NO added is plotted. The analyzer's response to changes in NO mixing ratio was linear, with a slope of 0.9984 and an R2 value of 1.0 (Figure S3.2). For multi-point precision checks of NO_2, required mixing ratios of NO_2 (40 ppbv, 50 ppbv and 60 ppbv) were added using gas-phase titration of NO with O_3.

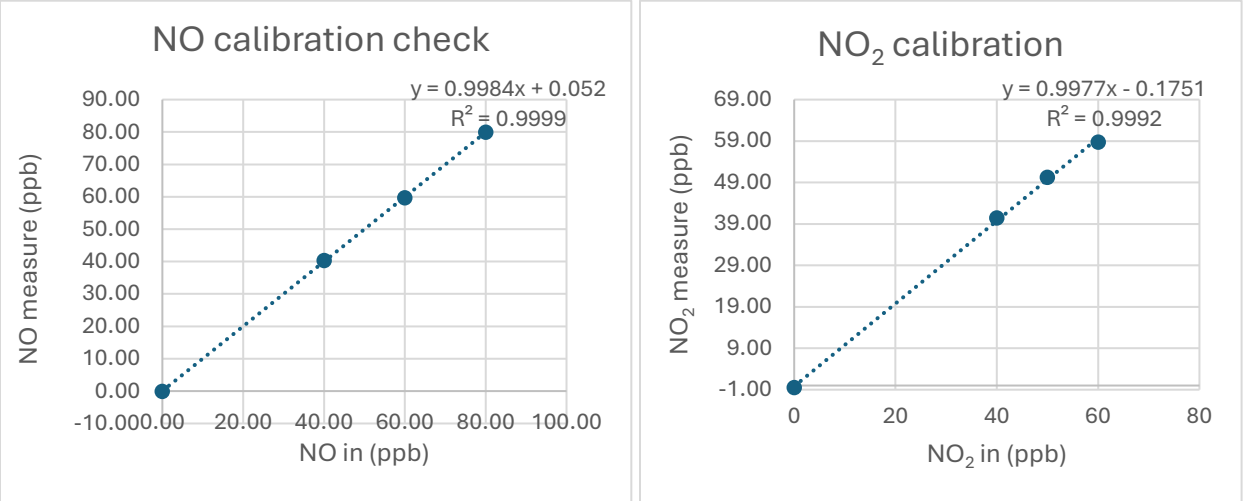

Figure S3.3: Calibration curve for NO and NO_2

S3.4: Calibration of soil probe

An oven-dried pooled soil sample was wetted with controlled amounts of water, and the resulting soil probe voltage was measured. The probe voltage is allowed to stabilize in each soil sample, and the known moisture content is also recorded. Repeated wetting of the soil with additional water is performed until the soil is fully saturated and the final probe voltage is obtained (**Table S3.4**). A calibration curve is then plotted for soil VWC vs raw soil probe voltage according to the manufacturer's instructions (**Figure S3.3**).

Table S3.4: Soil weight with incremental additions of water and the corresponding voltage readings. DIW water is calculated by taking the difference between the soil weight and the dry soil mass (1038.4 g). Gravimetric water content (*w*) is determined by dividing water mass by dry soil mass. The actual soil VWC was obtained by multiplying *w* by the bulk density (1.12 g cm^{-3}).

Points	Soil weight	DIW weight	Gravimetric water content (*w*)	Actual soil VWC	Sensor Measurements		
					Obs. 1	Obs. 2	Avg Obs.
	g	g	g g^{-1}	m^3 m^{-3}	mV	mV	mV
1	1045.82	7.45	0.0072	0.0080	1932.55	1931.16	1931.90
2	1136.15	97.78	0.0942	0.1055	2044.87	2042.87	2043.87
3	1224.14	185.77	0.1789	0.2004	2154.84	2153.07	2154.00
4	1297.83	259.46	0.2499	0.2799	2598.81	2598.82	2598.82
5	1325.4	287.03	0.2764	0.3096	2631.96	2632.8	2632.38

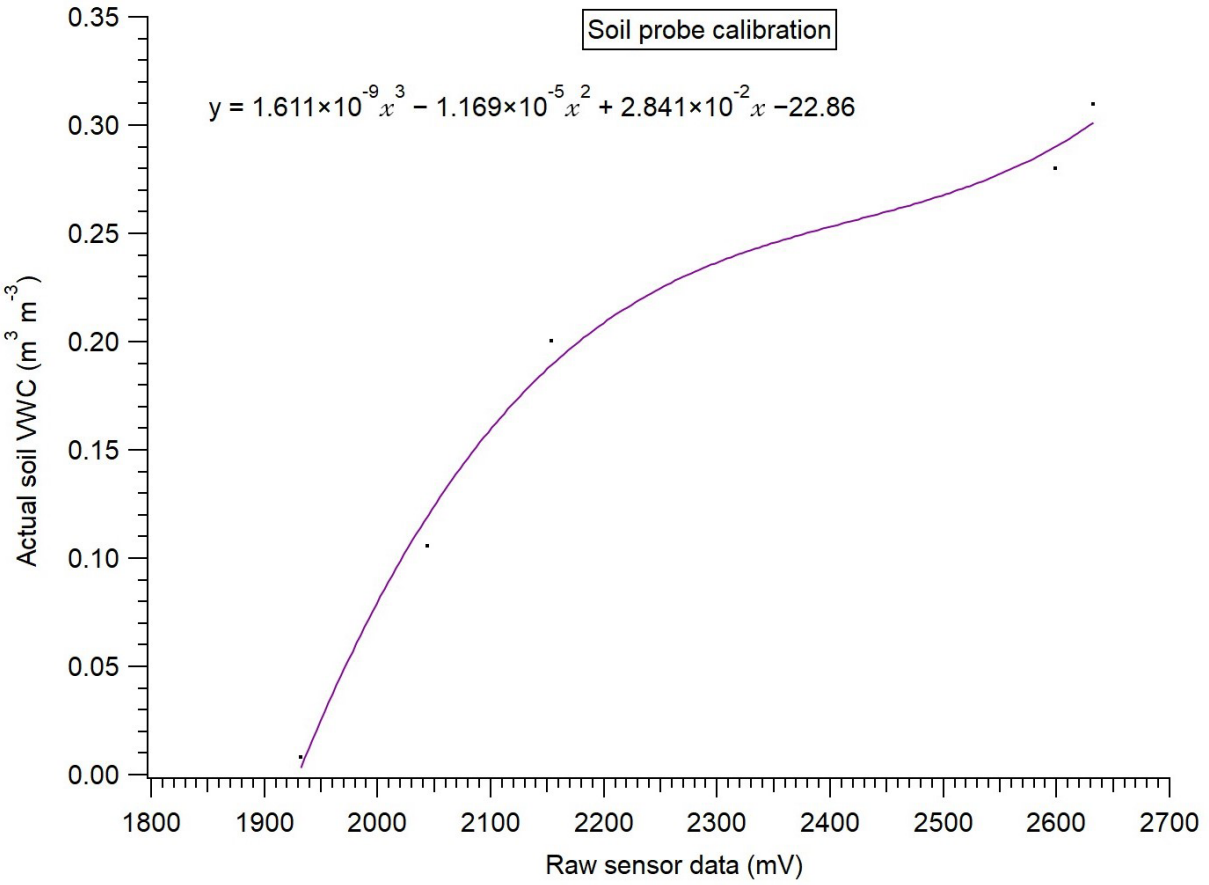

Figure 2.S3.4: Calibration curve for the soil probe (TEROS 11). The x represents the raw sensor data, ranging from 1930 mV to 2635 mV. The calibration was performed to ensure accurate measurement of soil volumetric water content (VWC) under experimental conditions.

S3.5: R code for one of the pooled replicates to calculate NO, NO_2 and HONO flux

To analyze the data, R code was used (https://github.com/moxy29/Soil-Data-Analyzer; soil flux). The multiple generated soil probe data files were imported and bound into one, followed by converting the epoch time to EST. Then, the valve data was imported and averaged over a minute. All datasets (NO, NO_2, HONO, valve state, and soil probe readings) were synchronized to one-minute intervals, producing a unified dataset on the same time base. Average hourly flux and integrated flux using the trapezoidal rule were calculated. The CSV file is then exported, and the data is plotted in Igor.

S3.5: Code to bin the data according to soil VWC (%)

An R code was produced to bin data (refer to https://github.com/moxy29/Soil-Data-Analyzer) into predefined soil VWC (e.g., 20-24). The code enables statistical comparisons among samples and trend visualization for NO_y across these regimes.

S3.6 Compute the average for the samples to compare with the obtained pooled sample

It calculates the weighted averages and uncertainties between sample replicates. It also performs a paired t-test to evaluate the similarities between the sample NO, NO_2 and HONO flux. The code can be found here https://github.com/moxy29/Soil-Data-Analyzer.

Table S3.5 Results of paired t-tests assessing the consistency between duplicate measurements within each plot (A–H) for NO, NO_2, and HONO. Each plot contained two replicate observation per parameter. The p-values indicate whether the replicate measurements are statistically similar ($p > 0.05$) or different ($p < 0.05$). Paired t-test results across all the plots. Please note that due to less data the results are not robust.

Plot	Parameter	p_value	Similar
A	NO	0.0001	No
A	NO_2	0	No
A	HONO	0.0474	Yes
B	NO	0.7741	Yes
B	NO_2	0.7538	Yes
B	HONO	0.7741	Yes
C	NO	0.0012	No
C	NO_2	0	No
C	HONO	0	No
D	NO	0	No
D	NO_2	0	No
D	HONO	0	No
E	NO	0.6198	Yes
E	NO_2	0.4949	Yes
E	HONO	0.0317	Yes
F	NO	0	No
F	NO_2	0	No
F	HONO	0	No
G	NO	0	No
G	NO_2	0	No
G	HONO	0	No
H	NO	0.8706	Yes
H	NO_2	0.3024	Yes
H	HONO	0.0166	Yes

Table S3.6: Average flux and mixing ratio of NO, NO_2, and HONO across similar soil VWC (20-24%). Values are reported as mean ± standard error.

Soil sample	Soil VWC (%)	Mixing ratio (ppb)			Avg Flux (μg N m^{-2} hr^{-1})		
		NO	NO_2	HONO	NO	NO_2	HONO
Pooled	23 ± 0.3	5 ± 0.22	1 ± 0.06	1 ± 0.07	1 ± 0.02	0.1 ± 0.01	0.1 ± 0.01
Obtained pooled	22 ± 0.1	17.6 ± 0.6	4.5 ± 0.06	3.4 ± 0.1	1.6 ± 0.02	0.4 ± 0.01	0.3 ± 0.001
A	22 ± 0.3	23 ± 0.6	4 ± 0.2	4 ± 0.1	2 ± 0.1	0.4 ± 0.02	0.4 ± 0.01
B	22 ± 0.1	10 ± 0.2	3 ± 0.2	0.6 ± 0.1	1 ± 0.02	0.3 ± 0.01	0.1 ± 0.01
C	22 ± 0.4	31 ± 0.5	7 ± 0.1	11 ± 0.2	3 ± 0.1	0.7 ± 0.11	1 ± 0.01
D	22 ± 0.01	7 ± 0.02	2 ± 0.1	0.3 ± 0.2	0.7 ± 0.01	0.1 ± 0.11	0.02 ± 0.03
E	24 ± 0.5	22 ± 0.5	7 ± 0.1	4 ± 0.3	2 ± 0.1	0.7 ± 0.01	0.4 ± 0.03
F	22 ± 0.1	10 ± 0.1	3 ± 0.02	0.7 ± 0.1	1 ± 0.01	0.2 ± 0.02	0.1 ± 0.01
G	22 ± 0.02	28 ± 0.5	7 ± 0.01	5 ± 0.01	2 ± 0.02	0.7 ± 0.02	0.5 ± 0.01
H	22 ± 0.2	10 ± 0.2	3 ± 0.1	0.6 ± 0.1	1 ± 0.01	0.2 ± 0.01	0.1 ± 0.01

Appendix C: Supporting information for Chapter Four

4.S1: Amount of double salts

To assess soil nitrogen fluxes, 350 g of pooled soil was used per experimental unit. Fertilizer solutions were applied at a rate equivalent to 1 g of nitrogen (N) per kilogram of soil, corresponding to 0.35 g N per treatment. The following fertilizer masses were applied based on calculated nitrogen content: 0.75 g of urea (46.67% N), 1.975 g of ammonium bicarbonate (ABC; 17.73% N), 3.16 g of magnesium ammonium carbonate (MAC; 11.1% N), and 3.56 g of zinc ammonium carbonate (ZAC; 9.84% N).

4.S2: Experimental setup of analyzers

Figure 4.S.2: The Moving rack consists of a multiplexer, NO_x, G2509, and O_3 analyzer from top to bottom.

Table 4.S1: Total N volatilized (%) was calculated by taking the ratio of the total nitrogen mass measured on the given day and the total mass of N added at the start of the experiment.

	Total N volatilized (%)		
Time (days)	Urea	MAC	ZAC
0	0	0	0
1	6.45	22.87	15.53
2	15.25	37.91	34.79
3	21.76	48.53	50.60